Bio tribology of the Patella Femoral Joint in Total Knee Replacement

Raman Maiti

Submitted in accordance with the requirements for the degree of

Doctor of Philosophy

The University of Leeds

School of Mechanical Engineering

January 2012

Supervisors: Dr. L. M. Jennings, Prof. Z.M. Jin, Prof. J. Fisher

The candidate confirms that the work submitted is her own and that appropriate credit has been given where reference has been made to the work of others.

Dedicated to mom (Baruna), dad (Surjya) and sister (Rakhi)

Acknowledgements

With blessings from GOD, mom, dad and sister, I choose this path to fulfil my dream. I am sure whatever I do in my life, everything I owe to them.

MY PhD life was similar to the joint replacement surgery. It consists of pre (consultancy), post (support and recovery) surgery stages and the surgery. I am thankful for all the help from different people throughout.

The main stage of this process is the replacement surgery on the capable hands of surgeons (supervisors) and nurses (technicians). 100% success rate was only possible because of talented supervisors (Dr. Louise Jennings, Prof. John Fisher and Prof. Zhongmin Jin) and hardworking technicians (Amisha Desai, Irvin Homan, Jane Cardie, Keith Dyer, Lee Wetherill and Phil Wood).

The pre-surgery consultancy was given by caring and friendly Claire Brockett, Mazen Al-Hajjar and Peter Ellison. The final and most vital stage is the post-surgery stage which consisted of financial, emotional and physical supports. The financial support was granted by EPSRC IDC, Cheryl Harris, Debra Baldwin and Rachel Cox. Emotional support was important at sad and difficult times. Many thanks to work mom (Jane Tillotson), Rae Taylor, iMBE family (Alison Jones, Dawn Groves, Laura McCann, Nagitha Wijayathunga, Nic Roberts, Phil Hyde, Rachel Vicars, Salah Hammouche, Sarah Junaid, Sarrawat Rehman, Silvia Carbone, Senay Mihcin, Sophie Williams, Susan Patridge, and Wei Jiang). Regular game of football with iMBE AFC (Abdul Abdellatif, Adam Liddle, Adam Stops, Antony Francis, Danny Skippy, Dave Horne, Dave Keeling, James Glover, Junyan Li, Martin Stanley, Mehran Moazen, Ondrej Holub, Qingen Meng, Sami Tarsuslugil, Simon Taylor, Stewart McClure and Xijin Hua), Illkley Moor (Todd Stewart) and sports day (Eileen Ingham, Joanne Tipper, Ruth Wilcox) kept me fit and ever ready for challenges.

Thanks to my close and dearest friends for being with me during my recovery stages Aparna Gondekar, Annalisa Morticelli, Daniele Dipresa, Bhakti Lad, Hitesh Sain, Lucrezia Morticelli Mansi Harjai, Mohit, Mridula Pillai and Navanshu Tripathi. Last not the least special thanks to my sisters, brothers, uncles, aunties and other relatives (Bahubalindra, Chaudhari, Das, Gantait, Maiti and Patra families).

Abstract

Total knee replacement remains the final treatment for patients suffering from knee arthritis and providing relief from pain and improvement in function. Despite the fact that the common reason for revisions of TKR is due to problems regarding patella femoral joint, the use of patella during TKA varies from country to country with popularity in USA (90%), Denmark (76%), Australia (43%), England and Wales (33%), Sweden (14%) and Norway (11%). Research was performed into the *in vitro* wear simulation of the patella femoral joint but to date none of these simulations have employed all six degrees of freedom.

The aim of this study was to

- develop a six axis patella femoral joint simulator for assessment of wear,
- develop a computational model to predict the kinematics of the patella femoral joint and validate using experimental knee joint simulator results,
- investigate the influence of kinematic parameters (patella rotation, displacement and tilt) and shape (round and oval dome patella) on the wear of the patella femoral joint,
- validate and develop other volumetric measurement techniques,
- validate the experimental wear results with the retrievals volumetric analysis.

The six station Leeds Prosim knee simulator was modified as a patella femoral knee simulator for the wear assessment process. Good overall agreement between the computational prediction and the experimental measurement were obtained for patella femoral kinematics. Increasing the medial lateral rotation significantly increased the wear rate from 8.6 mm^3/MC to 12.3 mm^3/MC. Decreasing the medial lateral displacement led to a no significant change in the wear rate. Changing the shape from round dome to oval dome led to a non significant decrease in wear rate from 8.7 mm^3/MC to 6.3 mm^3/MC. Ten retrievals were analyzed for volumetric and surface wear. Wear volume per year for retrievals were obtained in range of 0.9 mm^3/year to 18.7 mm^3/year. The wear scar area was similar in shape with the *in vitro* analysis validating the wear analysis.

Contents

Acknowledgements iv

Abstract v

Contents vi

Figures xiv

Tables xxv

Nomenclature xxix

Chapter 1: Introduction and Background 1

1.1 Introduction 1

1.2 Anatomy of Knee Joint 2

1.2.1 Tibia Femoral Joint 2

1.2.2 Patella femoral Joint 3

1.3 Need for Replacements 5

1.3.1 Patella Replacement in Total Knee Arthroplasty 6

1.3.2 Patella Femoral Arthroplasty (PFA) 7

1.3.3 Success and Revision of Knee and Patella Joint Replacement 7

1.4 Knee Joint Reference Plane 8

Coordinate system 8

1.5 TFJ Flexion Extension Rotation and Kinetics 11

1.6 PFJ Kinematics and Kinetics. 12

1.6.1 PFJ Kinematics of Normal Knee during Gait 13

1.6.2 PFJ Kinematics in Total Knee Replacement 16

1.6.3 PFJ Kinetics 23

1.7 Polyethylene Bearing Materials 25

1.7.1 Processing Methods 26

1.7.2 Limitation of UHMWPE 27

1.8 Wear Mechanism 28

1.9 Experimental Wear Simulations 29

1.9.1 Introduction 29

1.9.2 Patella Femoral Joint 29

1.10 Explant Analysis 36

1.11 Computational Kinematic Model 37

1.12 Research Rationale, Hypothesis, Aim, Objectives and Outline of the Thesis 39
1.12.1 Rationale 39
1.12.2 Aims, Hypothesis and Objectives 39
1.12.3 Outline 40

Chapter 2: Materials and Methods 41
2.1 Introduction 41
2.2 Materials used in *In Vitro* Wear Simulation 42
2.2.1 Femoral Component - PFC Sigma 42
2.2.2 UHMWPE Round Dome Patella 43
2.2.3 Test Lubricant 44
2.2.4 Poly methyl methacrylate (PMMA) Cement 44
2.3 Materials used in Explants Analysis 45
2.4 Cleaning Agents 45
2.5 Methods 45
2.5.1 The PFJ simulator 45
2.5.2 Development of Simulator for Patella Femoral Joint 47
2.5.3 Simulator Set Up 49
2.5.3.1 Station assembly 49
2.5.3.2 Calibration 54
2.5.4 Wear Model Control Strategy 55
2.5.5 In Vitro Kinematic Measurement 61
2.5.5.1 Calibration 61
2.5.5.2 Analysis 62
2.5.5.3 Statistical significance 62
2.6 Procedure of Operating the Wear Simulator 62
2.6.1 Specimen Preparation 63
2.6.1.1 Before the test 63
2.6.1.2 During the test 63
2.6.1.3 Measurement intervals 63
2.6.2 Gravimetric 64
2.6.2.1 Calibration 64
2.6.2.2 Test specimen 64
2.6.2.3 Analysis 65

2.6.2.4 Statistical significance 65
2.6.3 MicroCT 65
2.6.3.1 Calibration 66
2.6.3.2 Test specimen 67
2.6.3.3 Volume Analysis 67
2.6.3.4 Analysis 69
2.6.3.5 Statistical significance 69
2.6.4 Geometrical Measurement 69
2.6.4.1 Calibration 70
2.6.4.2 Test specimen 70
2.6.4.3 Analysis 71
2.6.4.4 Statistical significance 72
2.6.5 Pycnomatic ATC 73
2.6.5.1 Calibration 75
2.6.5.2 Test specimen 75
2.6.5.3 Analysis and statistical methods 76
2.6.6 Surface Topography Measurements 76
2.6.6.1 Calibration 78
2.6.6.2 Test specimen 78
2.6.6.3 Analysis 80
2.6.6.4 Statistical significance 82
2.6.7 Two Dimensional Measurements (Wear Area and Wear Grading) 82
2.6.7.1 Test specimen 83
2.6.7.2 Calibration 83
2.6.7.3 Analysis 84
2.6.7.4 Statistical methods 85
2.6.8 Wear Characteristics and Grading 85
2.7 Multi body solid dynamics (MBSD) model 87
2.7.1 Calibration 91
2.7.2 Analysis and Statistical Significance 91
2.8 Retrieval Analysis and Measurement Techniques 91
2.8.1 Retrieval Preparation 92
2.8.2 Measurement Techniques 92
2.8.3 Analysis and Statistical Significance 92

Chapter 3: Computational Modelling of Patella Femoral Kinematics during Gait Cycle and Experimental Validation 93

3.1 Introduction 93

3.2 Materials and Methods 94

3.2.1 Multi Body Solid Dynamics (MBSD) Model 96

3.2.1.1 Patella femoral contact 97

3.2.1.2 Contact parameters 99

3.2.1.3 Contact friction 100

3.2.2 Sensitivity Analysis 100

3.3 Results 100

3.3.1 Comparison of Kinematics at Different Radii of Rotation 101

3.3.2 Comparison of Kinematics for Unworn and Worn Patella 105

3.3.3 Comparison of Tilt for Round and Oval Dome Patella Buttons ... 106

3.3.4 Comparison of ML Tilt for Round Dome Patella with Literature 107

3.3.5 Sensitivity Analysis 109

3.4 Discussion 113

3.4.1 Comparison of Kinematics at Different Radii of Rotations 113

3.4.2 Comparison of Kinematics for Unworn and Worn Patella 115

3.4.3 Comparison of Kinematics for Round and Oval Dome Patella 115

3.4.4 Comparison of Kinematics for Round Dome Patella with Literature 115

3.4.5 Sensitivity Analysis 117

Summary 118

Chapter 4: Development of Volumetric Wear Measurement Techniques 119

4.1 Introduction 119

4.2 Materials and Methods 120

4.2.1 Pycnometer 121

4.2.2 CMM 121

4.2.3 MicroCT 121

4.3 Results 122

4.3.1 Pycnometer 122

4.3.2 CMM 124

4.3.3 MicroCT 126

4.4 Discussion 127

Summary 130

Chapter 5: *In Vitro* Wear Simulation of the PFC Sigma and Round Dome Patella 131

5.1 Introduction 131

5.2 Materials and Methods 131

5.2.1 Materials 131

5.2.2 Methods 132

5.3 Test Results 136

5.3.1 Soak and Load Soak Controls 136

5.3.1.1 Kinematics 136

5.3.1.2 Gravimetric volume measurements 136

5.3.1.3 MicroCT creep measurements 138

5.3.1.4 Geometrical creep measurements 138

5.3.1.5 Quantification of creep area, surface analysis, and creep depth 139

5.3.2 High ML Rotation (>3°) and Uncontrolled ML Displacement 142

5.3.2.1 Kinematics 142

5.3.2.2 Gravimetric volume measurements 145

5.3.2.3 MicroCT volume measurements 147

5.3.2.4 Geometric volume measurements 148

5.3.2.5 Volume loss with ML tilt 148

5.3.2.6 Quantification of wear scar area, surface analysis, and wear depth 149

Wear scar area 149

Visual inspection 152

Surface analysis 153

Wear depth 154

5.3.3 Low ML Rotation with Uncontrolled ML Displacement 155

5.3.3.1 Kinematics 155

5.3.3.2 Gravimetric volume measurements 158

5.3.3.3 MicroCT volume measurements 160

5.3.3.4 Volume loss with ML tilt 161

5.3.3.5 Quantification of wear scar area, surface analysis, and wear depth 162

Wear scar area 162

Visual inspection 164
Surface analysis 165
5.3.4 Low ML Rotation with Constrained ML Displacement 167
5.3.4.1 Kinematics 167
5.3.4.2 Gravimetric volume measurements 170
5.3.4.3 MicroCT volume measurements 172
5.3.4.4 Volume loss with ML tilt 173
5.3.4.5 Quantification of wear scar area, surface analysis, and wear depth 174
Wear scar area 174
Visual inspection 177
Surface analysis 177
Wear depth 178
5.3.5 Round Dome Wear Test – All Results 178
5.3.5.1 Gravimetric analysis 178
5.3.5.2 MicroCT volumetric measurements 179
5.3.5.3 Geometric volumetric measurements 182
5.3.5.4 Volume loss v/s tilt 184
5.3.5.5 Wear grading and location of centroid 185
Wear grading 185
Location of centroid 186
5.4 Discussion 186
Summary 192

Chapter 6: *In vitro* wear simulation of PFC Sigma and Oval Dome Patella 193
6.1 Introduction 193
6.2 Materials and Methods 193
6.2.1 Materials 193
6.2.2 Methods 194
6.3 Results 195
6.3.1 Kinematics 195
6.3.2 Wear Results 199
6.3.2.1 Gravimetric 199
Soak and load soak controls 199
Wear results at Low ML rotation with free ML displacement 199

Wear results of oval dome as compared to round dome patella 202

6.3.2.2 Geometrical volumetric measurements 202

6.3.3 Volume Loss with ML Tilt 208

6.3.4 Quantification of Wear Area, Centroid of the Scar Area, Surface Analysis and Wear Depth 209

6.3.4.1 Scar area 209

6.3.4.2 Location of centroid 213

6.3.4.3 Surface analysis for the femoral and patella components 213

Visual observations 213

Surface analysis 215

6.3.4.4 Wear depth 217

6.4 Discussion 219

Summary 222

Chapter 7: Tribological Analysis of Patella Femoral Joint Retrievals 223

7.1 Introduction 223

7.2 Materials and Method 224

7.3 Results 226

7.3.1 Position of Wear Scar Area 226

7.3.2 Oval Patella Retrievals 227

7.3.2.1 Geometric volumetric measurements 227

7.3.2.2 Quantification of surface analysis 230

Visual inspection 230

Wear scar area and location of centroid 233

Surface roughness parameters 237

7.3.3 Round Dome Patella Retrievals 238

7.3.3.1 Geometric volumetric measurements 238

7.3.3.2 Quantification of surface analysis 239

Visual inspection 239

Wear scar area and location of centroid 241

7.4 Discussion 243

Summary 246

Chapter 8: Overall Discussion and Conclusion 248

8.1 Overall Discussion 248

8.2 Conclusion 252
8.3 Future work 253
References 254
Appendix (List of Conference Publications) 272
Appendix A 273

Figures

Figure 1-1 Figure illustrates tibia femoral joint with tibia, femur, condyles menisci and ligaments (Brunkner and Khan 2005). 3

Figure 1-2 The Patella-femoral joint (Image taken from http://www.yoursurgery.com/ProcedureDetails.cfm?BR=5&Proc=30). 3

Figure 1-3 The Patellofemoral ligaments (Fulkerson, 1997). 4

Figure 1-4 Anatomical reference planes (Whittle, 2001) 9

Figure 1-5 Rotational movements of right tibia femoral joint (Ellison *et al.* 2007; Whittle, 2001). 10

Figure 1-6 Rotations of right knee joint with positive polarity (Ellison et al. 2007). 11

Figure 1-7 Patellar motion representation (Ellison et al. 2007). 11

Figure 1-8 TFJ flexion extension patterns during walking (Lafortune *et al.* 1992). 12

Figure 1-9 Translation and rotation of patellar tracking during normal gait cycle. A, E show the tibia femoral flexion during gait for comparison. B, C and D show the patella flexion, rotation and tilt respectively. F, G and H show the patella shift, anterior translation and superior translation respectively (Lafortune and Cavanagh 1987). 15

Figure 1-10 Variation of patella tilt versus knee flexion in TKR. 18

Figure 1-11: Variation of patella displacement versus knee flexion. 19

Figure 1-12 Variation of anterior posterior patella displacement versus knee flexion. 20

Figure 1-13 Variation of medial lateral patellar rotation with knee flexion. 21

Figure 1-14 Variation of patellar flexion extension rotation about x-axis with knee (tibia femoral) flexion. 22

Figure 1-15 Variation of superior inferior displacement with knee flexion. 23

Figure 1-16 Patellar medial-lateral shear force versus knee flexion for normal knee (Normal), PFC with patellar resurfacing (PFC-p), PFC without patellar resurfacing (PFC-np), PFCΣ with patellar resurfacing (PFCΣ-p) and PFCΣ without patellar resurfacing (PFCΣ-np). The positive force refers to force acting lateral direction (Singerman *et al.* 1999). 25

Figure 1-17 Four types of patella design (Hsu and Walker 1989). 30

Figure 1-18 Input waveforms of PFJ load and flexion angle for gait simulation (Burroughs *et al.* 2006). 31

Figure 1-19 Input waveforms of PFJ load and flexion angle for stair climbing simulation (Burroughs *et al.* 2006). 31

Figure 1-20 Wear rates for stair climbing (1 mc) and walking (0.25 mc) (Korduba *et al.* 2008). 32

Figure 1-21 Wear scars after 1 million cycles with misalignment in (a) conventional polyethylene and (b) high cross linked polyethylene (Burroughs *et al.* 2006). 33

Figure 1-22 Wear scar after 4 million cycle of in vitro simulation (Ellison *et al.* 2008). 34

Figure 1-23 Wear rate of patella femoral joint in mm^3/mc (Ellison *et al.* 2008; Korduba *et al.* 2008; Vanbiervliet *et al.* 2011) 35

Figure 1-24 Variation of cross shear with pin rotation (Kang *et al.* 2008). 38

Figure 2-1 Schematic drawing of patella articulation surface in PFC and PFC sigma femoral component (United States Patent – Modular knee replacement 1998, DePuy manufacturing drawing). 43

Figure 2-2 Range of PFC sigma patella: from left Oval and round dome designs. 44

Figure 2-3 General view of Leeds Prosim knee simulator and control unit (Barnett *et al.* 2002). 46

Figure 2-4 A typical station of the Prosim Knee Simulator 1 showing the degrees of freedom, directions and polarity. 47

Figure 2-5 Assembly of mounting and fixtures required for converting Leeds ProSim knee simulator to patella femoral joint. 50

Figure 2-6 PFC sigma femoral component with location of condyles removed from the femoral posterior. 51

Figure 2-7 Schematic diagram of femoral Mount A showing centre of rotation, screw and post holes. 52

Figure 2-8 Schematic drawing of femoral Mounting fixture showing readjusting the femoral component to ensure axial load passing through centre of patella (dotted and solid lines showing original and final setup respectively). 53

Figure 2-9 Schematic diagram of patella femoral joint showing six degrees of freedom and polarities of each degree in simulator and human body. (Modified from http://www.hughston.com/hha/a.extmech.htm). 56

Figure 2-10 Control waveform for patellar flexion during gait (Halloran *et al.* 2005; Ellison 2007). 57

Figure 2-11 Control strategy for superior patellar translation in the wear model (Ellison 2007). 59

Figure 2-12 Control strategy for patellar rotation in the simulator wear model (Ellison *et al.* 2008). Dotted and solid lined denote low and high medial lateral rotation for physiological and high kinematics wear simulation test. 60

Figure 2-13 Control waveform for axial force (Ellison *et al.* 2008). 61

Figure 2-14 Scanco MicroCT80. 66

Figure 2-15 Schematic diagram of MicroCT procedure (Vicars *et al.* 2009). 68

Figure 2-16 Holder for patella when used in CMM or Talysurf measurements. 70

Figure 2-17 A typical wear scar of explants. The olive region is the region of interest and the white mesh depicting the unworn surface for reference. 72

Figure 2-18 Image of Pycnomatic ATC helium gas Pycnometer (Pycnomatic and Pycnomatic ATC Instruction Manual 2007). 73

Figure 2-19 Schematic block diagram of Pycnomatic ATC (Pycnomatic And Pycnomatic ATC Instruction Manual 2007). 74

Figure 2-20 Profile showing peak and valley roughness over a sampling length. (ISO 4287:1997) 77

Figure 2-21 Profile showing average roughness over a sampling length (Flitney and Brown 2007). L: Sampling length 78

Figure 2-22 Surface texture analysis of a femoral component during measurement in Talysurf (Ellison 2007) 79

Figure 2-23 Surface texture analysis of a patella component during measurement in Talysurf (Ellison 2007). 79

Figure 2-24 Raw file for patella specimen from the Talysurf profilometer. 80

Figure 2-25 Roughness parameters for a patella specimen from the Talysurf profilometer. 81

Figure 2-26 Deformation for a patella specimen from the Talysurf profilometer. 81

Figure 2-27 Figure showing marking of wear scar area and division of specimen into four equal quadrants (M-medial, S-superior, I-inferior and L-lateral). 83

Figure 2-28 Position of centroid (star) in a patella specimen 85

Figure 2-29 Schematic plot of division of the total area in four quadrants and marking the modes of wear degradation. 86

Figure 2-30 Flowchart depicting the procedure of importing specimen scans from MicroCT to Adams/VIEW for in vitro analyses. 88

Figure 2-31 Segmentation of threshold in grey scale with threshold ranging from 20-255. 89

Figure 2-32 Smoothing of specimen using Morphological filters of 1,1,1. 89

Figure 3-1 Schematic diagram of femur component showing radius of patella mating (R_1), radius of condyles (R_3) and R_2 is the average of R_1 and R_3. 95

Figure 3-2 Station of Leeds knee Patella simulator for computational and experimental studies. 96

Figure 3-3 Contact model between two mating components (I and J); with I penetrating in J (MSC.Software 2008). 98

Figure 3-4 Load deformation hysteresis curve for PFC sigma round dome patella and low contact stress (LCS) with mobile bearing (MB) patella (Ellison 2008). 99

Figure 3-5 Medial lateral displacement for different radius of rotation (R_1 and R_2) when constrained with errors bar of 95% CL for the experimental results. 101

Figure 3-6 Medial lateral displacement for different radius of rotation (R_1 and R_2) when uncontrolled with error bars of 95% CL for the experimental results. 102

Figure 3-7: Anterior Posterior translation at different femoral radius of rotation (R_1 and R_2) when ML displacement was constrained with error bars of 95% CL for the experimental results. 103

Figure 3-8 Anterior Posterior translation at different femoral radius of rotation (R_1 and R_2) when ML displacement was uncontrolled with error bars of 95% CL for the experimental results. 103

Figure 3-9 Medial lateral tilt at different femoral radius of rotation (R_1 and R_2) when medial lateral translation was constrained with error bars of 95% CL for the experimental results. 104

Figure 3-10 Medial lateral tilt at different femoral radius of rotation (R_1 and R_2) when medial lateral translation was uncontrolled with error bars of 95% CL for the experimental results. 104

Figure 3-11: Medial lateral displacement for worn and unworn patella specimen when medial lateral translation was uncontrolled with error bars of 95% CL for the experimental results. 105

Figure 3-12 Anterior posterior displacement for worn and unworn patella specimen when medial lateral translation was uncontrolled with error bars of 95% CL for the experimental results. 106

Figure 3-13 Medial lateral tilt for worn and unworn patella specimen when medial lateral translation was uncontrolled with error bars of 95% CL of experimental results. 106

Figure 3-14 Medial lateral tilt for round and oval dome patella specimen when medial lateral translation was uncontrolled with error bars of 95% CL for the experimental results. 107

Figure 3-15 Comparison of computationally obtained medial lateral tilt for PFC sigma round dome patella for conditions, 1) without ligament force and constrained ML displacement, 2) without ligament force and uncontrolled ML displacement and 3) with ligament force and uncontrolled ML displacement (Lafortune and Cavanagh 1987; Halloran *et al.* 2005; Ellison *et al.* 2007) 109

Figure 3-16 Concept of tilt under the action of AP load and ML displacement of the patella. 114

Figure 4-1 Plot of volume calculated using Pycnomatic ATC and gravimetric measurements with 95% confidence limit. 123

Figure 4-2 R square between gravimetric and Pycnomatic volume for un-worn patella 123

Figure 4-3 Schematic diagram showing of the difference in volume estimated from CMM and gravimetric at 5, 10 and 15mm^3 material removals. 125

Figure 4-4 CMM scan of varied stages in validation process using surface fit from unworn area. S: Superior, I: Inferior, M: Medial and L: Lateral. 126

Figure 4-5 Schematic diagram showing difference in volume estimated from MicroCT and gravimetric at 5, 10 and 15mm^3 of material removals with 95% confidence limit error bars of MicroCT reference method. 127

Figure 5-1 Placement of round dome patella pegs in the patella mounting during the simulation test. 133

Figure 5-2 Flowchart describing the flow and number of cycles for all conditions. 135

Figure 5-3 Kinematic input and output AP force profiles for the creep station. 137

Figure 5-4 Weight change of soak samples over a course of 12 million cycles. 137

Figure 5-5 Cumulative weight gain (mg) of a load soak control under anterior posterior load in a 1 MC creep test as compared with mean weight of soak controls. 138

Figure 5-6 CMM analysis for specimen 4 from the creep test over 1MC. 139

Figure 5-7 Scar area from a MC of the creep test. S: superior, I: inferior, M: medial and L: lateral. 139

Figure 5-8 Roughness trace of creep test specimen after 1MC of the patella button. 140

Figure 5-9 Figure representing the penetration in a specimen undergone 1 MC creep test. 141

Figure 5-10 Anterior posterior load input (solid line) and simulator feedback (dotted line) plotted versus percentage of gait cycle. APF: Anterior Posterior Force 142

Figure 5-11 Superior inferior displacement input (solid line) and simulator feedback (dotted line) plotted versus percentage of gait cycle. 143

Figure 5-12 Medial lateral rotation input (solid line) and simulator feedback (dotted line) plotted versus percentage of gait cycle. 143

Figure 5-13 Medial lateral displacement plotted with 95% confidence limit versus percentage of gait cycle. 144

Figure 5-14 Medial lateral tilt (0-6MC) for all the stations plotted with 95% confidence limit versus percentage of gait cycle. 144

Figure 5-15 Cumulative volume loss, showing volume loss for every specimen at every MC for high ML rotation and uncontrolled ML displacement 146

Figure 5-16 Cumulative volume loss, showing volume loss for different stations at every MC for high ML rotation and uncontrolled ML displacement 147

Figure 5-17 Volumetric difference of high ML rotation and uncontrolled ML displacement wear test specimens over 6MC. 148

Figure 5-18 Relation of volume loss with tilt represented with linear correlation of R^2 value. 149

Figure 5-19 Wear scar area for 5 specimens with solid line indicating worn area over 6MC. 151

Figure 5-20 Scratches in the patella articulating femoral groove. While solid line highlights the scratches. 152

Figure 5-21 Wear characteristics of wear test specimen undergoing high ML rotation and uncontrolled ML displacement. 1: pitting wear (blue line), 2: burnishing (red line), 3: deformation (green line) and 4: scratching (yellow line). 153

Figure 5-22 Anterior posterior load input (solid line) and simulator feedback (dotted line) plotted versus percentage of gait cycle. 155

Figure 5-23 Superior inferior displacement input (solid line) and simulator feedback (dotted line) plotted versus percentage of gait cycle. 156

Figure 5-24 Medial lateral rotation input (solid line) and simulator feedback (dotted line) plotted versus percentage of gait cycle. 156

Figure 5-25 Medial lateral displacement plotted with 95% confidence limit versus percentage of gait cycle. 157

Figure 5-26 Medial lateral tilt (6-9MC) for all the stations plotted with 95% confidence limit versus percentage of gait cycle. 157

Figure 5-27 Cumulative volume loss, showing volume loss for every specimen at every MC for low ML rotation and uncontrolled ML displacement 159

Figure 5-28 Cumulative volume loss for different stations at every MC for low ML rotation and uncontrolled ML displacement 160

Figure 5-29 Volumetric difference of low ML rotation and uncontrolled ML displacement wear test specimens over 3MC. 161

Figure 5-30 Relation of volume loss with tilt represented with linear correlation of R^2 value. 162

Figure 5-31 Wear scar area for 5 specimens with solid line indicating worn area over 3MC. 164

Figure 5-32 Anterior posterior load input (solid line) and simulator feedback (dotted line) plotted versus percentage of gait cycle. 167

Figure 5-33 Superior inferior displacement input (solid line) and simulator feedback (dotted line) plotted versus percentage of gait cycle. 168

Figure 5-34 Constrained Medial lateral displacement plotted with 95% confidence limit versus percentage of gait cycle. 168

Figure 5-35 Medial lateral tilt (9-12MC) for all the stations plotted with 95% confidence limit versus percentage of gait cycle. 169

Figure 5-36 Cumulative volume loss, showing volume loss for every specimen at every MC for low ML rotation and constrained ML displacement 170

Figure 5-37 Cumulative volume loss for different stations at every MC for low ML rotation and constrained ML displacement 172

Figure 5-38 Volumetric difference of low ML rotation and constrained ML displacement wear test specimens over 3MC. 173

Figure 5-39 Relation of volume loss with tilt represented with linear correlation of R^2 value. 174

Figure 5-40 Wear scar area for five specimens with solid line indicating worn area over 3MC. 176

Figure 5-41 The variation of wear rate with change in kinematics. 179

Figure 5-42 Specimen volumetric difference from MicroCT and Gravimetric after the 12MC, linear regression analysis with R^2. 180

Figure 5-43 MicroCT reconstructed images of the patella specimens after 12MC wear test 182

Figure 5-44 3D images of patella specimens after 12MC of wear test 183

Figure 5-45 Volumetric difference of CMM with respect to gravimetric volumetric wear test specimens over 12MC. 184

Figure 5-46 Relation of volume loss with tilt. Figure shows the linear correlation with R^2 value. 185

Figure 5-47 Location of centroid (in star) of the wear scar in round dome patella. 186

Figure 5-48 Description of creep and wear debris formation (Rostoker et al. 1978). 188

Figure 5-49 Schematics diagram of centre of rotation 189

Figure 6-1 Schematic diagram showing position of oval dome with respect to femoral counterpart during a wear test (Scott *et al.* 1997) 195

Figure 6-2 Plot showing comparison between input profile (bold line) and feedback (dotted line) for anterior posterior force in N. 196

Figure 6-3 Plot showing comparison between input profile (bold line) and feedback (dotted line) for superior inferior displacement in mm. 196

Figure 6-4 Plot showing comparison between input profile (bold line) and feedback (dotted line) for medial lateral rotation in degrees. 197

Figure 6-5 Plot showing medial lateral displacement in mm with errors bar of 95% confidence limit. 197

Figure 6-6 Plot showing medial lateral tilt in degrees with errors bar of 95% confidence limit. 198

Figure 6-7 Change in weight of soak (bold line) and load soak (dotted line) specimen over 3 million cycles. 199

Figure 6-8 Cumulative volume loss for every specimen, showing volume loss at each MC for low ML rotation and free ML displacement. 200

Figure 6-9 Variation of cumulative volume loss with respect to varied station, showing volume loss at each MC for low ML rotation and free ML displacement 201

Figure 6-10 Chart showing the mean variation of wear rate (Mean with 95% confidence limit) with change in kinematics and shape of patella: RD stand for round dome and OD for oval dome patella. ANOVAs t-test are performed for each condition with significance at $p<0.05$ 202

Figure 6-11 Determination of total volumetric loss using CMM; R^2 value included for determining the correlation with gravimetric volume loss. The cumulative volume loss after every MC for the 3MC wear test is plotted. 203

Figure 6-12 CMM analysis of wear penetration of all five wear specimens following 3MC of in vitro simulation at physiological condition. Specimen 3 was damaged between 2-3MC and replaced by specimen 8. Specimen 7 was the creep test sample. 207

Figure 6-13 Relation of wear volume with tilt. Figure shows the linear correlation with R^2 value. 209

Figure 6-14 Wear Scar for all 5 specimens with solid line indicating total worn area. Specimen 7 underwent creep test. 210

Figure 6-15 Average patella scar area from 0 to 3MC. The solid line denotes for wear test and dotted line denotes increment of creep test. 211

Figure 6-16 Relation of wear volume with tilt. Figure shows the linear correlation with R^2 value. 212

Figure 6-17 Location of centroid (in star) of the wear scar in oval dome patella. 213

Figure 6-18 Wear characteristics of wear test specimens undergoing low ML rotation and uncontrolled ML displacement. 1: pitting wear (blue line),

2: burnishing (red line), 3: deformation (green line) and 4: scratching (yellow line). 214

Figure 6-19 Roughness of femoral component mating with wear specimen 2. The table shows average (R_a), skew (R_{sk}), peak (R_p) and valley (R_v) roughness of the femoral component 215

Figure 6-20 Roughness of wear patella specimen 2 after running for 3MC. 216

Figure 6-21 Wear depth of wear patella specimen 2 after running for 3MC. 218

Figure 6-22 Scatter plot of wear depth/deformation of the patella specimen during physiological conditions; ML rotation (<1°) and free ML displacement. 218

Figure 7-1 Wear scar area spread around quadrants ('M' for medial, 'L' for lateral, 'S' for superior and 'I' for inferior). Orientation of wear scar at (a) 0°, (b) 90° clockwise, (c) 180° clockwise and (d) 270° clockwise. 224

Figure 7-2 Position of patella with respect to femur during a) 0° b) 10° and c) 20° of femoral flexion in sagittal plane. 226

Figure 7-3 Position of patella with respect to the femur during a) 0°, b) 10° and c) 20° of femoral flexion in the frontal plane. 227

Figure 7-4 CMM analysis for volumetric wear determination (oval specimen A to F; round specimen G and H). 229

Figure 7-5 CMM analysis for volumetric wear determination (retrievals and *in vitro* test). 230

Figure 7-6 Wear characteristics for oval patella retrievals (Specimen A to H). 1: delamination/ pitting wear, 2: burnishing, 3: deformation, 4: scratching, 5: adhesive wear. 232

Figure 7-7 Wear scar area and location of centroid (shown in star) for oval patella retrievals (Specimen A to H). 235

Figure 7-8 Wear scar area (square mm) with respect to time in situ (in years) with linear trend line and linear correlation (R^2). 236

Figure 7-9 CMM analysis for volumetric wear determination (round retrieval I). 239

Figure 7-10 Wear characteristics for retrievals (Specimen I to J). 1: delamination/ pitting wear, 2: burnishing, 3: deformation, 4: scratching, 5: adhesive wear. 240

Figure 7-11 Wear scar area and location of centroid (shown in star) for oval patella retrievals (Specimen I and J). 242

Figure 7-12 Comparison of wear scar area and location of centroid (in star) between retrieval F, round dome and oval dome patella from experimental simulations and Schwartz's retrieval analysis (2002). 245

Tables

Table 1-1 Experimental data provided by previous investigators in patella tracking. 16

Table 1-2 Explants analysis based number of specimens, measurement types and device (Hood *et al.* 1983; Raimondi *et al.* 2000; Kooijman *et al.* 2003; Bowden *et al.* 2005; Rawlinson *et al.* 2006; Bills *et al.* 2007; Kurtz *et al.* 2007; Lindsey *et al.* 2010; Ellison *et al.* 2010). 36

Table 2-1 IPL commands for direct volume measurement 69

Table 3-1 Material properties of the fixtures used in ADAMS/View R3..... 97

Table 3-2 Values of AP displacement (mm) and Tilt (°) at the end of stance phase (60% of gait cycle) for constrained and uncontrolled ML displacements at varied conditions for R_1 radius of rotation: a) Actual input kinematics b) Ideal input kinematics..... 110

Table 3-3 Values of AP displacement (mm) and Tilt (°) at the end of stance phase (60% of gait cycle) for constrained and uncontrolled ML displacements at varied conditions at R_1 radius of rotation for a) actual input kinematics, b) 1.05 times actual input kinematics and c) 0.95 times actual input kinematics..... 111

Table 3-4 Values of AP (mm)and tilt (°) at the end of stance phase (60% of gait cycle) for constrained and uncontrolled ML displacements at varied conditions for R_1 radius of rotation for a) actual input, b) frictional coefficient = 0.01, c) frictional coefficient = 0.1, d) time step = 100, and e) time step = 2000. 112

Table 3-5 Values of tilt (°) at the end of stance phase (60% of gait cycle) for constrained and uncontrolled ML displacements at varied conditions for R_1 radius of rotation for a) actual input, b) 1.05 times stiffness coefficient, c) 0.95 times stiffness coefficient, d) 1.05 times force coefficient and e) 0.95 times force coefficient..... 113

Table 5-1 Lot numbers for femoral and patella specimen 132

Table5-2 Roughness parameters before and after 1MC creep test of the patella button. 141

Table 5-3 Absolute value of tilt in every station with 95% confidence limit..... 145

Table 5-4 Wear rate for High ML rotation with uncontrolled ML displacement by specimen number over 6MC..... 146

Table 5-5 Wear rate for High ML rotation with uncontrolled ML displacement by station number over 6MC..... 147

Table 5-6 Wear rate for High ML rotation with uncontrolled ML displacement using MicroCT over 6MC 148

Table 5-7 Progression of wear scar (in mm^2) and % of articulating surface area of 6MC in wear test. 150

Table 5-8 Progression of wear scar (in mm^2) in superior, inferior, lateral and medial quadrant during 6MC in wear test 150

Table 5-9 Mean roughness parameters with 95%CL of femoral component before and after the test over 6MC with P value (*p<0.05 significant) 153

Table 5-10 Mean roughness parameters with 95%CL of patella specimen before and after the test over 6MC with P value (*p<0.05 significant) 154

Table 5-11 Wear depth for patella specimens over 6MC 154

Table 5-12 Absolute value of tilt in every station for 6-9MC wear test with 95% confidence limit. 158

Table 5-13 Wear rate for low ML rotation with uncontrolled ML displacement by specimen number over 3MC 159

Table 5-14 Wear rate for low ML rotation with uncontrolled ML displacement by station number over 3MC 160

Table 5-15 Wear rate for low ML rotation with uncontrolled ML displacement using MicroCT over 3MC 161

Table 5-16 Progression of wear scar (in mm^2) and % of articulating surface area after 6MC and 9MC in wear test 163

Table 5-17 Progression of wear scar (in mm^2) in superior, inferior, lateral and medial quadrant during 3MC in wear test 163

Table 5-18 Mean roughness parameters with 95%CL of femoral component before and after the test over 3MC with P value (*p<0.05 significant) 165

Table 5-19 Mean roughness parameters with 95%CL of patella specimen before and after the test over 3MC with P value (*p<0.05 significant) 166

Table 5-20 Wear depth for patella specimens over 3MC 166

Table 5-21 Absolute value of tilt in every station for 9-12MC wear test with 95% confidence limit. 169

Table 5-22 Wear rate for low ML rotation with constrained ML displacement by specimen number over 3MC 171

Table 5-23 Wear rate for low ML rotation with constrained ML displacement by station number over 3MC 172

Table 5-24 Wear rate for low ML rotation with constrained ML displacement using MicroCT over 3MC 173

Table 5-25 Progression of wear scar (in mm^2) and % of articulating surface area after 9MC and 12MC in wear test 175

Table 5-26 Progression of wear scar (in mm^2) in superior, inferior, lateral and medial quadrant during 3MC in wear test 175

Table5-27 Mean roughness parameters with 95%CL of femoral component before and after the test over 3MC with P value (*p<0.05 significant) 177

Table 5-28 Mean roughness parameters with 95%CL of patella specimen before and after the test over 3MC with P value (*p<0.05 significant) 178

Table 5-29 Wear depth for patella specimens over 3MC. 178

Table 5-30 Wear depth for patella specimens over 12MC using CMM and Talysurf analysis 182

Table 5-31Wear grading of round dome test specimens using Hood *et al.*1983 ... 185

Table 6-1 Lot number for femoral and patella specimens 194

Table 6-2 Absolute value of tilt in every station with 95% confidence limit 198

Table 6-3 Wear rate for each specimen over 3 million cycles 200

Table 6-4 Wear rate for each stations over 3 million cycles 201

Table 6-5 Mean wear depth with 95% CL of worn specimens (1, 2, 5 and 6) and creep specimen (7) using CMM analysis. 207

Table 6-6 Mean wear rate with 95% CL of worn specimens (1, 2, 5 and 6) and creep specimen (7) using CMM analysis from 3 million cycles. Specimen 3 and 8 were excluded as the specimens were run less than 2 million cycles. 208

Table 6-7 Progression of wear scar (in mm^2) and % of articulating surface area during 3MC in wear and creep test specimens 211

Table 6-8 Progression of wear scar (in mm^2) in superior, inferior, lateral and medial quadrant during 3MC in wear test 212

Table 6-9 Grading of wear damage in oval dome test specimen 214

Table 6-10 Roughness parameters for the femoral components before and after the wear simulation test. Significant difference between the test interval with *p<0.05 216

Table 6-11 Roughness parameters for the patella specimen before and after the wear test. Significant difference between the test interval with *p<0.05 217

Table 6-12 Deformation of wear and creep test specimens after (3MC)..... 219

Table 7-1 Clinical data of patella retrievals (Retrieval database, University of Leeds) 225

Table 7-2 Volume loss of retrievals determined using CMM 229

Table 7-3 Wear rate (mm^3/year) of retrievals determined using CMM..... 229

Table 7-4 Frequency of patella damage with respect to the 8 retrievals dataset analysed 232

Table 7-5 Grading of oval patella based on Hood's grading (1983) 233

Table 7-6 Wear scar area and distribution of wear scar over the four quadrants 235

Table7- 7 Table of wear area in superior, inferior, lateral and medial quadrants of retrievals and *in vitro* specimens with p test between the two. 236

Table 7-8 Table of average, skew, peak and valley roughness parameters. 237

Table7-9: Table of average, skew, peak and valley roughness parameters of specimen (A, B, C and H) in mean±95% confidence limit and significance p test. 238

Table 7-10 Frequency of patella damage with respect to the 2 retrievals dataset and *in vitro* test specimens analysed..... 240

Table 7-11 Grading of round patella based on Hood's grading (1983) 241

Table 7-12 Wear scar area and distribution of wear scar over the four quadrants 242

Table 7-13 Table of average, skew, peak and valley roughness parameters. 243

Nomenclature

ANOVA	Analysis of variance
AP	Anterior Posterior
AR	Aspect ratio
BW	Body weight
CL	Confidence limit
CMM	Co-ordinate measuring machine
COR	centre of rotation
FE	Flexion Extension
IPL	Image processing language
ISO	International Organisation of standardization
ML	Medial Lateral
MicroCT	Microscopic computed tomography
MC	Million cycles
NHS	National Health Service
PE	Polyethylene
PFJ	Patella femoral joint
PMO	Principal molecular orientation
PTFE	Polytetrafluoroethylene
Pycnometer	Pycnomatic ATC
SD	Standard deviation
TKA	Total knee arthroplasty
TKR	Total knee replacement
UHMWPE	Ultra high molecular weight polyethylene

Chapter 1: Introduction and Background

1.1 Introduction

The history of knee stabilising began as early as 2730-2625 BC, when human remains were found with a device used to stabilise the knee (Seymour 2002). The work in biotribology started in year 175 AD by a physician named Galen. He described every joint covered with cartilage with greasy oil glutinous fluid on top giving easy movement and resistant to wear (May, 1968). This was the first documented literature found to explain the synovial joints.

Out of all the synovial joints present, the knee joint is considered as the major weight bearing joint commonly vulnerable to injuries and osteoarthritis. The injury leads to malfunction in daily normal life activities. The need to regain the normal function becomes essential. This has been obtained using total knee replacement (TKR) since the 1970's. The major reason behind the revisions of TKR is due to problems regarding the patella femoral joint (Berger *et al.* 1998; Fehring *et al.* 2000; Sharkey *et al.* 2002; Amis *et al.* 2005; Stiehl *et al.* 2005; Berti *et al.* 2006; Ma *et al.* 2007; Kessler *et al.* 2008; Anglin *et al.* 2009). The use of patella replacement during total knee arthroplasty (TKA) varies from country to country with popularity in USA (90%), Denmark (76%), Australia (43%), England and Wales (33%), Sweden (14%) and Norway (11%) (Clements *et al.* 2010; Robertsson *et al.* 2010; National Joint Registry for England and Wales 2009, 2010).

This introduction begins with the anatomy of the natural knee joint, followed by the need for replacement. Section four details the reference plane of tibia femoral and patella femoral joints. Kinematics of tibia femoral joint is discussed briefly in section five. Kinematics and kinetics of patella-femoral joint are explained in section six. Section seven and eight explain the polyethylene bearing material used in joint replacement and the wear mechanisms involved. Section nine highlights investigations of wear simulations in patella femoral joint. Retrieval analysis is detailed in section ten. Section eleven illustrates the progress in computer simulation of knee joint and the lack of research in patella femoral joint.

The rationale, aim, hypothesis and objectives of the project follow the literature review.

The purpose of project was to fill the gaps in artificial patella femoral joint research answering whether patella wear is important to quantify.

1.2 Anatomy of Knee Joint

The knee joint (Figure 1-1) is a form of hinge joint with condyles of the femur on top, tibial plateau bottom and the patella acting on the front. The articulating surfaces of the knee joint are covered with articular cartilage. Weight bearing and locomotion are the foremost function of the knee joint. These are facilitated through the connection with ligaments and tendons (Gray 1958; Goldblatt and Richmond 2003).

1.2.1 Tibia Femoral Joint

The joint formed by two largest bones, tibia and femur, of the body is known as tibia femoral joint (TFJ). The superior part of the joint, the femur, consists of condyles, medial and lateral. The condyles are curved in anterior posterior and medial lateral direction. The lateral femoral condyle can translate freely in anterior posterior and rotate in the transverse axis towards extension (Martelli and Pinskerova 2002). The curvature of lateral femoral condyle helps patella support against dislocation. The spherical shape of the medial femoral condyle helps the patella to translate within limits in the anterior posterior direction and to rotate in all 3 axes. The tibia is flat in the lateral plane and slightly concave in the medial plane to conform to femoral curvature. The surface of the tibial plateau slopes inferiorly and connects to the meniscus surface. In between the medial and lateral tibial plateau, an indentation of inverted cone (spline) is present to produce a femoral pivot to the tibial plateau during rotation about the transverse plane.

The tibia and femur are connected to each other using anterior and posterior cruciate ligaments, collateral ligaments and separated by fibro cartilage menisci as shown below in Figure 1-1.

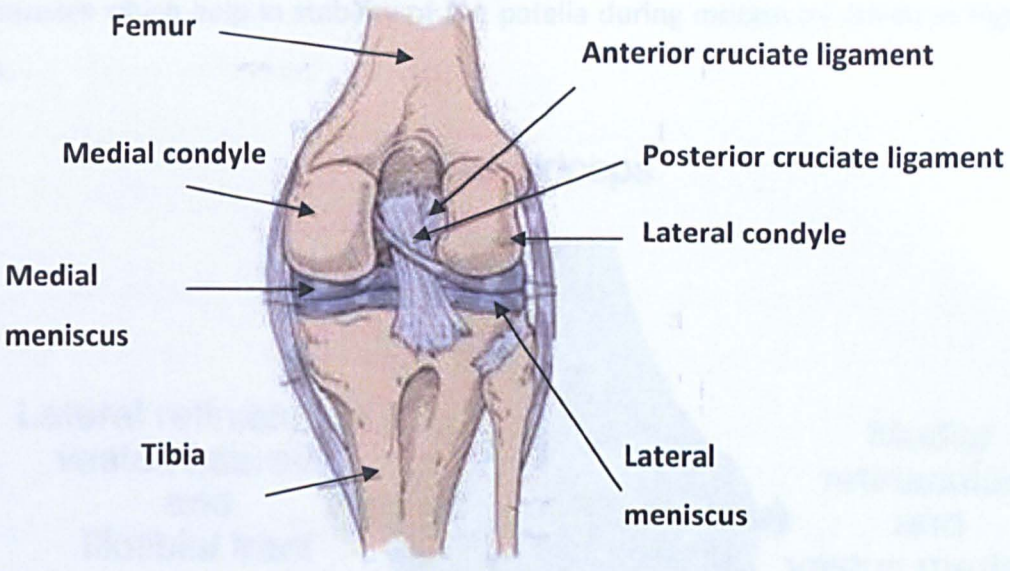

Figure 1-1 Figure illustrates tibia femoral joint with tibia, femur, condyles menisci and ligaments (Brunkner and Khan 2005).

1.2.2 Patella femoral Joint

The part of the knee joint that describes articulation between the patella and the femur is known as the patella femoral joint (PFJ) (Figure 1-2). The PFJ is subjected to high contact stress (6-8MPa), greater than the tibia femoral joint during flexion and extension of the knee. This is because the patella acts as a fulcrum in the knee joint and is subjected to higher compressive stress (Amis and Farahmand 1996).

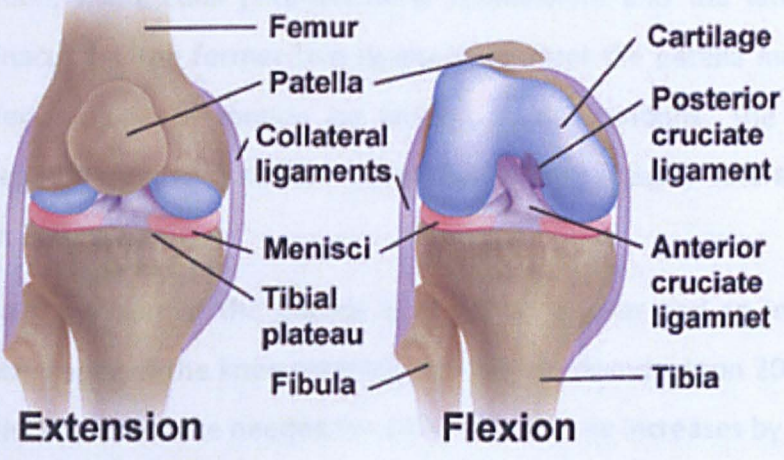

Figure 1-2 The Patella-femoral joint (Image taken from http://www.yoursurgery.com/ProcedureDetails.cfm?BR=5&Proc=30).

The patella is a triangular sesamoid bone surrounded by ligaments and muscles which help in stability of the patella during motion as shown in Figure 1-3.

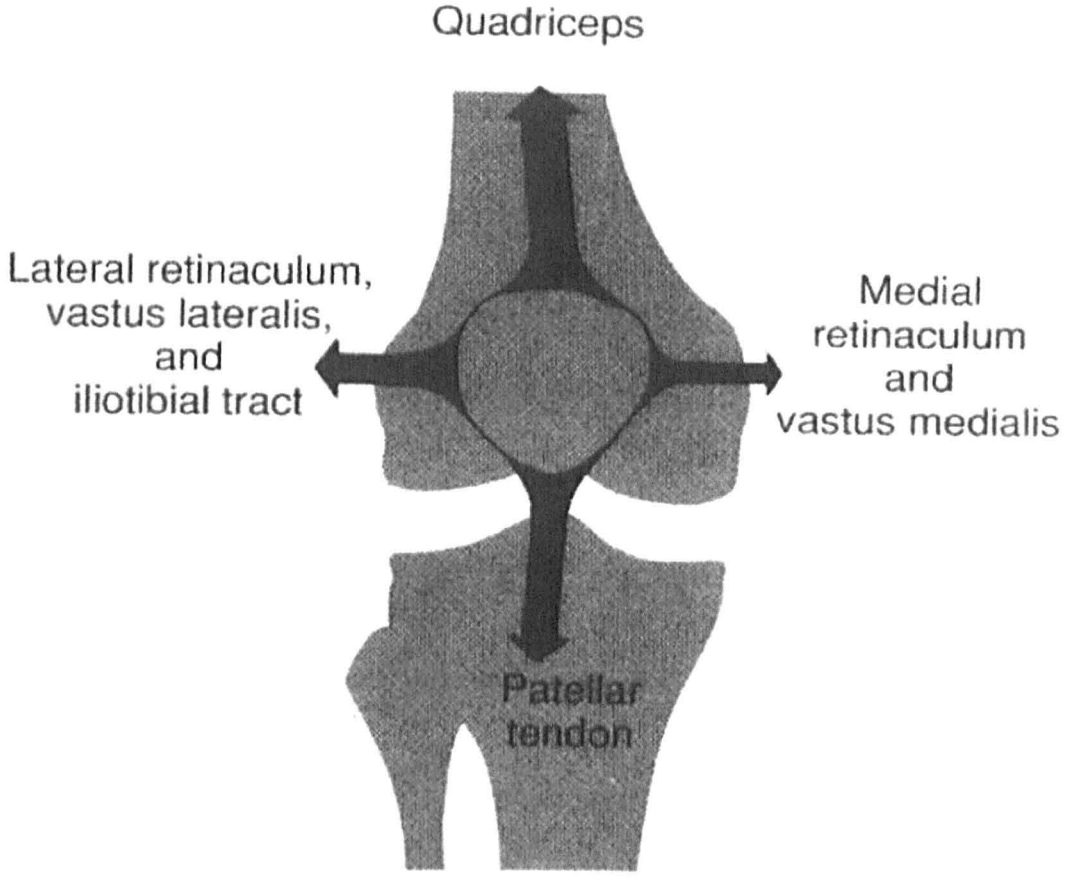

Figure 1-3 The Patellofemoral ligaments (Fulkerson, 1997).

The patella is acted on primarily by four ligaments the quadriceps tendon, the patellar tendon, the medial patellofemoral retinaculum and the lateral patella femoral retinaculum. The former two ligaments control the patella movement in superior inferior plane of motion by tension in the tendons. The latter two ligaments resist excessive patellar movement in the medial lateral direction (Hendrickson 2002).

The main function of the patella is to act as a lever and to increase the mechanical efficiency of the knee extensor mechanism (Hendrickson 2002). Kaufer (1979) showed that the force needed for extension of knee increases by 13% at 90° flexion and 31% at 0° knee flexion when the patella is absent. The other functions include providing anterior protection to the knee joint, and preventing wear of

quadriceps ligaments (Hendrickson 2002). The articular surface present in the PFJ is capable of bearing high compressive loads by presenting a low friction surface in the healthy knee (Garth 2001).

1.3 Need for Replacements

Approximately 9 million people in the UK are affected by osteoarthritis (Arthritis Research Campaign OA, 2008). Currently non surgical therapy for pain in the knee joint includes exercising and stretching. Surgical intervention consists of anterior advancement, debridement, chondrectomy, pallectomy, facetectomy and TKA (Cannon *et al.* 2008). Heatley *et al.* (1986) and Karlsson *et al.* (1992) on investigation of anterior advancement (removal of anterior cruciate ligament) as treatment of osteoarthritis found that the success rate is low (38%) with 6 - 10 years of follow up. As an early detection of osteoarthritis, debridement with lateral release can be a procedure to alleviate pain in cases of lateral tilt and excess load in lateral side. However for more complex cases, the process does not provide reduction of pain (Saleh *et al.* 2005*)*. Defective cartilages are removed in chondrectomy. This is often assisted with drilling in the bone for new cartilage growth. This method is often not suitable for patients over 30 years which is limiting age for reconstruction of bones and cartilage (Childers and Ellwood 1979; Schonholtz 1989). Removal of the patella due to chronic pain in the knee is known as Patellectomy. Patellectomy has disadvantage of weakening the knee joint and needs more time for recovery as reasonable amount of time is needed to achieve the strength for daily activities (Fulkerson 2005). This makes it less useful as a treatment for osteoarthritis. Facetectomy is a temporary procedure to relieve pain by removal of thick bones affected with osteoarthritis. However, the osteoarthritis may reappear after about 8 years of follow up (Yercan *et al.* 2005).

Knee replacement is considered the gold standard after all the other surgical intervention to cure knee disability and pain. Although arthritis predominantly affects older patients, the age of sufferers requiring intervention is decreasing (Crowninshield, et al. 2006) as patients become more and more active. The need for better replacements is increasing day by day.

Three types of replacement are most common. They are total knee replacement (TKR) with or without patella, patella femoral replacement (PFR) and uni-compartmental knee replacement. Replacement of the femur and tibial surface of the knee joint with metal and plastics with and without patella is known as total knee replacement or total knee arthroplasty (TKA). Patella femoral replacement involves replacement of part of the femur and back of the patella. It is also called patella femoral arthroplasty, PFA. The difference between PFR and TKR is that the unworn cartilage is left intact with the rest of the joint. The third type of replacement is the uni-compartmental knee replacement. In this type of replacement only one side of the arthritic joint is replaced. It is also called uni-compartmental arthroplasty or partial knee replacement.

1.3.1 Patella Replacement in Total Knee Arthroplasty

Patella femoral mechanisms remain one of the major problems in total knee revision surgery (Berger *et al.* 1998; Fehring *et al.* 2000; Sharkey *et al.* 2002; Amis *et al.* 2005; Stiehl *et al.* 2005; Berti *et al.* 2006; Ma *et al.* 2007; Kessler *et al.* 2008; Anglin *et al.* 2009). Despite the known problem the use of patella replacement is popular among only a few number of countries with USA (90%) leading followed by Denmark (76%), Australia (43%), England and Wales (33%), Sweden (14%) and Norway (11%) (Robertsson *et al.* 2010, Clements *et al.* 2010 and National Joint Registry for England and Wales 2009, 2010). Damage of the patella button can also lead to revision in TKA. Many studies have reported the failure of patella button, mostly the metal-backed designs (Lombardi *et al.* 1988; Piraino *et al.* 1990; Collier *et al.* 1991; Huang *et al.* 2005). The metal backed patella induces additional contact stress and failures on the edges were reported. All-polyethylene patellar buttons have also been considered. However, wear and loosening were found to be significantly high (Wright et al. 1986; Collier *et al.* 1991; Schwartz *et al.* 2002). The question remains whether or not to resurface the patella.

1.3.2 Patella Femoral Arthroplasty (PFA)

Research has shown that PFJ osteoarthritis is more common than TFJ and a cause of knee disability (McAlindon et al. 1992; Hunter et al. 2003; Szebenyi et al. 2006; Kornaat et al. 2006; Duncan et al. 2009). PFA is the largest popular intervention for patella femoral joint osteoarthritis. For investigating the long term results of patella femoral arthroplasty, Kooijman *et al.* (2003) studied the outcome of 51 patients. Out of 51 patients, 7 cases (15.5%) needed PFA revision. The reason for PFA revision was patellar loosening, malposition of patella and maltracking. 3 patients had patellectomy. 12 cases needed TKA surgery after PFA because of presence of osteoarthritis in tibia. Most of the revisions were caused through neglecting tibial osteoarthritis during PFA (Kooijman *et al.* 2003; Nicol *et al.* 2006; Farr and Barrett 2008). Mean survival time of the PFA was 19.5 +/- 0.45 years. One patient among 51 was satisfied with the outcome of PFA (Kooijman *et al.* 2003). PFA has an advantage over total knee arthroplasty as the original menisci, collateral ligaments are left unharmed. This feature makes it suitable for youngsters and more active patients (Cannon *et al.* 2008). PFA success rate are lower than that of total knee replacement. Considering the lack of exposure and success rate of PFA (44% - 90%) in 17 years follow up, total knee arthroplasty with PFA is preferred by majority of the surgeons for achieving consistent results (Kooijman *et al.* 2003; NJR 2010).

1.3.3 Success and Revision of Knee and Patella Joint Replacement

The common causes of revision in knee patella replacement depend on factors of failure. Due to an increase in demand the failures are studied and reported in this section (SJR.se 2007; NJR.uk 2003)

1. Aseptic loosening – Loosening is considered as a factor leading to revision surgery. The articulation of the polyethylene insert with the metal components generates small particles of polyethylene leading to osteolysis and consequently loosening.

2. Infection – Infection was prevalent in patients with rheumatoid arthritis, ulcers in the skin, patients with previous history of knee operations, recurrent urinary tract infections, and oral use of steroids (Wilson *et al.* 1990).

3. Fracture – Fracture in the metal backed patella component was investigated by Lombardi *et al.* (1988). Fracture of patella includes separation of polyethylene component from metal base and fracture of polyethylene due to excessive wear.

4. Instability – Instability created due to improper balance of soft tissue may lead to revision surgery.

5. Maltracking - Subluxation in the total knee replacement leads to increased wear and postoperative complaints like pain in the knee.

6. Overstuffing – Overstuffing in knee replacement leads to increase in contact forces, which may lead to increase in wear. An increase in thickness of 10% results in 7.5% increase in joint forces at 95 degrees of knee flexion (Mountney *et al.* 2008). This causes an increase in wear leading to knee replacement.

Studies of misalignment have been reported after total knee arthroplasty which results in increased patella femoral contact force during flexion by 20% (Hollinghurst *et al.* 2007; Miller *et al.* 1998). The kinematics of the knee joint must be considered to understand the cause of failures.

1.4 Knee Joint Reference Plane

Coordinate system

As discussed earlier in section 1.2, the tibia femoral joint (TFJ) consists of tibia and femur collectively known as TFJ. The movement in TFJ is due to rolling and sliding of femoral condyles over tibial plateau. The basic anatomical figure of a knee joint (Whittle, 2001) is described in Figure 1-4, the X-axis is perpendicular to the sagittal plane, Y-axis is perpendicular to the transverse plane and the Z-axis is perpendicular to the frontal plane.

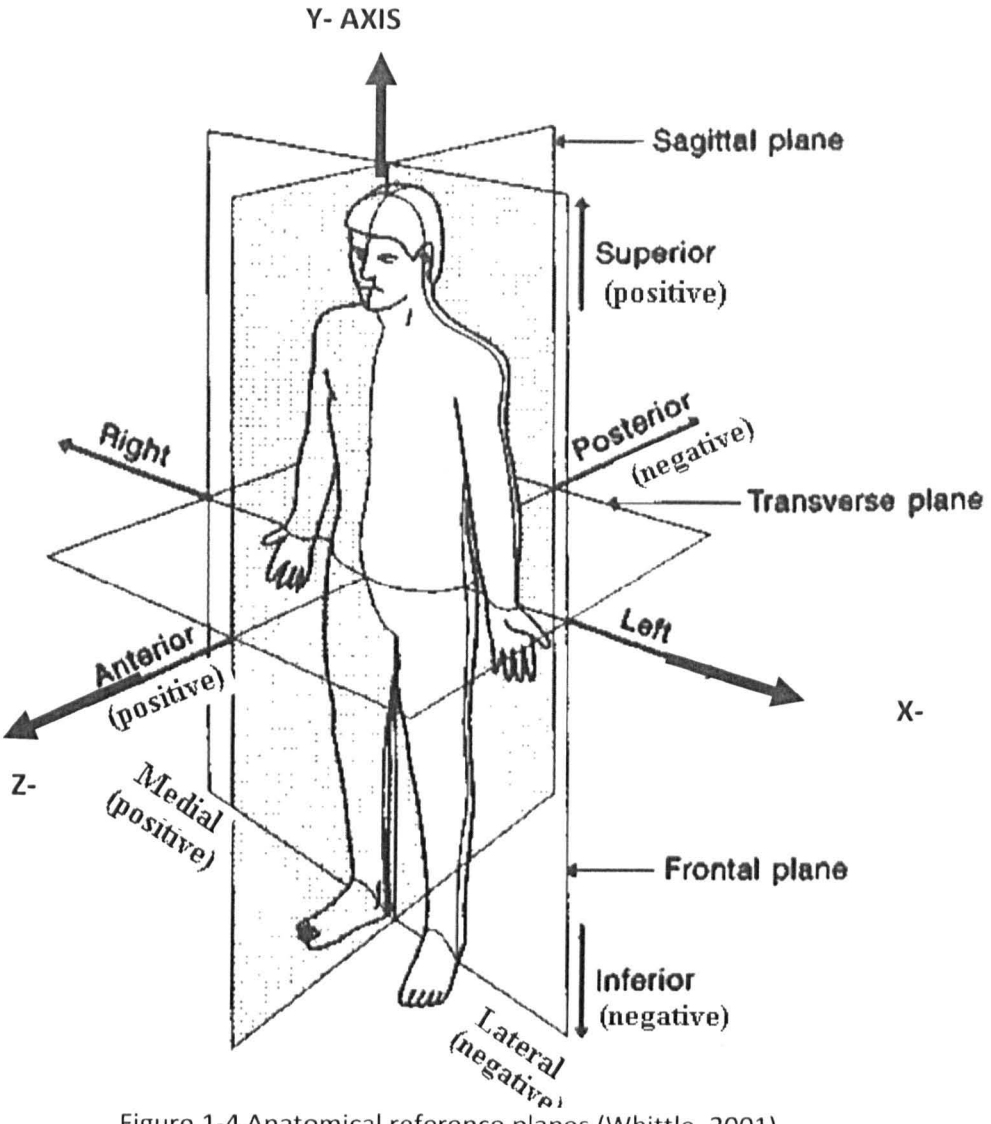

Figure 1-4 Anatomical reference planes (Whittle, 2001)

For this study the polarity of the displacements and rotations were based on Ellison and co-authors (2008). About X axis, the rotation of tibia is known as knee flexion, with extension as positive. The motion of tibia along the X-axis is known as medial-lateral shift with medial displacement as positive. The rotation of tibia about Y-axis are internal-external rotations with internal as positive. Tibial rotation about Z-axis is termed as abduction adduction rotation with adduction being positive. The translation motion of the tibia along Z-axis is proximal-distal translation, proximal translation being positive. The rotations of the tibia are systematically shown in Figure 1-5.

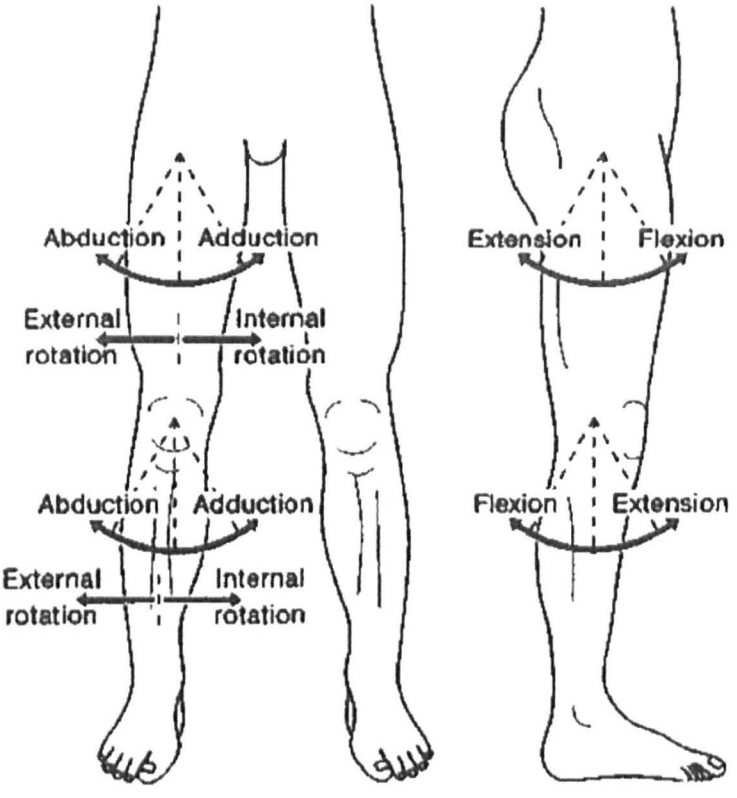

Figure 1-5 Rotational movements of right tibia femoral joint (Ellison *et al.* 2007; Whittle, 2001).

Figure 1-6 describes the different rotations of the patella in the knee joint defined with polarity from Ellison (2007). About X axis, the rotation of the patella is known as patella flexion, with flexion as positive. The motion of the patella along the X-axis is known as medial lateral displacement with medial displacement as positive. Motion of the patella about the Y-axis is termed as medial lateral tilt with medial tilt as positive. Motion along the Y-axis is termed as inferior superior translation with superior as positive. The patellar rotation about Z-axis is termed as medial lateral or abduction adduction rotation, with medial and adduction being positive with apex of patella moving towards medial direction. The translation motion of the patella along Z-axis is anterior posterior translation, anterior translation being positive. The movements of the patella are systematically shown in Figure 1-7.

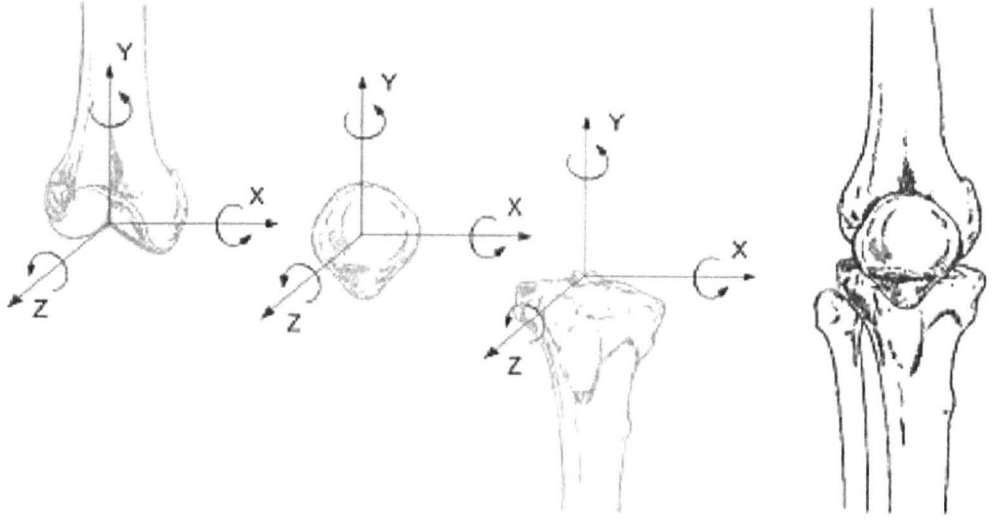

Figure 1-6 Rotations of right knee joint with positive polarity (Ellison et al. 2007).

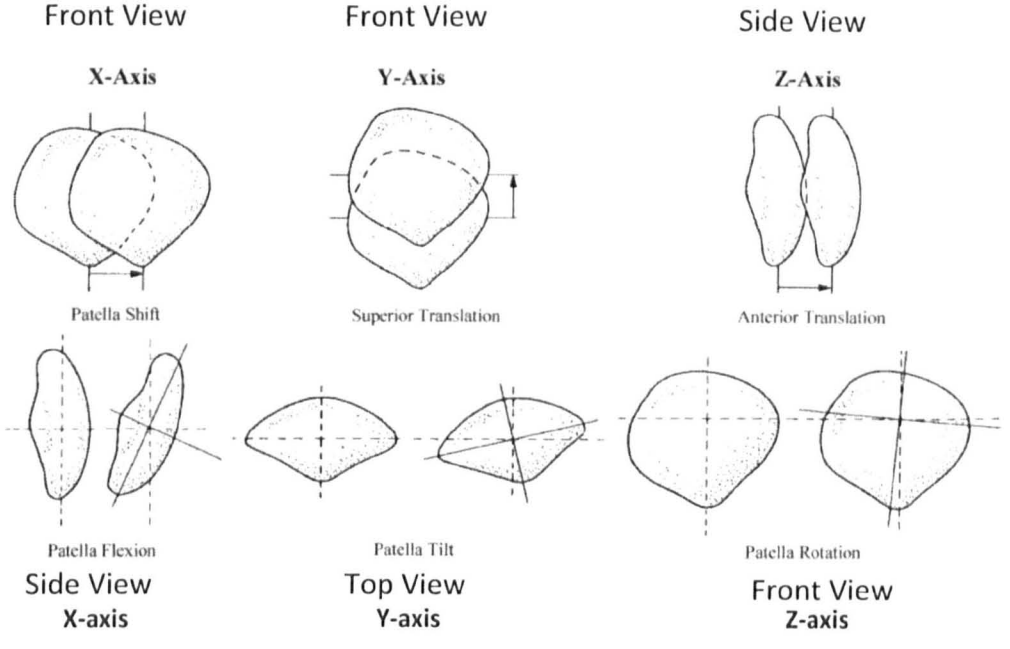

Figure 1-7 Patellar motion representation (Ellison et al. 2007).

1.5 TFJ Flexion Extension Rotation and Kinetics

The flexion extension motion of the tibia femoral joint was obtained from five subjects by Lafortune *et al.* (1992) for a walking cycle. Steinmann pins were inserted into the right femur of the healthy subjects. The position of the pins was recorded through radiography. Flexion extension was an important parameter in determining the kinematics of the PFJ. The pattern is shown in Figure 1-8. The

pattern follows a biphasic nature with small flexion followed by extension in stance phase and larger flexion in swing phase. After heel strike, the knee flexes to 20 ° in approximately 190 ms for all five subjects. Following, the flexion the knee follows extension and returns to 1.3 ° short of full extension in approximately 300 ms, before the end of stance phase. Again, the knee starts to flex to 35 ° by toe off and follows the trend till maximum flexion 60 ° was attained. In the next 30 ms, the knee extends and returns back to full extension in the swing phase to start the new heel strike-toe off cycle. The position of the pins was difficult to analyse as the pictures were taken 3 dimensionally. Hence the accuracy of the method is questionable.

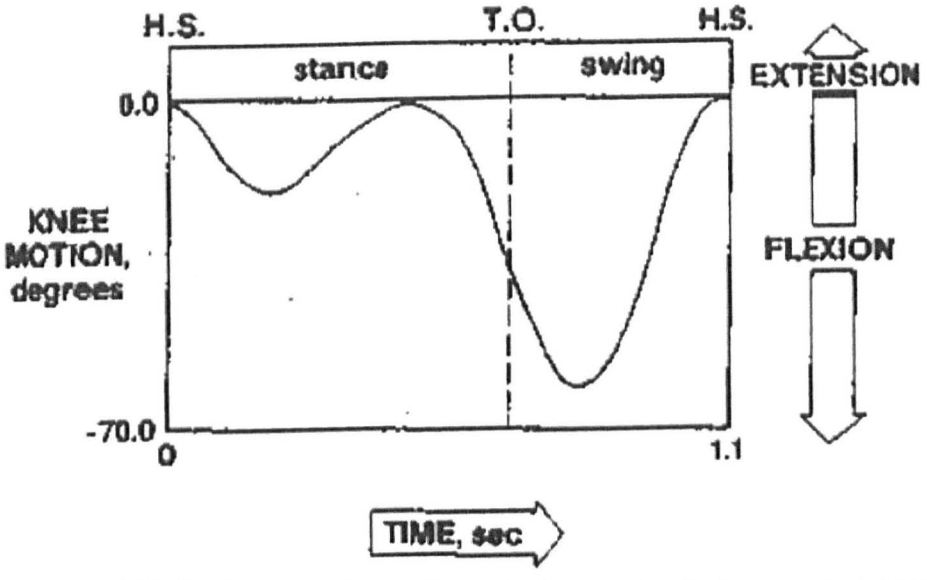

Figure 1-8 TFJ flexion extension patterns during walking (Lafortune *et al.* 1992).

The tibia femoral joint is subjected to a force of 3 BW during walking to 8 BW during downhill walking (Mow and Huiskes 2005).

1.6 PFJ Kinematics and Kinetics.

Patellar pain syndrome is often associated with the disorientation of the patella from the normal configuration. Many authors have tried to outline the complex motion of the patella and the forces acting during varied activity. The

following sections outline the previous investigations on patellar motion and the various forces acting during varied static and dynamic activities.

1.6.1 PFJ Kinematics of Normal Knee during Gait

Research on patellofemoral joint kinematics during gait cycle has received not much attention from researchers. As the surface area of the patella is small in the saggital plane, difficulties in measurement are the main reason behind insufficient research in the gait cycle patellar kinematics *in vivo*. The investigation by Lafortune and Cavanagh (1987) and Abbas *et al.* (2011) are highlighted in this section.

The test by Lafortune and Cavanagh (1987) was conducted by fixing Steinmann pins in the anaesthetic legs of five patients. The movement of the pins were observed from four high speed cameras operating at 100 frames per second. Due to problems of fixation of the pins in the patella, two studies of subject were removed from the investigations. X-ray recording along with camera recording was done to get a better preview of the patellar kinematics. The accuracy of the camera recording was 0.5 mm and that of X-ray was 0.4 mm. Only three specimens were analysed. The accuracy of the kinematics and radiographs cannot be relied upon.

The gait cycle is shown in Figure 1-9. TFJ flexion and extension serve as the basis reference cycle for the gait study. The cycle starts with heel strike (HS) to toe off (TO), followed by swing motion from TO to HS. Graph B, C and D show flexion extension, adduction abduction (internal external) rotation and medial lateral tilt of the patella respectively. Graph F, G and H show lateral-medial, anterior-posterior and superior-inferior translation of the patella respectively.

The results obtained for flexion extension and internal external rotation are consistent in all three subjects. The curve of flexion extension of the patella is similar to the TFJ curve. However, the patellar curve is offset in magnitude with reference to TFJ by -20°. This is due to the resistance offered by the quadriceps tendon to the pull by the patellar tendon. From the beginning of HS, the patella flexes to neutral position at 20° of TFJ flexion. The patella extends to 12.5° at the later stage of stance before moving for a maximum flexion of 28.1° during swing phase just after TO. Following this the patella extends to the next HS.

In the case of internal external rotation, there are two peaks obtained in between consecutive HS. The first peak of 2° internal rotation is obtained at stance phase when TFJ reaches the maximum positive flexion. The second peak of the patella is external rotation of 7.2° shortly after TO, when TFJ reaches maximum flexion in swing phase. After the second peak, the patella reverses and reaches HS position marking the end of the gait cycle.

During the stance stage, two subjects showed consistency in results for patella tilt. At the beginning of the TFJ flexion, the patella has medial tilt followed by lateral tilt of 5°. Just during TO, there is a secondary patella tilt of 4° medially. In case of third subject, instead of medial tilt, there was a lateral tilt of 12.5° till maximum TFJ flexion and the curve rapidly returned to the next HS position.

The patterns of anterior posterior and superior inferior translations of the patella were similar to the flexion extension pattern of TFJ. There were two differences in the curves obtained. Firstly the posterior translation occurred before HS and was having less magnitude in stance stage. Secondly, there was a superior movement in the stance phase after HS. An Average movement of 21mm for anterior posterior and 45mm for superior inferior translation was obtained. In the case of medial lateral displacement, increment in lateral displacement (8mm) from heel strike to maximum flexion in swing phase, followed by medial displacement after the knee extension.

As only three specimens were considered for this investigation, this experiment cannot be validated for patient variation. More than three patients are required to get an range of kinematics variation.

The other study (Abbas *et al.* 2011) was performed by placing retro-reflective markers on 16 healthy subjects. The movements were recorded using a 9-infrared camera system (Vicon 612, Oxford). However errors due to the difference in movement of exo-skeletal markers and the bones were not considered in the measurements. Maximum and minimum measurement of ML displacement and tilt were measured at different knee flexion angles during different gait cycle. The trend was not specified for any single gait cycle. The position of 4 markers on the distal, proximal, medial and lateral were used for kinematics measurement. The

measurements were calculated with reference to the centre of the knee in degrees. As the four markers present could move and rotate. Accurate ML displacement and tilt could not be measured.

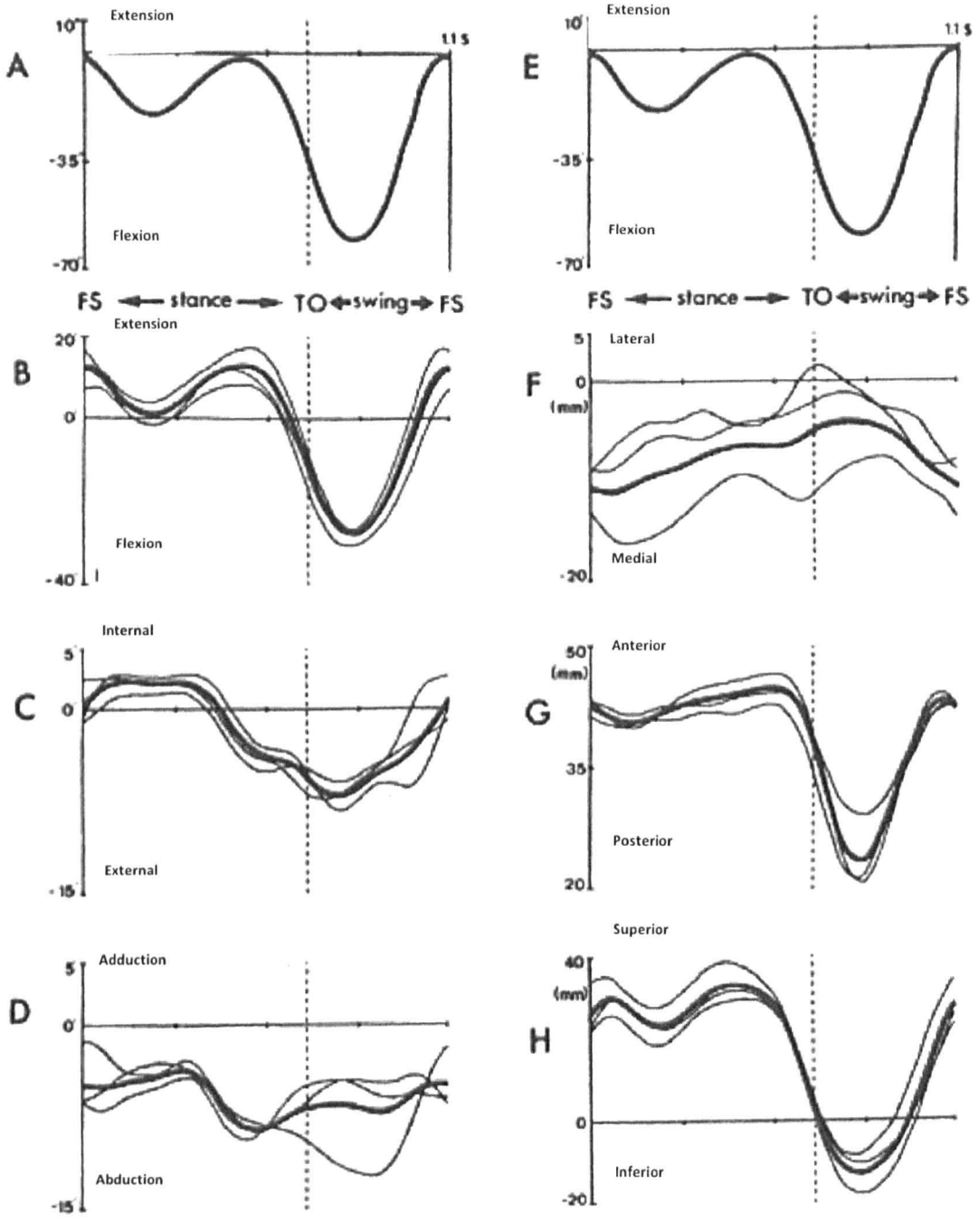

Figure 1-9 Translation and rotation of patellar tracking during normal gait cycle. A, E show the tibia femoral flexion during gait for comparison. B, C and D show the patella flexion, rotation and tilt respectively. F, G and H show the patella shift, anterior translation and superior translation respectively (Lafortune and Cavanagh 1987).

1.6.2 PFJ Kinematics in Total Knee Replacement

This section deals with authors investigating patellar tracking in artificial knee replacement and report the variation of patella with knee flexion angle. The authors who investigated patellar tracking in total knee replacement are listed in Table 1-1. The table illustrates the number of specimens, range of flexion, method of capturing data and additional details on loading.

Table 1-1 Experimental data provided by previous investigators in patella tracking.

Authors	Number/ type	Flexion Range(°)	Method	Loading
Chew *et al.* (1997)	9/ Cadaveric	0 to 105	Magnetic tracking system	30N
Komistek *et al.* (2000)	65/ subject	0 to 90	Fluoroscopic video analysis	No data
Belvedere *et al.* (2007)	6/ Cadaveric	0 to 140	Knee navigation system	100N quadriceps force
Barink *et al.* (2007)	15/ Cadaveric	0 to 100	Electromagnetic tracking system	27 X 3 N quadriceps force and 50N compression
Ostermeier *et al. (2005)*	5/ Subject	0 to 120	Three dimensional motion analysis	2000N
Ahmed *et al.* (1999)	32/ Cadaveric	0 to 120	Radiography	28 X 4 N

Fresh cadaveric knees were used for kinematics measurement in most investigations (Chew *et al.* 1997; Belvedere *et al.* 2007; Barink *et al.* 2007; Ahmed *et al.* 1999). While other investigations used healthy human subjects (Komistek *et al.* 2000; Ostermeier *et al.* 2005).

Medial lateral (ML) tilt

Three authors investigated patellar tilt with knee flexion for different types of total knee replacement. The results are provided in Figure 1-10.

Chew *et al.* (1997) found notable differences between normal and all three replaced knees. There was a large amount of lateral tilt in the three implanted knees compared to the intact knee. At 60° knee flexion, the patella in the intact knee showed 0.44 ° of lateral tilt, whereas the patella in the three implants showed 7.32 °, 5.88 ° and 6.69 ° lateral tilt. The lateral tilt in the press fit condyle (PFC) implant (Johnson and Johnson, New Brunswick, NJ) was less than others due to the presence of a deep femoral groove. This result was supported by the clinical results on PFC (Chew *et al.* 1997). Komistek *et al.* (2000) suggested the abnormality in the results of patellar tilt compared with normal knee was due to an increase in tension of the quadriceps ligaments, flange size of femoral components, malposition of patella, variation in thickness of flanges and variation of friction between the articulating surfaces. The cruciate retaining Scorpio (Allendale, NJ, USA) TKR with patellar resurfacing was used in the investigation by Belvedere *et al.* (2007). The femoral component was set to zero degrees in the frontal plane and 2 degrees in the sagittal plane with respect to the tibial plateau. No internal/external tibial rotation was applied to the femur. Belvedere *et al.* (2007) with investigation on patellar tilt found a large difference in the lateral tilt compared to other implants (Genesis II, NexGen and PFC) in the beginning of knee flexion. The difference was noted because of the presence of a single medial-lateral implant radius designed to control area of contact and avoid lift off. This feature helps in reducing the tilt which can be highlighted in above figure. Neither of the authors investigated the effect of tibial rotation on tilt.

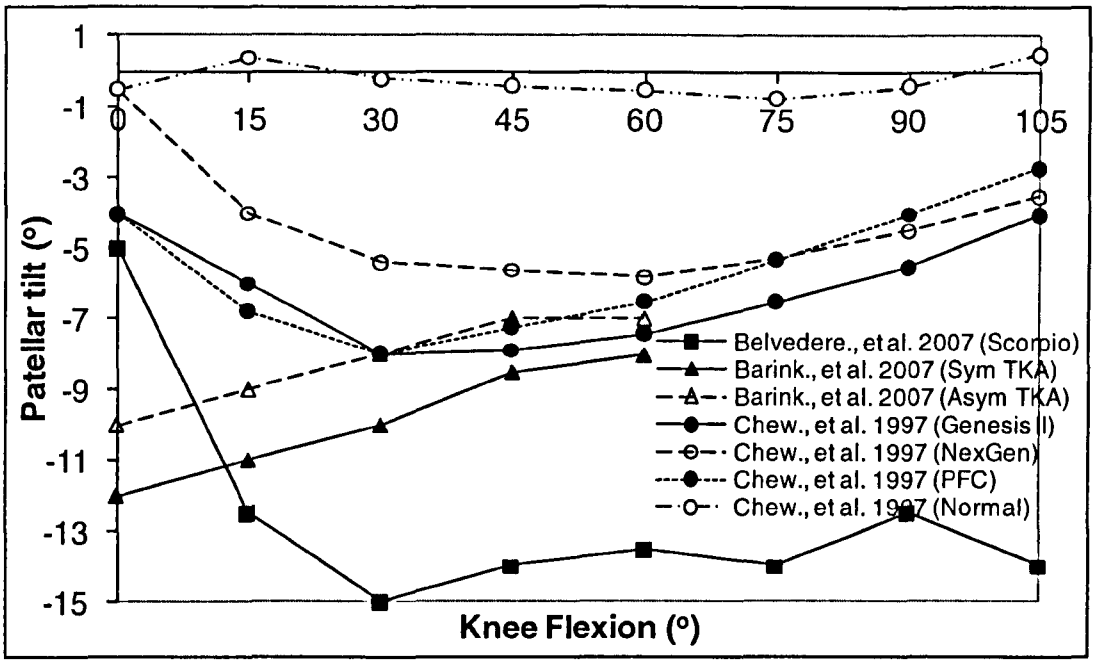

Figure 1-10 Variation of patella tilt versus knee flexion in TKR.

The only author to investigate the effect of tibial rotation on patella tilt for symmetrical and asymmetrical femur trochlea groove in TKR was Barink *et al.* (2007). The results signified that the patella tilted more medially between 20° – 30° of knee flexion. It was also reported that the difference in tilt was due to the addition external tibial rotation of 3° provided. This made the medial condyle elevate in anterior position compared to the lateral condyle causing the patellar tilt medially as compared to the normal knee. All the results presented were different to the anatomical knee data.

ML displacement

The results of three previous authors investigating patellar displacement in the artificial knee joint are shown in Figure 1-11.

Lateral displacement in three samples increased with an increase in knee flexion (Chew *et al.* 1997). The PFC implant displacement pattern was close to the actual knee. Among the three implants investigated by Chew *et al.* (1997), the PFC femur component showed the lowest displacement due to the presence of deeper

a femur grove in comparison to other implants. The groove restricted the movement for PFC knee implant.

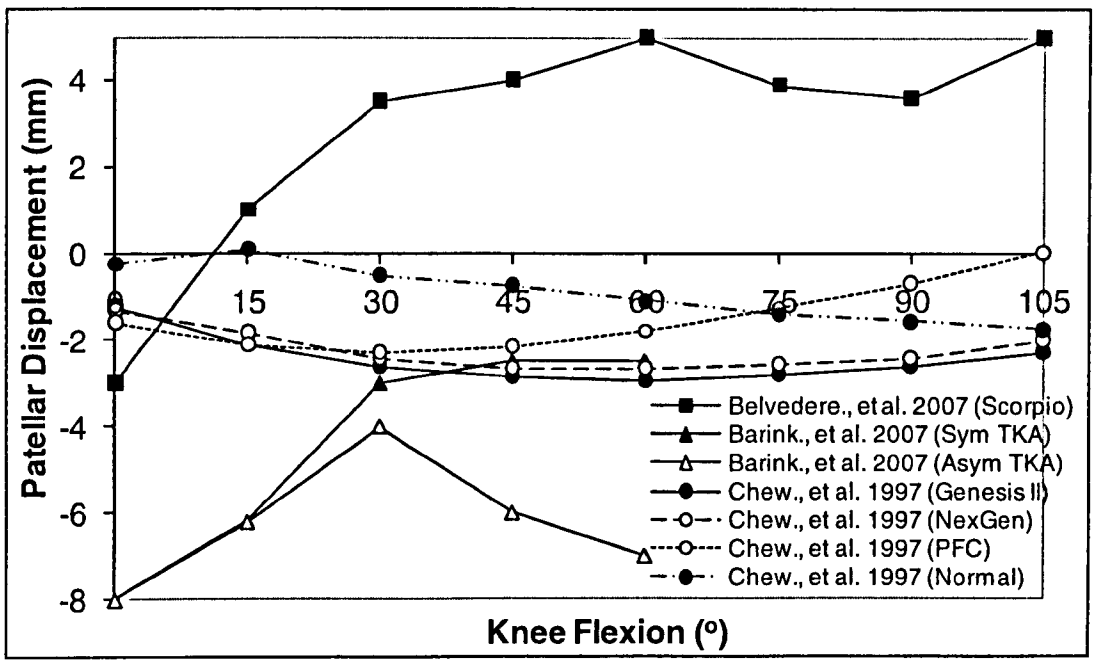

Figure 1-11: Variation of patella displacement versus knee flexion.

Barink *et al.* (2007) and Belvedere *et al.* (2007) showed more medial displacement with an increase in flexion. The results by Barink *et al.* (2007) indicated that both the implants (symmetrical TKA and asymmetrical TKA) examined followed the same trend of increase in medial displacement at the beginning of the knee flexion (5-10°). However, at the later stage (80 - 90 °), the patella displacement was different; the difference was due to the orientation of the groove. Belvedere *et al.* (2007) results were similar to Barink *et al.* (2007) in trend but were higher in magnitude (five times) as compared to Barink *et al.* (2007) till 30° knee flexion.

Anterior posterior (AP) displacement

The results obtained by Ostermeier *et al.* (2005) regarding study of patella in AP movement are illustrated in Figure 1-12.

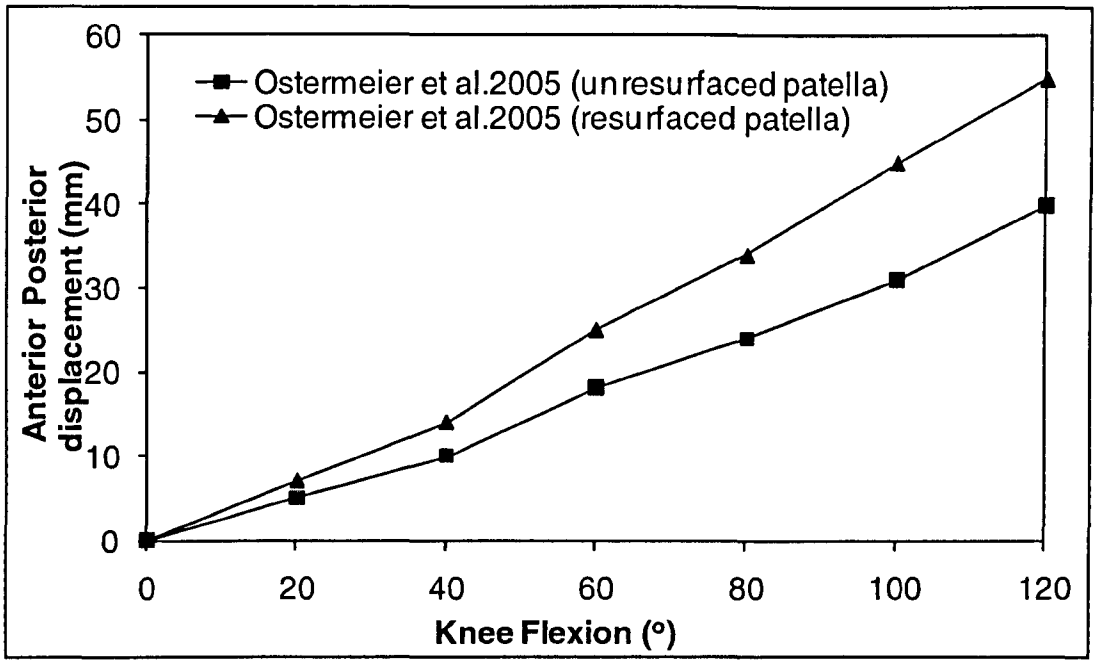

Figure 1-12 Variation of anterior posterior patella displacement versus knee flexion.

The effect of patellar resurfacing on knee flexion was studied in the investigation of AP displacement. The results of both the implants (Interax ISA prosthesis with and without resurfacing) were the same compared to the pattern shown by Ahmed *et al.* (1999). Both the trend of implants (Figure 1-12) showed no significant difference in the AP translation whether the patella was resurfaced or not. However, the resurfaced patella had higher posterior displacement because of the non conformity of the patella to the femoral articulating surface.

Patellar ML rotation

Chew *et al.* (1997) and Belvedere *et al.* (2007) investigated the effect of ML rotation with knee flexion after TKR. The results have been illustrated in Figure 1-13.

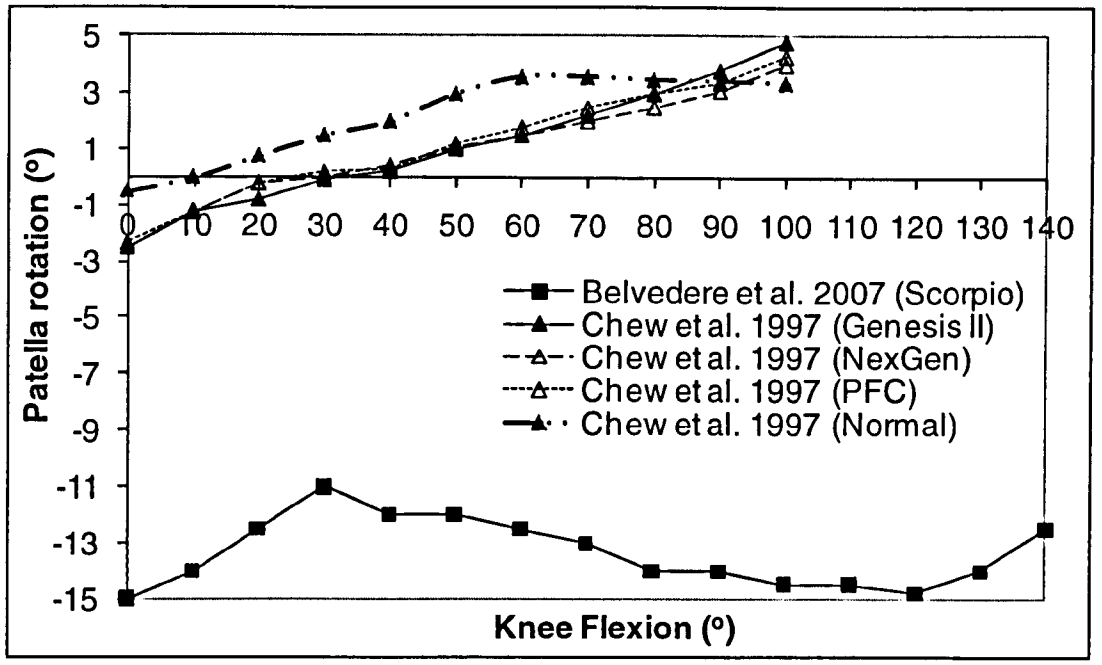

Figure 1-13 Variation of medial lateral patellar rotation with knee flexion.

All three specimens tested by Chew *et al.* (1997) and one specimen by Belvedere *et al.* (2007) followed the same pattern as in the intact knee. The patella rotated medially at the beginning of knee flexion for all the knee implants. The difference between the two investigations was the magnitude of the ML rotation. The ML rotation increased medially with knee flexion (Chew *et al.* 1997). However, the presence of posterised stabilised knee design in tibia of Scorpio (cruciate retaining, Allendale, NJ, USA) led to a higher lateral rotation of the femur (Belvedere *et al.* 2007).

Flexion extension (FE) rotation

Figure 1-14 shows the findings of two authors (Barink *et al.* 2007; Belvedere *et al.* 2007) on patella flexion post TKR. The patella in knees with TKR followed the same trend of flexion before and after surgery. This indicated that sagittal geometry of the normal and TKR implant were the same. The presence of a deeper patellar groove in the Scorpio cruciate retaining implant (Allendale, NJ, USA) compared to symmetrical and asymmetrical implants (Barink *et al.* 2007) balanced the extensor mechanism by easing the tension and providing deeper flexion. The positive patellar flexion in Belvedere *et al.* (2007) showed the difference all through

the flexion cycle in comparison with the investigation by Barink *et al.* (2007) although; the same gradient was obtained in both the investigations.

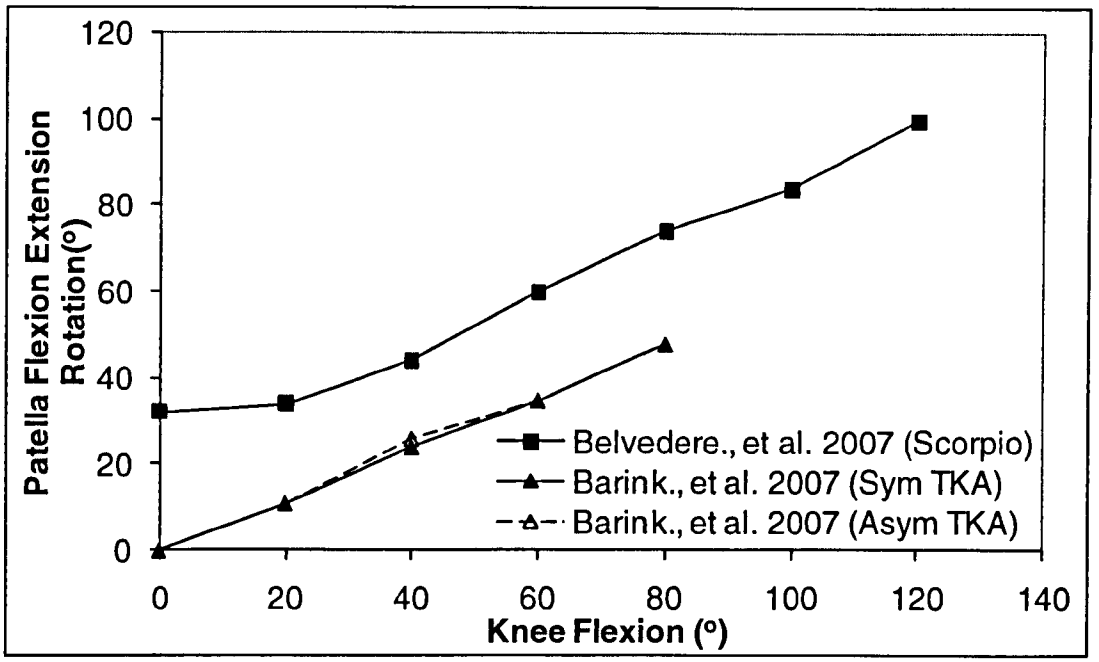

Figure 1-14 Variation of patellar flexion extension rotation about x-axis with knee (tibia femoral) flexion.

Superior inferior patella displacement

The present author could find only one author (Komistek *et al.* 2000) who investigated the superior inferior (SI) displacement of the patella after total knee replacement (Figure 1-15). SI displacement in normal knee has been plotted showing the difference of superior inferior translation between the normal and implanted knee.

The patella in the normal knee was inferior by -8 mm at full extension with respect to other knee replacements designs. The displacement in posterior cruciate retaining (PCR) TKA and posterior stabilized, PS TKA (Johnson and Johnson Orthopedics, Raynham, MA, USA) implanted knees were inferior by -1 and -3.8 mm respectively. The two implants increased superiorly with an increase in knee flexion. The trend of the pattern is exactly same as the normal knee. However, the magnitude was different.

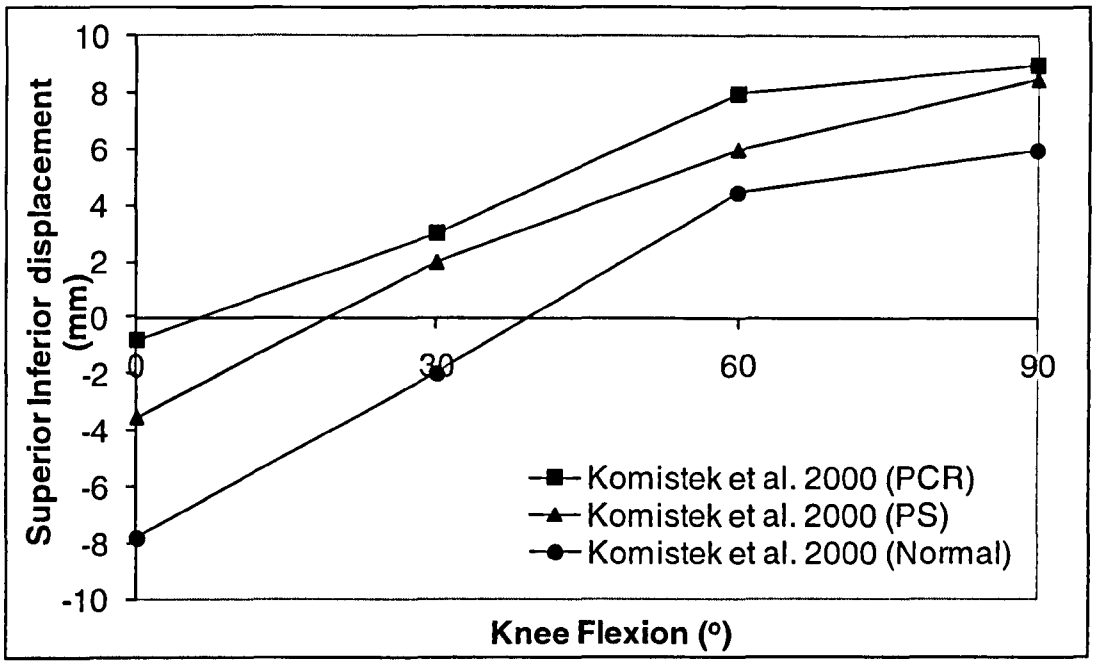

Figure 1-15 Variation of superior inferior displacement with knee flexion.

Summary

The TKR designs are followed the same trend as the normal knee with a few exceptions. The variation of patellar tilt in the artificial knee lies in the range of anatomical knees. Patella shift started with medial shift and changed to lateral shift with knee flexion. There were few exceptions from Chew *et al.* (1997) studies which showed lower displacement due to lower loading. Anterior and superior translation followed the same trend as normal knee. Investigations from Belvedere *et al.* (2007) were different from Chew *et al.* (1997) and Barink *et al.* (2007) in rotation and flexion because of the cruciate retaining Scorpio having +/- 15 ° medial-lateral tilt. The large intra specimen variability due to the variation in patients bone structure caused a large variation in kinematics.

1.6.3 PFJ Kinetics

The forces on the patella range from between 0.2 – 1.4 times body weight during walking (Dixit *et al.* 2007; Reilly *et al.* 1972; Komistek *et al.* 1997). The force increases to 3 body weight during stair climbing, and up to 7 body weight during squatting (Dixit *et al.* 2007; Reilly *et al.* 1972). Komistek *et al.* (1997) performed an

investigation with one healthy female with the help of markers placed on three different bones of the knee and fluoroscopy image was used for calculation of forces. Data was collected through four 60 Hz video cameras and 1000 Hz force platform sampling. The joint reactions were calculated using relative joint motions and ground reactions as input in a mathematical model. Only one healthy subject was considered which could make the investigation unreliable.

Investigations of finding contact stress using plastic micro-indenter transducer (Ahmed *et al.* 1983) and Fuji Pressensor™ film (Haut *et al.* 1989; Huberti *et al.* 1988; Huberti *et al.* 1984) were indirect ways to find contact force by a few investigators. The contact force was then found by integrating the contact stress over the entire area. The complexity in the geometry of the patellar articular surface makes it difficult to integrate over the entire area, which results in errors in the calculation of contact force. Singerman *et al.* (1994; 1999) directly investigated the contact force of 7 fresh frozen cadaver samples by designing a six degree of freedom patellofemoral force transducer. The force transducer was used to measure three forces and the location of patella at the point of action of the forces. Uni-axial force was applied at the hip and ankle to obtain forces in the orthogonal direction. The results of medial lateral shear force are shown in Figure 1-16. The coordinate system defined in Singerman *et al.* (1994; 1999) are opposite to the translation coordinate system adopted in this report.

In the case of medial-lateral component of patellar shear force, there was no significance difference reported by Singerman *et al.* (1999) for either design with or without patellar resurfacing. As the patella in the knee moves in the lateral direction (VanKampen *et al.* 1990; Koh *et al.* 1992; Heegaard *et al.* 1995; Sheehan *et al.* 1999; Tennant *et al.* 2001), the resultant shear force will act in the opposite direction to resist the movement as shown in Figure 1-16. After TKR, both the designs (PFC and PFCΣ) with or without patellar resurfacing tend to have M-L shear forces in lateral direction as the patella moves in medial direction.

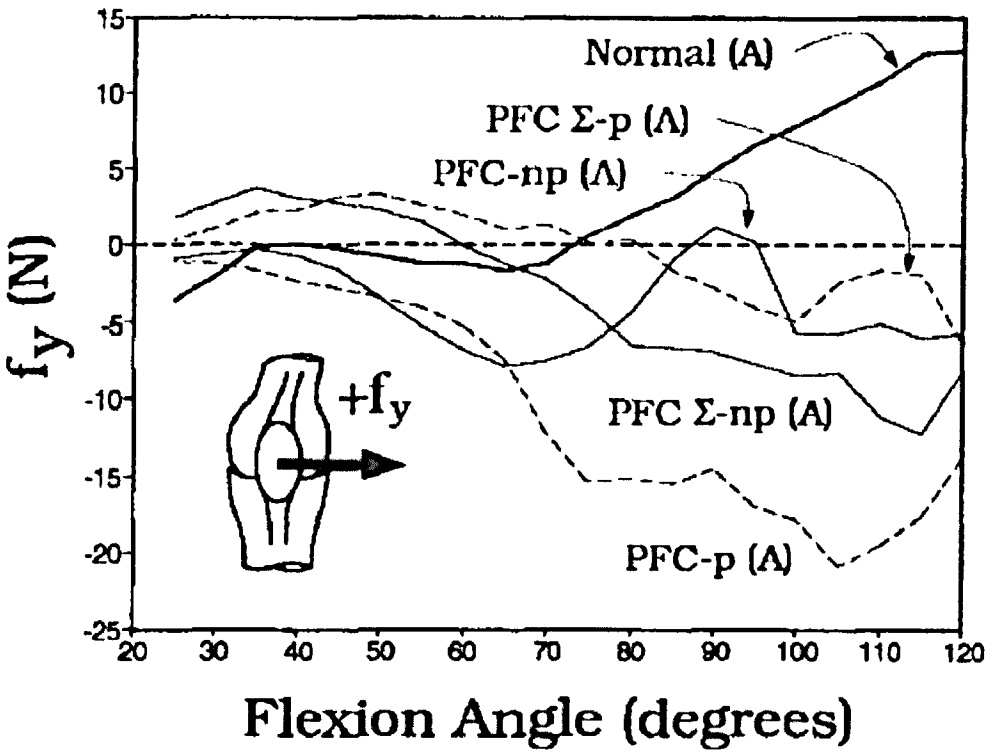

Figure 1-16 Patellar medial-lateral shear force versus knee flexion for normal knee (Normal), PFC with patellar resurfacing (PFC-p), PFC without patellar resurfacing (PFC-np), PFCΣ with patellar resurfacing (PFCΣ-p) and PFCΣ without patellar resurfacing (PFCΣ-np). The positive force refers to force acting lateral direction (Singerman *et al.* 1999).

1.7 Polyethylene Bearing Materials

The optimum bearing material to be used as a medical implant is a material with good biocompatibility with low wear rate, long term mechanical and chemical properties. The various biomaterials in implant history so far since the advent of knee replacement are polytetrafluoroethylene (PTFE), high density polyethylene (HDPE), ultra high molecular weight polyethylene (UHMWPE) and carbon reinforced UHMWPE.

The first polyethylene PTFE hip arthroplasty was implanted by Charnley for its low friction properties and chemical inertness. Radiological observation found that 6-7mm of material was removed due to poor abrasive wear and low creep resistance properties (Semlitsch 1991; Li and Burstein 1994). In 1962 the implant

material PTFE was replaced by UHMWPE by Charnley which had good resistance to wear and low frictional properties at high stress. UHMWPE is a long chain of semi crystalline ethylene molecules; formed by a polymerisation reaction; with a molecular weight of about 400,000. It also has good lubrication properties with synovial fluid helping to reduce wear (Charnley 1979).

Apart from low frictional properties, wear resistance, lubrication properties, UHMWPE is also biocompatible producing low wear debris, chemically stable when not irradiated, is ductile and has a good damping capacity which makes it suitable for knee replacements. Three other biomaterials evolved during this time for example, Polyacetal, PolyTwo (Zimmer, IN, US), Hylamer and Hylamer M (DePuy, IN, US). However, the former two materials gave good wear resistance only for seven years (Wright *et al.* 1988; Li and Burstein, 1994) and the latter two had catastrophic failure following irradiation *in vivo* (Schmalzried *et al.* 1998; Livingston *et al.* 1997).

1.7.1 Processing Methods

Orthopaedic implants are made of UHMWPE powder with average molecular weight of over 75,000 (Whelan and Goff 1990) using three methods. First method is direct moulding which moulds the exact shape of the implants by compressing the powder enclosed in a mould. The second is preparation of rods (5-15 cm diameter) by ram extrusion where the powder is extruded into the mould. The third and final way is moulding large sheets of thickness 20cm and length 240cm. All the methods include heating the powder to a temperature above melting point which decreases the crystallinity. However, the crystallinity is improved by successive treating at high pressure and temperature (Li and Burstein 1990).

Recently, cross linked polyethylene has been introduced. Cross linking induces wear resistance under the action of multidirectional movements (Wang *et al.* 1996) by forming linear chains between the polymers with strong permanent bonds. Under the action of unidirectional sliding, the polymers align itself to the sliding direction to resist deformation (strain hardening). However, when rotation is

involved, sliding in the transverse direction weakens (strain hardening). Therefore with cross linking, the orientation of the polymers was reduced. Cross linking is induced using irradiation or by a chemical process. Irradiation can be using gamma rays or electron beam, or chemical processes involving the use of peroxide or silane.

Following irradiation the UHMWPE is sterilised after packaging and before implanting. For example, one of the current cross linking sterilization method used by DePuy International is gamma irradiation at 2.5-4MRad dose in the presence of an inert atmosphere (vacuum). The sterilised UHMWPE (at inert atmosphere) has been shown to have good resistance to wear and delamination failure as compared to irradiation in air (Fisher et al. 1997; Reeves *et al.* 1998; Kurtz *et al.* 1999; Collier *et al.*2005).

1.7.2 Limitation of UHMWPE

UHMWPE is stabilised with or without irradiation process. The stabilisation process is followed by heat treatment to remove free radicals formed as a part of the irradiation process. This treatment removes the failure due to delamination (Reeves *et al.* 1998; Bell *et al.* 1998). This leaves surface wear as the major concern in polyethylene. The production of wear particles of micron size during surface wear when metal and polyethylene slides against each other. These particles result in loosening and osteolysis (Ingham and Fisher 2000). The generation of particles leads to joint inflammation, loss of bone followed by loosening. The volume of particles generated in knee joint is lower than hip generally (Ingham and Fisher 2000). However, with increase in implantation time the possibility of osteolysis will increase (Peters *et al.* 1992). Therefore, the life of an implant is dependent on the osteolysis formed due to the size and total volume of particles and the presence within a tissue area. To improve success rate, the number of particles and wear volume should be reduced. Osteolysis depends on factors like surgical alignment, implant design, type of cement used and number of follow up years. Fisher *et al.* (2005) have reported that polyethylene with high molecular weight and high cross linked generated smaller and high reactive particles compared to low molecular

weight. Patellar misalignment has been commonly shown in patients with osteolysis clinically but studies to evaluate this relationship have been neglected in the past. Lwano *et al.* (1990) evaluated 108 knees and found that 28% of the patients had earlier history of subluxation. Osteolysis is more substantial in non-conforming TKR as compared to conforming as in conforming the load is distributed uniformly along larger areas so wear is less for earlier generation of UHMWPE (Lwano *et al.* 1990*)*. However, in vitro investigations have shown with higher contact area, the wear rate increases (Galvin *et al.* 2009). As the wear rate increases, the possibility of osteolysis will increase with implantation time. Collier *et al.* (2005) investigated the effect of osteolysis by changing properties of implant. The decrease in occurrence of osteolysis (25%) was noticed when the knee with gamma irradiated in air and having a rough base plate surface was changed to knee insert with gamma irradiation in inert gas and have polished base plate. Prevalence of osteolysis was observed (6% decrease) when the insert was sterilised with nitrogen and mated with polished base plate surface with the same conformity. Loosening of implants caused as a result of osteolysis may lead to bone fracture in extreme cases (Collier *et al.* 2005).

The generation of wear debris is dependent on the surface roughness in the metallic femoral component, artificial knee joint design, oxidative degradation of polyethylene and kinematic input profiles (Lwano *et al.* (1990); Engh *et al.* 1992; Fisher *et al.* 1995; Besong *et al.* 1997; Tipper *et al.* 2000; Barbour *et al.* 2000; Collier *et al.* 2005; McEwen *et al.* 2005; Galvin *et al.* 2009).

1.8 Wear Mechanism

Wear is progressive damage involving the removal of material from two articulating moving parts (Bayer 2002; Stachowiak 2005).

There are various types of wear mechanisms as follows.

- Abrasive wear: Wear caused by removal of material through hard particles or protuberances. This can also have a third body involved.

- Adhesive wear: Removal of material due to localised bonding being formed between mating surface leading to loss of material from one or both the surfaces.
- Burnishing wear: Polishing of the surface such that the roughness is less than machined roughness.
- Deformation: Wear involving deformation rather than material loss.
- Delamination wear: Wear involving thin layers (2-5mm) being formed and removed from one surface. This involves formation of cracks in the surface ultimately leading to material loss.
- Pitting: A form of wear where flakes of material (0-2mm) are removed due to repeated cyclic stress.

1.9 Experimental Wear Simulations

1.9.1 Introduction

Wear in artificial knee joints can be studied through knee joint simulators. In a knee simulator the actual knee prosthesis can be tested resembling the functions obtained in human body. This section deals with the wear simulations in patellofemoral joint.

1.9.2 Patella Femoral Joint

Wear in the patella-femoral joint has received little attention from researchers. The present author has found five investigations that have documented patellar wear.

The authors who investigated on wear from in vitro conditions were Hsu and Walker (1989), Korduba *et al.* (2008) and Burroughs *et al.* (2006). Two degrees of freedom (Flexion extension rotation and axial load) were used by the investigators for the wear analysis under walking (Burroughs *et al.* 2006; Korduba *et al.* 2008),

stair climbing (Hsu and Walker 1989, Korduba *et al.* 2008 and Burroughs *et al.* 2006), descending stairs and rising from a chair (Hsu and Walker 1989).

Hsu and Walker (1989) used different shapes of patella for testing wear in knee flexion from 55 ° to 100 ° for activities such as stair climbing and descending and rising from a chair. Four patellar designs, all-plastic dome, metal-backed dome, all-plastic conforming and metal-backed conforming shapes were used for the investigation under a load of 750 N or 1500N as shown in Figure 1-17. The common wear mechanisms of the all-plastic dome patellar component due to wear test (1600- 192000 cycles) were: 1) presence of loose wear debris, 2) distortion of the plastic component and 3) components failed due to compression at load bearing regions. The metal-backed dome lasted for more cycles as compared to the all-plastic patellar components. However, the wear penetrated through the polyethylene causing damage to the femoral component. The patella was conventional polyethylene irradiated in air during the investigation which was improved by cross linking in recent years. The comparison between the various test specimens can be performed as there was variation in number of cycles among the test specimen.

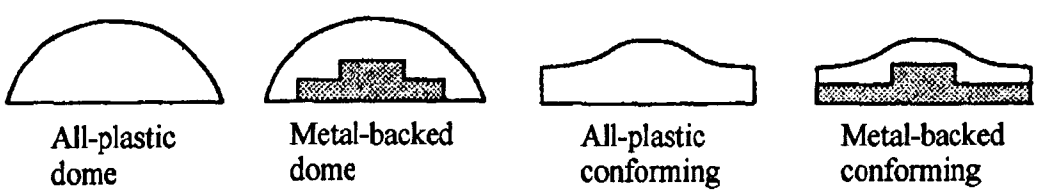

Figure 1-17 Four types of patella design (Hsu and Walker 1989).

Burroughs *et al.* (2006) and Korduba *et al.* (2008) worked with knee simulator under single load and displacement as shown in Figures 1-18 and 1-19.

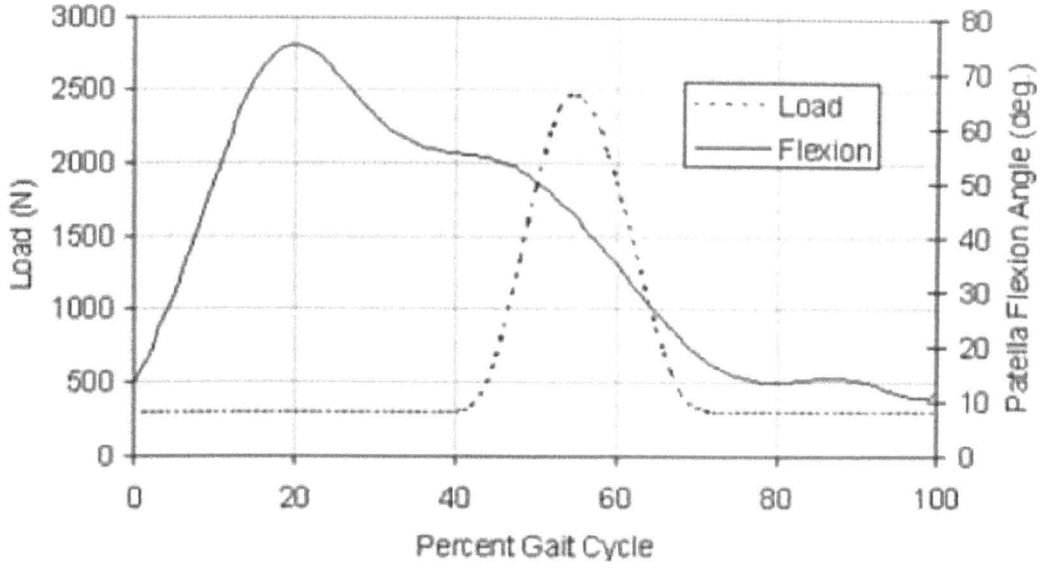

Figure 1-18 Input waveforms of PFJ load and flexion angle for gait simulation (Burroughs *et al.* 2006).

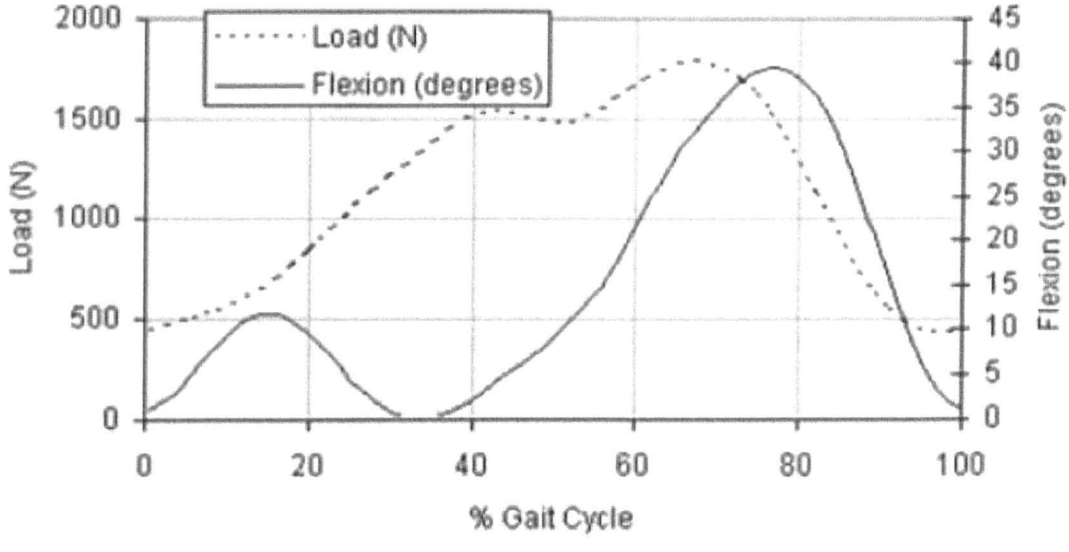

Figure 1-19 Input waveforms of PFJ load and flexion angle for stair climbing simulation (Burroughs *et al.* 2006).

Two set of implants, one with passive M-L motion and other with constrained M-L motion was used for stair climbing conditions. Wear rate of both the conditions are shown in Figure 1-20 (Korduba *et al.* 2008). The patella with constrained medial-lateral translation in stair climbing (5.1 mm^3/mc) showed

higher wear rate than in walking conditions (3.3 mm^3/mc). However, the walking cycle was tested for 0.25MC. During stair climbing wear rate for patella having passive medial lateral displacement (0.75 – 1.07 mm^3/mc) were much lower than constrained medial lateral (2.78 – 5.0 mm^3/mc). A large wear scar was found in the lateral surface and a few scars on the medial surface were found in case of the patella with passive translation, whereas as the wear scar was centrally located in the dome for the patella with constrained medial lateral motion. Constrained ML translation showed higher wear and the wear scar obtained in passive ML patella was due to the shift of patella during the flexion.

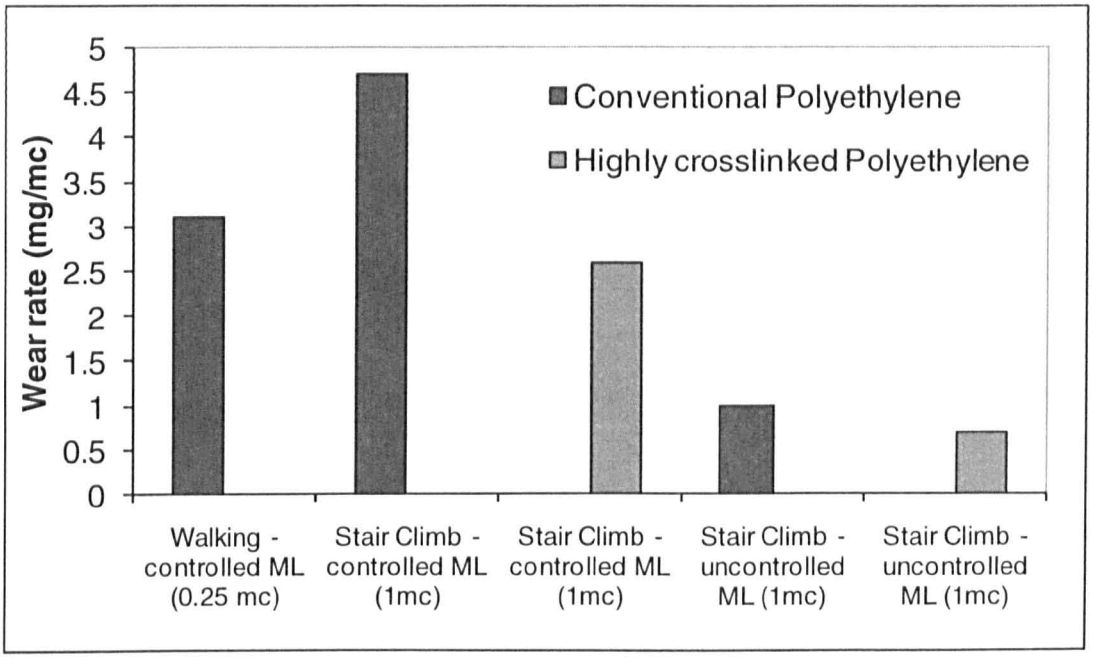

Figure 1-20 Wear rates for stair climbing (1 mc) and walking (0.25 mc) (Korduba *et al.* 2008).

Burroughs *et al.* (2006) found cracks and delamination in conventional polyethylene patellar components (GUR 1020 compression moulding and sterilization with 25-40kGy gamma irradiation in oxygenless environment) due to presence of high contact pressure during stair climbing and oxidative state of polyethylene. The highly cross linked polyethylene patellar component (GUR 1050 compression moulded and sterilised using ethylene oxide gas) however, didn't show any crack or delamination after stair climbing, even with 4 $^{\circ}$ misalignment of femoral components as shown in Figure 1-21(b).

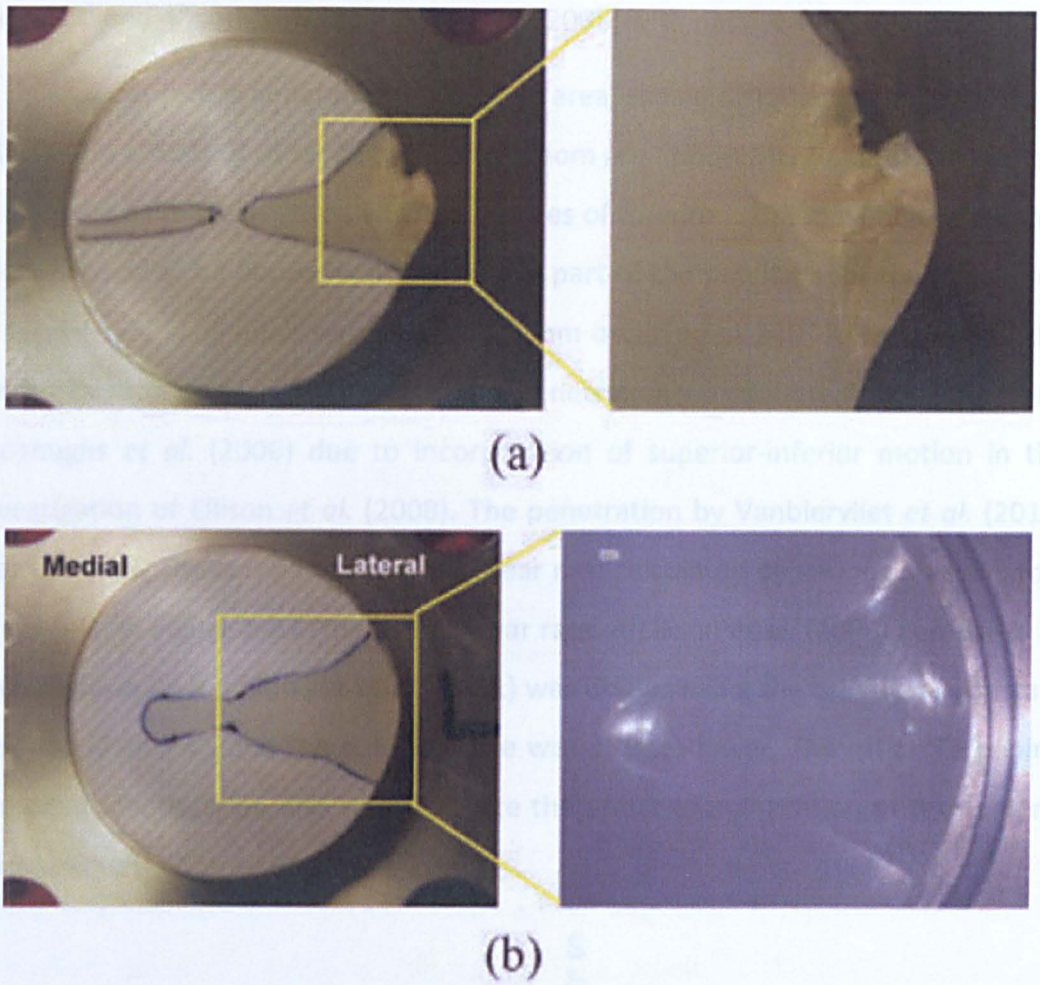

Figure 1-21 Wear scars after 1 million cycles with misalignment in (a) conventional polyethylene and (b) high cross linked polyethylene (Burroughs *et al.* 2006).

All the previous authors reported so far have concentrated on two motions; flexion extension rotation and anterior posterior load in their investigation, which are non physiological considering cases in vivo. The investigations to find the wear were based on visual inspection except in Korduba *et al.* (2008). The authors considering the effect of other patellar motions are Ellison *et al.* (2008) and Vanbiervliet *et al.* (2011). Ellison and co-authors (2008) investigated wear under axial load (200-1200N), patellar rotation (0-1°), flexion extension (0-22°), patellar displacements restricted to 1mm and superior inferior displacement (-5 to 20mm). Compared to Ellison *et al.* (2008), Vanbiervliet and co-authors (2011) had lower force (-50 to 400N), patellar rotation (-10° to 10°), flexion (0° to 40°), patellar and

superior inferior displacements (-10 to 10mm). The sixth degree of freedom tilt was fixed at 0 and 4° compared to Ellison *et al.* (2008) with passive tilt movements.

As wear rate is dependent on contact area, sliding distance and load (Archard 1953). The effects of other degrees of freedom are important. None of the authors in the past have investigated with six degrees of freedom. The maximum wear rate was analysed to be occurring in the medial part of the patellar specimen as shown in Figure 1-22. The penetration of -0.947 mm occurred at 240° from lateral in the medial portion of the articular face. This penetration was double that predicted by Burroughs *et al.* (2006) due to incorporation of superior-inferior motion in the investigation of Ellison *et al.* (2008). The penetration by Vanbiervliet *et al.* (2011) was 0.05mm. The comparisons of the wear rate calculated by various investigators are shown in Figure 1-23. The higher wear rate of Ellison *et al.* (2008) compared to investigation by Vanbiervliet *et al.* (2011) was due to fixing the tilt to two constant degrees (0 and 4°) and the contact force was 3 times lower. The rationale behind the wear investigation was to investigate the effect of malrotation of the femoral compartment (Vanbiervliet *et al.* 2011).

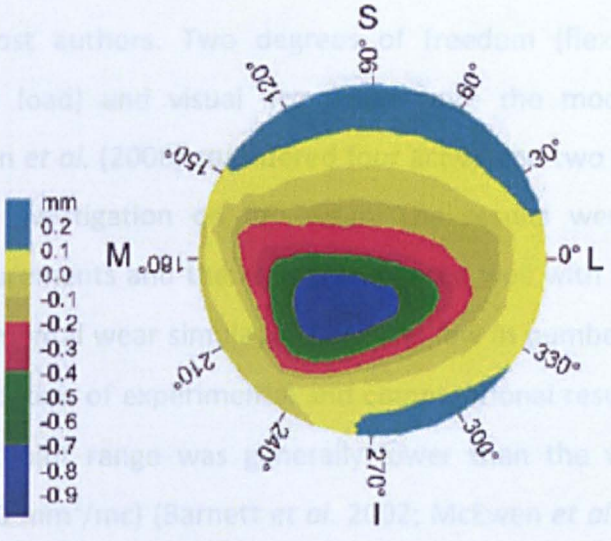

Figure 1-22 Wear scar after 4 million cycle of in vitro simulation (Ellison *et al.* 2008).

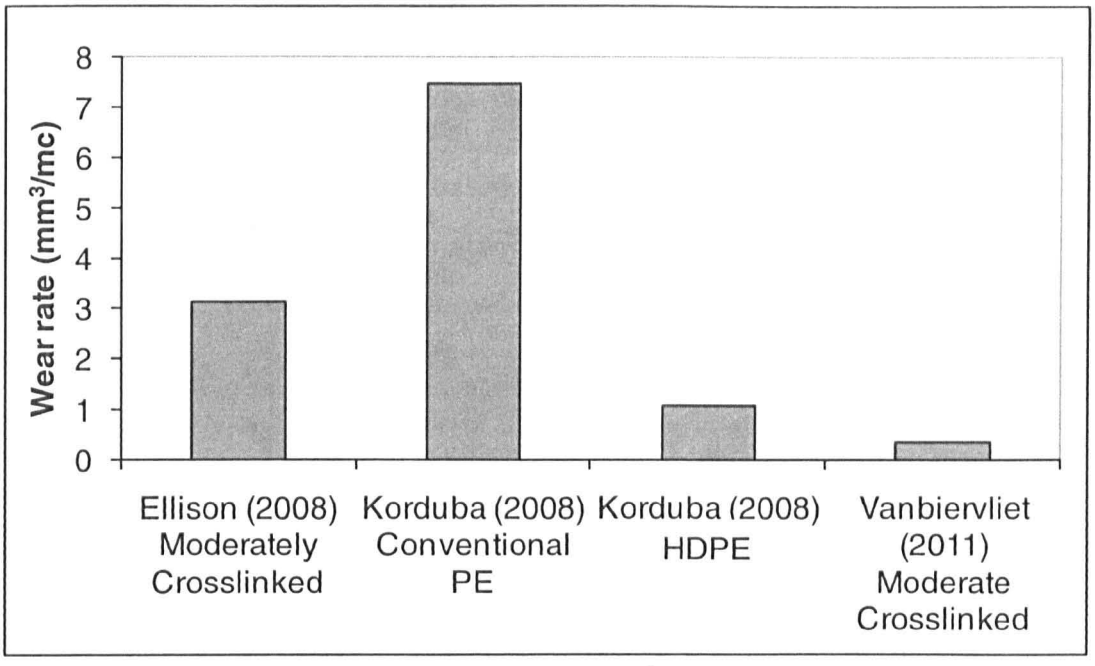

Figure 1-23 Wear rate of patella femoral joint in mm^3/mc (Ellison *et al.* 2008; Korduba *et al.* 2008; Vanbiervliet *et al.* 2011)

Summary

PFJ wear has been investigated by several authors. The conditions of testing were, however, limited to non physiological (less than 6 degree of freedoms) conditions by most authors. Two degrees of freedom (flexion-extension and anterior-posterior load) and visual inspection were the mode used for wear assessment. Ellison *et al.* (2008) considered four active and two passive degrees of freedom for his investigation on PFJ wear. The results were analyzed using gravimetric measurements and the results compared well with in vivo specimens. Studies on experimental wear simulations are still low in numbers and need to be expanded for validation of experimental and computational results. The wear rate in patellofemoral joint range was generally lower than the wear rate in tibia femoral joint (5-40 mm^3/mc) (Barnett *et al.* 2002; McEwen *et al.* 2005; Affatato *et al.* 2008; Wang *et al.* 2008).

1.10 Explant Analysis

Several methods have been developed in the past to evaluate clinical retrievals. These can be divided based on joint type and measurement techniques as shown in Table 1-2. Gravimetric and MicroCT analysis was used for the measurement of volume when pre-wear data was available.

Table 1-2 Explants analysis based number of specimens, measurement types and device (Hood *et al.* 1983; Raimondi *et al.* 2000; Kooijman *et al.* 2003; Bowden *et al.* 2005; Rawlinson *et al.* 2006; Bills *et al.* 2007; Kurtz *et al.* 2007; Lindsey *et al.* 2010; Ellison *et al.* 2010).

Investigations	**Retrieval Type**	**Number of samples**	**Measurement type**	**Device**
Hood *et al.* 1983	Patella buttons	48	Grading	Visual
Raimondi *et al.* 2000	Acetabular cups	65	Linear wear	Mathematical
Kooijman *et al.* 2003	Patella	42	Score/ Radiography	Direct/ Radiograph
Bowden *et al.* 2005	Acetabular liners	6	Volume	MicroCT
Rawlinson *et al.* 2006	Tibia	25	Wear patterns	Digital image analysis
Bills *et al.* 2007	Hips	2	Volume	CMM
Kurtz *et al.* 2007	Total disc replacements	21	Linear wear	MicroCT
Lindsey *et al.* 2010	Patella	13	Wear patterns	Visual
Ellison *et al.* 2010	Patella	2	Volume	CMM

Limited research has been performed to calculate the wear volume of the patella. However, the number of specimens is very low (Ellison *et al.* 2010). Retrievals volumetric wear are important to determine the validity of in *vitro* tests.

1.11 Computational Kinematic Model

For development of artificial joint replacements, pre clinical studies need to be carried out. This can be done using a combination of clinical studies, experimental measurements and theoretical modelling. Clinical involves running *in vivo* animal model studies; whereas experimental studies can involve running wear simulator. Experiments can provide wear data and biological responses of wear particles but they are time consuming, expensive and complex in nature. Theoretical modelling is becoming more established and are validated with the help of experimental simulation. It can provide better screening of design, materials and surgical variables. In majority of theoretical modelling finite element analysis (FEA) was the tool used for evaluating contact stresses in the implant and its wear (Kang *et al.* 2006). The inherent complexity of the knee joint makes it difficult to model computationally (Komistek *et al.* 1997).

In hip or knee theoretical modelling, Archard's wear law (Archard 1953) in many forms has been used to calculate wear. The wear depth ΔH was expressed (Kang *et al.* 2006) as follows.

$$\Delta H = K_D \sigma_i S_i \qquad \text{(Equation 1)}$$

where, K_D is the wear factor, σ_i is the contact stress between articulating surfaces, S_i is the sliding distance, σ_i and S_i both being function of time,

Further investigations into Archard's wear law (1953) have shown wear is dependent on cross shear (Fisher *et al.* 1994; Kang *et al.* 2008; Galvin, *et al.* 2009). Cross shear is the shear in the motion transverse to the direction of strain hardening in a polyethylene material during sliding (Kang *et al.* 2008). As K_D is a function of aspect ratio (AR), AR function of strain hardening and strain hardening function of cross shear. Therefore K_D is a function of cross shear. Ingham and Fisher

(2000) stated that the majority of hip replacement failure and revisions are due to the debris generated from UHMWPE. One of the major causes of generation of wear debris in conventional UHMWPE is cross shear. For single dimensional motion, the cross shear causes hardening of the surface, but for multidirectional motion hardening in one direction causes weakening in transversal direction, which accelerated formation of wear debris. Cross shear was also an important factor dependent on friction (Kang *et al.* 2008). The analysis of cross shear showed that it is directly proportional to the polymer orientation. The more the rotation of the pin, more is the cross shear effect (Figure 1-24). Saikko *et al. (2004)* also investigated the effect of variation of AR and wear factor k. When AR is more than 5.5, the wear factor decreases to unrealistic values and the wear scar are different from that seen in explants. The wear particles however were found of same size irrespective of AR values.

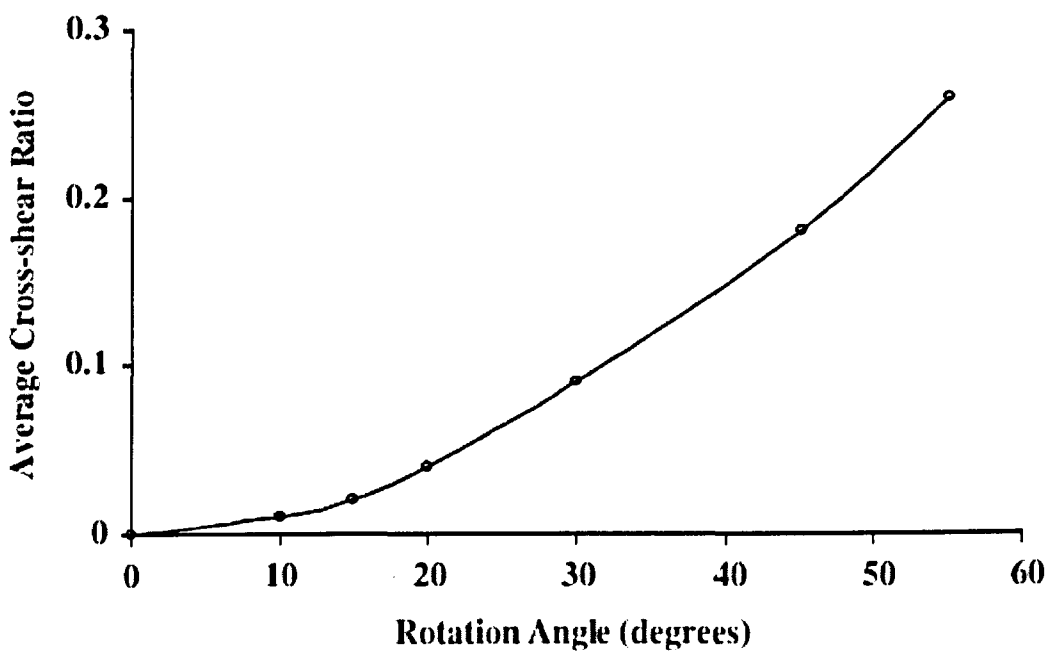

Figure 1-24 Variation of cross shear with pin rotation (Kang *et al.* 2008).

In addition to cross shear, Korduba *et al.* 2008, Ellison *et al.* 2008, and Vanbiervliet *et al.* 2011 have observed that with increase in kinematics, the wear rate increases. Therefore, the first step of creating a wear model is developing a computational model and validating the kinematics with experimental results.

Models have been created to validate tibia femoral joint (Godest *et al.* 2002; Knight *et al.* 2007; Halloran *et al.* 2010), and patella femoral joint (Baldwin *et al.* 2009; Halloran *et al.* 2010). Godest *et al.* (2002) and Knight *et al.* (2007) validated the Stanmore knee wear simulator. Baldwin *et al.* (2009) and Halloran *et al.* (2010) validated the Kansas knee simulator. The validation of the Leeds Knee simulator has not yet been performed. Hence, an active comparison of the computational model with experiments will be useful.

1.12 Research Rationale, Hypothesis, Aim, Objectives and Outline of the Thesis

1.12.1 Rationale

Despite a revision rate of the patella femoral joint of 14.7% at 5 years and 20.37% at 7 years (NJR 2010), the information on PFJ implants are limited. The research on patella maltracking at various dynamic conditions like walking, jumping, running etc. has not been properly examined. The numbers of published biomechanical studies on patella tracking are few (Sheehan *et al.* 1999) in cadaveric specimens due to complexity and invasive nature. These studies are needed for an examination of the role of the quadriceps tendon and patellar ligaments on the stability of the patella during knee flexion. Studies on computational wear model of TFJ have been reported, but investigation on the PFJ is low. The determination of wear in relation to kinematics and design is important. The computational simulation is an important tool for evaluation of the PFJ performance and wear. Very limited data on *in-vivo* wear is available. As this information is required for validation of computational and experimental models appropriate experimentation to measure wear data of explants are required.

1.12.2 Aims, Hypothesis and Objectives

The aim of the present project is to investigate the in vitro wear behaviour of the artificial patella femoral joint in total knee replacement. Hypothesis of this

study is that a six degree of freedom simulator with high kinematic input will result in increase in wear. Specifically, the objectives are as follows.

1. Design, modify and use the existing Leeds knee simulator as a six station patella femoral joint simulator for prediction of wear. Compare the data by with previous testing results (Ellison *et al.* 2008).
2. To determine the influence of kinematics and shape of patella on the wear behaviour.
3. Develop a computational model to predict kinematics and validate with experimental results.
4. Develop methods to measure wear volume in clinical retrievals.
5. Validate experimental testing of wear volume in patella-femoral joint with clinical retrievals.

1.12.3 Outline

Chapter two explains the method and materials used to do the in vitro wear test, computational model and retrieval analysis. Chapter three discusses the validation of three volume measurement techniques with gravimetric for repeatability and accuracy. Chapter four analyses the kinematics using computational modelling and validates with experimental results. Fifth and sixth chapter discusses the result of wear test of PFC sigma with round and oval dome patella respectively. Seventh chapter is on retrieval analysis. Finally the discussion of all chapter and future plans of the project are highlighted in chapter eight.

Chapter 2: Materials and Methods

2.1 Introduction

This chapter details the materials and methodologies used in the study. The rationale behind various machines and measurement techniques used in this project are detailed below.

Knee simulator as patella femoral joint simulator: The presence of six degrees of freedom and motions similar to patella femoral joint and possibility to test 5 wear specimens and 1 creep test at the same time makes knee simulator best suited to be used and modified for the patella femoral joint.

Gravimetric: The most standard and accurate method of measuring mass loss of polyethylene specimen during wear simulation.

Due to problems regarding soaking, cement fixtures, and cement debris in test specimens, additional methods to measure volume were necessary. These are as follows:

Micro computed tomography (MicroCT): X-ray techniques have been used for volumetric measurement of polyethylene explants (Kurtz *et al.* 2007) and total disc replacements (Vicars *et al.* 2009). However, measurements of volume have never been adopted in patella specimens.

Coordinate measuring machine (CMM): CMM has been used for measurement of change in volume for hip retrievals (Raimondi *et al.* 2000; Bills *et al.* 2007). The need for measurement of retrieved patella specimens was required. The coordinate measuring machine (CMM) at present remains the only available method to find the volume change in retrievals with no pre-wear data present.

Pycnometer: Helium is an inert gas not affecting the volumetric calculation. As no investigations have been performed in the past for determination of polyethylene volume, this project examines the method potential for volume calculation of the patella.

Computational simulation – Computational modelling remains the fastest way to investigate any joint mechanics in detail. In this project multi body solid dynamics (MBSD) was used to design and test the fixtures of the patella femoral joint simulator for robustness prior to manufacturing.

Retrieval analysis: The validation of the specimens from *in vitro* wear simulations with *in vivo* retrievals is essential for clinical relevance. The relevance was investigated in this project.

2.2 Materials used in *In Vitro* Wear Simulation

The components used for the wear simulation test were commercially available; Co-Cr metallic femoral component and an ultra high molecular weight polyethylene (UHMWPE) polyethylene patella button; supplied by DePuy International (Leeds, UK). The composition and brief manufacturing methodologies of the materials are detailed below.

2.2.1 Femoral Component - PFC Sigma

The press fit condylar (PFC) design has been in usage since 1984 (Schai *et al.* 1998). It was upgraded to PFC sigma later on in 1996. The PFC and PFC sigma knee femoral component are manufactured with Cobalt-28 Chromium-6 Molybdenum (Co-Cr-Mo) alloy. After manufacturing, the components were heat treated and machine polished to obtain an average surface roughness (R_a) of 0.02μm (ASTM-F75-01, 2001). The surface finish was well within accepted orthopaedic implants surface finish (R_a) of 0.1μm (ISO 7207-2:2011).

The main difference between the PFC sigma when compared to the PFC knee system is the angulation of the trochlear femoral groove. The angulation of 7 degrees in the trochlear femoral groove is similar to the natural knee (Figure 2-1). Introduction of the angulation reduced the medial lateral (M-L) shear by 10% as compared to the straight alignment of trochlear femoral groove in PFC knee (Petersilge *et al.* 1994). The other difference between the two types of PFC is the introduction of conformity in the tibia and femoral condyle interface as suggested by Uvehammer *et al.* (2001). The articulating surface of PFC knees; mating with

patella; have been designed based on the dome curvature of the UHMWPE dome patella. For current *in vitro* experiments 'Right' knee PFC Sigma femoral component was used.

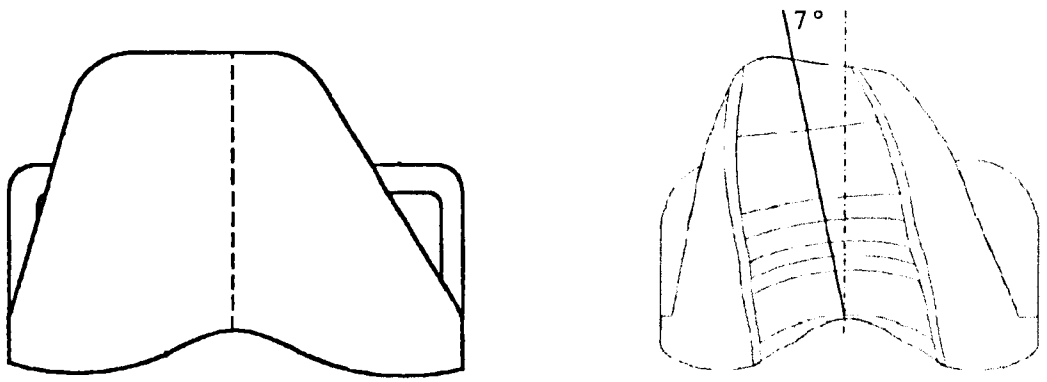

Figure 2-1 Schematic drawing of patella articulation surface in PFC and PFC sigma femoral component (United States Patent – Modular knee replacement 1998, DePuy manufacturing drawing).

2.2.2 UHMWPE Round Dome Patella

High grade GUR 1020 UHWMPE as the patella specimen was used in the experimental simulation. The sterilization was obtained by using gamma irradiation under vacuum with a standard radiation range of 2.5-4.0MRad while sealed in foil packaging (GVF sterilisation). The irradiation results in moderate cross linking of the polymer (Endo *et al.* 2001). The types of patella used were all polyethylene design of round and oval dome shape (Figure 2-2). The specimen were clipped to the metallic fixtures during *in vitro* simulation and cemented to the bone using PMMA surgical cement during *in-vivo* implantation. The radius of curvature for both types of patella was 25.4mm. The size was 38mm and 38 mm x 33mm for the round and oval dome respectively (DePuy International, Leeds, UK). The superior surface for the patella specimen articulated with the trochlear femoral groove. The inferior surface of the patella had 3 posts designed for greater rigidity when attached to the bone *in vivo* or mountings *in vitro* (United States Patent – oval dome patella 1997). The average roughness surface finish (R_a) was 0.03μm (Ellison 2007). The density of the polyethylene specimen used for volumetric calculation was 0.935 kg/mm^3 (Kurtz *et al.* 1999).

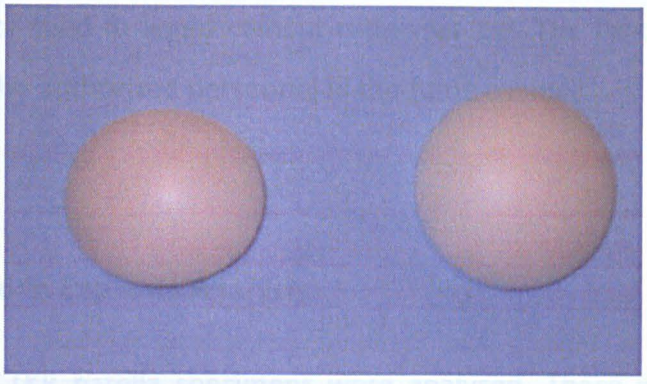

Figure 2-2 Range of PFC sigma patella: from left Oval and round dome designs.

2.2.3 Test Lubricant

The lubricant used for the test was 25% newborn calf serum (Seralab, Haywards Heath, West Sussex, UK) supplemented with 0.03% of sodium azide (Sigma-Aldrich Company Ltd, Gillingham, UK) solution. Sodium azide was used to minimise the bacterial growth. The properties (protein concentration of 6g/dl) obtained (Certificate of Analysis, Sera Laboratories International) after mixing were similar to the properties of ISO standard fluid used for total hip replacement or total knee replacement wear testing methodology (ISO: 14242-3 2009; ISO: 14243-1 2009). The lubricant was changed every third of a million cycles. The serum used was collected every million cycles and stored for potential wear debris analysis.

The rationale of using 25% of serum solution was to obtain the similar protein level as observed in the physiological scenario of the body fluid. The protein present in the serum acted as a boundary layer causing decrease in wear (Saikko *et al.* 2003; Wang *et al.* 2004; John *et al.* 2010; Harsha *et al.* 2011).

2.2.4 Poly methyl methacrylate (PMMA) Cement

PMMA cement mixture (WHW Plastics, Hull, UK) was used to secure the position and orientation of femoral component with the mounting for the wear simulation test. The cement mixture consists of solid powder (Cold Cure) and liquid monomer (Rapid Repair Liquid) mixed in proportion as specified in the instruction

manual. The ratio of solid to liquid cement ratio was 2:1. The fixation procedure was performed by the authorised personnel in the fume cabinet.

2.3 Materials used in Explants Analysis

A total of 10 TKR patella specimens were analysed. These were retrieved specimens from Leicester Nutfield Hospital, Glenfield Hospital, Bradford Royal Infirmary and Leeds General Infirmary. These specimens were either retrieved during revision surgery or at post mortem by the surgeons. The specimens after sterilisation were cleaned with iso-propanol solution and dusted with compressed air before measurements.

2.4 Cleaning Agents

Trigene (MediChem International Ltd, Seven Oaks, UK) is a detergent solution used for cleaning the specimen before any measurement procedure.

Iso-propanol solution (Fisher Scientific, Loughborough, UK) mixed with water (70% iso-propanol: 30% water) were used to clean the specimens in ultra sonic cleaning (VWR Labshop, IL, USA) for 10 minutes (IMBE simulator test protocol, Leeds University, UK).

2.5 Methods

2.5.1 The PFJ simulator

This section deals with the design of the PFJ wear simulator and associated fixtures. As the simulator used in the project was originally described as a tibia femoral knee simulator, the simulator was modified to act as a patella femoral

simulator. The fixtures manufactured were designed to obtain the required knee patella motions.

The first knee simulator was designed by Shaw and Murray in 1973 (Shaw and Murray 1973). The Leeds Prosim knee simulator (Simulation Solutions Ltd, Stockport, UK) (Figure 2-3) is a platform for wear testing at controlled loading and kinematic conditions and has been used extensively in over a billion cycles of knee wear testing (Barnett *et al.* 2001; Barnett *et al.* 2002, Fisher *et al.* 2004, McEwen *et al.* 2005, Jennings *et al.* 2006, Jennings *et al.* 2007, Fisher *et al.* 2009; Galvin et al. 2009; Brockett et al. 2011). The simulator consisted of 6 stations therefore allowing six specimens to be tested simultaneously at similar conditions.

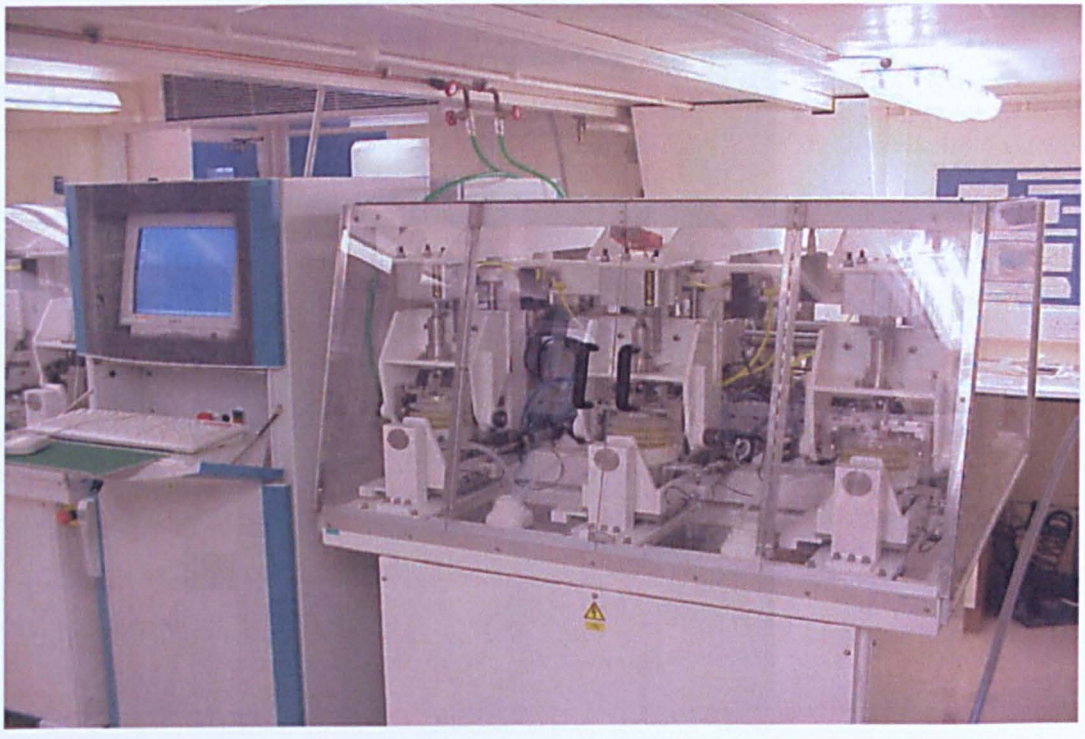

Figure 2-3 General view of Leeds Prosim knee simulator and control unit (Barnett *et al.* 2002).

The simulator was chosen to be adapted to create a patella femoral joint simulator. There were six stations in the simulator and six axes of freedom, 4 of which were controlled. The other benefit of using the knee simulator as patella femoral simulator was to avoid the manufacturing cost and manual labour incurred in building a completely new simulator.

2.5.2 Development of Simulator for Patella Femoral Joint

The Leeds knee simulator I was chosen for the design of the patella simulator in this project. The capability to control the 6 degrees of freedom can be properly handled in the existing knee simulator as compared to the previous simulator using the Leeds 1 hip simulator. The medial lateral displacement was constrained to 1mm in the earlier study. The presence of six stations made the simulator most suitable for the study as compared to two stations in the previous study (Ellison 2007).

The parameters acting on the femur were flexion extension (FE) and the axial load, which passed through the centre of patella as shown in Figure 2-4. The motions on the patella were medial lateral (ML) rotation, ML tilt, ML displacement and superior inferior (SI) displacement.

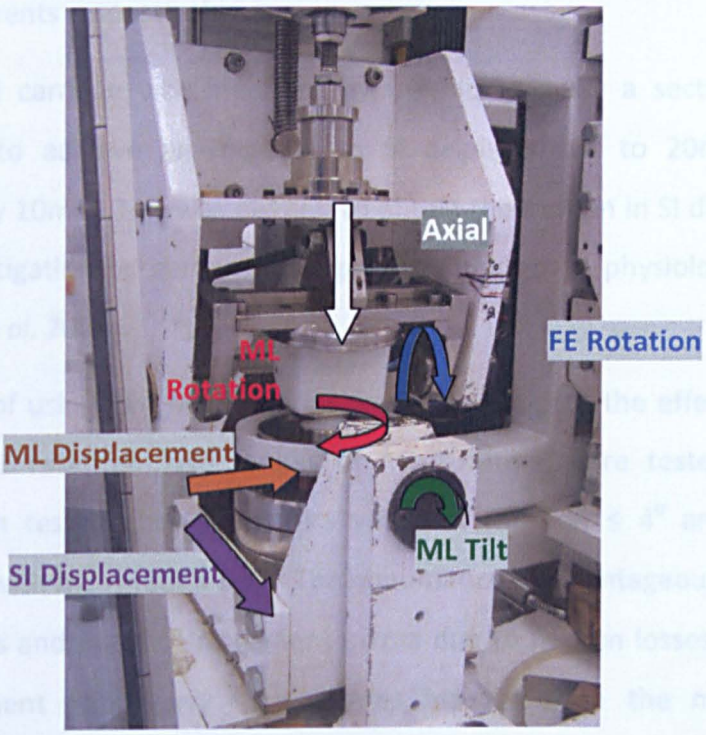

Figure 2-4 A typical station of the Prosim Knee Simulator 1 showing the degrees of freedom, directions and polarity.

In this investigation, five stations were used for wear testing. The sixth station was used for part of the testing as a creep station. The creep station was only under the action of axial (anterior posterior) load. The flexion extension rotation was removed by disengaging the connecting rod between the motor and the

flexion extension cradle. ML rotation and SI displacement were reduced to zero by lowering the air pressure in the pneumatics.

The design of the other five stations was modified to obtain the required control strategy as listed below.

- ML displacement was constrained in the conventional knee simulator set up (Ellison et al. 2008). In this study the displacement was unconstrained by using a Monorail BM20K bearing (Schneeberger, Germany) to enable free-floating. However, to replicate the earlier study, restrictions were obtained using cylindrical blocks for constrained ML displacement. The variation of the ML displacement on the wear rate was investigated. A maximum displacement of ±10mm and ±1.5mm were obtained in unconstrained and constrained ML displacements respectively.
- The tibial carriage was modified by machining away a section of the end carriage to achieve an increase in SI displacement to 20mm which was previously 10mm. This was needed to obtain the motion in SI direction close to the investigation by earlier investigator and closer to physiological waveform (Ellison *et al.* 2008).
- The aim of using two ML rotations was to investigate the effect of wear with varied ML rotation. Two ranges of ML rotation were tested in the wear simulation test, higher kinematics with ML rotation $\leq 4^{\circ}$ and physiological scenario with ML rotation $\leq 1^{\circ}$. The pneumatics is advantageous for low inertia conditions and avoid displacement errors due to friction losses. However, low displacement and heavy load creates inaccuracy in the movement. This limitation of the pneumatics was observed at lower amplitudes of rotation.
- The femoral radius of rotation R_1 was taken on the basis of the inner groove dimension where the patella articulates with the PFC sigma knee (DePuy manufacturing drawing).
- The resistance by medial retinaculum equivalent to 10N (Singerman *et al.* 1999) created a moment of 267 N-mm (force x moment arm). This was taken into account by introducing a load of 0.2 Kg at a moment arm distance of 136mm

(from the centre of rotation) placed on the lateral side of the piston balance of outer cradle. This load induced a resistance; similar to the medial retinaculum in an anatomical state; to medial translation during the knee flexion. This load also helped avoid 'patella slip' at higher tilt angles. 'Patella slip' was a slip of the patella from the articulating contact due to higher tilt or higher superior motion. This was further caused due to the lack of resistance offered from the trochlear femoral groove.

- Patella slip was observed when the ML tilt was above 5.2°. This could have led to damage of the components. This was avoided by introducing wedges at the bottom of the tilt cradle limiting the ML tilt to maximum 5° on both the medial and lateral sides. It was an artefact of the simulation and not likely to happen *in vivo* due to presence of ligaments. The ligaments offered a resistance to balance the joint thereby stopping from the slip.
- At the beginning of the test damage was caused to the patella specimen due to excess displacement in the inferior direction. This caused slip of patella from the articulating contact and hence, damage of the specimen. To avoid further damage, rubber blocks were introduced to prevent excess movement and thereby, eliminate patella 'slip' in the superior inferior direction.

2.5.3 Simulator Set Up

2.5.3.1 Station assembly

The various fixtures and mounting required to convert the Leeds ProSim Knee simulator to a patella femoral joint simulator are shown in Figure 2-5. This section introduces all fixtures and mountings explaining the important features associated with it.

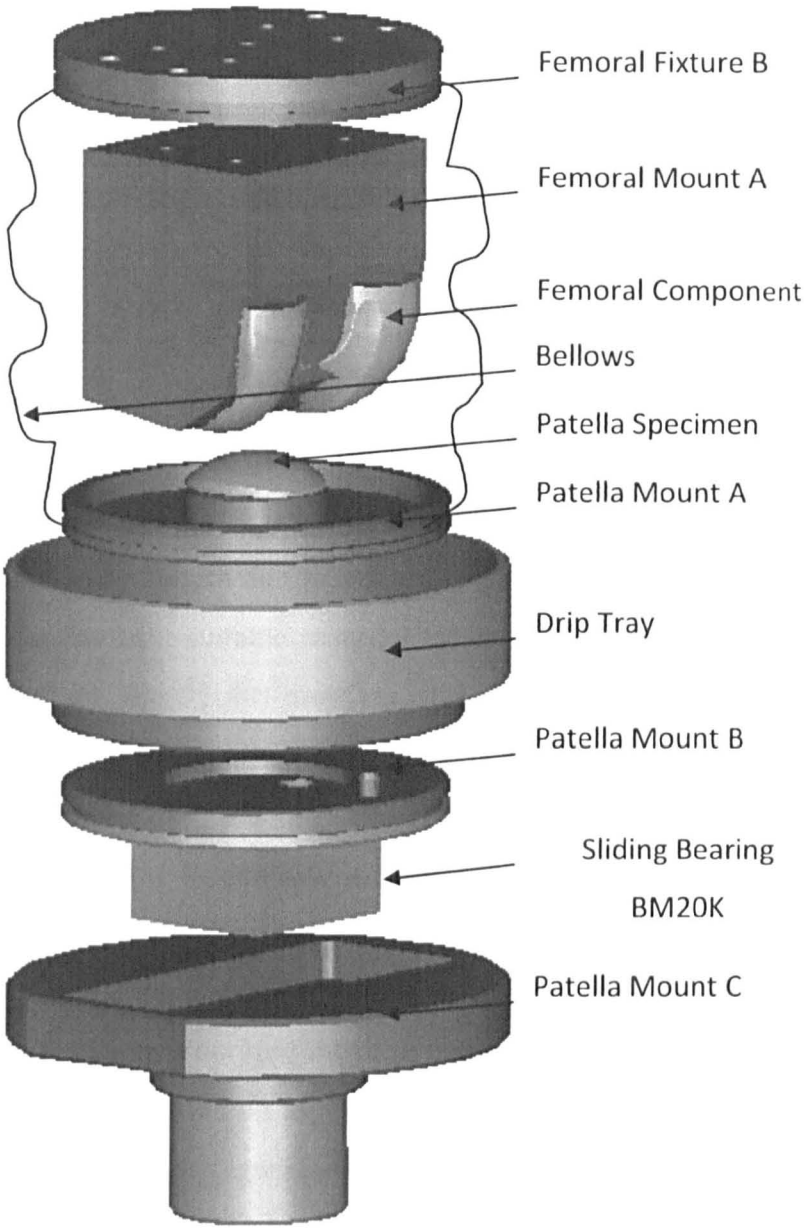

Figure 2-5 Assembly of mounting and fixtures required for converting Leeds ProSim knee simulator to patella femoral joint.

The Femoral component (PFC Sigma) and Patella specimen were supplied from DePuy International (Leeds, UK) for wear test.

Femoral Component

The posterior condyles were not required, and also in order to facilitate mounting in the simulator, were removed as shown in Figure 2-6

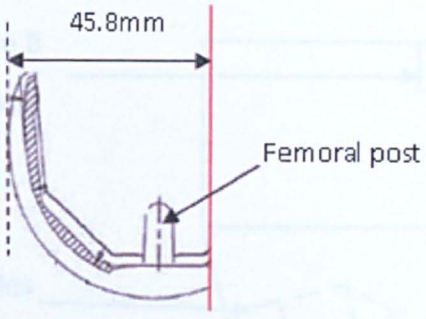

Figure 2-6 PFC sigma femoral component with location of condyles removed from the femoral posterior.

The femoral mount 'A' (Figure 2-7) was manufactured from DELRIN. The toughness, mechanical strength and resistance to solvents were the properties to classify DELRIN as the best suitable material for femoral mount (DELRIN product and properties, 2000). The DELRIN products were designed to geometrically fit to the back of the femoral components (Appendix A-1). An additional setup of 12° was included while designing the mounting. The 12° angular deviation was considered as a result of change in the flexion extension profile. Ellison and co authors (2008) predicted the flexion extension rotation to start at 12° extension. Due to the start position of knee simulator at 0° flexion, the waveform was shifted by 12°. The change in rotation was incorporated into the mounting design. The dimension of the femoral mount A was based on the centre of rotation (R_1) of the articulation of patella specimen with the PFC Sigma femur. As the patella was in contact from the top of the femoral component to 21mm inferior, the radius corresponding to the contact patch was considered (R_1) (DePuy Manfacturing Drawing). The mount was designed to ensure that the centre of rotation of the machine matched the centre of rotation of the femoral component.

During fixation of the femoral component in the mount, the femoral posts were inserted into the post holes as shown in Figure 2-7. The side grub screws were tightened considering cement thickness of 1mm was maintained between the femoral component and femoral mount A. PMMA bone cement was left in the cavity and the post hole for fixation for 48 hours. Excess cement was removed from

the mounting and the cement was covered in silicone sealant to prevent cement debris entering the lubricant during the experiment.

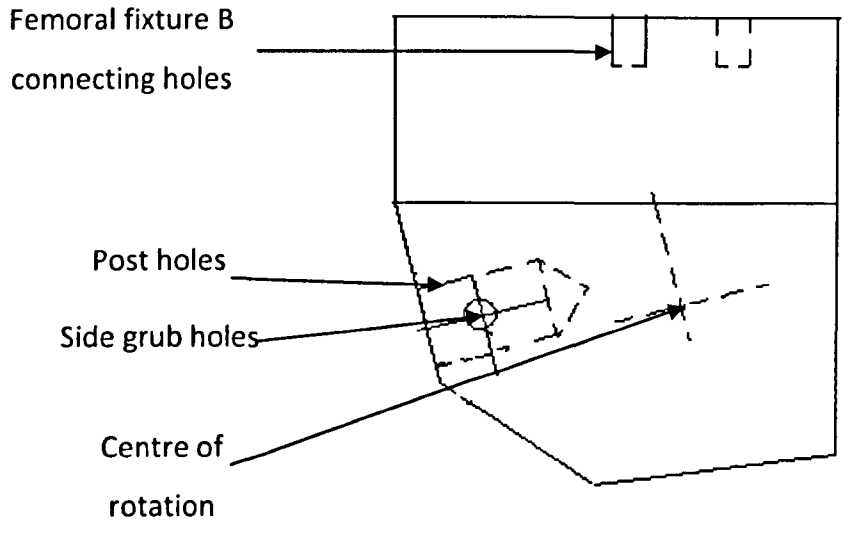

Figure 2-7 Schematic diagram of femoral Mount A showing centre of rotation, screw and post holes.

The patella articulating groove in the femoral component was at an inclination of 7° (Figure 2-1). To ensure the anterior posterior load acting through the centre of femoral mount A in frontal plane, the holes connecting the femoral mount A with femoral fixture B were drilled at 7.5 mm medially as shown in Figure 2-8. This was necessary to avoid any unnecessary torque on patella specimen created due to misaligned anterior posterior load during the experiments.

The femoral fixture B was created to connect the femoral component and femoral mounting A to the flexion extension cradle. The fixture was made of stainless steel.

Patella mount A was manufactured using stainless steel. The backing of the patella was embossed in the mount to prevent backside wear between the patella specimen and the patella mount A. Three peg holes were drilled to ensure proper fitting of the patella specimen in the mount (Appendix A-2). The patellae were clipped to the patella mount A.

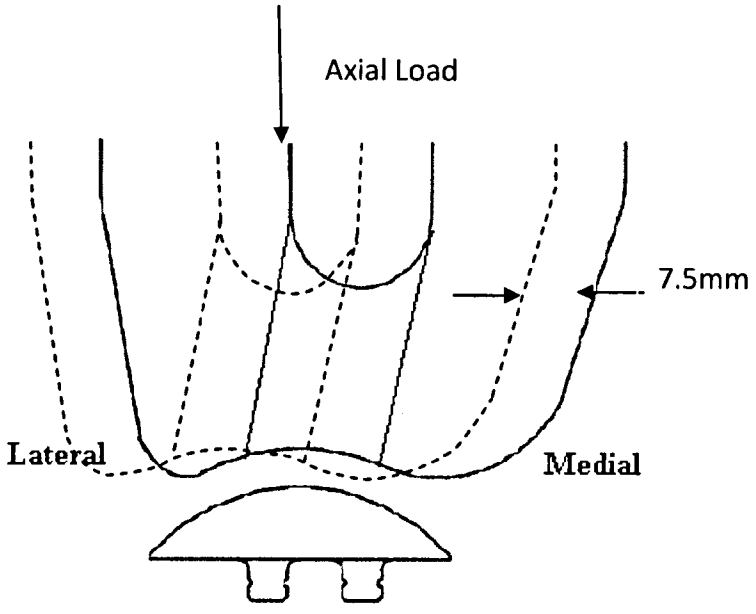

Figure 2-8 Schematic drawing of femoral Mounting fixture showing readjusting the femoral component to ensure axial load passing through centre of patella (dotted and solid lines showing original and final setup respectively).

Gaiters

Serum bags/bellows are flexible silicon bags provided in each assembly to hold the serum for lubrication. The bags were taped and clipped using a jubilee clip to the Patella mount A and femoral fixture B to contain the serum and provide lubrication during the experimental simulations.

Drip trays were provided in the assembly to prevent leakage of the serum from damaging the simulator bearings. These were made of DERLIN (Appendix A-3).

Patella mount B was the connection between the Patella mount A and the sliding bearing (Appendix A-4). The mount was manufactured with stainless steel. The sliding bearing BM20K (Schneeberger bearing, UK) was used for articulation of the patella specimen in the patella groove of the femoral component in the medial lateral plane due to the 7° femoral trochlear groove. The sliding bearing consisted of two parts, the rail and the bearing. The bearing was attached to the patella mount B and the rail was attached to patella mount C. The mount made of stainless steel held the rail part of the sliding bearing (BM20K). The slot provided for the rail

had grease as a lubricant to prevent sliding bearing failure. The manufacturing drawing is provided in Appendix A-5.

2.5.3.2 Calibration

The calibration procedure included calibration of load and motion systems before and after every test. The calibration was started by running the simulator without air and motor connection. Calibration key switch was inserted to put the simulator in calibration mode. During the calibration the simulator AD output at the display screen was recorded.

Calibration of the axial load cell

The calibration alignment jig was located in the specimen holder. The axial force transducer was introduced into the station along with the knee simulator load transducer. Using a compressed air supply the load was increased by 500N from 0N to 5kN recording the simulator output. The axial load versus the simulator AD output was plotted. The procedure was repeated for the 5 other stations. These are provided in Appendix A-6.

Calibration of motion cycles

The AP calibration blocks and calibrated angle protractors were placed in the station. Medial lateral rotation was calibrated with bespoke calibrated angles 10^{o}, 5^{o}, 0, -5^{o} and -10^{o}. AD outputs were recorded for each angle. Similarly with the calibration block, the superior inferior displacement was calibrated in all stations at 0, 10mm and -10mm. The AD output data from the screen was recorded. The calibration factors were determined by calculating the displacement or rotation against the AD output using the slope gradient function. These are provided in Appendix A-6.

Calibration of test rig frequency

The frequency of the simulator was monitored for 100 seconds using a stop watch. The frequency should be in the range of 1.0±0.1Hz.

The calibration factors in the form of slope was determined and recorded in a new calibration file. After the calibration, the simulator was restarted with motor and air on. The calibration key switch was turned back to normal.

The calibration file was loaded in the software before the test started.

2.5.4 Wear Model Control Strategy

The aim of the wear model was to represent the physiological kinematics of the patella. This section explains the importance of kinematic data combined with normal and post patella femoral joint (PFJ) replacement data to get a control strategy for the PFJ wear model. As the kinematic data for the PFJ in gait cycle was not completely available in literature, information from the normal PFJ gait cycle was integrated to obtain the control strategy for the test. The kinematics used in the wear simulation test were similar to those used by Ellison and co authors (2008).

The majority of the patella tracking was displacement controlled. The control of all six degrees of freedom was avoided as this would complicate the model resulting in unrealistic joint forces (Ellison 2007). The schematic diagram of the patella femoral joint with six degree of freedoms and the polarities are shown in Figure 2-9. The control strategy for each degree of freedom is explained below.

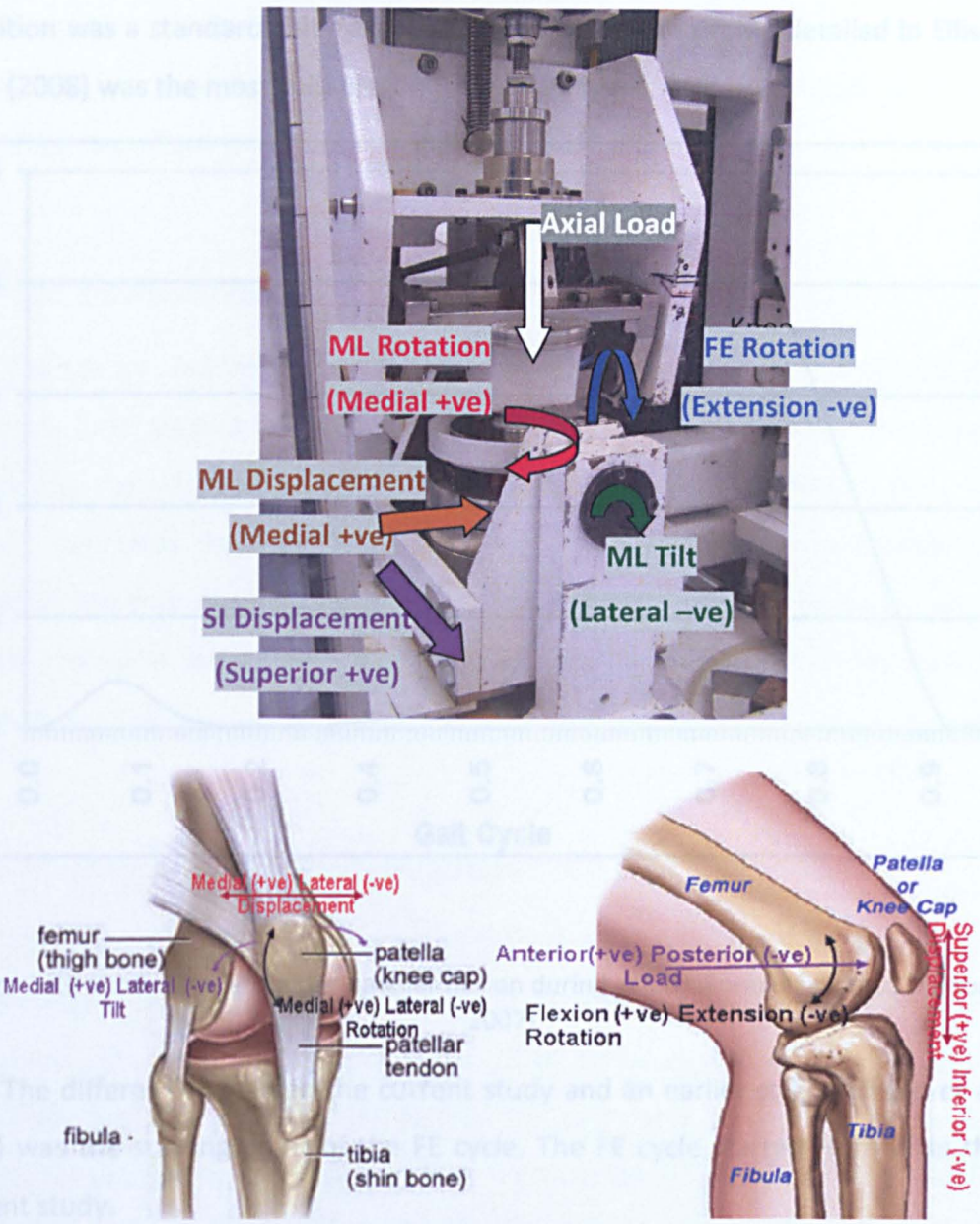

Figure 2-9 Schematic diagram of patella femoral joint showing six degrees of freedom and polarities of each degree in simulator and human body. (Modified from http://www.hughston.com/hha/a.extmech.htm).

Patella flexion extension rotation (Ellison 2007)

Patella flexion is dependent primarily on the quadriceps muscles and patellar tendon and secondly on the geometry of the femur trochlear groove. It was necessary to control this degree of freedom as it was not totally controlled by the femur trochlear groove. The flexion extension data presented (Figure 2-10) by Ellison and co authors (2008) and Halloran et al. (2005) was used in the control strategy of the present study due to the same condition being tested. As the test

condition was a standard gait cycle, the flexion extension profile detailed in Ellison et al. (2008) was the most suitable.

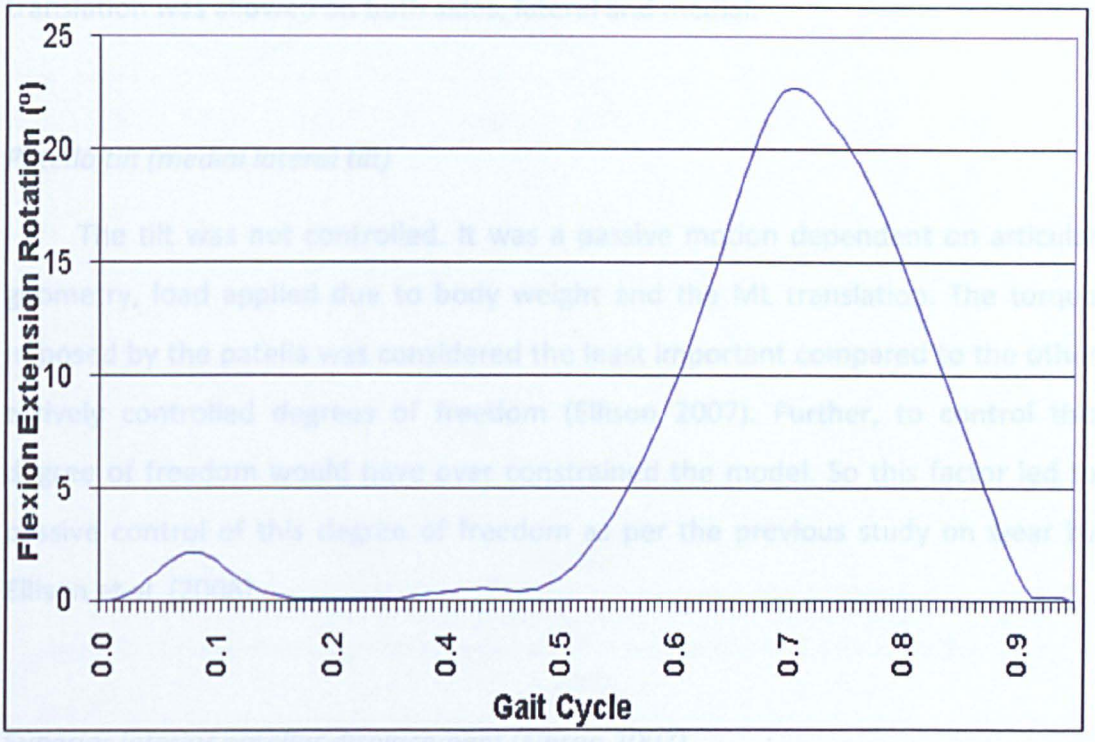

Figure 2-10 Control waveform for patellar flexion during gait (Halloran *et al.* 2005; Ellison 2007).

The difference between the current study and an earlier study (Ellison *et al.* 2008) was the starting point of the FE cycle. The FE cycle started from 0° in the present study.

Patella shift (Medial lateral displacement)

The controlling factor in the patellar shift is the 'Q angle', the angle formed between the quadriceps and patellar tendons. As the knee flexes, the quadriceps muscles produce force in the lateral direction. So patellar shift is dependent on the Q angle and articular geometry. This degree of freedom was not controlled. Lafortune and Cavanagh (1987) reported a patellar shift of 2 mm laterally and 8 mm medially during a normal knee gait cycle. Halloran *et al.* (2005) reported the variation of patellar shift for TKA in the Purdue knee simulator was less than 1 mm. The translation was passively controlled, depending on the femur geometry. In

Ellison's study (2008), the medial lateral displacement was restricted to 1mm. However in this project, this constraint was overcome and a maximum of 10 mm translation was allowed on both sides, lateral and medial.

Patella tilt (medial lateral tilt)

The tilt was not controlled. It was a passive motion dependent on articular geometry, load applied due to body weight and the ML translation. The torque imposed by the patella was considered the least important compared to the other actively controlled degrees of freedom (Ellison 2007). Further, to control this degree of freedom would have over constrained the model. So this factor led to passive control of this degree of freedom as per the previous study on wear by Ellison et al. (2008).

Superior inferior patellar displacement (Ellison 2007)

The superior inferior translation of the patella is considered as the result of flexion angle and forces imposed by the quadriceps and patellar ligaments constraints. Therefore it was considered as an active degree of freedom to be controlled. Halloran *et al.* (2005) studied the gait cycle after TKA; the control strategy for patellar superior translation is represented in Figure 2-11. The data for this degree of freedom was adopted from Ellison due to the similar nature of the study.

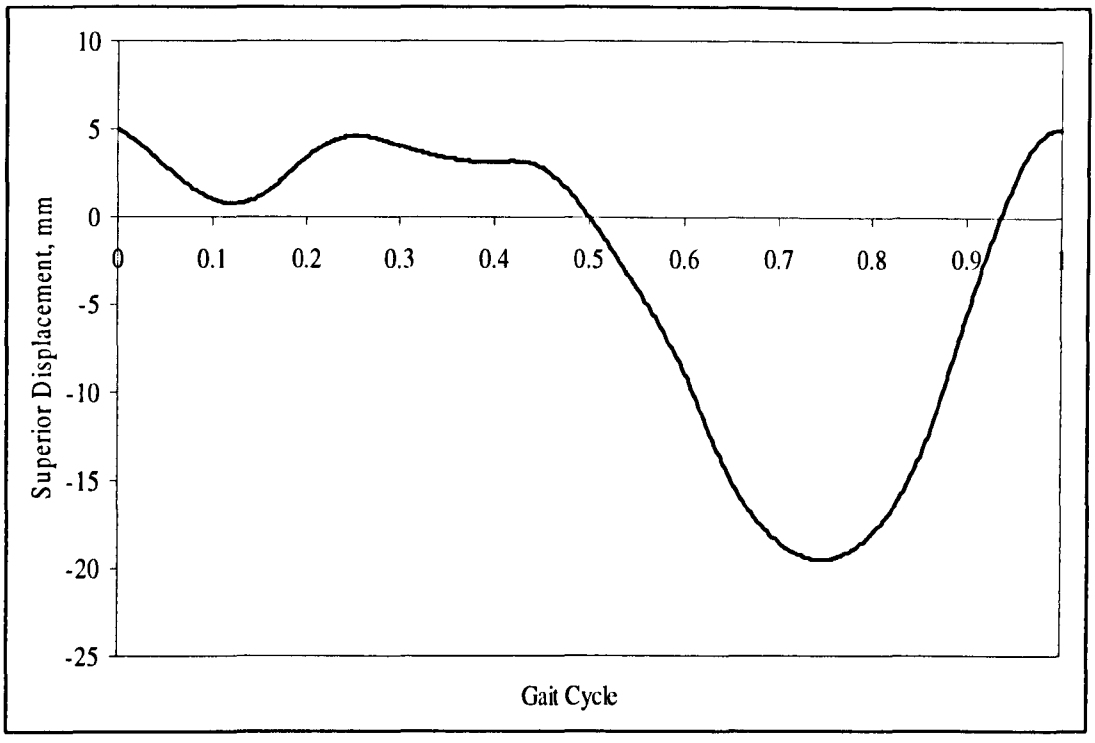

Figure 2-11 Control strategy for superior patellar translation in the wear model (Ellison 2007).

Patellar rotation (Medial lateral rotation)

Patellar rotation depends on tibia-femoral kinetics. This degree of freedom needs to be actively controlled. The control waveform is shown in Figure 2-12. Halloran *et al. (2005)* and Zachman *et al.* (1978) stated that the maximum rotation from the Purdue knee simulator was 1º. This computational model was verified using data from experimental simulation using two cadaveric knees by Zachman and co authors (1978). The waveform used in this wear study was taken from Lafortune and Cavanagh (1987) and modified to obtain a maximum patellar rotation of 1º. To investigate the effect of patellar rotation on wear rate and kinematics, the rotation was increased by a factor of 4, producing a 'high kinematics' condition. The previous investigator (Ellison *et al.* 2008) investigated the effect of lower patellar rotation on wear rate. This is the first study to consider the effect of patellar rotation and higher kinematics on wear rate.

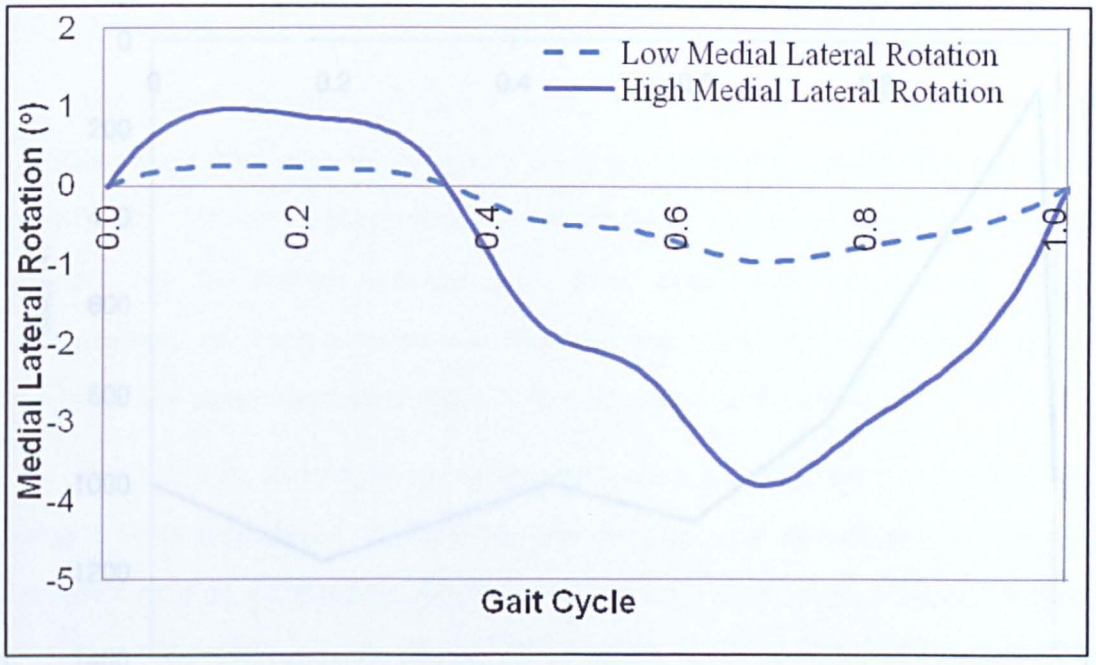

Figure 2-12 Control strategy for patellar rotation in the simulator wear model (Ellison *et al.* 2008). Dotted and solid lined denote low and high medial lateral rotation for physiological and high kinematics wear simulation test.

Axial load (anterior posterior patellar force)

Gill and O'Connor (1995) investigated the patella femoral forces during the gait cycle and described a maximum compressive load of 1.4 +/- 0.2 times body weight acting at 29 +/- 0.2 º knee flexion during the peak of stance phase. Zavatsky *et al.* (2004) stated that patella-femoral compressive force increased with knee flexion below 60 º of tibia flexion and the force was highest when the leg was under the action of full body weight. Therefore, control strategies of anterior force for a wear model incorporating all the known factors are (Ellison *et al.* 2008)

- Force increases from heel strike to peak of 1.4 BW at 29 +/- 0.2 º (A).
- Decrease from peak with increase in tibia femoral joint flexion (B).
- Second increase in stance phase with increase in knee flexion (C).
- Reduction from second peak till Toe off (D).
- Increase in reduction after peak of knee flexion (E).
- Sudden increase in force to heel strike.(F)

The control strategy of anterior patellar force for the wear model is shown in Figure 2-13.

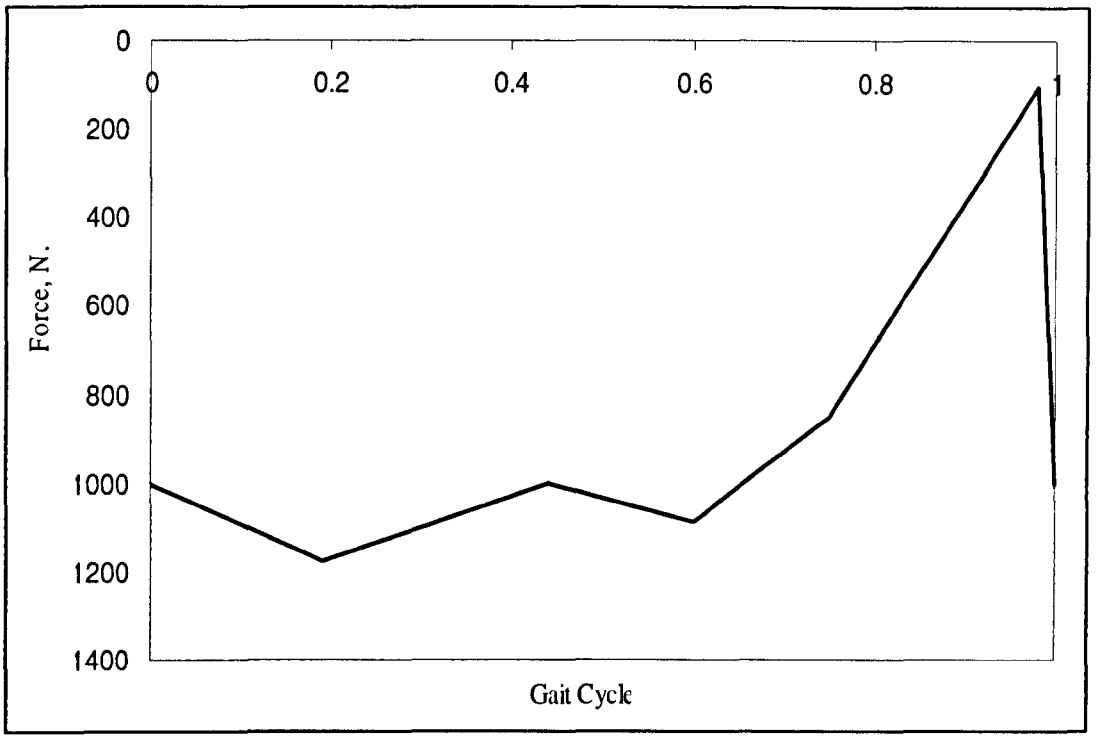

Figure 2-13 Control waveform for axial force (Ellison *et al.* 2008).

2.5.5 In Vitro Kinematic Measurement

2.5.5.1 Calibration

The calibration of a linear variable direct transducer (LVDT) (RDP Group CE S7M Transducer, Wolverhampton, UK) and potentiometer was required for determination of the translational and angular displacements obtained using an oscilloscope (Tektronix TDS 210, Florida, USA) with respect to voltage respectively. As the LVDT and potentiometer were connected to the output in voltage, defining the relation between voltage and displacements were necessary.

The LVDT was calibrated using slip gauges. Slip gauges were introduced from 0 to a maximum of 5mm with an increment of 0.5mm. The change in voltage due to the addition of the slip gauge was recorded through the oscilloscope. The potentiometer was calibrated by checking the voltage corresponding to angles ranging from 0 to a maximum of 5° in clockwise and anticlockwise directions at 0.5° increments. The angles were monitored using a protractor. The voltage corresponding to an increase in angle was recorded and plotted against voltage.

2.5.5.2 Analysis

The input motions (Axial/AP load, FE rotation, ML rotation and SI displacement) were directly observed using the simulator output. The output in form of ML shift, AP displacement and ML tilt were measured directly. As wear is proportional to sliding distance and cross shear (McEwen, et al. 2005), measurement of these motions was required and these motions were important inputs for the determination of wear in the computational model.

The ML shift and AP displacement data were recorded with an oscilloscope using a LVDT transducer. The tilt was obtained using a potentiometer and was recorded with an oscilloscope. Three measurements every million cycles for every station were performed and plotted with respect to time. These plots were later compared with the computational kinematic model as explained in Section 2.7. The tilt was plotted against wear volume change and linear correlation (R square) was performed.

2.5.5.3 Statistical significance

The output from each station and specimen was compared among stations and specimens. A student t-test was performed to check the significance between stations and specimens ($p<0.05$).

2.6 Procedure of Operating the Wear Simulator

The temperature of the surrounding environment was maintained constant at 20°C. Liao *et al.* (2003) have reported that with higher temperature, the boundary lubrication property of the serum reduces as the protein content precipitates thereby, increasing wear. Hence, the temperature was kept closer to the room temperature.

2.6.1 Specimen Preparation

2.6.1.1 Before the test

The femoral component and polyethylene specimen were first etched with identification numbers. Following marking they were cleaned with detergent solution. Ultrasonic cleaning of component and specimens were employed with iso-propanol/ water solution to clean the remaining contamination (Leeds Standard operating procedure). The polyethylene specimens were then placed in distilled water for a minimum period of 2 weeks to stabilise the water absorption in polyethylene. Two days prior to the test, the specimens were cleaned following the above standard operating procedure. Immediately after cleaning, the specimens were placed in controlled temperature and humidity conditions for 48 hours for stabilising.

Femoral components cemented to the mountings were cleaned using iso-propanol solution prior to the test as described in Chapter 2 Section 5: Station Assembly.

2.6.1.2 During the test

Serum was changed every 333,333 cycles. Serum was disposed or collected out of the bags before cleaning. The patella specimen, femoral components and their respective mountings were washed in a detergent to remove serum contamination. They were further soaked in Trigene for 10 minutes. Following soaking, the specimen were rinsed and dried with tissues and wiped clean with 70% iso-propanol/water solution before assembling it for the next third of a million cycles run as stated in standard operating procedure (Leeds Standard operating procedure).

2.6.1.3 Measurement intervals

After a million cycles were completed, the components and the mountings were completely disassembled. The serum obtained from the last third of a million

cycles was stored in containers for potential wear debris analyses. The patella specimens and femoral components were initially cleaned with detergent solution followed by soaking in 10 minutes with Trigene solution. Following soaking all the steps were repeated as described in earlier section. In addition, the patella specimens were cleaned in ultrasonic bath as described in Section 2.6.

2.6.2 Gravimetric

Gravimetric measurement technique is the most standard method of measuring mass loss of UHMWPE in wear simulation (McEwen *et. al* 2001; Affatato *et al.* 2002; D'Lima *et al.* 2003). In this test, the loss of mass was measured gravimetrically using a Mettler AT201 digital balance (Mettler Toledo Inc., Columbus, Ohio, USA) with resolution of 0.01mg (Davidson 1999).

2.6.2.1 Calibration

Calibration of the Mettler balance was performed annually to UKAS standard. Calibration was verified at each measurement point by using a cylindrical metallic specimen with known mass. The metallic specimen was used as a calibration specimen as moisture has no effect on the change in mass of the specimen.

2.6.2.2 Test specimen

The specimens were measured before starting the test and after a million cycles as specified in standard protocol for polyethylene (Standard Operating Procedure, Leeds University). To compensate for the error due to absorption of liquid, two soak specimens were included. The soak specimens were kept under same control temperature and fluid level as in the experiment. Soak and test specimens were measured until five readings with difference of ±50μg was obtained.

2.6.2.3 Analysis

The equivalent volume was calculated by using the density of medical grade polyethylene for patella specimens (ρ_{po}=0.935kg/mm^3). After the volume has been calculated for the patella specimen, the soak volumes were subtracted to get the actual volume independent of soaking. The volumes before and after the test were calculated based on equation 1 below.

$$Volume_i = Mass_i \times density \quad \ldots (1)$$

Where, i signify before or after the test, density is the ρ_{po} and mass is measured using AT201 digital balance.

Loss in volume (mm^3) was calculated by,

$$Volume_{loss} = Volume_{before} - Volume_{after} \quad \ldots (2)$$

The volume loss from the entire test was added to obtain cumulative volume loss for each specimen. The cumulative volume loss over the million cycles was plotted against number of cycles. Wear rate was calculated using gradient of cumulative volume loss over number of million cycles for all specimens. Mean wear rate was calculated based on five specimens with 95% confidence limit using slope function.

2.6.2.4 Statistical significance

One way ANOVA student t-test (p value) was conducted between different condition and tests to check the significance with significance taken at $p<0.05$. 95% confidence limits of the volume of all specimens after every million cycles was calculated.

2.6.3 MicroCT

Micro Computed topography (MicroCT), as shown in Figure 2-14, is a technique using x-ray to create three dimensional geometries. It was found the most reliable and accurate approach to determine the volume of retrieved

acetabular liners (Bowden *et al.* 2005; Bills *et al.* 2007). The MicroCT used in this investigation was a Scanco MicroCT80 (Scanco Medical, Busserdorf, Switzerland).

Figure 2-14 Scanco MicroCT80.

2.6.3.1 Calibration

The calibration for the scanner was performed weekly using calibration of phantom (QRM Quality Assurance in Radiology and Medicine, Germany). The phantom consists of five cylindrical inserts of various densities of calcium hydroxyapatite (CaHA). It was used for calibrating *in vivo* and *in vitro* polyethylene specimen. The densities found from the scan were compared with manufacturing specifications.

Threshold is the most important factor in image analysis (Ding et al. 1999; Fajardo et al. 2002; Hara et al. 2002; Kerckhofs et al. 2008). Threshold is defined as the number which differentiates the specimen from the background. The number is important for calculation of body mass index, volume and density. The threshold changes with variation of geometry, shape and light intensity. Using phantom calibration, the fixed value of threshold was not acceptable during scans based on past investigations (Kuhn *et al.* 1990, Sips *et al.* 2008). Hence, a methodology of calculating threshold at each scan was required. A calibration process during every scan was employed involving scanning a cylindrical polyethylene specimen with known volume of 936 mm^3 with every patella specimen. This volume was calculated in Image processing language (Scanco Medical Module, version V5.01a); an in-built software available in MicroCT. All the patella specimens were scanned

with a known calibration polyethylene specimen to ensure the threshold values for estimation of volume remained consistent with each scan. Based on known volume of cylindrical polyethylene specimen, a threshold was calculated. This threshold was then used for calculation of volume for all the patella specimens.

2.6.3.2 Test specimen

Prior to the measurement process in the MicroCT, the sample was measured gravimetrically. The MicroCT scans were taken at standard resolution of 36μm with the use of a 1024 x 1024 plane image matrix at 70kVp and current 114μA. Other settings (different current and voltage settings) were tested to identify the sensitivity of current and voltage settings in distinguishing the background and specimen. However, the 70kVp voltage and 114μA current were the best settings found from the sensitivity analysis. The samples were placed in poly (methyl methacrylate) specimen holder and positioned using packaging with foam to ensure stability during scans. The scans took approximately 90 minutes each and a minimum of 5 GB storage space. A scan of the sample was performed using X-rays which were assembled after the scan to be reconstructed into three dimensional greyscale images.

2.6.3.3 Volume Analysis

Volume Calculation

Image processing language (IPL) software was used for calculation of specimen volume, body mass index and density. For the current investigation, volumetric measurement was important. Using the IPL the volume of the sample was calculated by selecting the region of interest in the two dimensional slice. The threshold parameters and scaling values (sigma and support) were selected based on the greyscale image. The 'threshold' value was selected such that the pixel of the sample defined was classed as part of the object material. Everything apart from the pixel was considered as background and thereby removed from the volume calculation. The 'threshold' used was a user defined parameter; adding or

removing led to addition or deletion of pixels from the object boundary and hence affected the volume calculation. The threshold was an important factor which distinguished the specimen from the background. The other software parameter, Gaussian filters (sigma 1.2 and support 2), were selected to evaluate smoothing of the image noise (Eckhardt et al. EORS abstract, 2002; Wong et al. 2007; Ding et al. 2011). The scanning and analysing processes are illustrated in Figure 2-15 and the IPL commands are summarised in Table 2-1.

The in vitro specimens were scanned before and after the experimental simulation. Volume was calculated using IPL and the volumetric difference for each condition was plotted with reference to the gravimetric analysis.

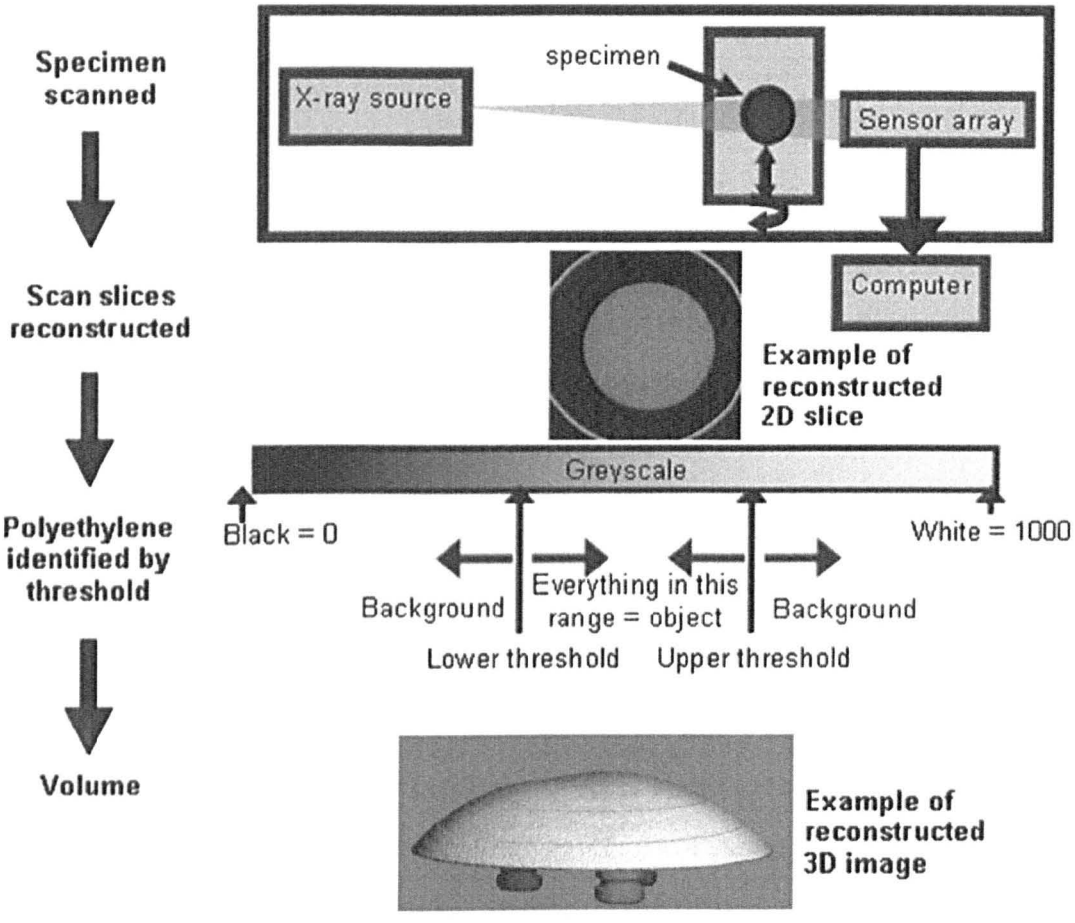

Figure 2-15 Schematic diagram of MicroCT procedure (Vicars *et al.* 2009).

Table 2-1 IPL commands for direct volume measurement

Step	Commands	Description
1	isq_to_aim	Converts *.ISQ file to *.AIM file
2	write (aim)	Write *.AIM to disk
3	gobj	Uses a '.gobj' file and cuts away the part of image not required to be analysed
4	gauss_seg	Segments the image based on threshold value. Below the threshold value is the image is background and above the threshold value the image is the object/specimen.
5	cl_ow_rank_extract	Extracts the largest volume from the segmented image. It removes and unattached particles.
6	examine	Summarises the output in form of largest volume obtained after segmentation.

2.6.3.4 Analysis

The total specimen volume was obtained from IPL in MicroCT. The volume obtained was plotted against gravimetric volume to assess the linear correlation between the two. The volume loss was calculated by subtracting the volume of the specimen after every million cycles from the original unworn volume. The mean volume was calculated from all five specimens and presented with 95% confidence limit.

2.6.3.5 Statistical significance

The total volume of each specimen and the volume loss during the experimental simulation presented in mean±95% confidence limit were compared with gravimetric measurements. The comparison was presented in linear correlation (R square). In addition, student t-test was conducted to check the significance between the results for $p<0.05$.

2.6.4 Geometrical Measurement

A co-ordinate measuring machine (CMM) *(Legex 322, Mitutoyo)* measured the specimen geometry producing a point cloud with a probe of size 1mm. The

resolution of this CMM was 0.01µm (Mitutoyo Legex 322 Catalogue). This method did not register the influence of fluid uptake or embedment of bone or metals. As this method depended on the surface, any creep deformation on the specimen surface was included in the measurement. Only a perfect spherical specimen could be analysed with the post processing software available (SR3D, Tribosol), which meant that the measurement was limited to spherical shaped patella buttons.

2.6.4.1 Calibration

A calibration was performed before every set of measurements with a ceramic calibration ball. Four points on the periphery were taken to calculate the probe dimension. Any error in the probe dimension was included in the specimen measurements.

2.6.4.2 Test specimen

The test specimens were cleaned with iso-propanol solution and dusted with compressed air to remove dust particles. Immediately after cleaning they were placed in the stainless steel holder as shown in Figure 2-16 for measurements. The holder had three peg holes to hold the patella with diameter ± tolerance as 7mm±0.2mm.

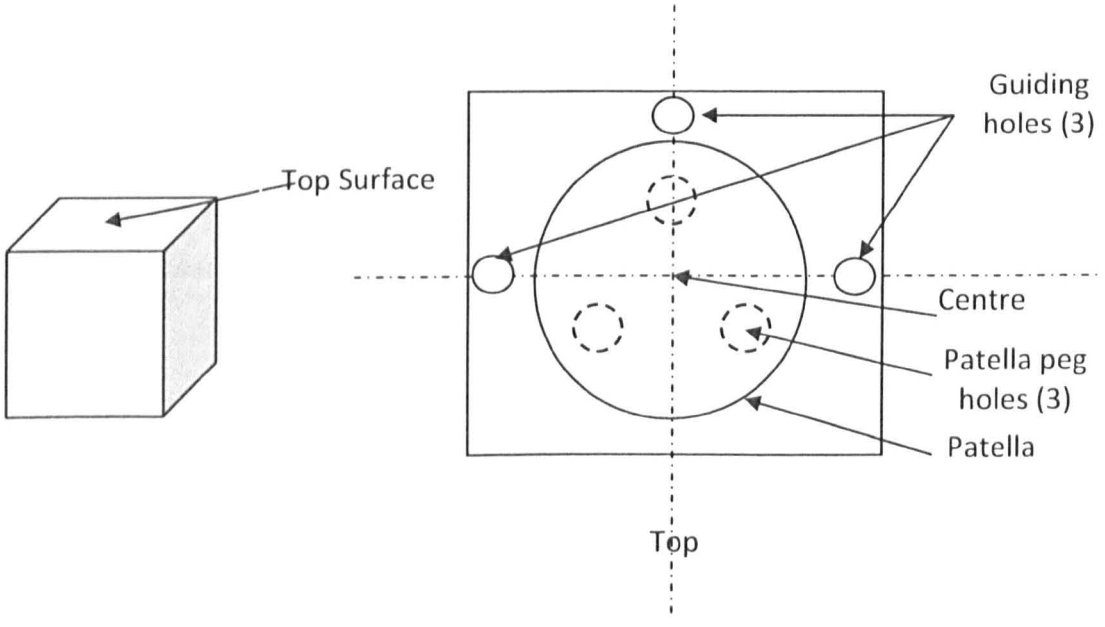

Figure 2-16 Holder for patella when used in CMM or Talysurf measurements.

The probe first selects the datum based on the three guiding holes of 4mm±0.2mm diameter ± tolerance and the top surface 50mm±0.2mm length ± tolerance from base. Once the datum was selected, the axis and the top point of the sample were identified considering the sample to be perfect sphere. Thirty six traces each of 48 points were measured around the patella i.e. every 10^{0} a trace was taken from the centre to the edge. The points were stored in the form of co-ordinates in a '.dat' text file. This method was used for both *in vitro* and *explants* volumetric calculation.

2.6.4.3 Analysis

The volume measurement analysis was carried out with SR3D software (Tribosol Ltd Pontefract, UK). The software read and created a surface based on the stored co-ordinate points from the '.dat' text file.

There were two different ways to calculate the volume loss of any *in vitro* samples or retrievals. They were either comparing the surface of whole specimen with complete pre-wear surface (known as reference comparison) or by creating a surface based on an unworn part of the specimen (known as unworn surface). Both these methods are explained below.

Comparison with pre-wear reference specimen

This method was applicable only for *in vitro* specimens with known pre-wear data. A pre-wear specimen was the reference and compared with worn specimen in SR3D software; the loss in volume was hence calculated.

Comparison with unworn surface

This method can also be used for explants or retrievals where the pre wear data was not available. This method used an unworn region for the 'reference'. The unworn region was taken as the reference and a nominal sphere was generated through surface-fit as shown in Figure 2-17. As shown in Figure 2-17, the white mesh/patch defined the area of reference. The olive region was the region of the worn surface. A complete nominal sphere was created based on the non olive area.

The difference between a nominal surface and surface was the volume change of the specimen.

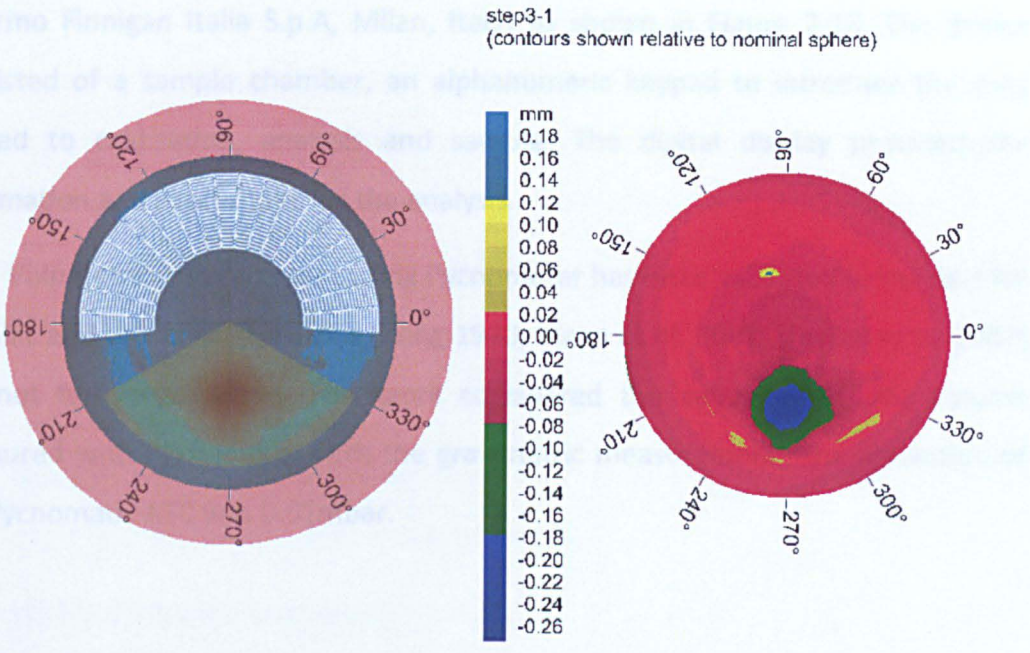

Figure 2-17 A typical wear scar of explants. The olive region is the region of interest and the white mesh depicting the unworn surface for reference.

The white mesh considered for creation of the nominal surface should completely cover the unworn region to accurately determine the volume.

The volume changes obtained from the two methods (MicroCT and CMM) were plotted against the gravimetric volume change.

2.6.4.4 Statistical significance

The total volume of each specimen and the volume loss during the experimental simulation presented in mean±95% confidence limits were compared with gravimetric measurements. The comparison was presented in linear correlation (R square). In addition, students t-test was conducted to check the significance between the results for $p<0.05$. A linear correlation between the two CMM methods and gravimetric was calculated. The two CMM methods were checked with student's t-test against each other.

2.6.5 Pycnomatic ATC

The helium Pycnometer used in this investigation was a Pycnomatic ATC (Thermo Finnigan Italia S.p.A, Milan, Italy) as shown in Figure 2-18. The device consisted of a sample chamber, an alphanumeric keypad to introduce the data related to calibration, analysis and sample. The digital display provided the information and procedures for the analysis.

Volumetric measurement using Pycnometer has been validated in the past for metallic and composite particles (Keng 1970; Viana *et al.* 2002; Lievers *et al.* 2007) but not for polyethylene. This work considered the validation of the volume measured with Pycnometer with the gravimetric measurement. The resolution of the Pycnomatic ATC was 0.01mbar.

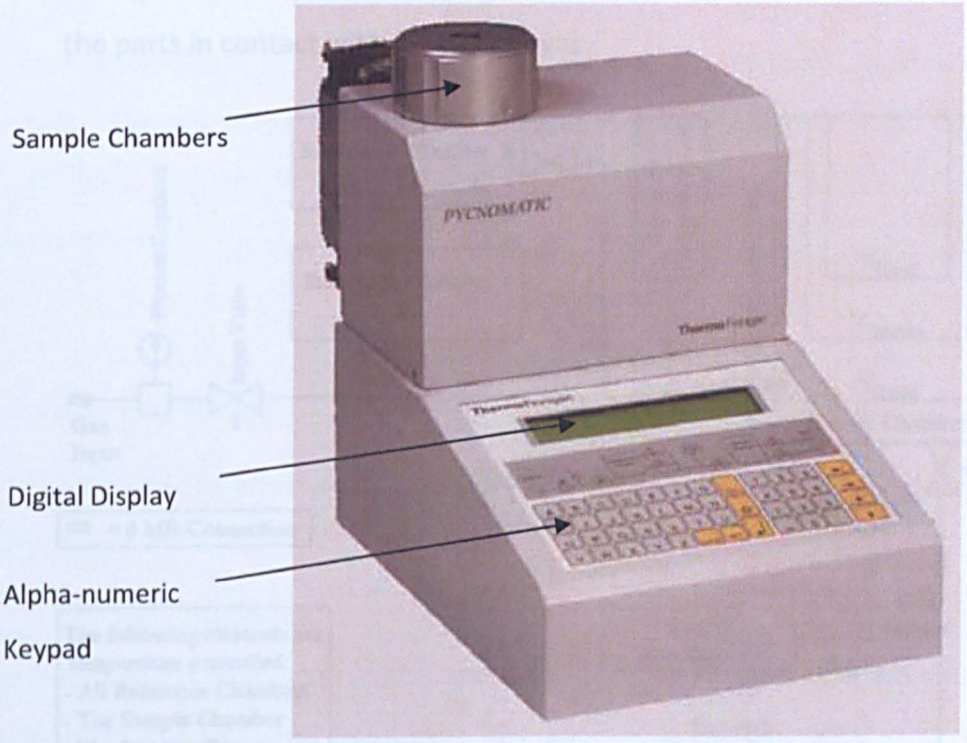

Figure 2-18 Image of Pycnomatic ATC helium gas Pycnometer (Pycnomatic and Pycnomatic ATC Instruction Manual 2007).

The aim of this investigation was to use the Pycnomatic ATC for volumetric measurement and compare with gravimetric measurements as a means for validation.

Pycnomatic ATC used 99.995% pure helium gas for the measurement of the volume of the sample by measuring the pressure change of helium in a calibrated volume based on Boyles pressure volume law (PV=constant). The schematic block diagram of Pycnomatic ATC is shown in Figure 2-19. The main components of the Pycnomatic ATC are

- reference calibrated volumes (Vr_I, Vr_{II} and $Vr_{III} = Vr_I + Vr_{II}$).
- three different calibrated volume reducers to analyse chamber volumes (Vc extra small, medium, large and extra large).
- absolute pressure transducer.
- three temperature sensors.
- a temperature control device to maintain constant temperature throughout the parts in contact with the helium gas.

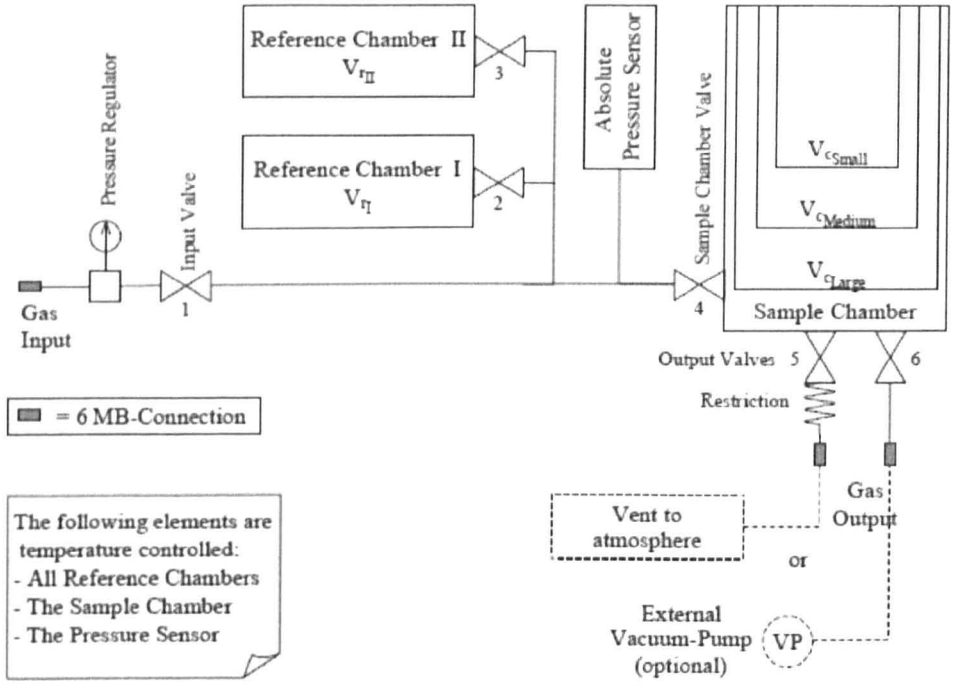

Figure 2-19 Schematic block diagram of Pycnomatic ATC (Pycnomatic And Pycnomatic ATC Instruction Manual 2007).

2.6.5.1 Calibration

The calibration was performed by inserting a calibrated ball in the chamber (60cc). The volume of the ball was inserted in the digital display. The chamber was closed to begin the cycle. The cycle started with helium passing through the system to remove atmospheric gas. The reference volume (Vr) was loaded with helium at an absolute pressure of 2bar higher than atmospheric pressure (Pycnomatic And Pycnomatic ATC Instruction Manual 2007). The pressure value (Pr) was recorded at this stage at a stable temperature. Valve 4 was opened and the helium gas expanded to the chamber volume (Vc) from Vr. The helium reached a pressure which was equivalent to the function of the empty space between the sample and the sample chamber. The pressure of the chamber (Pc) was recorded when the temperature was stable. Finally gas was discharged through valve 6. The Chamber Volume was calculated using *equation* 3

$$Pc * Vc = \mathrm{Pr} * Vr \qquad \text{....3}$$

The difference in Vc and the empty chamber volume gave the volume of the sample. The comparison to the volume obtained and the volume of the ball imported earlier was the error of the machine which was accounted for in further measurements.

2.6.5.2 Test specimen

The test specimen was first cleaned with iso-propanol solution and dusted with compressed air.

At the beginning the sample was placed in the sample chamber corresponding to the size of the specimen's diameter. The procedure similar to calibration was repeated five times. The average volume in the Pycnomatic ATC was displayed in the digital display after five successive readings.

2.6.5.3 Analysis and statistical methods

The volume change calculated from the Pycnometer was plotted with gravimetric volumetric measurements. A linear correlation was found. The volume of worn and unworn specimens was compared by students t-test analysis. The statistical approach (p value) was employed to evaluate the significance between the volume calculated by gravimetric and Pycnomatic measurements. A value of $p<0.05$ was deemed significant for the comparison (Lievers *et al.* 2007).

2.6.6 Surface Topography Measurements

Form Talysurf (Rank Taylor Hobson, France) is a contacting profilometer for measuring surfaces with 3.2nm resolution. Talysurf can be used over a small area depending on the range of movement of the stylus. The surface texture plays an important role in the wear process (Affatato *et al.* 2002). To understand the difference in surface in terms of deformation and roughness, Talysurf profile measurements were taken. Roughness measurements are required to evaluate the specimens for accepted roughness level. In the case of orthopaedic implants, the accepted standard value is 0.1μm for CoCr femoral components (ISO 7207-2:2011). After the test these measurements were required to determine the change in surface texture and relate these to the wear measurements. The following surface parameters were investigated before and after the wear test simulations:

Peak roughness (R_p): The roughness corresponds to the highest peak in any sampling length as shown in Figure 2-20.

Valley roughness (R_v): The roughness corresponding to the highest valley in a sampling length (Figure 2-20).

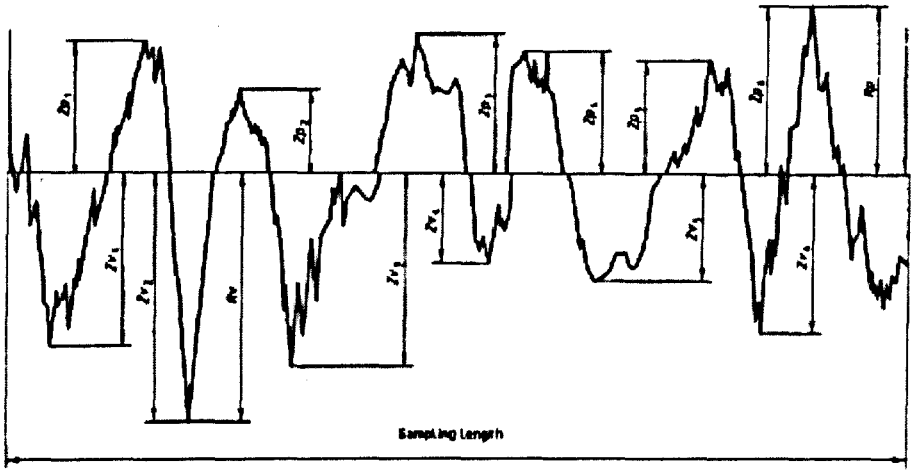

Figure 2-20 Profile showing peak and valley roughness over a sampling length. (ISO 4287:1997)

Average roughness (R_a): R_a is the arithmetic mean of deviation of profile from the average mean line within a sampling length (Flitney and Brown 2007). The average roughness is derived as shown in Figure 2-21, the mean height of the roughness profile from the mean line is termed as R_a.

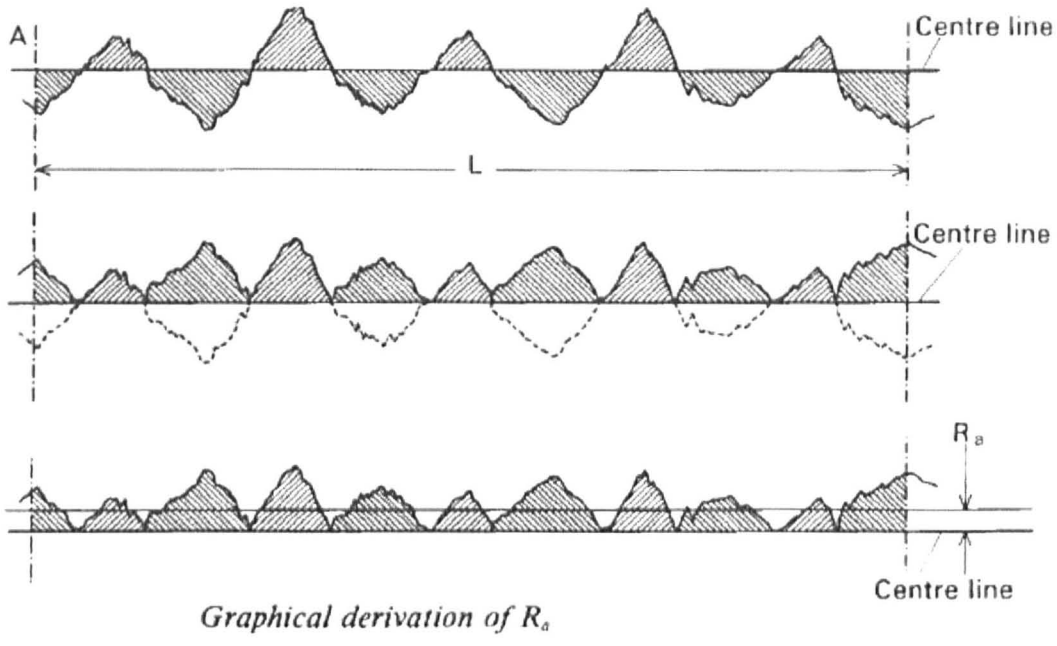

Figure 2-21 Profile showing average roughness over a sampling length (Flitney and Brown 2007). L: Sampling length

Skew roughness (R_{sk}): R_{sk} is a measurement of skewness. It signifies whether the surface is filled with peaks or valley or combination of both. A surface with peaks is considered positive skew and with valleys has negative skew roughness (Flitney and Brown, 2007).

2.6.6.1 Calibration

External calibration was performed annually by Talysurf. A Calibration check was performed using the stylus travelling in the measuring direction on a calibrated spherical ball to make contact at all points. The profile obtained determined the state of damage (if any) in the stylus. Calibration check was performed before every set of measurements.

Gauge linearity in terms of average roughness parameter (R_a) was calculated by measuring over a factory calibrated R_a patch. The variation of Ra from the measurement and the patch showed the accuracy of the stylus.

2.6.6.2 Test specimen

The test specimens were initially cleaned with iso-propanol solution and dusted with compressed air to remove dust particles.

Femoral Component

The highest point on the medial condyle of the femoral component was located as shown in Figure 2-22. This point was taken as the reference for all measurement. Five traces 25mm long of surface texture analysis were taken at spacings of 5mm in the inferior and superior direction as shown in Figure 2-22. The traces were saved in RAW format for analysis.

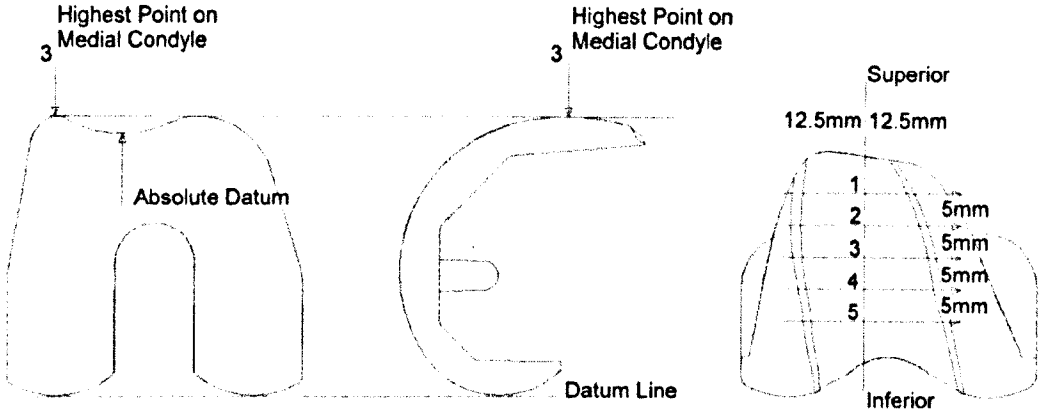

Figure 2-22 Surface texture analysis of a femoral component during measurement in Talysurf (Ellison 2007)

Patella Component

The patella was mounted on a fixture as shown in Figure 2-5 and placed under the Talysurf probe such that the patella wear scar was placed in the bottom half. The centre of the patella was obtained through the guiding holes present on the surface of the patella fixture. The centre of the patella was the reference for all the measurements. Four traces (three horizontal and one vertical trace) of 30mm length were taken as shown in Figure 2-23. The horizontal traces were taken every 9.5mm. All the traces were saved in RAW format.

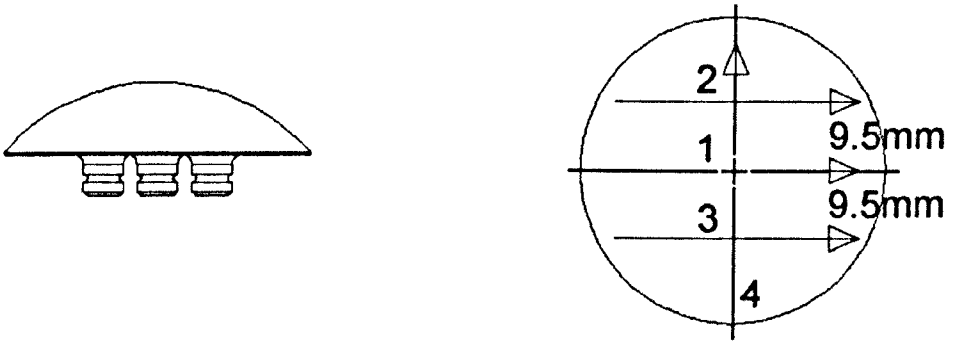

Figure 2-23 Surface texture analysis of a patella component during measurement in Talysurf (Ellison 2007).

2.6.6.3 Analysis

The RAW file (Figure 2-24) was analysed using LS arc for roughness calculation for femur and patella (Figure 2-25). Figure 2-25 shows the roughness parameters (Ra, Rsk, Rp and Rv) for a patella specimen. The deformation or the wear depth in patella was important and was calculated based on the RAW file using a primary LS arc (Figure 2-26).

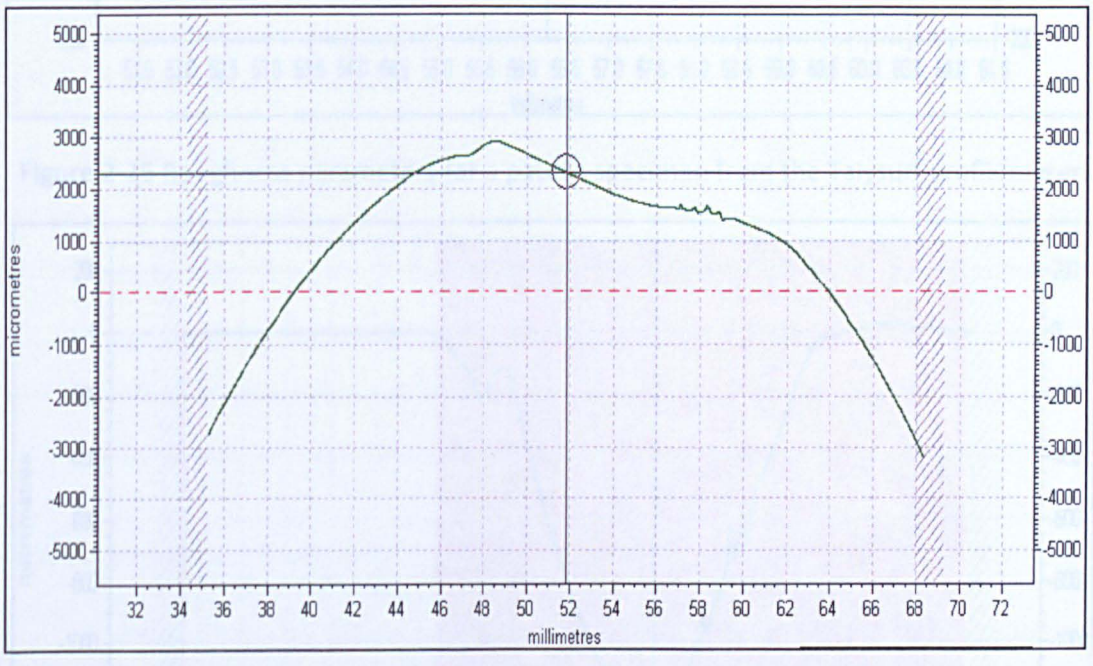

Figure 2-24 Raw file for patella specimen from the Talysurf profilometer.

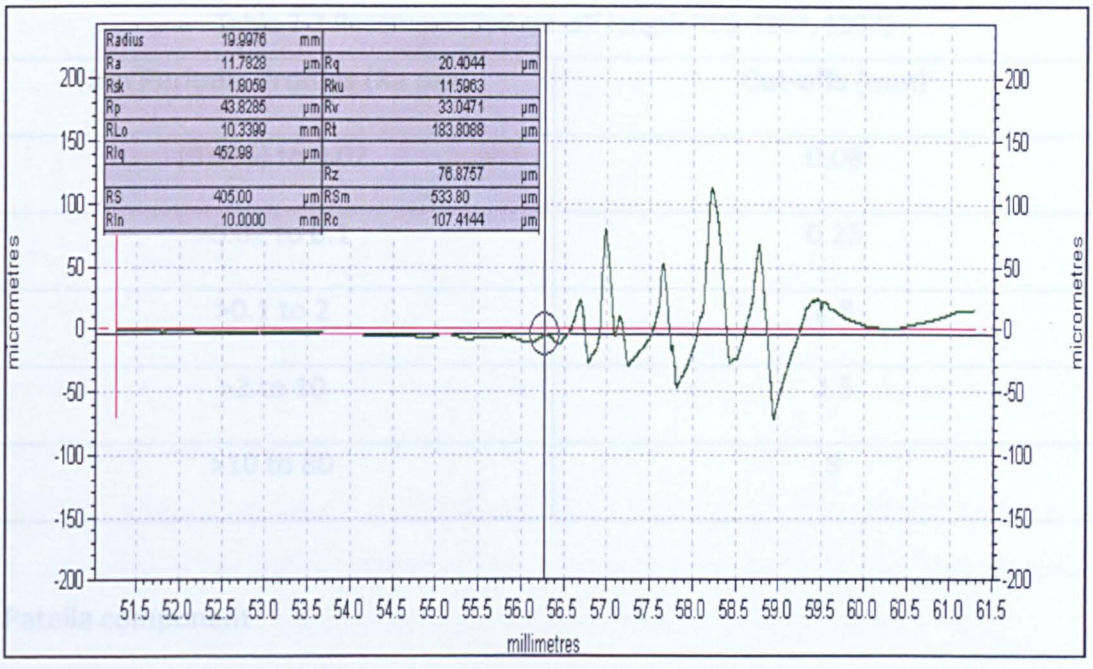

Figure 2-25 Roughness parameters for a patella specimen from the Talysurf profilometer.

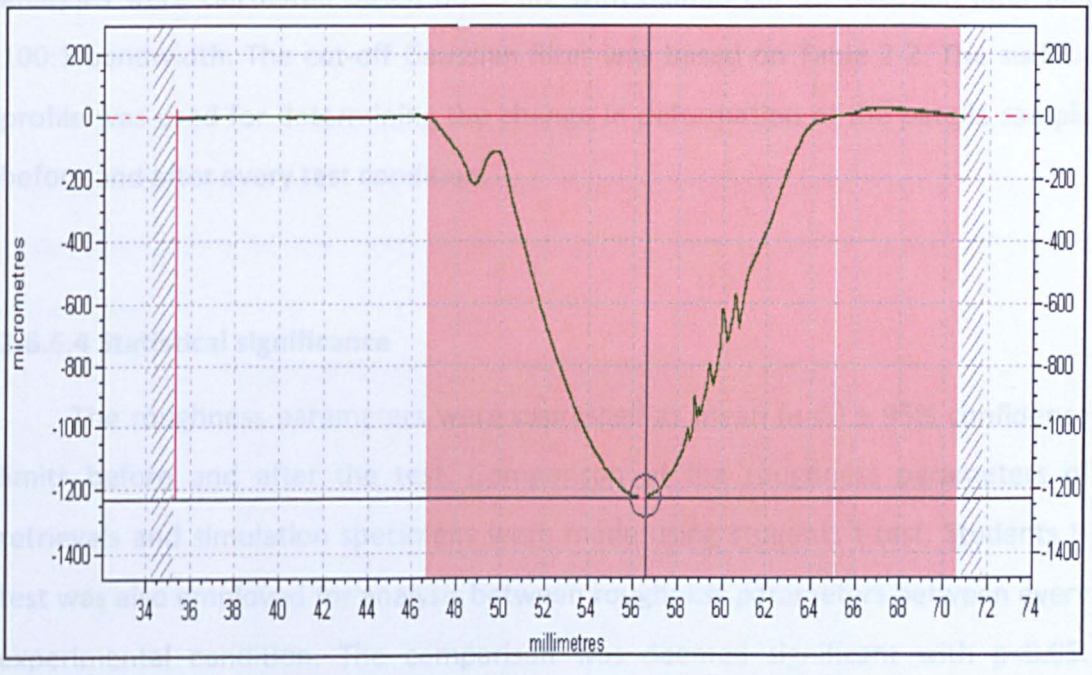

Figure 2-26 Deformation for a patella specimen from the Talysurf profilometer.

Femoral component

The surface texture was calculated based on LS arc with 0.25mm cut-off Gaussian filter and 100:1 bandwidth. The cut-off arc was based on the values of R_a after comparing with data of Table 2-2. The roughness (R_a) of the femoral component was obtained by averaging all the traces in the component.

Table 2-2 Recommended cut-off length (ISO-4287, 1997)

Non Periodic Profiles (Ra µm)	Cut-offs (mm)
(0.006) to 0.02	0.08
>0.02 to 0.1	0.25
>0.1 to 2	0.8
>2 to 10	2.5
>10 to 80	8

Patella component

Surface parameters and profiles were recorded for each trace. Both the analyses were calculated based on LS arc with 0.8mm cut-off Gaussian filter and 100:1 bandwidth. The cut-off Gaussian filter was based on Table 2-2. The surface profile was used for determining the change in deformation of the patella sample before and after every test condition.

2.6.6.4 Statistical significance

The roughness parameters were expressed as mean (n=5) ± 95% confidence limits before and after the test. Comparison of the roughness parameters of retrievals and simulation specimens were made using students t-test. Students t-test was also employed for analysis between roughness parameters between every experimental condition. The comparison was deemed significant with $p<0.05$. Linear correlation (R square) plots between the roughness parameters and time were calculated.

2.6.7 Two Dimensional Measurements (Wear Area and Wear Grading)

Two dimension measurements included measurement of wear scar area, percentage of area in quadrants and location of Centroid. These are important

characteristics when determining the shape and location of wear scar area as a comparison between *in vitro* specimens and retrievals.

2.6.7.1 Test specimen

The specimens (*in vitro and retrievals*) were initially marked with non permanent ink marking the boundaries of the wear scar. The specimens were divided into four quadrants so that medial, lateral, inferior and superior quadrant covered a fourth of the total area as shown in Figure 2-27. The marked specimens were captured in 'JPEG' format using a camera (Cannon SLR 80). The captured pictures were then imported in Image ProPlus (MediaCybernetics, MD, USA).

2.6.7.2 Calibration

Calibration of the images was performed using the scale present in the JPEG images. A line was drawn and total units defining the length of the line from the scale was added in the calibration system. All the specimen were calibrated separately.

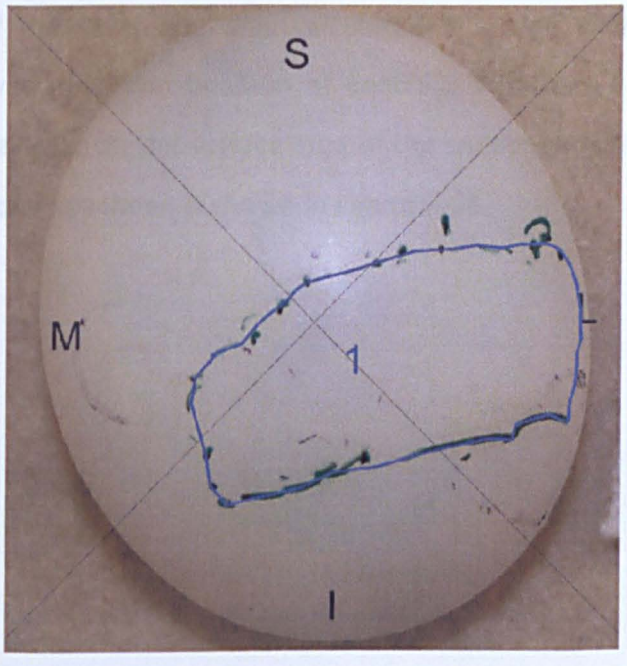

Figure 2-27 Figure showing marking of wear scar area and division of specimen into four equal quadrants (M-medial, S-superior, I-inferior and L-lateral).

2.6.7.3 Analysis

The analysis included marking the boundaries and calculating the total wear area and wear spread along different quadrants as described below:

Wear area

The wear area was calculated of the selected wear scar area in Image ProPlus. The wear scar area was measured three times for each specimen and represented as mean area in mm^2 and percentage of the total surface area (%). The wear area for all the specimens during the test was plotted against number of million cycles.

Percentage of wear area in quadrants

Similar to wear scar area, area spread over four quadrant was calculated individually in Image ProPlus. The areas in each quadrant for in vitro specimens were recorded for comparison with retrievals.

Centroid of wear area

Centroid of the wear scar was calculated in Image ProPlus. The unit for representation was mm. The position of centroid determined the position and spread of the wear scar on the surface area of the specimen over the quadrants. A typical centroid for a specimen is shown in Figure 2-28

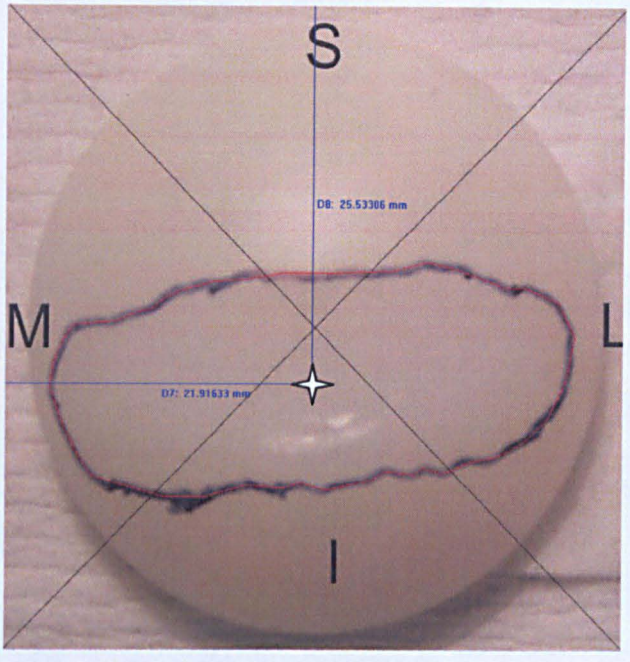

Figure 2-28 Position of centroid (star) in a patella specimen

2.6.7.4 Statistical methods

The mean area for all the *in vitro* specimens was presented with respect to the number of million cycles and the linear correlation (R square) was calculated. The wear scar area from the *in vitro* simulations was compared to the retrievals wear scar area to predict the validity of the *in vitro* simulations.

The distribution of area in every quadrant was compared with students t-test for significance. The variation of the area was plotted against time to investigate the gradual increment of area with time.

2.6.8 Wear Characteristics and Grading

The wear scar area was visually inspected and categorised for varied wear properties (Hood *et al.* 1983). The boundary of the wear scar area was marked using a non permanent marker.

The whole specimen was divided into four quadrants to ensure that the area in all quadrants remained constant as shown Figure 2-29.

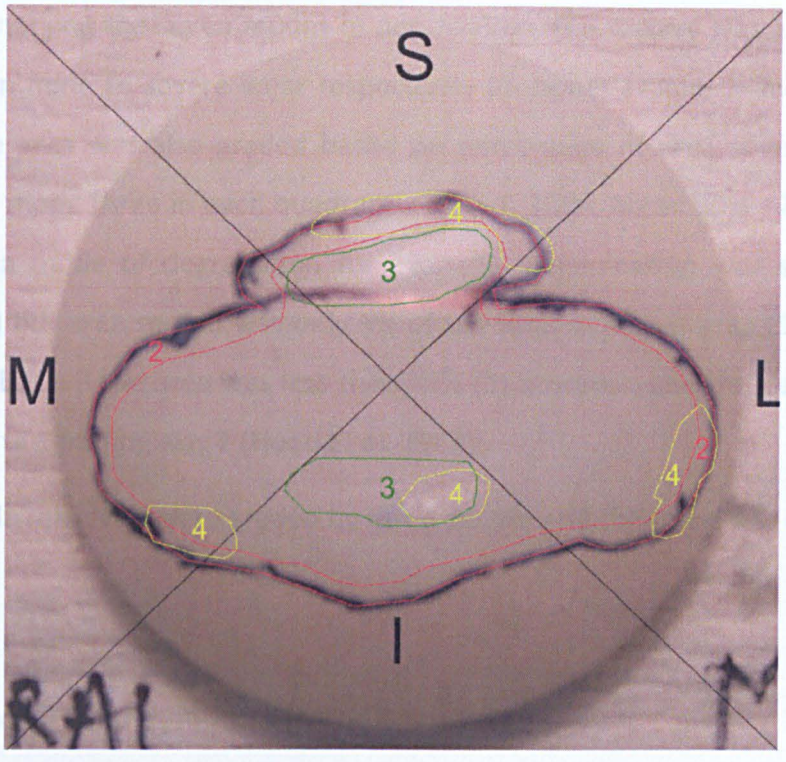

Figure 2-29 Schematic plot of division of the total area in four quadrants and marking the modes of wear degradation.

Seven modes of surface degradation were considered here namely, deformation, pitting, embedded poly-methyl methacrylate (PMMA) debris, scratching, burnishing, and abrasion. The different regimes of wear modes were characterised by identifying different modes of surface degradation as explained below.

- Deformation: Deformation caused on the articulating surface due to creep or cold flow of the polyethylene specimen.
- Pitting: Depressions on the polyethylene surface smaller in size and irregular in shape. The sizes varied from 2-3mm across and 1-2mm deep.
- Embedded PMMA debris: Wear debris from polyethylene surface embedded and protruded on the surface leading to rougher surface.
- Scratching: Indented lines on the surface of the polyethylene aligned parallel to the direction of anterior posterior displacement.
- Burnishing: Wear pattern where the surface formed was smoother and highly polished as compared to the original surface.
- Abrasion: Areas shredded due to contact with a bone

After marking the seven modes of degradation, the surface was graded from 0-3 based on none to severe wear respectively (0- none, 1- low, 2- moderate, 3- severe). The area was also graded based on percentage of area covered by the degradation mode (Area in each quadrant <10% -1, 10%< Area< 50% - 2 and area> 50% -3). If a mode of degradation for example, delamination was severe in a quadrant (3) but area spread was only 9% of the total quadrant area (1), then the grading will be 3. If the area was less than 50% (2) however, and the delamination was low (1), the grading was 2 (Hood *et al.* 1983).

All the patella retrievals were graded by three people and the score was recorded.

2.7 Multi body solid dynamics (MBSD) model

A three dimensional model of the Leeds knee simulator was created in IDEAS NX (Siemens, Texas, US). The CAD drawing of the femur was obtained from DePuy (DePuy International, Leeds, UK). The patella specimen was scanned before and after the experimental simulation in MicroCT and images in form of 'dicom' files were exported. The image files were imported to SCANIP (Simpleware software, IN) directly to MSC Adams/VIEW R3 (MSC.Software Corporation, CA) to investigate the variation of kinematics with a change in geometry of the specimen. The flowchart explaining the steps from reconstruction of model in SCANIP is shown in Figure 2-30.

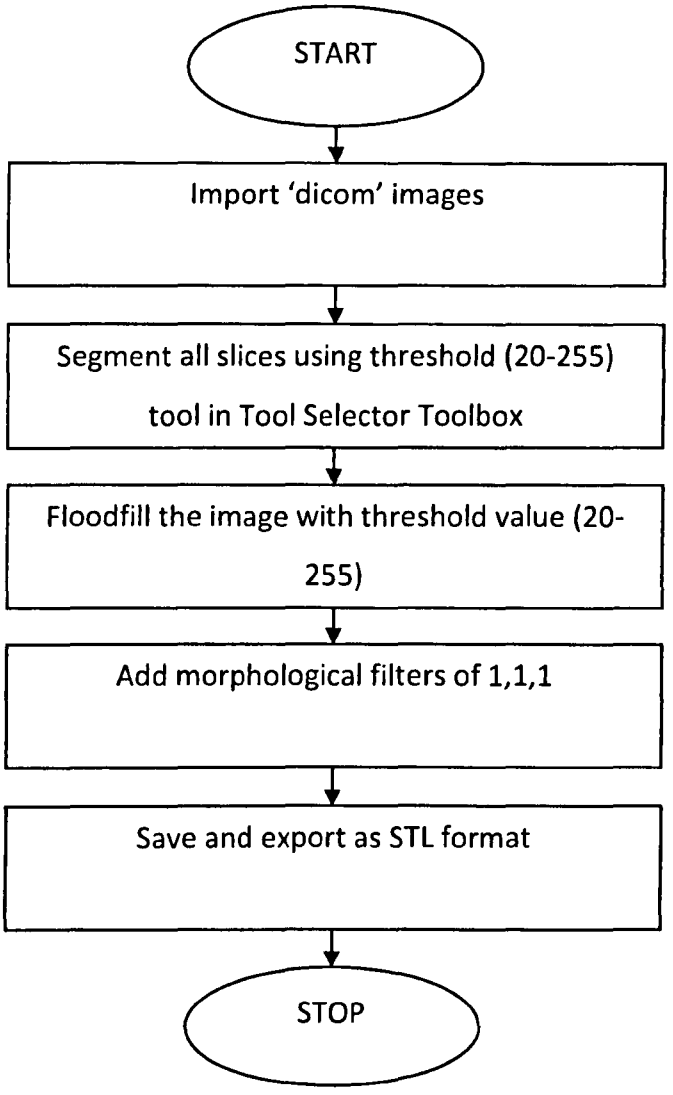

Figure 2-30 Flowchart depicting the procedure of importing specimen scans from MicroCT to Adams/VIEW for in vitro analyses.

The images in 'dicom' files were imported in SCANIP software for reconstruction. The images were segmented in grey scale with minimum threshold 20 and maximum threshold 255. Anything between threshold 20 and 255 was considered part of specimen, the rest was considered to be background and was not included in reconstruction as shown in Figure 2-31

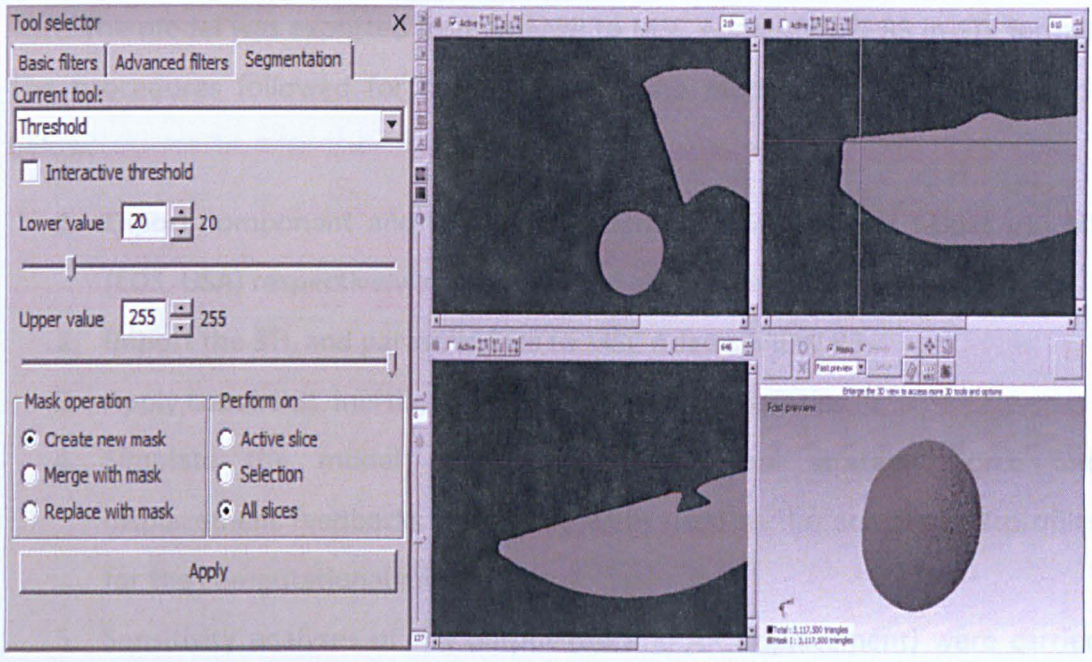

Figure 2-31 Segmentation of threshold in grey scale with threshold ranging from 20-255.

The segmentation was followed by floodfilling the image to change from grey scale to coloured image. This was required for image to be distinguished from background at coloured scale. This was followed by smoothing the edges of the specimen using morphological filters of 1,1,1 in x,y and z axes respectively as shown in Figure 2-32.

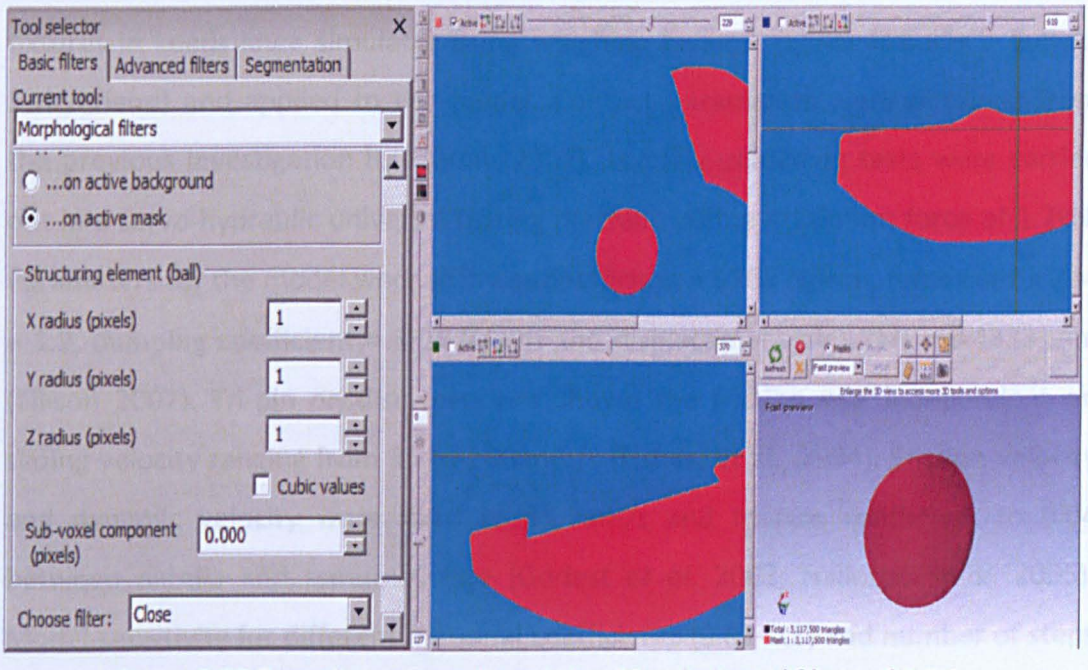

Figure 2-32 Smoothing of specimen using Morphological filters of 1,1,1.

The model was exported from SCANIP to MSC Adams/VIEW R3 in STL format. The procedures followed for construction of the model are briefly highlighted below.

1. Export component and simulator design from SCANIP and I-Deas v11 NX (EDS, USA) respectively in STL and parasolid format.
2. Import the STL and parasolid files to MSC Adams/VIEW R3.
3. Apply constraint, inertia, friction and material properties.
4. Simulate the model under simulator control strategy. Force and displacement feedbacks for patella were used as the actual input profiles for the computational model.
5. Sensitivity analyses of the output (tilt and AP displacement) were carried out by varying frictional coefficient (0.01-0.1), time steps (100-1000) and percentage of input kinematics (95-105%).

All connecting fixing links between the fixtures/parts were modelled as perfect unions. No additional movements were observed between the fixtures, this assumption was an ideal case which makes the model simple for analysis. The revolute links and translational links were considered frictionless for simplicity. The station centre of gravity and the moment of inertia were measured from the fixtures in Leeds knee simulator using weighing balance (KERN FTB 35K1, Eyholz, Switzerland) and applied to the model. Contact parameters were obtained from the previous investigation by Ellison (2007). Loading-unloading tests were carried out in a servo-hydraulic universal testing machine with a maximum force of 1.2kN. Parameters for the model were stiffness coefficient = 5702 N/mm, force coefficient = 1.9, damping coefficient = 35.4 N/mm and displacement at 1.2kN = 0.4333 mm (Ellison 2007). Tri-pin on disc tests has shown the friction was independent on sliding velocity ranging from 35 to 240 mm/s (Fisher, et al., 1994). Stiction velocity and dynamic velocity were fixed to 35 mm/s and friction coefficient to 0.04 between patella and femur surface (Godest *et al.* 2002; Halloran *et al.* 2005). Model sensitivity for different frictional coefficients (0.01-0.1) and number of steps were considered. The sensitivity to ±5% change in input kinematics was considered to get a range of output profiles and dependency on inputs.

The assumptions to simplify the model are listed below.

1. All bodies were considered to be rigid
2. Patellofemoral contact was represented as spring damping element based on simple elastic impact algorithm.
3. All joints had zero friction except the patellofemoral joint contact.
4. All fixtures were manufactured without consideration of tolerance.
5. There was no material loss due to surface wear.
6. All materials were considered to be homogeneous.

2.7.1 Calibration

Calibration was performed by linking the outputs from the computational model to experimental simulation at constrained ML displacement. The outputs were matched by changing the load acting on the lateral side of outer cradle which represented the ligament load.

2.7.2 Analysis and Statistical Significance

The output kinematics in form of ML tilt, AP displacement and ML shift were plotted against percentage of gait cycle. Students t-test was performed between the experimental simulation output and computational kinematics for significance ($p<0.05$) at uncontrolled ML shift. The change due to geometry of the specimen were analysed and significance between worn and unworn specimen were investigated.

2.8 Retrieval Analysis and Measurement Techniques

This section describes the investigation of evaluating the wear characteristics of retrievals. Retrieval characteristics are required to relate them to *in vitro* wear characteristics.

2.8.1 Retrieval Preparation

The explants were obtained from surgeons from various hospitals as detailed in Section 2.3. After removal the retrievals were sterilised by soaking in 10% neutral buffered formalin for a period of 48 hours. Following soaking the retrieval specimen were cleaned for tissue using detergent solution. Following the procedure, the specimens were passed on to the university. The same procedures were followed in the university. Finally, the specimens were cleaned with iso-propanol solution and left to dry for 48 hours at controlled temperature prior to the measurements. During handling, care was taken to avoid damage to the retrievals.

2.8.2 Measurement Techniques

As the pre wear data for the retrieval specimens was not known, the specimen volume was measured using the CMM as detailed in Section 2.6.4. The surface analysis was performed in Form Talysurf as reported in Section 2.6.6. The wear scar analysis and area calculation were performed as described earlier in Sections 2.6.7 and 2.6.8.

2.8.3 Analysis and Statistical Significance

After the measurements, the volume change was compared with the in vitro specimen for justification of the experimental simulations. The data obtained from both retrieval and experiments analyses were compared using Student t-test. The wear depth and roughness were linearly correlated (R square) with number of implant years. The CMM images for oval and round dome patella were compared with the in vitro specimens for modes and locations of wear.

Chapter 3: Computational Modelling of Patella Femoral Kinematics during Gait Cycle and Experimental Validation

3.1 Introduction

Investigation of the *in vitro* kinematics using computational modelling and validation against experimental studies is detailed in this chapter. A computational model can provide robustness in the design before manufacturing thereby reducing the development time and cost associated with manufacturing. The other benefits are the prediction of kinematics associated with different designs and possible explanation of the change in contact between the mating specimens *in situ*, which are difficult to understand *in vivo* or *in vitro*. This validation also acts as an important step towards the development of a wear model.

The aim of the investigation was to formulate a computational model to predict the patella femoral kinematics and validate it using experimental results. Further, the objective of the current study was to evaluate an explicit kinematics study (computational and experimental) for predicting the motion between round/oval dome patella and PFC sigma knee at two femoral radii of rotation during constrained and uncontrolled medial lateral (ML) displacements. The detailed objectives for the computational model are listed as follows.

1. Design of the femur and patella mounting in accordance with the existing knee simulator.
2. Adopt the control strategy by Ellison and co authors (2008) and modify as per the simulator specifications.
3. Modelling for kinematics at different femoral radii of rotation and validating against experimental results. This supported the rationale for choosing the radius for the simulator studies.
4. Modelling for kinematics for worn and unworn patella buttons and comparing with experimental results. The controlled motions for the computational model were axial load, superior inferior displacement, flexion extension and

medial lateral rotations. The medial lateral tilt, medial lateral and anterior posterior displacements were passively controlled.

5. Predicting and comparing the kinematics of different shapes of patella button - round and oval dome.
6. Comparing the kinematics output with previous listed sources of data.
7. Sensitivity analysis of the kinematics for specific changes in the control strategy.

3.2 Materials and Methods

The materials used in the modelling purpose are detailed in section 2.7. The design of mountings and fixtures are listed in Chapter 2 Section 5. The control strategy for the computational and experimental analyses is shown in Figures 2-10 to 2-13. The kinematics profile used was chosen to represent the physiological behaviour of the patella during the complete gait cycle. All the input data were displacement control except the axial load or anterior posterior load with closed loop feedback acting through the centre of the patella. This was needed to avoid over constraining the model which can result in unrealistic joint loads. The control of axial load as force controlled had an additional benefit of controlling the contact force between the mating components as outlined in Archard's wear equation (Archard 1953). Two radius of rotation R_1 and R_2 (Figure 3-1) were used for experimental and computational models to investigate the change in kinematics at different radii of rotation. The radius of rotation R_1 was taken on the basis of the inner groove dimension where the patella articulates with the PFC sigma knee. Another radius of rotation R_2 considered in this investigation was based on that of a previous investigator (Ellison *et al.* 2008). The radius R_2 was taken as the average of radius of femoral condyles and radius of rotation; R_1. A ligament load with 2N was applied on the lateral side of the cradle to act as a ligament force restricting ML displacement.

Two cases of ML displacement were considered; one being constrained and the other uncontrolled translation. Two designs of patella button were used; oval

and round dome patella buttons. The output kinematics of tilt, anterior posterior displacement and medial lateral displacement were investigated based on shape and restrictions in ML displacements. The effect of a worn specimen on tilt was investigated compared to an unworn specimen.

The schematic diagrams of a single station of the knee simulator in experimental and computational studies with degrees of freedom are shown in Figure 3-2.

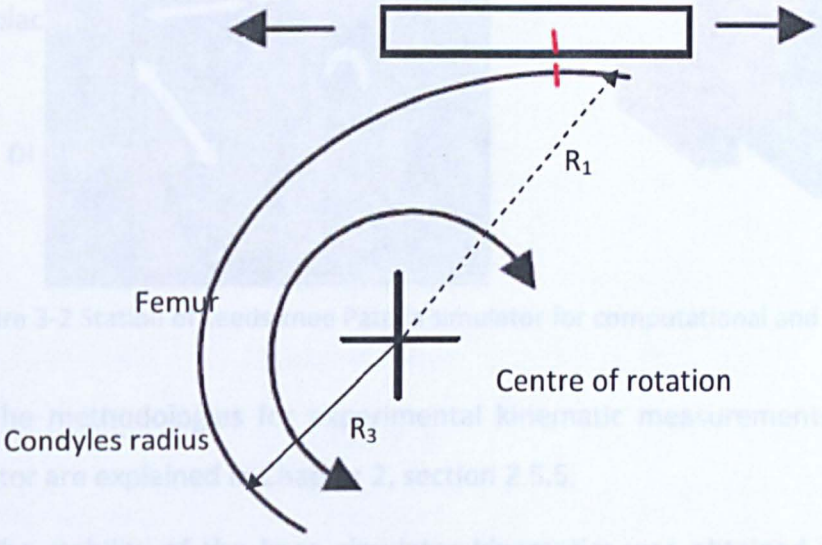

Figure 3-1 Schematic diagram of femur component showing radius of patella mating (R_1), radius of condyles (R_3) and R_2 is the average of R_1 and R_3.

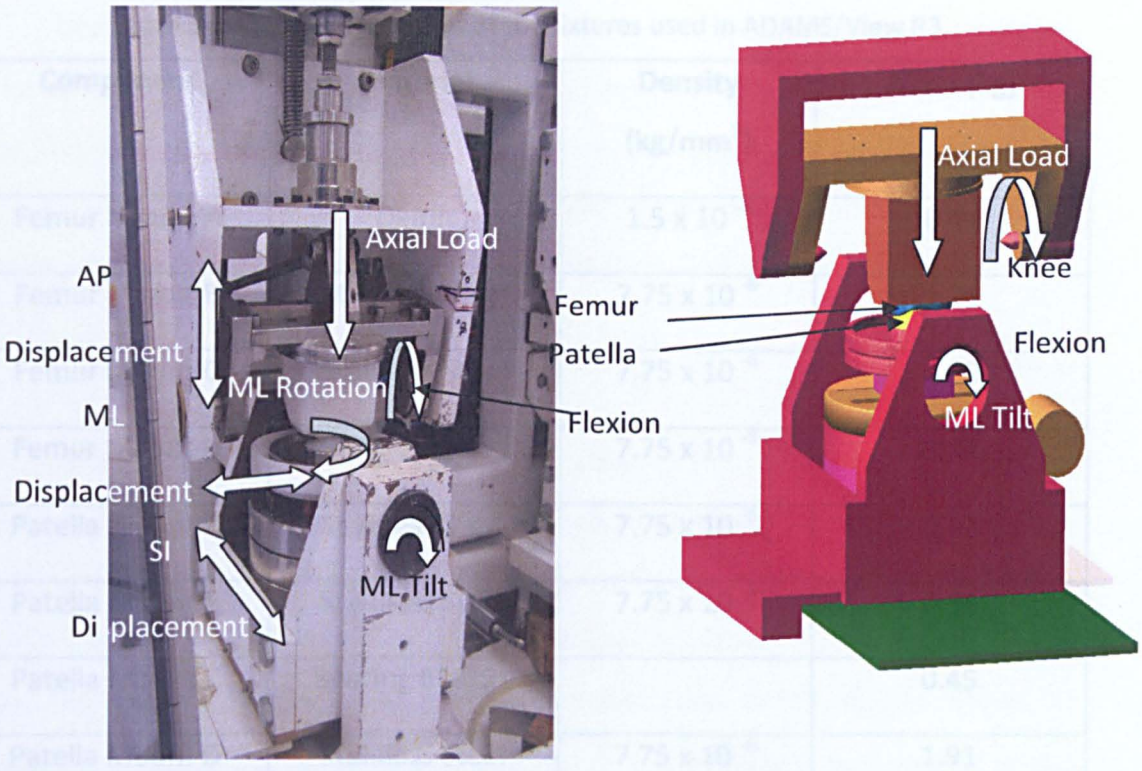

Figure 3-2 Station of Leeds knee Patella simulator for computational and experimental studies.

The methodologies for experimental kinematic measurements in the knee simulator are explained in Chapter 2, section 2.5.5.

The stability of the knee simulator kinematics was obtained after the first thousand cycles. Three measurements in the experimental model were taken after every 1000 cycles and presented with mean ± 95% confidence limits.

3.2.1 Multi Body Solid Dynamics (MBSD) Model

A three dimensional model of the Leeds knee simulator was created in IDEAS NX (Siemens, Texas, US). The CAD drawing of the femur (PFC Sigma) knee model was obtained from DePuy (DePuy International, Leeds, UK). The patella was scanned in MicroCT and transferred to MSC ADAMS/View R3 (MSC.Software Corporation, CA) after reconstruction in SCANIP (Simpleware software) as detailed in Chapter 2 Section 7. The material properties of the fixtures were obtained using weighing balance (KERN FTB 35K1, Eyholz, Switzerland) as shown in Table 3-1. The mass was included in ADAMS/View R3.

Table 3-1 Material properties of the fixtures used in ADAMS/View R3

Component	Material	Density (kg/mm^3)	Mass (kg)
Femur Mount A	Delrin	1.5×10^{-6}	0.49
Femur Mount B	Stainless Steel	7.75×10^{-6}	1.21
Femur Mount C	Stainless Steel	7.75×10^{-6}	4.00
Femur Mount D	Stainless Steel	7.75×10^{-6}	10.00
Patella Mount A	Stainless Steel	7.75×10^{-6}	0.42
Patella Mount B	Stainless Steel	7.75×10^{-6}	0.53
Patella Mount C	Bearing BM20K		0.45
Patella Mount D	Stainless Steel	7.75×10^{-6}	1.91
Patella Mount E	Stainless Steel	7.75×10^{-6}	2.31
Patella Mount F	Stainless Steel	7.75×10^{-6}	0.28
Patella Mount G	Stainless Steel	7.75×10^{-6}	2.80
Patella Mount H	Stainless Steel	7.75×10^{-6}	0.60
Outer Cradle	Stainless Steel	7.75×10^{-6}	12.00

3.2.1.1 Patella femoral contact

The contact between the mating parts; patella and femoral; was modelled based on standard collinear elastic algorithm present in ADAMS/View. The algorithm was based on the following assumptions (Johnson 1985)

- The contact was quasi static. The transfer of mass was ignored in the contacting bodies.
- The mass of the body acted at the centroid and moved with constant velocity
- Hertzian contact occurred at a local area rather than the whole bulk of material.

These assumptions led to the contact between two components represented by a spring element in a static solver. The spring element ensured contact between the two components. In a dynamic solver, an additional damping element was present. The two elements together stabilised the load transmission in any two mating components represented by Equation 1 (MSC.Software 2008).

$$F_n = k\delta^e + C\frac{d\delta}{dt} \qquad \text{(Equation 1)}$$

Where, F_n is the force acting perpendicular to the contact surface, k is the stiffness coefficient, δ is the penetration depth of one body on the other equals x-x_1 (Figure 3-3), e is the Meyer's index; force coefficient expressing linearity of the contact and C is the damping constant expressed in terms of initial C_o, maximum C_{max} damping coefficients, and maximum penetration depth δ_{max} as shown in Equation 2. The damping coefficient ensured that stability was not created at the initial contact of the mating components.

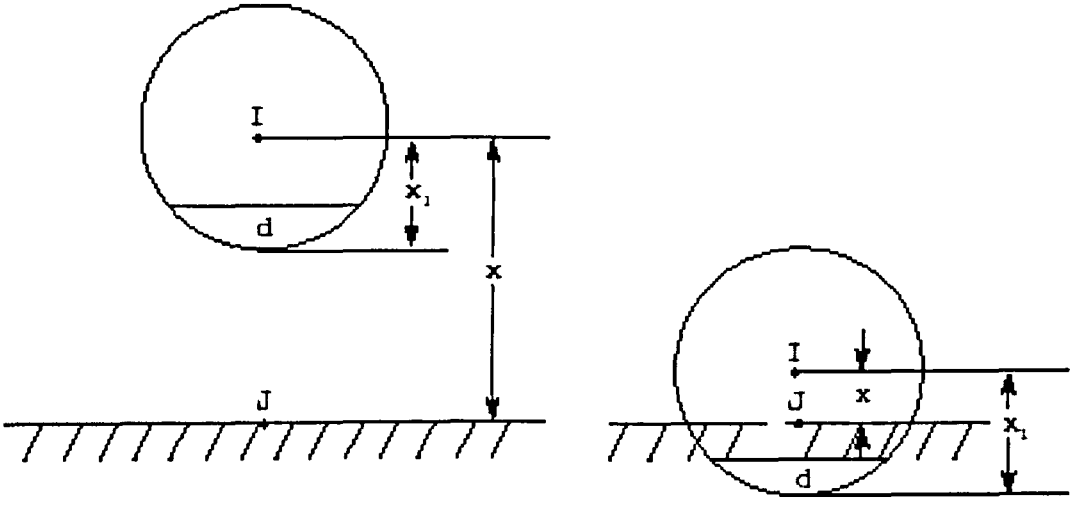

Figure 3-3 Contact model between two mating components (I and J); with I penetrating in J (MSC.Software 2008).

$$C = \begin{bmatrix} \delta \le 0 : C_o \\ 0 < \delta < \delta_{max} : C_o + (C_{max} - C_0)\left(\frac{\delta}{\delta_{max}}\right)^2 \left(3 - 2\left(\frac{\delta}{\delta_{max}}\right)\right) \\ \delta \ge \delta_{max} : C_{max} \end{bmatrix} \qquad \text{(Equation 2)}$$

3.2.1.2 Contact parameters

The contact parameters were predicted using load displacement testing by Ellison and co authors (2008). The testing was carried out on a servo hydraulic universal testing machine with 20kN subcell (Dartec, UK). The patella component was aligned to the femoral groove to obtain maximum conformity. Load was applied and released at 150N/s and deformation in the patella button was observed. The values of stiffness coefficient k, force coefficient e, and maximum deformation of patella surface at 1200N load δ_{max} were calculated using curve fitting of load deformation curve (Figure 3-4) and using first function of Equation 1 (neglecting the damping function).

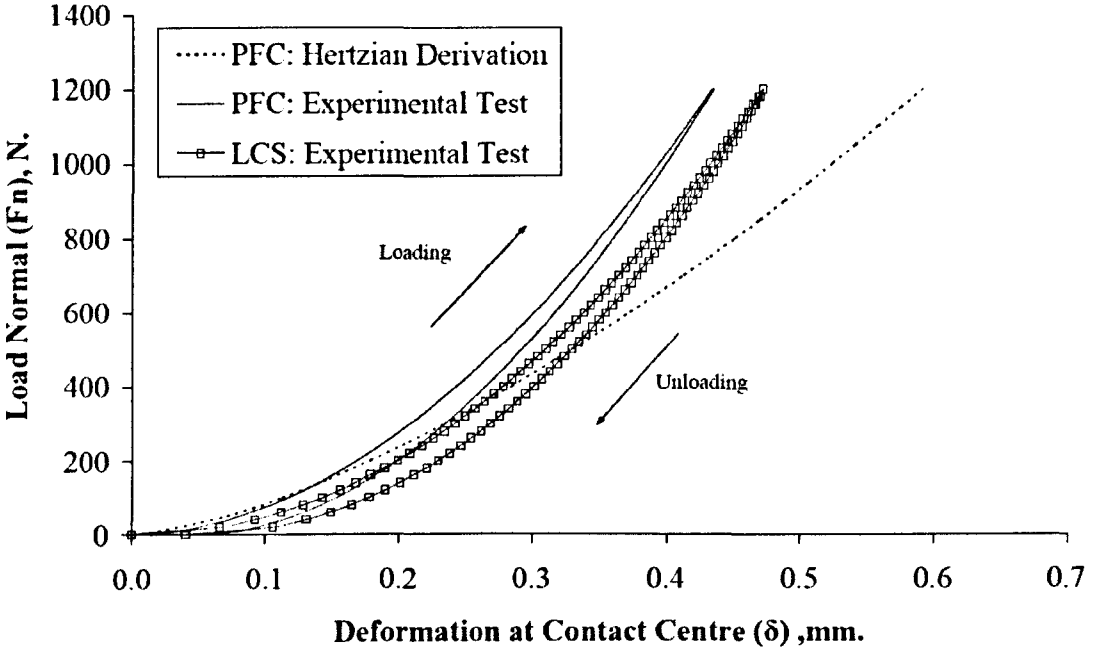

Figure 3-4 Load deformation hysteresis curve for PFC sigma round dome patella and low contact stress (LCS) with mobile bearing (MB) patella (Ellison 2008).

The maximum damping coefficient was found by Equation 3 (Rao 1995), where hysteresis damping constant (h) was assumed approximately equal to C_{max}, ΔW was the energy dissipated found by calculating the area enclosed between the loading and unloading hysteresis curve.

$$\Delta W = \pi h \delta_{max}^{2} \qquad \text{(Equation 3)}$$

As the radius of curvature in the round dome and oval dome were same (38mm), the value for stiffness coefficient (k) 5907.2 N/mm, force coefficient (e)

1.9, displacement at maximum load (δ_{max}) 0.433 mm and maximum damping coefficient (C_{max}) 35.4 N/mm were kept the same for both the oval and round dome patellae in the computational simulation. The sensitivity analysis based on stiffness, force and damping coefficients were performed on the kinematics.

3.2.1.3 Contact friction

The contact friction between the patella femoral mating surfaces was represented in the form of standard Coulomb friction algorithm in ADAMS/View. The values of static (μ_s), dynamic (μ_d) friction coefficients and velocities at which the friction acted V_s and V_d respectively were determined from fundamental tests carried out with a tri-pin disc experiment (Fisher et al. 1994). The friction between the UHMWPE and femoral component were found independent of the velocity ranging from 35 to 240 mm/s. Based on the test and previous computational literature, the friction coefficient and the velocity were set to 0.04 and 35mm/s respectively (Fisher *et al.* 1994, Godest 2002, Halloran *et al.* 2005).

3.2.2 Sensitivity Analysis

Sensitivity analyses of the output (tilt and AP displacement) were carried out by varying frictional coefficient (0.01-0.1), time steps (100-1000), contact parameters (95-105% change in contact parameters) and percentage of input kinematics (95-105%) in the computational model.

3.3 Results

The validity of the model was obtained from comparison of computational outputs with the experimental results. The kinematics were not sensitive to the time step. The kinematics modelling was based on surface contact rather than material contact, hence, the mesh sensitivity was not performed. Hence the model was validated by comparing computational and experimental results.

3.3.1 Comparison of Kinematics at Different Radii of Rotation

The kinematic trends from the computational model showed consistency with the experimental predictions. The medial lateral (ML) displacement for constrained displacement is presented in Figure 3-5 with 95% confidence limit (CL). The uncontrolled case of medial lateral displacement considered free translation in both directions is as shown in Figure 3-6. The ML displacement followed the flexion extension trend with maximum amplitudes of 1.6 and 4.5mm of medial displacement obtained for constrained and uncontrolled ML displacement respectively at R_1 radius of rotation. The maximum peaks were obtained at the highest flexion angle during the swing phase. There was a large difference between the computational and experimental ML displacement of the radius of rotation R_2. The ML displacement was lower for R_2 when constrained.

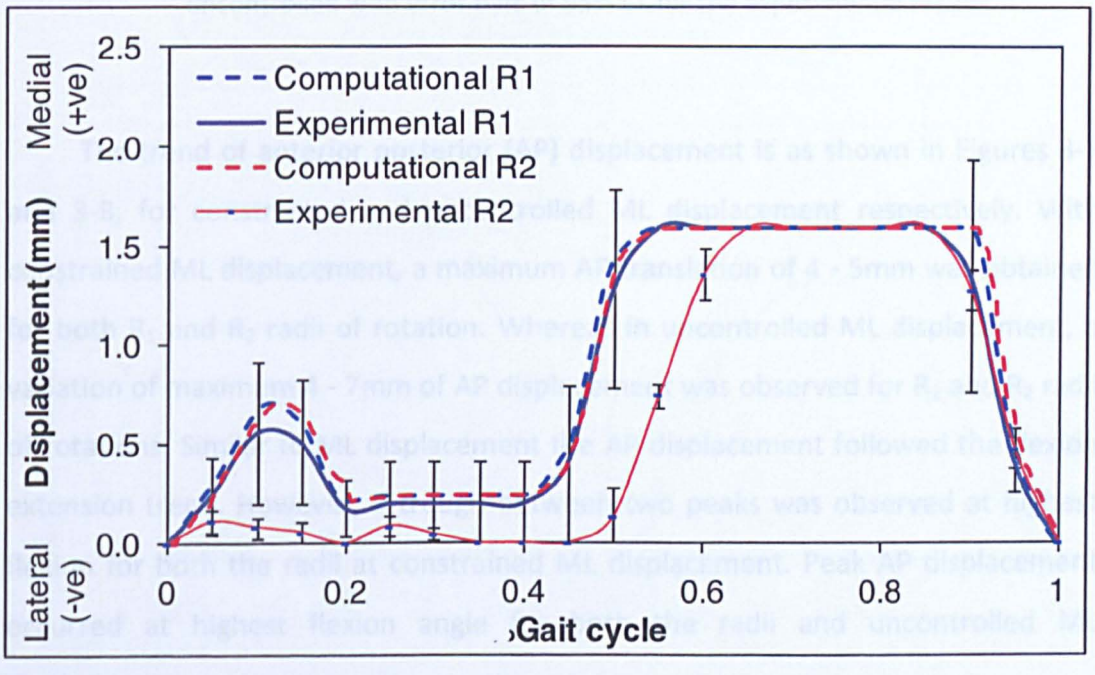

Figure 3-5 Medial lateral displacement for different radius of rotation (R_1 and R_2) when constrained with errors bar of 95% CL for the experimental results.

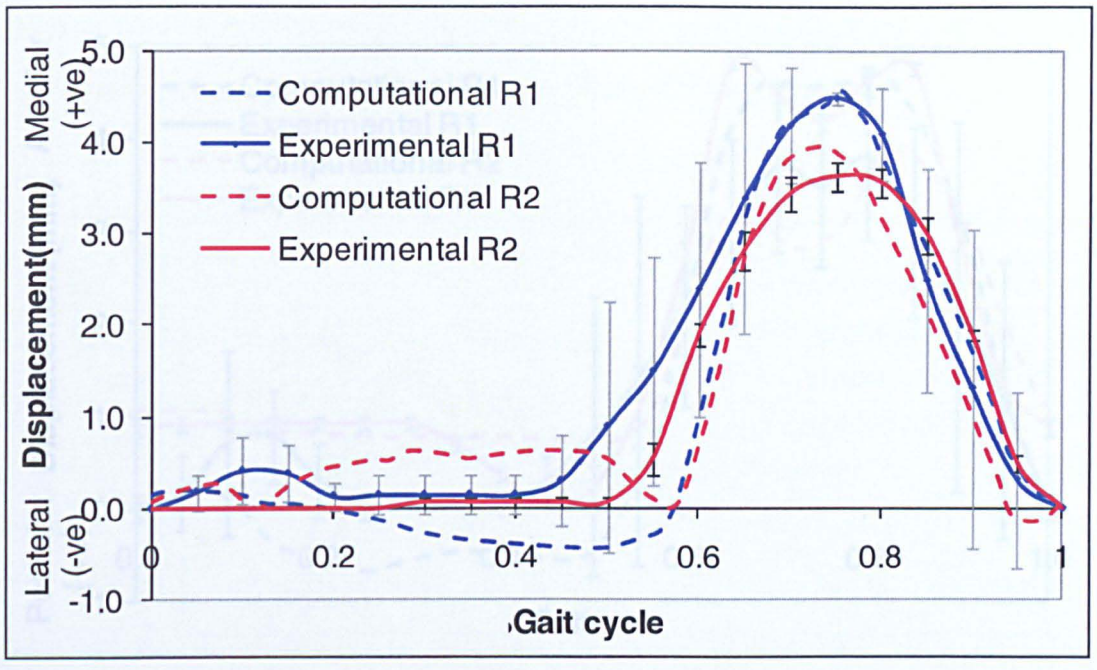

Figure 3-6 Medial lateral displacement for different radius of rotation (R_1 and R_2) when uncontrolled with error bars of 95% CL for the experimental results.

The trend of anterior posterior (AP) displacement is as shown in Figures 3-7 and 3-8, for constrained and uncontrolled ML displacement respectively. With constrained ML displacement, a maximum AP translation of 4 - 5mm was obtained for both R_1 and R_2 radii of rotation. Whereas in uncontrolled ML displacement, a variation of maximum 4 - 7mm of AP displacement was observed for R_1 and R_2 radii of rotations. Similar to ML displacement the AP displacement followed the flexion extension trend. However, a trough between two peaks was observed at highest flexion for both the radii at constrained ML displacement. Peak AP displacement occurred at highest flexion angle for both the radii and uncontrolled ML displacement.

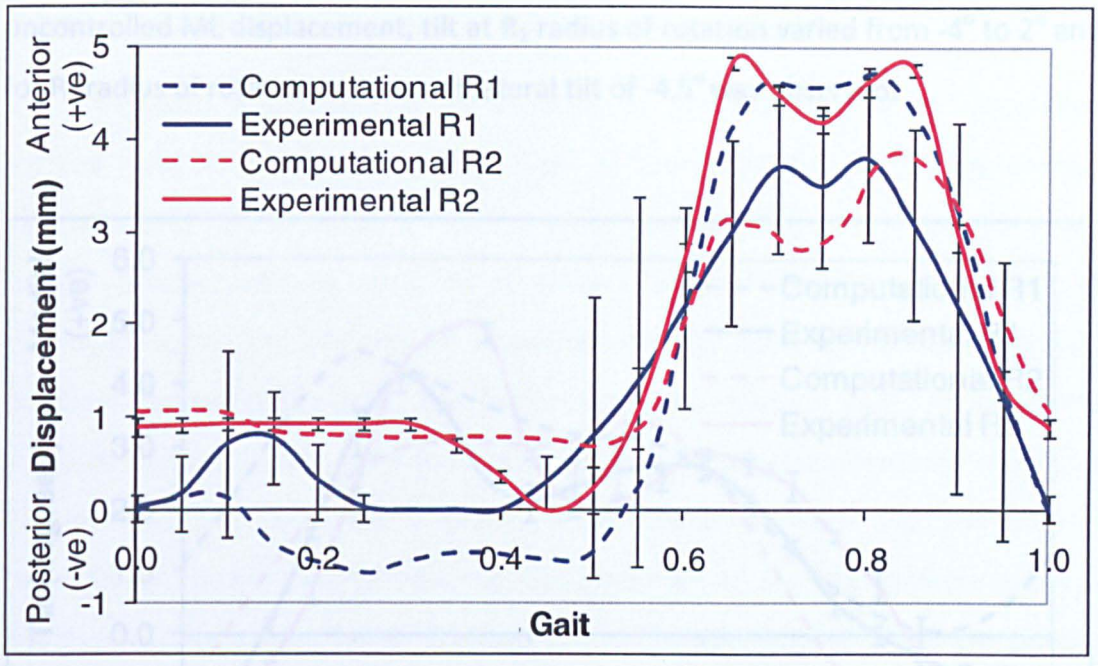

Figure 3-7: Anterior Posterior translation at different femoral radius of rotation (R_1 and R_2) when ML displacement was constrained with error bars of 95% CL for the experimental results.

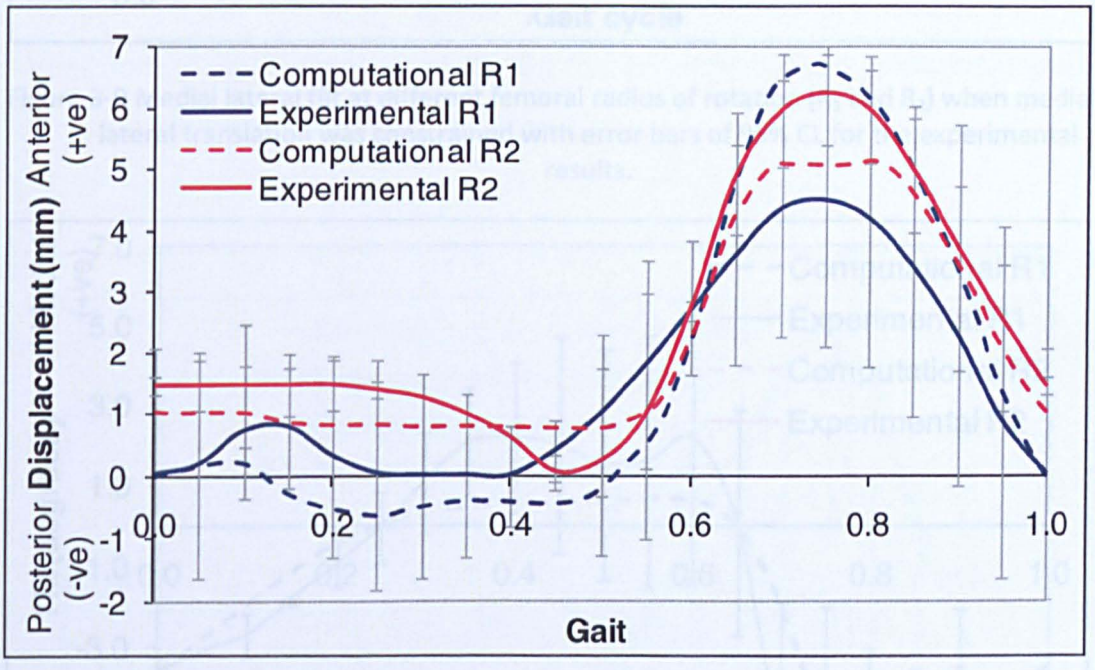

Figure 3-8 Anterior Posterior translation at different femoral radius of rotation (R_1 and R_2) when ML displacement was uncontrolled with error bars of 95% CL for the experimental results.

Tilt (shown in Figures 3-9 and 3-10) was dependent on ML displacement. At constrained ML displacement, a variation of maximum tilt (4-5°) was noticed for both the radii of rotation. Two peaks of 3.5° and 2.5° were obtained at 20% and 60% of the gait cycle for R_2 radius of rotation at constrained ML displacement. With

uncontrolled ML displacement, tilt at R_1 radius of rotation varied from -4° to 2° and for R_2 radius of rotation, a constant lateral tilt of -4.5° was observed.

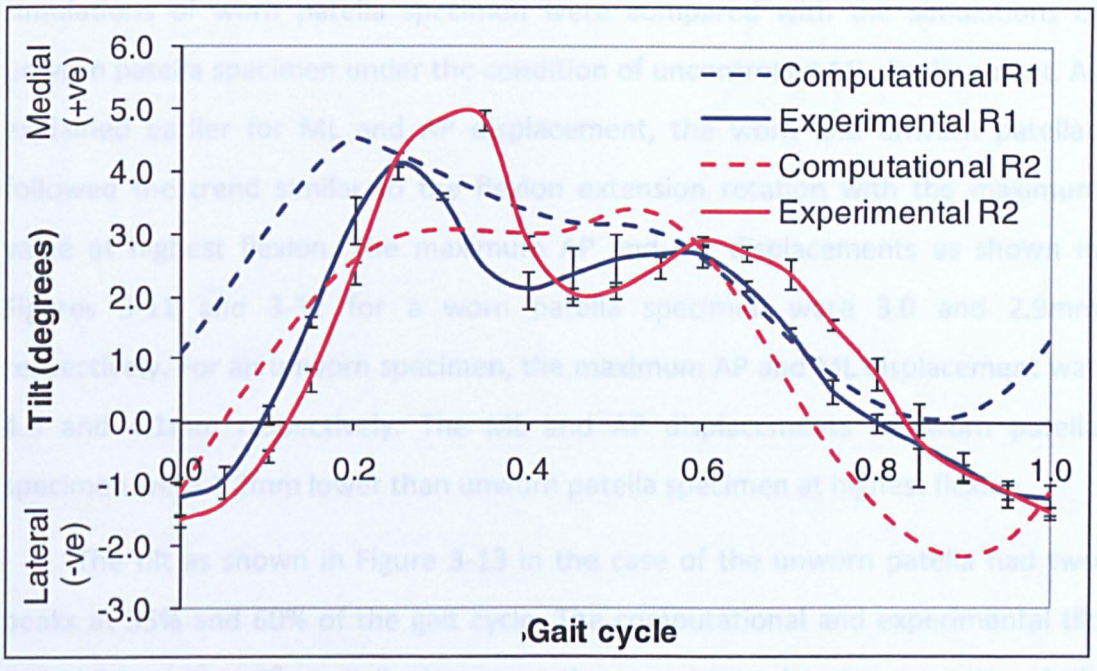

Figure 3-9 Medial lateral tilt at different femoral radius of rotation (R_1 and R_2) when medial lateral translation was constrained with error bars of 95% CL for the experimental results.

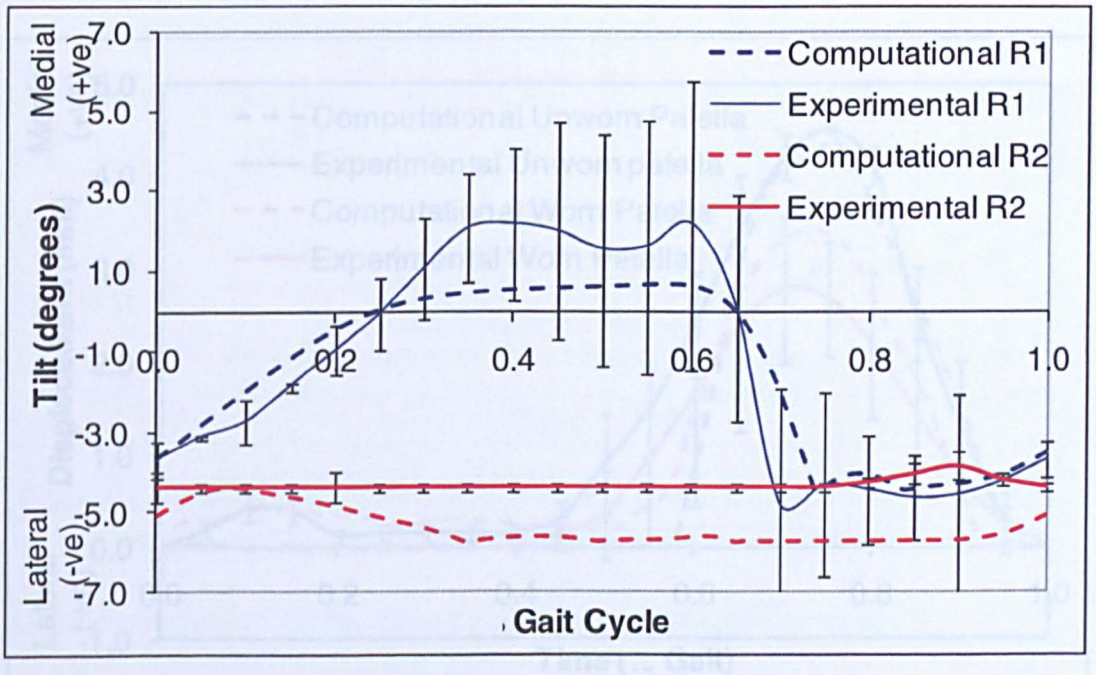

Figure 3-10 Medial lateral tilt at different femoral radius of rotation (R_1 and R_2) when medial lateral translation was uncontrolled with error bars of 95% CL for the experimental results.

3.3.2 Comparison of Kinematics for Unworn and Worn Patella

The worn specimen had deformation in the inferior side of articulating surface due to wear test. Kinematics of computational and experimental simulations of worn patella specimen were compared with the simulations of unworn patella specimen under the condition of uncontrolled ML displacement. As explained earlier for ML and AP displacement, the worn and unworn patellae followed the trend similar to the flexion extension rotation with the maximum value at highest flexion. The maximum AP and ML displacements as shown in Figures 3-11 and 3-12 for a worn patella specimen were 3.0 and 2.9mm respectively. For an unworn specimen, the maximum AP and ML displacement was 4.3 and 4.1mm respectively. The ML and AP displacements for worn patella specimen were 1.2mm lower than unworn patella specimen at highest flexion.

The tilt as shown in Figure 3-13 in the case of the unworn patella had two peaks at 35% and 60% of the gait cycle. The computational and experimental tilt varied from -4° to 2° medially. However, the experimental and computational tilt for worn patella was constant 2° of lateral tilt.

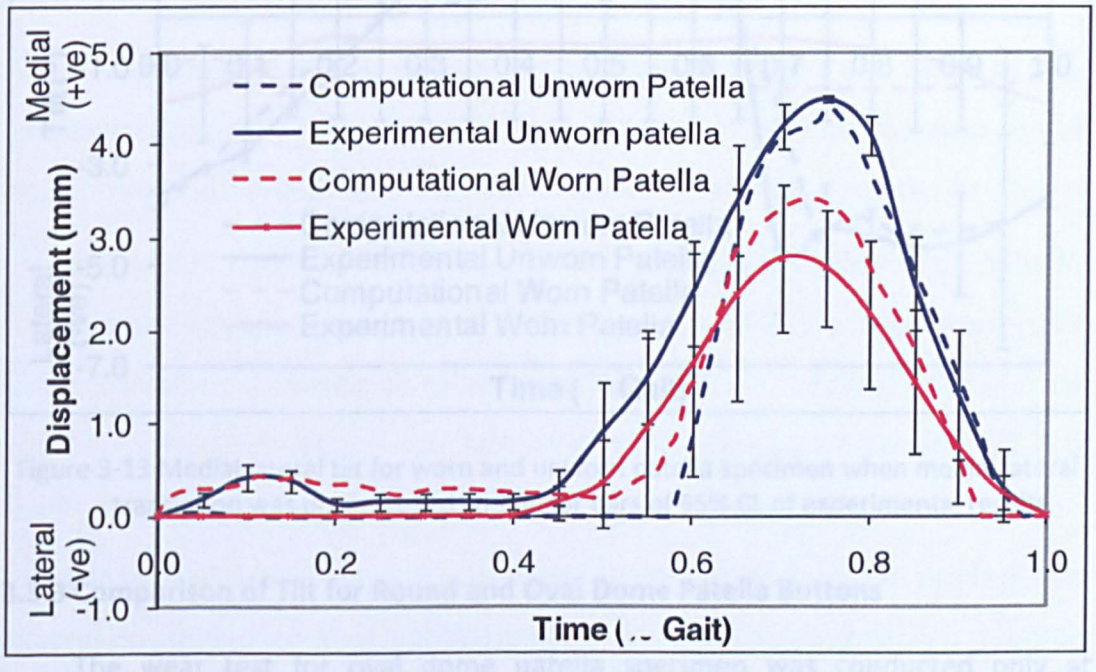

Figure 3-11: Medial lateral displacement for worn and unworn patella specimen when medial lateral translation was uncontrolled with error bars of 95% CL for the experimental results.

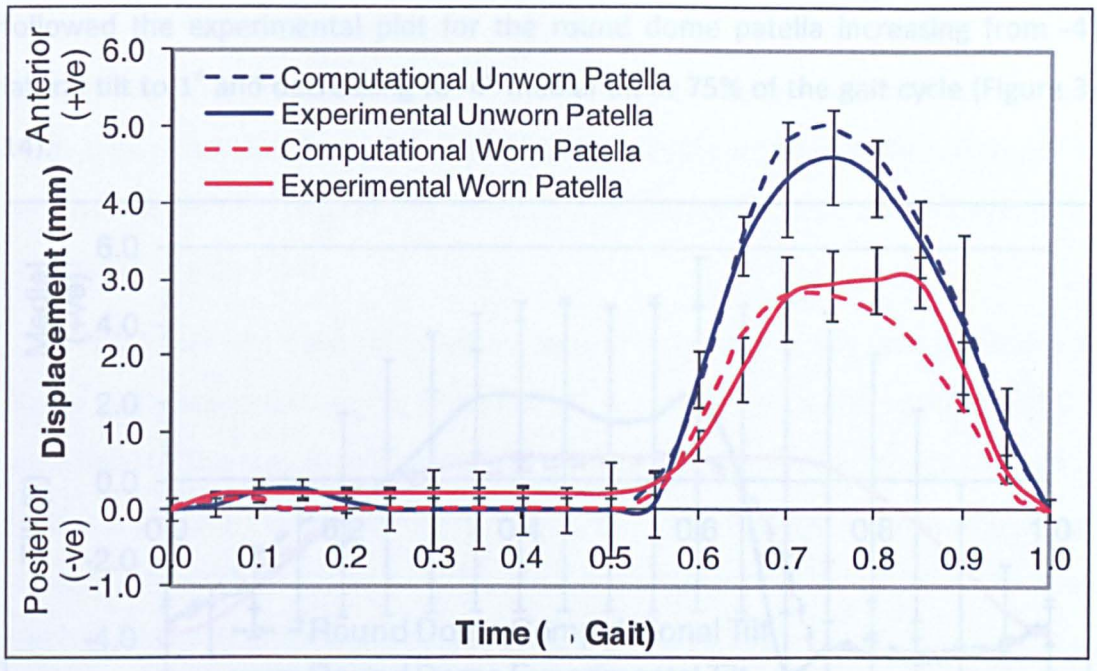

Figure 3-12 Anterior posterior displacement for worn and unworn patella specimen when medial lateral translation was uncontrolled with error bars of 95% CL for the experimental results.

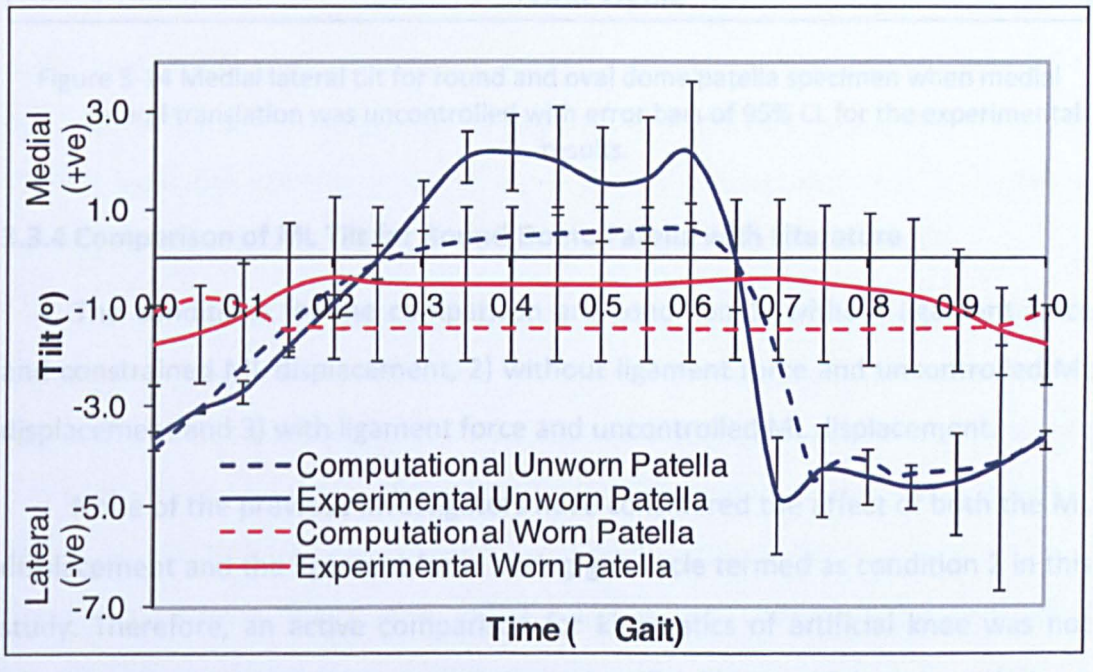

Figure 3-13 Medial lateral tilt for worn and unworn patella specimen when medial lateral translation was uncontrolled with error bars of 95% CL of experimental results.

3.3.3 Comparison of Tilt for Round and Oval Dome Patella Buttons

The wear test for oval dome patella specimen was conducted only at physiological scenario; hence the ML displacement was kept uncontrolled for comparison of round and oval dome specimens. Both the computational plots

followed the experimental plot for the round dome patella increasing from -4° lateral tilt to 1° and decreasing to -4° medial tilt at 75% of the gait cycle (Figure 3-14).

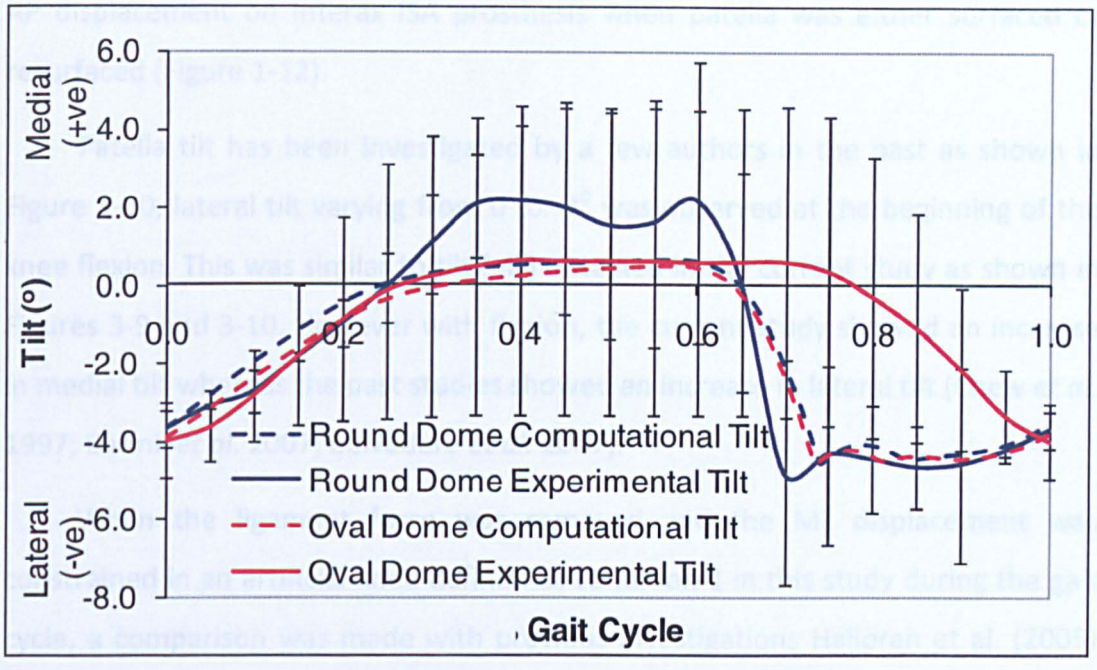

Figure 3-14 Medial lateral tilt for round and oval dome patella specimen when medial lateral translation was uncontrolled with error bars of 95% CL for the experimental results.

3.3.4 Comparison of ML Tilt for Round Dome Patella with Literature

The conditions for the comparison are condition 1) without ligament force and constrained ML displacement, 2) without ligament force and uncontrolled ML displacement and 3) with ligament force and uncontrolled ML displacement.

None of the previous investigators have considered the effect of both the ML displacement and the ligament force during gait cycle termed as condition 2 in this study. Therefore, an active comparison for kinematics of artificial knee was not possible. However, kinematics comparison of artificial knee with increment in knee flexion was investigated.

The ML displacement (4.5mm) was similar to the medial displacement observed by Belvedere *et al.* (2007). However, the femoral specimen was a Scorpio type femur as shown in Figure 1-11. When compared to PFC sigma type femur (Chew *et al.* 1997), the displacement was 3mm lateral.

The AP displacement was found to be approx 7mm in the literature (Ostermeier *et al.* 2005) similar to the displacement (5mm) found in the current study (Figure 3-12). Ostermeier and co authors (2005) worked on the difference of AP displacement on Interax ISA prosthesis when patella was either surfaced or resurfaced (Figure 1-12).

Patella tilt has been investigated by a few authors in the past as shown in Figure 1-10, lateral tilt varying from 0 to -4° was observed at the beginning of the knee flexion. This was similar to tilt (-4°) obtained in the current study as shown in Figures 3-9 and 3-10. However with flexion, the current study showed an increase in medial tilt whereas the past studies showed an increase in lateral tilt (Chew *et al.* 1997; Barink *et al.* 2007; Belvedere *et al.* 2007).

When the ligament force was removed and the ML displacement was constrained in an artificial knee defined as condition 1 in this study during the gait cycle, a comparison was made with previous investigations Halloran et al. (2005) and Ellison (2007) as shown in Figure 3-15. The tilt at condition 1 varied from 0.5 to -4.5° as compared to average tilt by previous investigators varying from 1 to -4°. The tilt from the PFC sigma round dome patella was not different from the tilt obtained from both the authors; Halloran et al. (2005) and Ellison (2007).

For the scenario when ligament force was included and ML displacement was uncontrolled, comparison with the literature was based on the natural knee (Lafortune and Cavanagh 1987). The tilt of PFC sigma round dome patella (condition 3) was high medially compared with the natural knee. As compared to PFC sigma, the tilt in the natural knee was -5 to -8° laterally. There was no similarity between the trends. The removal of the ligament force (condition 2) did not affect the tilt. The variation of tilt was from -4 to 2°.

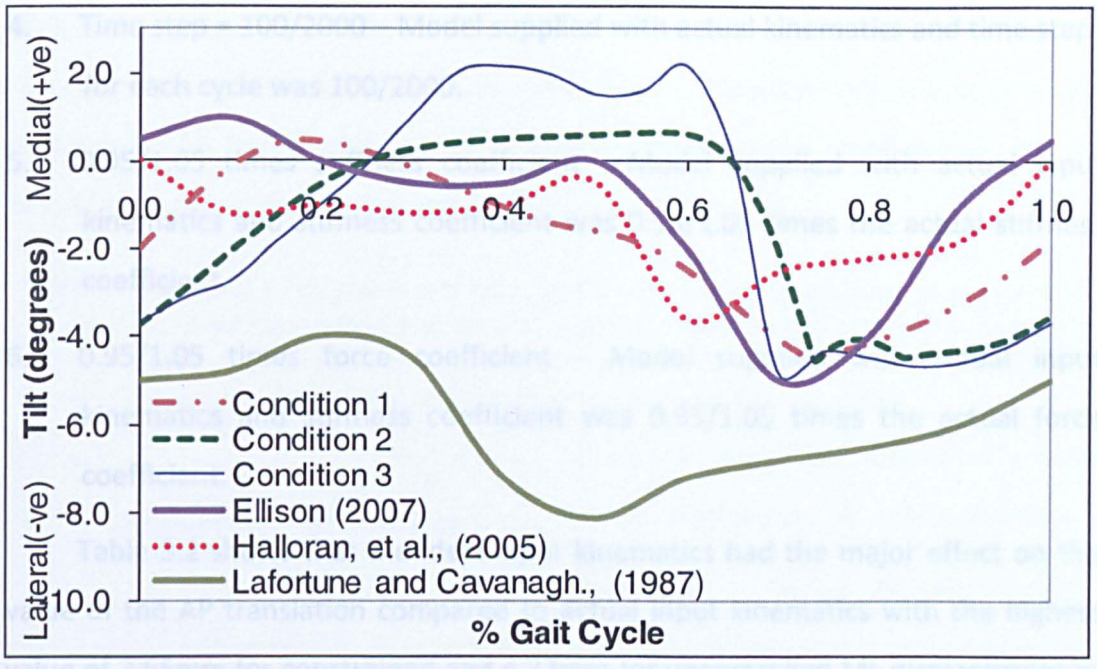

Figure 3-15 Comparison of computationally obtained medial lateral tilt for PFC sigma round dome patella for conditions, 1) without ligament force and constrained ML displacement, 2) without ligament force and uncontrolled ML displacement and 3) with ligament force and uncontrolled ML displacement (Lafortune and Cavanagh 1987; Halloran *et al.* 2005; Ellison *et al.* 2007)

3.3.5 Sensitivity Analysis

As discussed earlier in Chapter 2 section 7, the sensitivity analysis of the outputs in form of tilt and AP displacement were evaluated based on the change in the input kinematics (Axial load, FE rotation, ML rotation and SI displacement). The AP and tilt for femur with R_1 radius of rotation was considered for computational sensitivity analysis with constrained and free ML displacement at highest axial load (60% gait cycle), tabulated in Tables 3-2, 3-3 and 3-4 respectively. The terminologies used in the sensitivity analysis are:

1. Actual/Ideal input kinematics – the actual/Ideal kinematics followed by simulator when used as input kinematics for the computational model with frictional coefficient as 0.05 and time step =127.
2. 0.95/1.05 times actual input kinematics – The input kinematics to the model was 0.95/1.05 times the actual input kinematics.
3. Frictional coefficient = 0.01/0.1- Model supplied with actual input kinematics and frictional coefficient was 0.01/0.1.

4. Time step = 100/2000 – Model supplied with actual kinematics and time steps for each cycle was 100/2000.

5. 0.95/1.05 times stiffness coefficient - Model supplied with actual input kinematics and stiffness coefficient was 0.95/1.05 times the actual stiffness coefficient.

6. 0.95/1.05 times force coefficient - Model supplied with actual input kinematics and stiffness coefficient was 0.95/1.05 times the actual force coefficient.

Table 3.2 shows that the ideal input kinematics had the major effect on the value of the AP translation compared to actual input kinematics with the highest value of 3.65mm for constrained and 4.33mm for uncontrolled ML displacement at the end of stance phase. The tilt (2.65° for constrained and 0.63° for uncontrolled ML translation) at actual input kinematics did not vary from the tilt (2.5° for constrained and 0.52° for uncontrolled ML translation) obtained from model supplied with ideal input kinematics.

Table 3-2 Values of AP displacement (mm) and Tilt (°) at the end of stance phase (60% of gait cycle) for constrained and uncontrolled ML displacements at varied conditions for R_1 radius of rotation: a) Actual input kinematics b) Ideal input kinematics.

Output (AP/ Tilt) from	**Constrained ML displacement**		**Uncontrolled ML displacement**	
	AP mm	Tilt °	AP mm	Tilt °
Actual input kinematics	*2.2*	*2.65*	*2.21*	*0.63*
Ideal input kinematics	*3.65*	*2.5*	*4.33*	*0.52*

The change in actual input kinematics by 5% as tabulated in Table 3.3 gave significant difference with the actual kinematics at end of stance phase. Increase or decrease of actual input kinematics by 5% led to a significant difference in AP displacement and tilt compared to the model when supplied with actual input kinematics. The AP displacement varied from 2.2mm to 2.53mm in case of constrained ML displacement and 2.11mm to 2.26mm in case of uncontrolled ML

displacement. In the case of the tilt, the variation was 2.65° to 2.78° for constrained and 0.25° to 0.75° for uncontrolled ML displacement. It was however noted that the trend at all varied conditions followed the standard AP and tilt trends as shown in Figures 3-8 and 3-10 respectively.

Table 3-3 Values of AP displacement (mm) and Tilt (°) at the end of stance phase (60% of gait cycle) for constrained and uncontrolled ML displacements at varied conditions at R_1 radius of rotation for a) actual input kinematics, b) 1.05 times actual input kinematics and c) 0.95 times actual input kinematics

Output (AP/ Tilt) from/for	**Constrained ML displacement**		**Uncontrolled ML displacement**	
	AP mm	Tilt °	AP mm	Tilt °
Actual input kinematics	*2.2*	*2.65*	*2.21*	*0.63*
1.05 times actual input kinematics	*2.53*	*2.68*	*2.26*	*0.25*
0.95 times actual input kinematics	*2.27*	*2.78*	*2.11*	*0.75*

Frictional coefficient made a major significance to the change in tilt. The tilt varied from 1.77° to 3.74° and 2.94° to -0.63° for constrained and uncontrolled ML displacement respectively when frictional coefficient was changed from 0.01 to 0.1. Time step when increased from 100 to 2000 led to no change in AP displacement or tilt as shown in Table 3-4. In the case of AP displacement, the frictional coefficient and time step had no dependency on the sensitivity at uncontrolled and constrained ML displacement.

Table 3-4 Values of AP (mm)and tilt (°) at the end of stance phase (60% of gait cycle) for constrained and uncontrolled ML displacements at varied conditions for R_1 radius of rotation for a) actual input, b) frictional coefficient = 0.01, c) frictional coefficient = 0.1, d) time step = 100, and e) time step = 2000.

Output (AP/ Tilt) from/for	Constrained ML displacement		Uncontrolled ML displacement	
	AP mm	Tilt °	AP mm	Tilt °
Actual input kinematics (μ = 0.05)	*2.2*	*2.65*	*2.21*	*0.63*
Frictional coefficient = 0.01	*2.26*	*1.77*	*2.14*	*2.94*
Frictional coefficient = 0.1	*2.2*	*3.74*	*2.21*	*-0.63*
Time step = 100	*2.21*	*2.62*	*2.23*	*0.61*
Time step = 2000	*2.23*	*2.61*	*2.24*	*0.65*

The variation of kinematics with contact parameters (stiffness, force and damping coefficients) was analysed as tabulated in Table 3-5. There was no variation in ML and AP displacements with contact parameters. The tilt varied with stiffness and force coefficients for uncontrolled ML displacement. The damping coefficient had no effect on tilt. The increase and decrease in stiffness coefficient by 5% led to increase (from 0.63° to 0.75°) and decrease (from 0.63° to 0.56°) in tilt respectively. However, the increase and decrease in force coefficient by 5% led to decrease (from 0.63° to 0.51°) and increase (from 0.63° to 0.88°) in tilt respectively. There was no variation of tilt with any coefficients at constrained ML displacement.

Table 3-5 Values of tilt (°) at the end of stance phase (60% of gait cycle) for constrained and uncontrolled ML displacements at varied conditions for R_1 radius of rotation for a) actual input, b) 1.05 times stiffness coefficient, c) 0.95 times stiffness coefficient, d) 1.05 times force coefficient and e) 0.95 times force coefficient.

Output (AP/ Tilt) from/for	Constrained ML displacement	Uncontrolled ML displacement
	Tilt °	Tilt °
Actual input kinematics	*2.65*	*0.63*
1.05 times stiffness coefficient	*2.65*	*0.75*
0.95 times stiffness coefficient	*2.65*	*0.56*
1.05 times force coefficient	*2.65*	*0.51*
0.95 times force coefficient	*2.65*	*0.88*

3.4 Discussion

Verified computational models present an efficient way to understand patella femoral mechanics addressing relevant clinical issues due to maltracking for example. This also helped in evaluating the performance of the implant during the design stage. Previous investigations predicted PFJ kinematics in the Kansas knee system using finite element analysis at gait cycle (Haloran *et al.* 2005a, 2005b 2006). These studies have not previously been applied to the Leeds knee simulator. The objective of the current study was to evaluate computational and experimental kinematics study for predicting the motion between round/oval dome patella and PFC sigma knee at two femoral radii of rotation during constrained and uncontrolled ML displacements.

3.4.1 Comparison of Kinematics at Different Radii of Rotations

The medial translation displacement was due to the curvature of the inner groove and SI translation. The deviation of inner groove from the centre line passing through the mid-axis of femoral condyles led to ML displacement. The AP displacement was dependent on load and flexion extension rotation. There was a

difference in ML displacement between computational and experimental model at R_2 radius of rotation (Figure 3-6). ML tilt was highly dependent on the ML translation. At constrained or uncontrolled translation, a minor movement of the patella in the medial direction caused a change in tilt. This can be explained as the increase in fulcrum length led to an increase in tilting torque at constant load as shown in Figure 3-16.

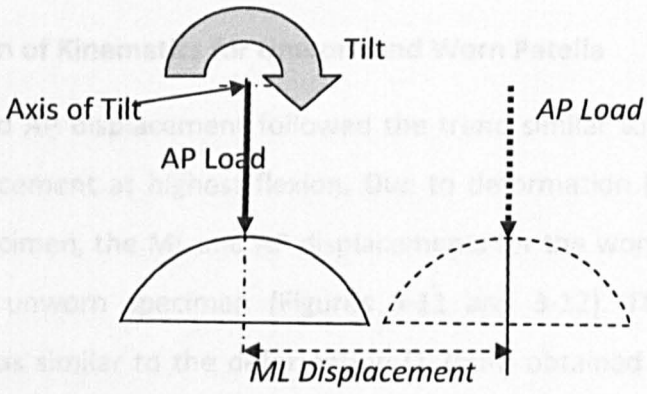

Figure 3-16 Concept of tilt under the action of AP load and ML displacement of the patella.

At the beginning of the flexion cycle during the stance phase the patella tilted medially due to the load in piston balance corresponding to the ligament tension and the absence of confinement within the femoral groove. With an increase in ML translation during the swing phase, the tilt changed from medial to lateral. The tilt oscillated during the end of the flexion cycle due to sudden change of tilt from medial to lateral. This can be considered due to the restriction obtained as the outer cradle, under the sudden increase in axial load, contacted with the base of knee simulator. The base acts as a restriction to the movement of cradle, thereby stopping the patella slip for tilts higher than 5.2°. At higher radius of rotation and uncontrolled ML displacement, the area of contact, hence conformity between the femoral component and patella specimen led to a constant lateral tilt of -4°.

The AP displacement was dependent on the axial load and flexion extension (FE) rotation. AP translation was in phase with FE rotation however, was affected by change in tilt in case of constrained ML displacement. There was a dip in AP translation for both femoral centres of rotation (R_1 and R_2) at 75% of gait cycle which showed the change in AP displacement due to the change in tilt. As the

radius of rotation increased the AP displacement increased when ML displacement was uncontrolled. For constrained ML translation, this was not applicable as the patella did not follow the inner groove due to restrictions in the ML displacements. The motors driving the flexion/extension motion in the experimental simulator tripped out due to overloading after a certain amount of cycles for R_2 radius of rotation. Hence, R_1 radius of rotation was found to be the optimum and physiological option for running the wear simulation test.

3.4.2 Comparison of Kinematics for Unworn and Worn Patella

The ML and AP displacement followed the trend similar to FE rotation with maximum displacement at highest flexion. Due to deformation (1200 μm) in the worn patella specimen, the ML and AP displacements for the worn specimen were lower than the unworn specimen (Figures 3-11 and 3-12). This difference in displacements was similar to the deformation (1.2mm) obtained during the wear test as measured by the Talysurf profilometer.

The tilt for the worn specimen followed the same trend as the trend observed higher radius of rotation (R_2) (Figure 3-10). The tilt at R_2 was a constant lateral tilt due to conformity of the patella specimen to the femoral counterpart as a result of wear deformation as explained in section 3.3.2 (Figure 3-13).

3.4.3 Comparison of Kinematics for Round and Oval Dome Patella

The tilt for round dome and oval dome patella were similar to the experimental simulation (Figure 3-14). However, there was no difference found between the tilt in the two domes as the curvature of the dome was the same in both round dome and oval dome patellae. The difference in elliptical shape of oval dome as compared to round dome did not affect the tilt at the unworn stage.

3.4.4 Comparison of Kinematics for Round Dome Patella with Literature

The ML displacement changed with knee flexion. The direction of the displacement was dependent on the direction of the patella articulating groove which in the current study was medial. Hence, there was medial displacement. Chew and co authors (1997) also reported that most of the ML displacement in

other specimens was medial. However, their PFC sigma control specimen showed lateral displacement. The AP displacement increased with flexion. The displacement was higher in the investigation by Ostermeier *et al.* (2005) compared to the current study. This can be due to the shape of patella and pull of ligaments which were absent in current study.

There were only two kinematic investigations performed in the past with an artificial patella femoral joint at gait cycle (Halloran *et al.* 2005, Ellison 2007). Halloran and co-authors (2005) investigated two oval dome specimens using the Purdue knee simulator, out of which only one observation was recorded. The second specimen was neglected as there was no variation in tilt monitored with change in flexion. In Ellison's investigation (2007), the number of round dome patella specimens were more than five, tested in a modified hip simulator. However, all the degrees of freedom (ML displacement) were not included in the wear study. Comparing the patellar tilt predicted by PFC sigma round dome patella without the ligament force at constrained ML displacement (condition 1) with that recorded in literature (Halloran *et al.* 2005; Ellison 2007), the tilt (-2.0° to 0.5°) was found to have similar trend and magnitude. Hence, good agreement with the literature (-4.0° to 1.0°) was observed showing the validity of the model.

No previous literatures have been reported with a six degree of freedom and ligament force simulation. When the ML displacement was unconstrained and the ligament force included, the tilt showed a large variation with the two past authors. The reason for this difference was the introduction of uncontrolled ML displacement and ligament force (condition 3) that caused additional torque which produced higher lateral tilt as shown in Figure 3-16. The removal of the ligament load (condition 2) caused a change in the magnitude of tilt. However, the trend was similar between the two conditions (2 and 3). Condition 3 was compared with natural knee kinematics (Lafortune and Cavanagh 1987), the tilt obtained was different in terms of magnitude and trend. Higher values of lateral tilt (-4.0° to 2.0°) were observed in the natural knee due to the presence of additional ligaments, muscle forces and contact geometry.

3.4.5 Sensitivity Analysis

AP translation increased and tilt decreased as the input parameters were changed from actual to ideal conditions for uncontrolled and constrained ML displacements. The simulator followed the actual kinematic due to presence of pneumatic motors. As the actual kinematics were less than the ideal kinematics, the value of the translations was lower compared to the ideal scenario. The FE and superior inferior displacement when lower in actual kinematics led to a decrease in AP translation.

With an increase in 5% of the input kinematics (105% of the input kinematics), the AP displacement and tilt increased and decreased respectively. Conversely, AP and tilt decreased and increased with a decrease in input kinematics by 5% (Table 3-3).

The frictional coefficient had an effect on tilt; with an increase in friction leading to a stiffer joint and hence, a decrease in tilt was observed in constrained and uncontrolled ML displacements (Table 3-4). AP displacement did not vary with change in frictional coefficient. The time step had no effect on the tilt or AP displacement. The frictional contact had higher effect when contact between the joints was higher. In AP displacement, there was point/line or lower surface contact. However, the tilt had high surface contact and hence, tilt was affected due to change in the frictional coefficient

The contact parameters had no effect on ML and AP displacements with constrained and uncontrolled ML displacements. Tilt at constrained ML displacement was not affected by an increase or decrease in contact parameters by 5%. However, tilt with uncontrolled ML displacement was affected by force and stiffness coefficients $\leq 0.25^{\circ}$. The increased of force coefficient (0.1) led to a decrease in deformation and conformity increases. Hence, tilt was inversely proportional to force. With an increase in stiffness, the deformity was lower, hence conformity decreased and we observed higher tilt. Therefore, tilt was directly proportional to the stiffness coefficient.

Summary

A computational model has been developed and validated with experimental results. A good (80%) agreement was found between the two for most conditions. The model predicted the kinematics of different shapes, radii of rotation at constrained and uncontrolled ML displacement. The model was tested for sensitivity and found to be robust against change in the time step.

Chapter 4: Development of Volumetric Wear Measurement Techniques

4.1 Introduction

Measurement of the volume change is very important to accurately determine the wear rate and volume loss of the ultra high molecular weight polyethylene patella specimens. In the literature, there are many methods of determining the volume change of UHWMPE in the hip, spine and knee either using contact or non contact procedures. Geometric procedures includes coordinate measuring machine (CMM) (Raimondi *et al.* 2000; Bills *et al.* 2007) whereas, non contact procedures include Micro computed topography (MicroCT) (Vicars *et al.* 2009), Pycnomatic ATC (Pycnometer) (Keng 1970; Viana *et al.* 2002) and gravimetric (Affatato *et al.* 2002; D'Lima *et al.* 2003). However, the most standard and validated method is gravimetric analysis. The gravimetric measurement has certain issues like fluid uptake, inclusion of wear debris in the polyethylene counterpart, specimen attached to fixtures fixed with cement which required mass of fixturing during measurements, cement attached to the specimen, transfer of materials into the back of components (Bills *et al.* 2005; Bills *et al.* 2007). These factors gave errors in the volumetric calculation of gravimetric analysis (Blunt et al. 2007). Gravimetric measurements always need the pre test measurements for calculation of volume change which are unavailable in retrievals. Therefore, there is always a need for development of advanced measuring machines for measurement of volumetric wear due to issues with gravimetric. Some methods which can be used for volumetric wear measurement purposes are CMM, MicroCT, and Pycnometer. Recently, these methods have been developed for accuracy and repeatability (Raimondi *et al.* 2000; Bills *et al.* 2007; Vicars *et al.* 2009; Keng 1970; Viana *et al.* 2002).

This chapter investigates three volumetric measurement methods using Pycnometer (Thermo Finnigan Italia S.p.A, Milan, Italy), CMM (Legex 322, Mitotoyo) and MicroCT (Scanco Medical, Busserdorf, Switzerland). Pycnometer, CMM and MicroCT are not affected by the fluid intake in polyethylene. The

principles behind the methodology of the three measurement techniques are explained in Chapter 2: Section 6. The presence of pre-wear data accurately determines the volume change of the specimen. However, it is impossible to obtain details of pre-wear data for specimens like retrievals. Methods like MicroCT (Bowden *et al.* 2005) and CMM (Bills *et al.* 2005; Bills *et al.* 2007) do not depend on the pre-wear data and have been used for volumetric analysis of retrievals in the past. The Pycnometer has never been previously employed for polyethylene specimens.

The aim was to assess the Pycnometer, CMM and MicroCT based procedure to calculate volume of UHWMPE patella specimens and compare the results with the standard gravimetric quantification. The validation was needed, to be used in *in vitro* or *in vivo* specimen analysis. To achieve the goal, a series of artificially created wear were generated and the volume was determined using the CMM and MicroCT volumetric measurement methods. Pycnometer was used to measure a worn and an unworn specimen; the results were hence compared with gravimetric volumetric technique. The methods will also be assessed for accuracy and repeatability.

4.2 Materials and Methods

The specimens used for the measurement and validation process were UHMWPE round dome (38mm diameter) patella specimens (DePuy, UK). The specimens were cleaned with iso-propanol solution and then dusted with compressed air to remove dust particles. Before any measurement in Pycnometer, CMM and MicroCT, all the specimens were weighed in the AT 201 balance.

The methodologies for the volumetric measurements are explained in detail in Chapter 2: Materials and Methods, Section 6.

4.2.1 Pycnometer

A Pycnometer was used to measure the volume of two patella specimens (a worn and an unworn sample); the methodology is explained in Chapter 2, section 2.6.5. The worn specimen was a test specimen from the simulator wear test.

4.2.2 CMM

The patella specimens were measured using gravimetric and CMM at different stages of known artificially created wear. The stages were pre-wear, volume loss of 5mm^3, 10mm^3 and 15mm^3. The results obtained were compared and validated against gravimetric measurements.

An unworn patella specimen was used for the analysis. The artificial wear was generated by removing material using files from the specimen after each stage by a technician. The amount of material equivalent to volumes of low (5), medium (10) and high (15) mm^3 was verified by measuring the mass loss in the AT 201 balance. The selection of the volume loss was decided based on the wear volume loss per million cycles in a wear test. The specimen was cleaned and prepared for measurement purposes as detailed in Chapter 2: section 2.6.1. The pre-wear test measurement was used as a reference for all the techniques.

CMM techniques on the other hand analysed the volume using two methodologies as explained in Chapter 2, section 2.6.4. The method 1 was determination of volume with respect to reference volume. Method 2 was generation of an unworn specimen based on the surface fit of the unworn surface.

4.2.3 MicroCT

Measurements were performed for low, medium and high volume loss similar to CMM. MicroCT volumetric analysis was carried out based on two methods a) reference to gravimetric analysis (Vicars *et al.* 2009) and b) based on cylindrical reference volume. In the first method, reference to gravimetric method, knowing the volumetric difference from gravimetric measurement was the key requirement for calculation of volume in the MicroCT. The threshold was adjusted in the image processing language (IPL) software in MicroCT scanner so as to obtain the similar

volumetric difference by gravimetric analysis (Vicars *et al.* 2009). This method was dependent on gravimetric analysis. The latter method of calculating the volume was based on using a cylindrical reference volume. A volume of the reference specimen (936mm^3) was kept at constant environment throughout the test. Based on the reference volume, the threshold was calculated. The threshold obtained was used as a method to determine the volume of the polyethylene specimen.

All measurements were performed three times on each specimen. The mean volume change was then calculated with 95% confidence limits.

4.3 Results

4.3.1 Pycnometer

The Pycnometer volume analysis estimated the volume of worn and unworn patella as 5716 and 5833±15 mm^3 respectively. Only one volume result was calculated for worn patella leading to inaccuracy in results. All the other results are shown in Figure 4-1 with 95% confidence limits. The 95% confidence limit on the volume calculated using the Pycnometer was higher than the gravimetric technique. The measurement took 20 minutes per specimen.

The student's t-test found no significance difference between the Pycnomatic ATC and gravimetric results of un-worn patella (p=0.27). This led to the determination of Linear least squared regressions as shown in Figure 4-2.

The R square value (0.24) was much less than 1 showing no correlation between the Pycnometer and gravimetric volume for the unworn specimen.

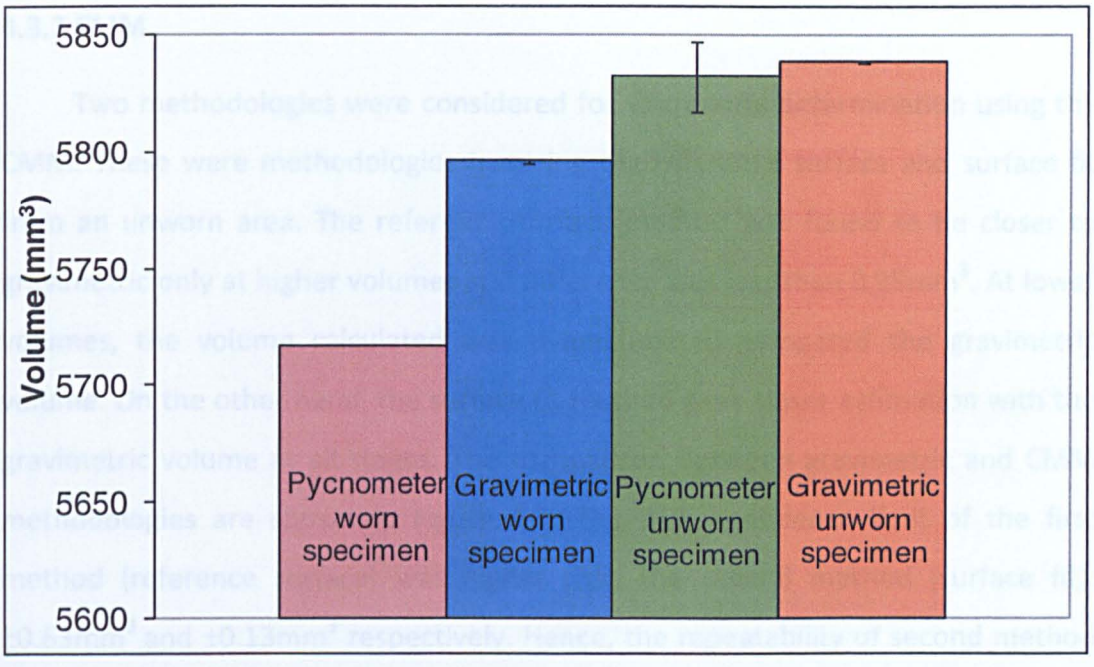

Figure 4-1 Plot of volume calculated using Pycnomatic ATC and gravimetric measurements with 95% confidence limit.

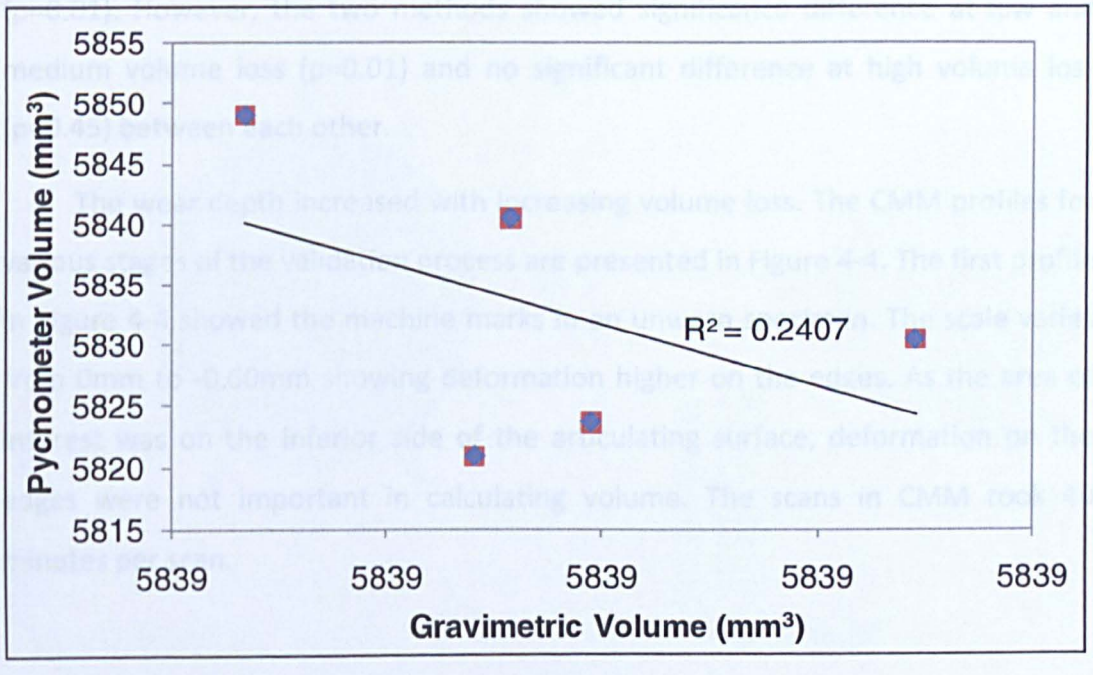

Figure 4-2 R square between gravimetric and Pycnomatic volume for un-worn patella

4.3.2 CMM

Two methodologies were considered for volumetric determination using the CMM. These were methodologies involving the reference surface and surface fit from an unworn area. The reference surface method was found to be closer to gravimetric only at higher volumes and difference was less than 0.95mm^3. At lower volumes, the volume calculated was overestimated compared the gravimetric volume. On the other hand, the surface fit method gave closer estimation with the gravimetric volume at all stages. The comparison between gravimetric and CMM methodologies are shown in Figure 4-3. The 95% confidence limit of the first method (reference surface) was higher than the second method (surface fit); ±0.63mm^3 and ±0.13mm^3 respectively. Hence, the repeatability of second method was better compared to the first method. However, the repeatability of both methodologies was weaker than gravimetric (±0.02mm^3). The student t-test showed significance difference of the two types of methods with gravimetric ($p=0.01$). However, the two methods showed significance difference at low and medium volume loss ($p=0.01$) and no significant difference at high volume loss ($p=0.45$) between each other.

The wear depth increased with increasing volume loss. The CMM profiles for various stages of the validation process are presented in Figure 4-4. The first profile in Figure 4-4 showed the machine marks in an unworn specimen. The scale varies from 0mm to -0.60mm showing deformation higher on the edges. As the area of interest was on the inferior side of the articulating surface, deformation on the edges were not important in calculating volume. The scans in CMM took 40 minutes per scan.

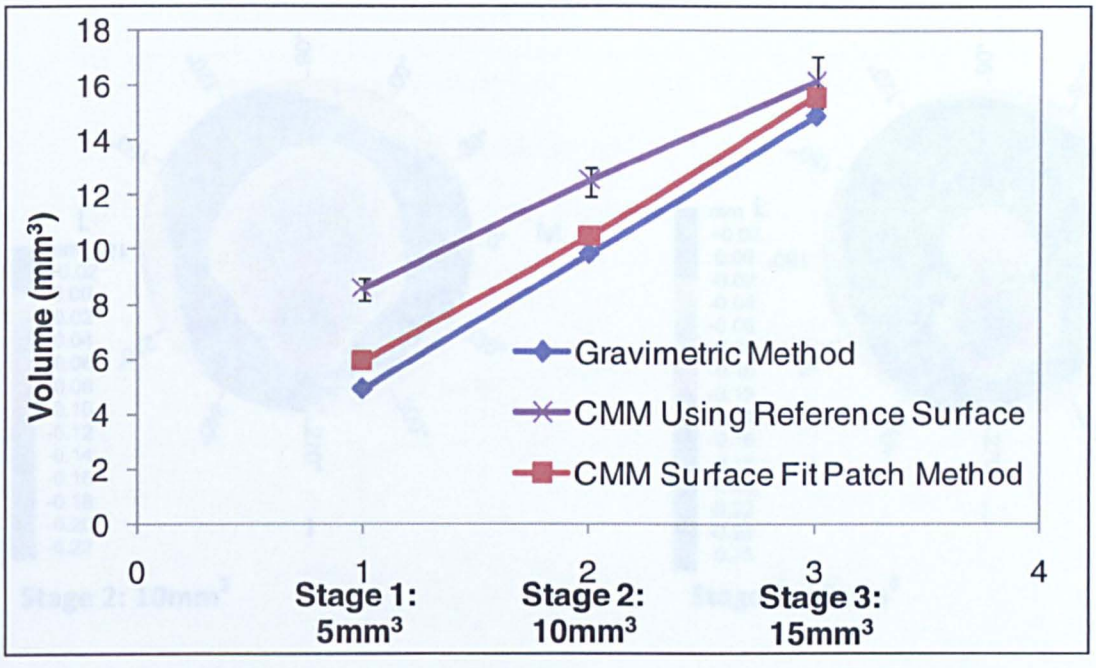

Figure 4-3 Schematic diagram showing of the difference in volume estimated from CMM and gravimetric at 5, 10 and 15mm^3 material removals.

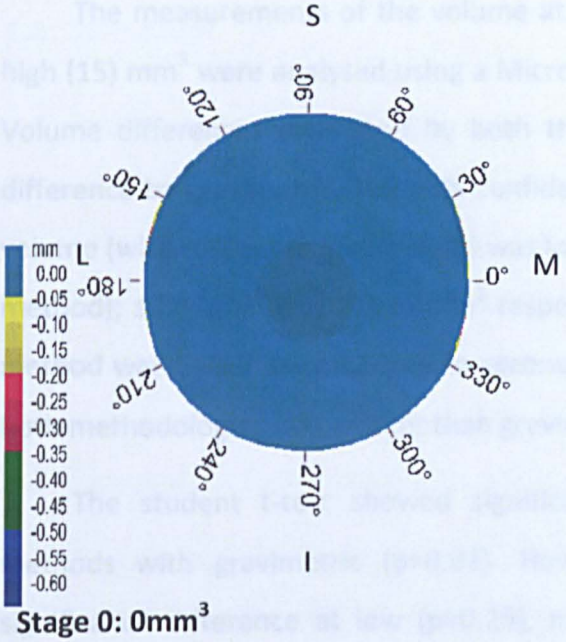

Stage 0: 0mm^3

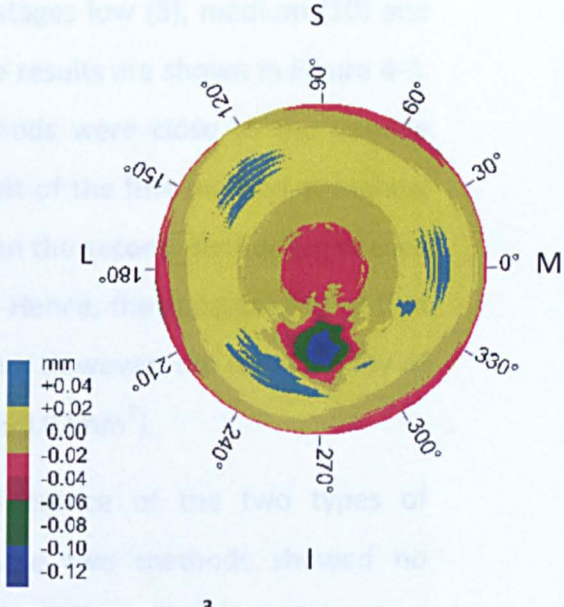

Stage 1: 5mm^3

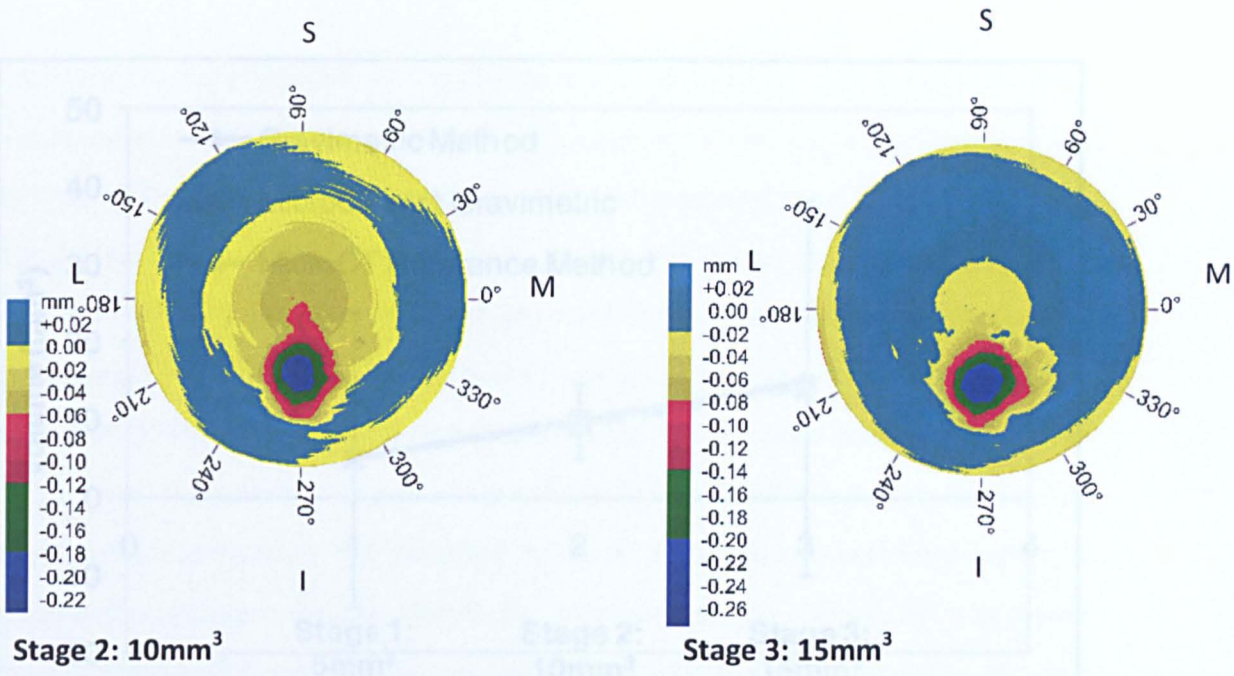

Figure 4-4 CMM scan of varied stages in validation process using surface fit from unworn area. S: Superior, I: Inferior, M: Medial and L: Lateral.

4.3.3 MicroCT

The measurements of the volume at three stages low (5), medium (10) and high (15) mm^3 were analysed using a MicroCT. The results are shown in Figure 4-5. Volume differences estimated by both the methods were close to the volume difference by gravimetric. The 95% confidence limit of the first method at highest volume (with respect to gravimetric) was lower than the second method (reference method); ±0.84mm^3 and ±15.94mm^3 respectively. Hence, the repeatability of first method was better as compared to second method. However, the repeatability of both methodologies was weaker than gravimetric (±0.02mm^3).

The student t-test showed significance difference of the two types of methods with gravimetric (p=0.01). However, the two methods showed no significance difference at low (p=0.29), medium (p=0.16) and high volume loss (p=0.06) between each other. The scans in MicroCT took around 45 minutes.

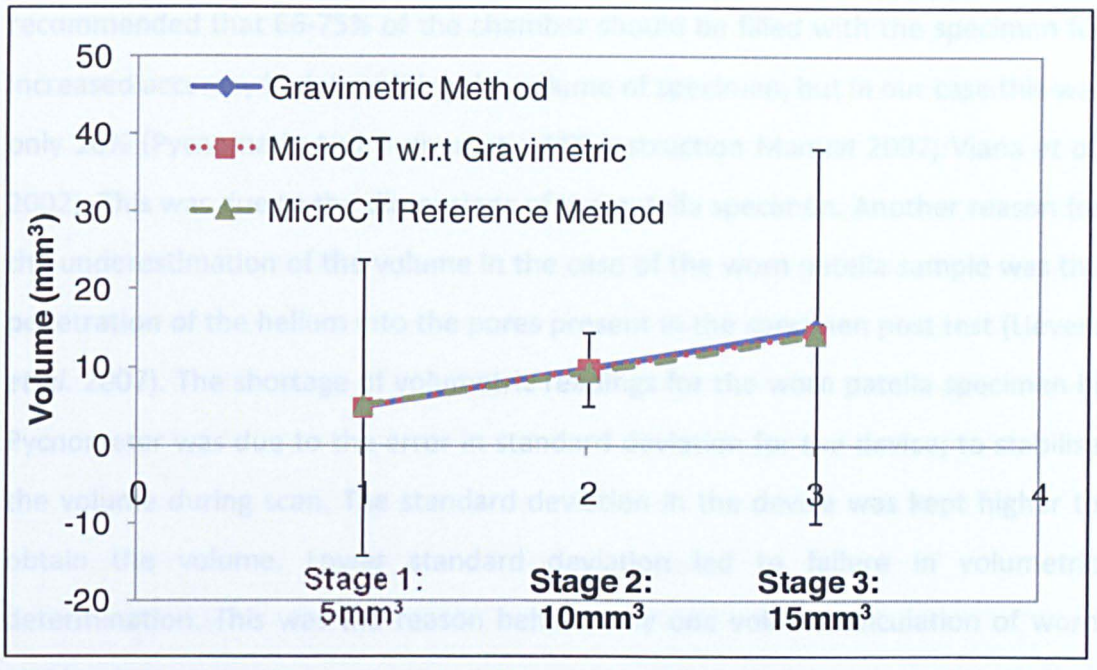

Figure 4-5 Schematic diagram showing difference in volume estimated from MicroCT and gravimetric at 5, 10 and 15mm^3 of material removals with 95% confidence limit error bars of MicroCT reference method.

4.4 Discussion

Gravimetric analysis is the most widely used standard method in the determination of the volume of any specimen. However, there are limitations in the measurement of UHMWPE due to fluid absorption, metallic debris inclusion and mass of cement mantle. A call for new methodologies to measure volume was needed with greater accuracy and repeatability. The aim of the project was to validate new methods of measuring the volume of polyethylene with gravimetric analysis considered as the reference value.

The results using the Pycnometer showed a best volume repeatability of ± 15 mm^3, which is significantly larger than for gravimetric measurement of ±0.9 mm^3. A typical patella wear volume was 3.13mm^3 per million cycles from the past (Ellison *et al.* 2008). As the linear least squared regressions was low (0.24) between the volumes calculated using gravimetric and Pycnomatic ATC procedures. The Pycnometer was not found to be a reliable method to calculate volume compared to gravimetric measurements. The reasons were the estimation of sample volume in comparison with the volume of the chamber (6000:60000 mm^3). It is

recommended that 66-75% of the chamber should be filled with the specimen for increased accuracy in determining the volume of specimen, but in our case this was only 10% (Pycnomatic And Pycnomatic ATC Instruction Manual 2007; Viana *et al.* 2002). This was due to the dimensions of the patella specimen. Another reason for the underestimation of the volume in the case of the worn patella sample was the penetration of the helium into the pores present in the specimen post test (Lievers *et al.* 2007). The shortage of volumetric readings for the worn patella specimen in Pycnometer was due to the error in standard deviation for the device; to stabilise the volume during scan. The standard deviation in the device was kept higher to obtain the volume. Lower standard deviation led to failure in volumetric determination. This was the reason behind only one volume calculation of worn specimen.

The CMM over estimated the volume change as compared to gravimetric. The average repeatability of CMM reference surface and surface fit ($\pm 0.63 mm^3$ and $\pm 0.13 mm^3$ respectively) were higher than that of gravimetric ($\pm 0.02 mm^3$). However, there were significant differences found between the two methods with gravimetric.

The CMM methodology of reference surface gave less accurate results of material removed. This may be the result of different datum between the reference specimen and the worn specimen. In the case of volume determination from surface fit method, the volume determined was close to the gravimetric measurement. The difference between volumes determined by this method was less than $1 mm^3$ with respect to the gravimetric methodology. However, there were significance differences found between the two methodologies in CMM at low (<0.01) and medium (<0.01) volume loss and no significant difference at high volume loss (0.45). The surface fit method gave better accuracy compared to the reference method. For retrievals, due to the absence of pre-wear data, the reference surface is not available. Hence, the surface fit method will be used for volume determination in the following chapters.

The MicroCT estimated the volume accurately as compared to gravimetric volume. However, the repeatability of the results was quite high. The average

repeatability of MicroCT with respect to gravimetric and reference method ($\pm 0.84 mm^3$ and $\pm 15.94 mm^3$ respectively) were higher than that of gravimetric ($\pm 0.02 mm^3$). The MicroCT methodology of predicting the volume with respect to gravimetric was very accurate. However, the gravimetric results were needed to obtain the volume. In the other methodology, the measurement was independent on the gravimetric volume. However, repeatability of the results was very weak. The errors in volume calculation were found to be similar to Bowden and co authors (2005). It has been reported that the difference in volumetric wear was due to error in thresholding and scanner which affected the intensity of light. This was however solved by using a calibration volume, the volume of which was known. The repeatability of the MicroCT was found to be acceptable in the later chapter when testing cumulative volume loss of higher magnitude more than $20 mm^3$ in Chapter 5 and 6. As there was a need to accurately determine the volume change of specimen without depending on gravimetric, the second method of reference volume was used in the following chapters.

MicroCT and gravimetric measurements can be used when the pre-wear data is available. However, in the case of retrievals, the method becomes incapable to determine the volume. CMM can be used to determine the volume in retrievals. It was found to be very accurate when surface fit methodology was used. However, more specimens should be tested to determine the accuracy of the method at lower volume.

Gravimetric volume measurement is the most accurate and easiest way to determine the volume of polyethylene specimens. However, in many scenarios like compensation for moisture uptake, specimen attached to a fixture, specimen cemented to the fixture can lead to inaccurate volumetric determination. Pycnometer, MicroCT and CMM were the other potential methods used to determine volume. Pycnometer used helium gas to determine the volume. However, the reason of inaccuracy in volumetric determination was due to the presence of empty space (>60%) in the measuring chamber. MicroCT has two methodologies, one which required constant gravimetric measurement to calculate the volume loss. The other methodology used a calibration specimen to obtain the threshold and this threshold determined the volume of the specimen. Out of the

two methods, the second method was the most independent and accurate method to be used for volumetric measurement. CMM also considered two methodologies to calculate the volume. One was comparing with the original profile and the other considered creating a nominal surface based on the unworn surface. The second method was found more accurate and could be used for retrieval volumetric analysis. In the absence of pre-wear data, CMM was found more accurate and useful in determining the volume of retrievals as compared to gravimetric and MicroCT. The gravimetric measurement took the least time compared to other measurement techniques.

Summary

Gravimetric remains the most accurate and quickest way to determine wear volume. CMM can be used for retrievals when no pre-wear data exists and offers additional information on the geometry, penetration depth and deformation.

Chapter 5: *In Vitro* Wear Simulation of the PFC Sigma and Round Dome Patella

5.1 Introduction

Previous *in vitro* studies (Halloran *et al.* 2005) that investigated the movements of the patella in the ML plane have restricted the movement to 1mm. However, the movement was found to be more than 1mm due to the varied stiffness of ML ligaments (Lafortune and Cavanagh 1987; Chew *et al.* 1997; Barink *et al.* 2007; Belvedere *et al.* 2007). Therefore, the test was conducted with higher and lower ML displacement to investigate the influence on wear. The earlier test controlled five degrees of freedom (Halloran *et al.* 2005). There was no investigation on the variation of kinematics on wear. This study investigated the influence of kinematics on the wear simulation of the PFC sigma and round dome patella. The results were compared to the other varied kinematic parameters and the difference on the wear rate and the influence of parameters on the wear rate are discussed. This chapter details the results of the tests performed on the new 6-axis patella femoral joint (PFJ) simulator. The initial test was performed for the validation of the simulator itself. The results were then compared with other *in vivo* and *in vitro* data.

5.2 Materials and Methods

5.2.1 Materials

Five wear, one load and two soak round dome patellae were used for the test. The lot numbers for the PFC sigma femur and round dome patella are listed in Table 5-1. The specimens were all UHMWPE polyethylene type round dome patella with diameter 38mm.

Table 5-1 Lot numbers for femoral and patella specimen

Specimen number	Femoral lot number	Patella lot number
Group 1-1	2999022	3006157
Group 1-2	2999022	2998670
Group 1-3	2999022	2998672
Group 2-1	2998552	2994444
Group 2-2	2998552	3006156
Group 2-3	2998552	2994443
Soak Specimens		3006156

5.2.2 Methods

The new six-axis PFJ simulator was developed to test five specimens of PFC Sigma femoral component with round dome patellae under relevant kinematic conditions, divided with three specimens in Group 1 and two specimens for Group 2 stations. Both the groups ran with different flexion extension motors to facilitate the active degree of freedoms. As the patella articulating surface was round in shape, the position of pegs at the back of the patella did not matter as compared to oval dome specimen. Hence, the specimens were placed in the mountings in such an order that no two pegs of the patella were collinear in horizontal or vertical plane as shown in Figure 5-1. One specimen was tested under the influence of AP load (200N-1200N) for conditions pertaining to creep at the end of the test for one million cycles (MC) in Group 2 station 3. Two other specimens were placed into a container of the serum for the test duration, thus acting as soak controls minimising the error arising from the absorption of fluid in polymers as outlined in tibia femoral wear testing in ISO 14243-3 (2009) when measuring gravimetrically.

The test ran under three conditions in the following order;

- 'High medial lateral (ML) rotation and uncontrolled ML displacement for 6MC',
- 'Low ML rotation (<1°) with uncontrolled ML displacement' for 3MC
- 'Low ML rotation with constrained ML displacement (<1.6mm)' for 3MC.

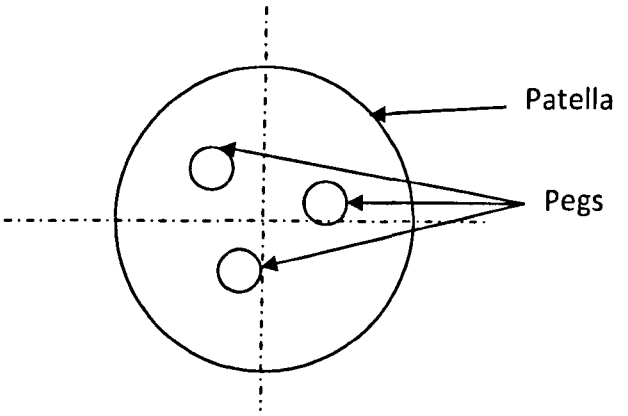

Figure 5-1 Placement of round dome patella pegs in the patella mounting during the simulation test.

Low ML rotation with uncontrolled ML displacement' was the most physiologically relevant condition according to the available literature, 'High ML rotation with uncontrolled ML displacement' was used to investigate the influence of rotation and 'Low ML rotation with constrained ML displacement' was used to investigate the influence of ML displacement. The physiological scenario ran for 3 million cycles (MC). The ML rotation was increased by four folds (<4°) and the scenario ran for 6MC. The physiological case with constrained ML displacement ran for 3MC. The first condition ran for 6MC to validate the simulator with literature results (Ellison *et al.* 2008). After the initial 6MC test, the further conditions each ran for 3MC. In total the test ran for 12 MC as shown in Figure 5-2. The other degrees of freedom are mentioned in Chapter 2: Section 2.5.4. The ML displacement was constrained by including a cylindrical block thus, limiting the movement to 1.6mm.

The wear volume was determined using gravimetric analysis and geometric methods using coordinate measuring machine (CMM) surface fit and micro computed tomography (MicroCT) reference specimen measuring techniques. As gravimetric is the standard method of wear determination (Dowson and Jobbins 1988; Barnett 2002; Liao *et al.* 2003; McEwen *et al.* 2005), the method was used every 1 MC of the test. While, other methods; CMM and MicroCT; were used before and after every condition. Talysurf was used for the evaluation of surface parameters (R_a, R_{sk}, R_p and R_v) before and after every set of conditions. Throughout the test, the wear scar, deformation, surface analyses were measured and reported after every condition.

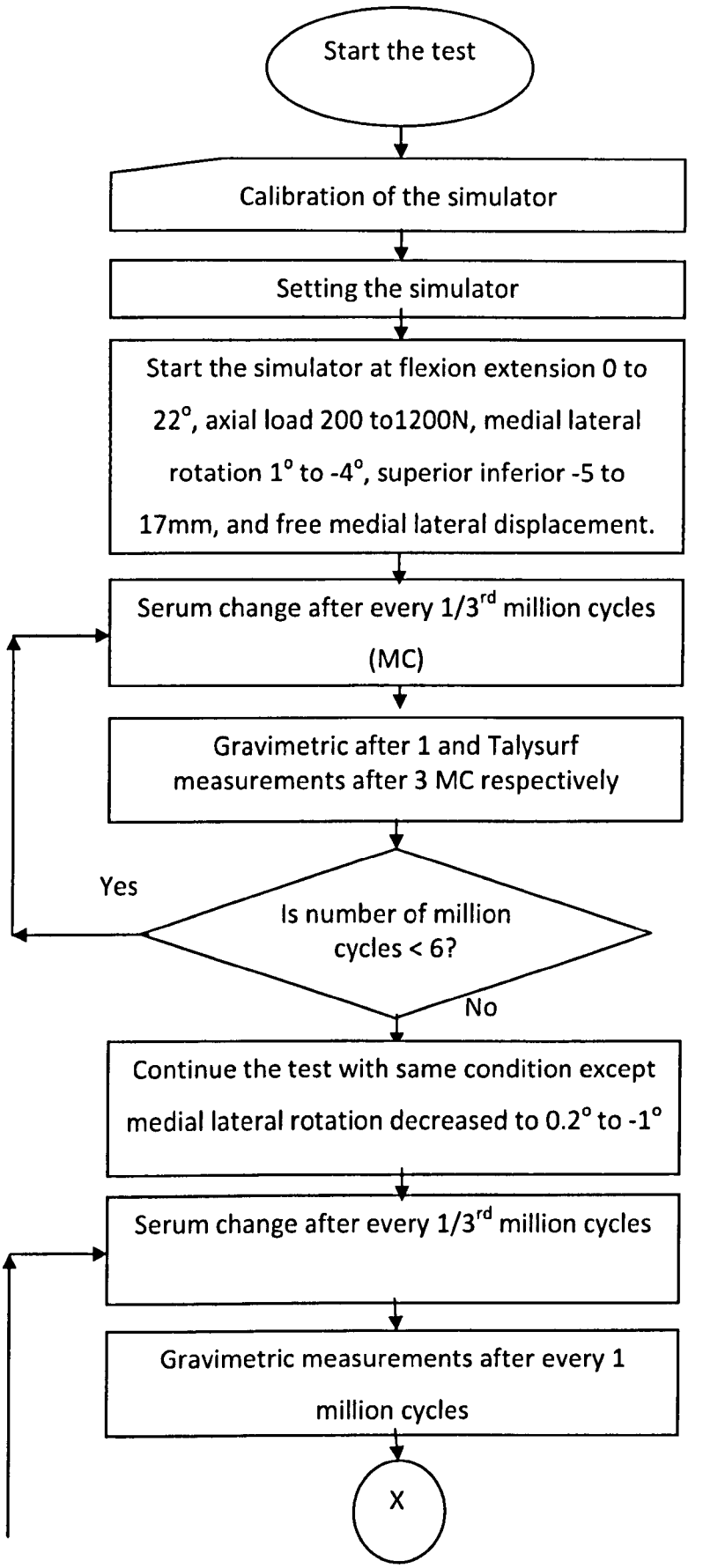
Start the test
Calibration of the simulator
Setting the simulator
Start the simulator at flexion extension 0 to 22°, axial load 200 to1200N, medial lateral rotation 1° to -4°, superior inferior -5 to 17mm, and free medial lateral displacement.
Serum change after every 1/3rd million cycles (MC)
Gravimetric after 1 and Talysurf measurements after 3 MC respectively
Is number of million cycles < 6?
Yes
No
Continue the test with same condition except medial lateral rotation decreased to 0.2° to -1°
Serum change after every 1/3rd million cycles
Gravimetric measurements after every 1 million cycles
X

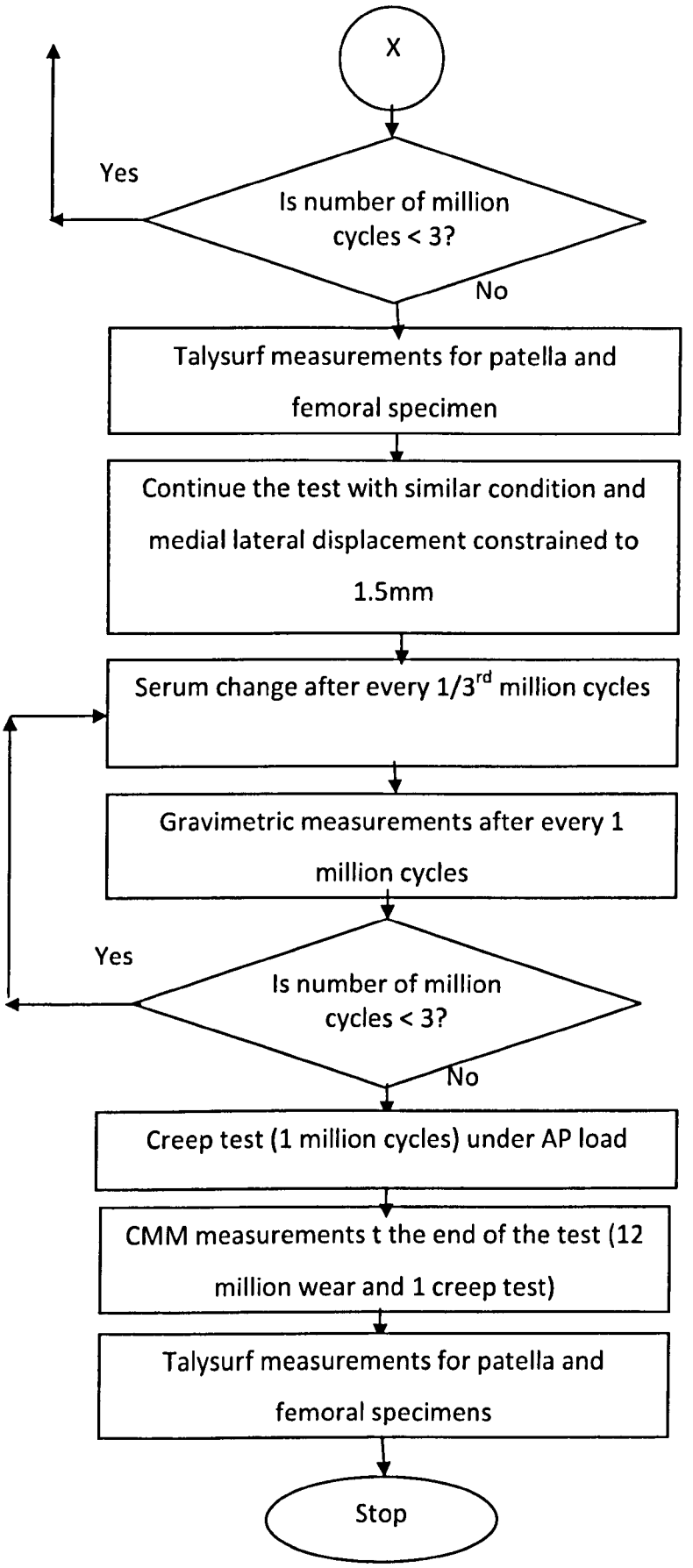

Figure 5-2 Flowchart describing the flow and number of cycles for all conditions.

5.3 Test Results

In total, the test ran for 12 MC. 6MC with high ML rotation and uncontrolled ML displacement, 3MC with low ML rotation and uncontrolled ML displacement and another 3MC with low ML rotation and constrained ML displacement.

There was a patella slip recorded due to higher tilt, larger than 5°, in one station. This problem was rectified by introducing wedges in all the stations of both groups to stop excessive tilt. Another problem of patella slipping from the femoral contact was observed during the first half MC. This was observed when patella moved in superior direction due to error in pneumatic motors. The problem was resolved by introducing rubber blocks to restrict the excessive movements.

5.3.1 Soak and Load Soak Controls

5.3.1.1 Kinematics

The soak controls were not under any action of displacement or load. The load soak controls were loaded with AP or axial load. The input and output AP load profile for the load soak control is shown in Figure 5-3 along with feedback from simulator.

5.3.1.2 Gravimetric volume measurements

The total mean weight gain of the soak controls over 12MC was 3.7mg. The mean weight gain in the first MC was 0.92mg. Following the first MC, the weight gain reduced to 0.2-0.4mg/MC thereafter. Figure 5-4 shows the cumulative weight change for two soak specimens throughout 12 MC.

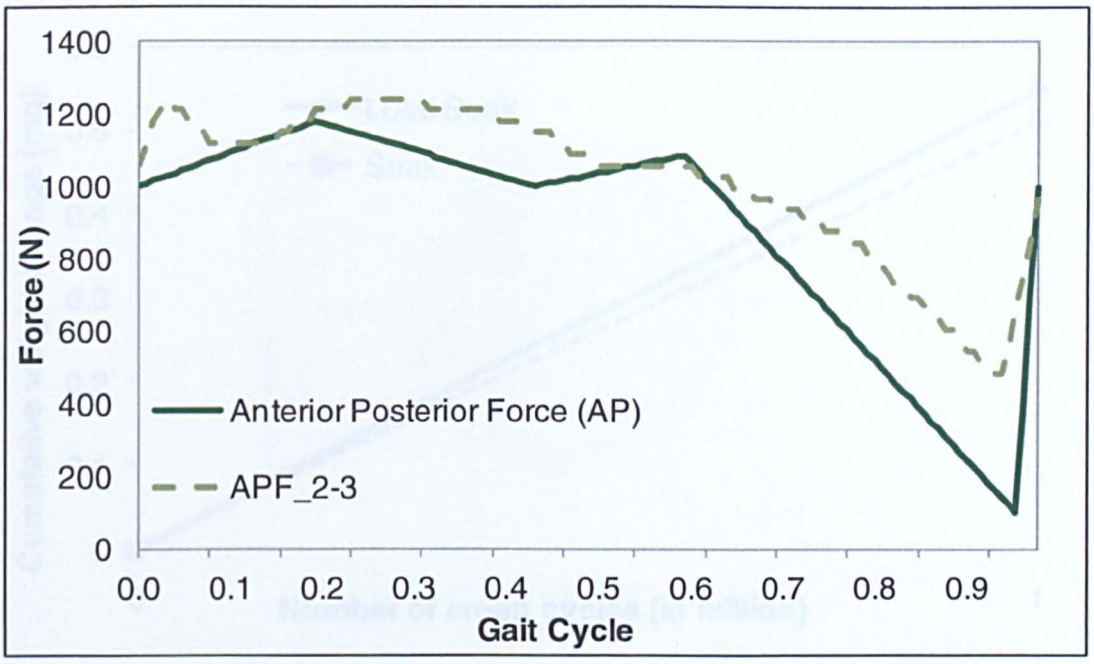

Figure 5-3 Kinematic input and output AP force profiles for the creep station.

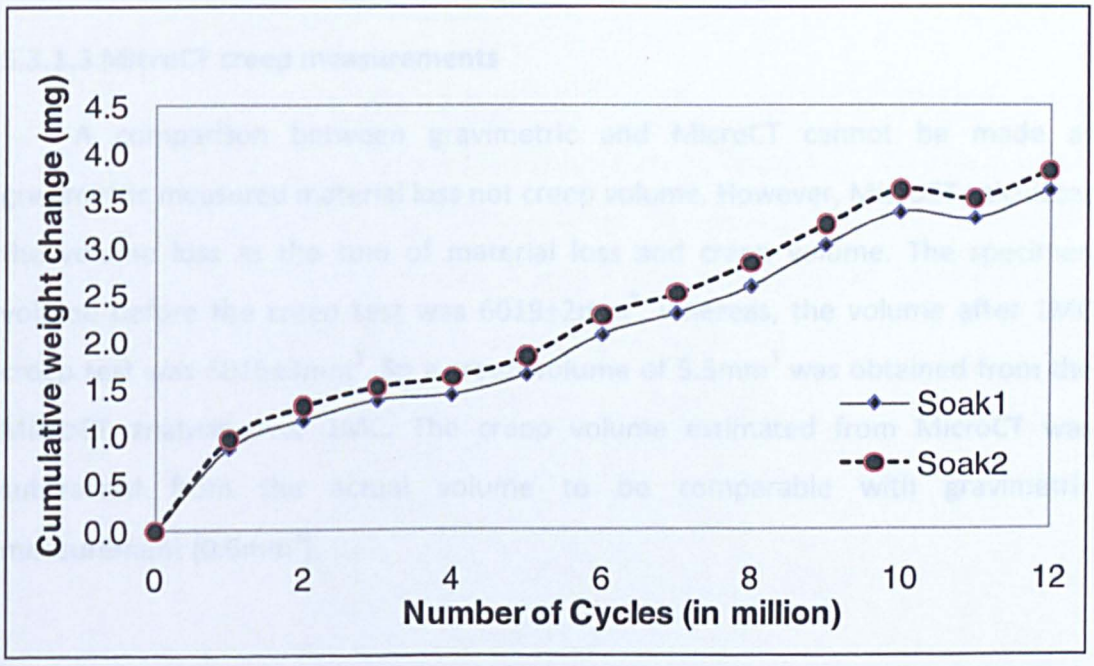

Figure 5-4 Weight change of soak samples over a course of 12 million cycles.

A gain of 0.04mg weight (0.04mm^3 volume) was observed in the load soak control as compared to the mean weight of soak controls (Figure 5-5).

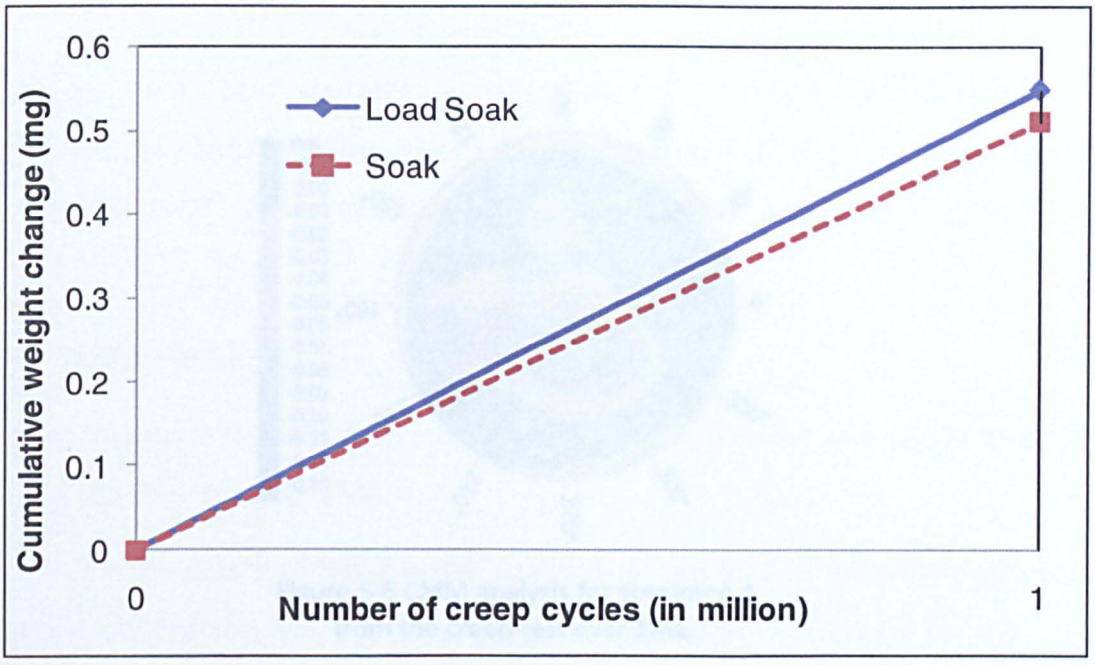

Figure 5-5 Cumulative weight gain (mg) of a load soak control under anterior posterior load in a 1 MC creep test as compared with mean weight of soak controls.

5.3.1.3 MicroCT creep measurements

A comparison between gravimetric and MicroCT cannot be made as gravimetric measured material loss not creep volume. However, MicroCT calculates the volume loss as the sum of material loss and creep volume. The specimen volume before the creep test was 6019±2mm^3, whereas, the volume after 1MC creep test was 6015±3mm^3. So a creep volume of 5.5mm^3 was obtained from the MicroCT analysis over 1MC. The creep volume estimated from MicroCT was subtracted from the actual volume to be comparable with gravimetric measurement (0.6mm^3).

5.3.1.4 Geometrical creep measurements

The volume change from the creep test was determined using geometrical volumetric techniques; CMM. The volume calculation from CMM was 5.9mm^3 (Figure 5-6), which was higher compared to the volume calculated from gravimetric (0.6mm^3). The deformation due to AP load caused a higher change in volume reported in CMM. However, it was due to creep, not material loss. A penetration depth of 113 µm was obtained from CMM analysis.

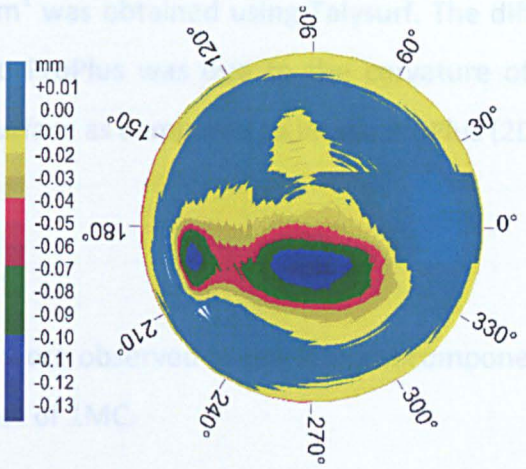

Figure 5-6 CMM analysis for specimen 4 from the creep test over 1MC.

5.3.1.5 Quantification of creep area, surface analysis, and creep depth

Superior surface scar area

The scar area from the superior surface after one MC of creep test was 171.9±11.48mm^2 i.e. 13.5% of the total surface area (Figure 5-7). The scar area was present in the lower bottom of the specimen. The distribution of the articulating scar area over the four quadrants are 0.1mm^2, 46.6mm^2, 36.7mm^2 and 88.5mm^2 in superior, inferior, lateral and medial quadrant respectively.

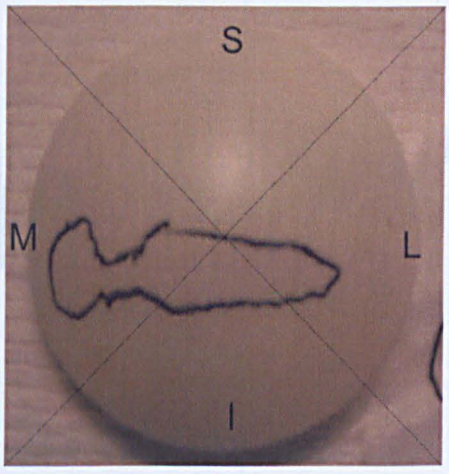

Figure 5-7 Scar area from a MC of the creep test. S: superior, I: inferior, M: medial and L: lateral.

The scar area was also measured with Talysurf form profilometer. A creep scar area of 175mm^2 was obtained using Talysurf. The difference in area between Talysurf and Image ProPlus was due to the curvature of the specimen. Talysurf measures the 3D surface as compared to Image ProPlus (2D measurement).

Visual observations

No scratches were observed in the femoral component and patella specimen during the creep test of 1MC.

Deformation was found in the superior surface area of the patella specimen after creep test of 1 MC. The creep characteristic is shown in Figure 5-7.

Surface analysis

The roughness parameters of the creep test specimen patella button (sample example as shown in Figure 5-8) are tabulated in Table 5-2. The selected area for roughness measurement defines only the wear scar. The average surface (R_a), skew (R_{sk}), peak (R_p) and valley (R_v) roughness decreased after one MC of creep test.

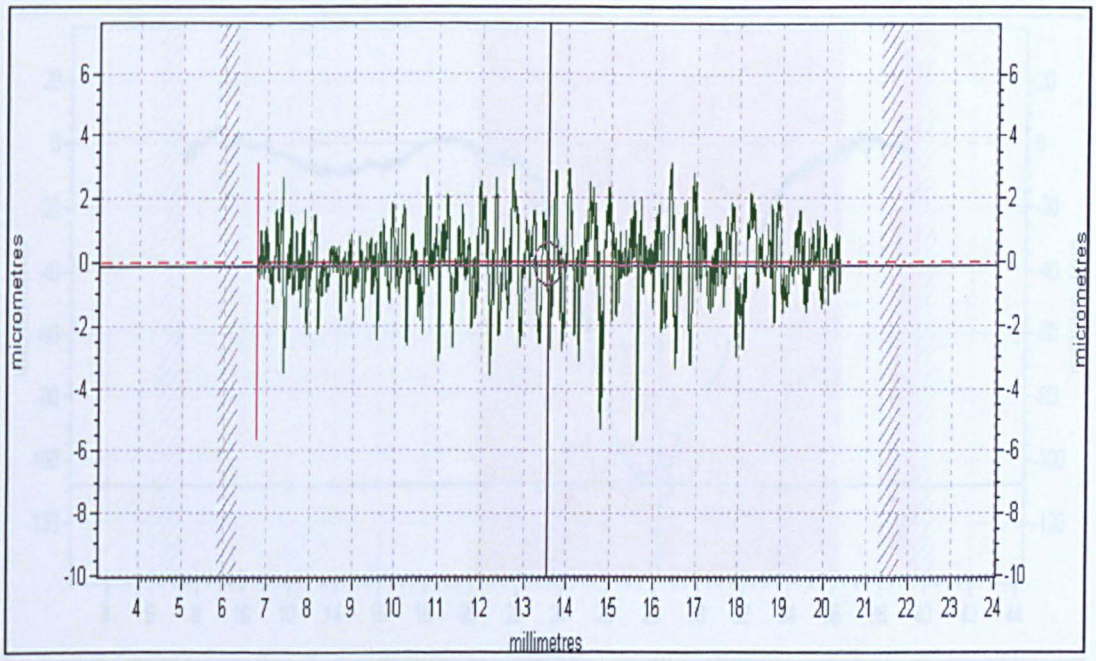

Figure 5-8 Roughness trace of creep test specimen after 1MC of the patella button.

Table5-2 Roughness parameters before and after 1MC creep test of the patella button.

Parameters	Before Test	After Test
R_a (μm)	1.15	0.71
R_{sk}	-0.17	-0.61
R_p(μm)	3.39	2.00
R_v(μm)	3.77	2.64

Creep depth

The deformation of the patella specimen is shown as example in Figure 5-9. The deformation in the specimen after the creep test of 1 million cycles was 110μm as measured by Talysurf. The penetration observed in current study was double the creep deformation as compared Vanbiervlier *et al.* (2011) (50μm) and similar to deformation by Ellison *et al.* (2008) 120μm. Good correlation with CMM (120μm) was observed.

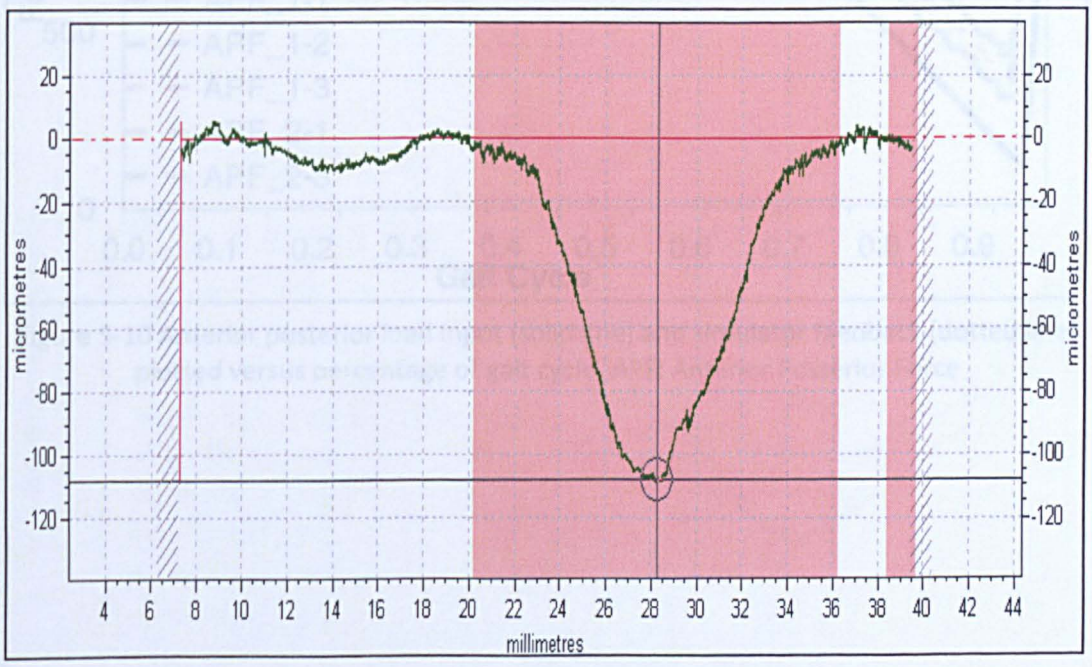

Figure 5-9 Figure representing the penetration in a specimen undergone 1 MC creep test.

5.3.2 High ML Rotation (>3°) and Uncontrolled ML Displacement

5.3.2.1 Kinematics

The first 6MC of the test was carried out at high ML rotation (>3°) and uncontrolled ML displacement. As the simulator used pneumatic motors for ML rotation, there were errors between the required control routine and obtained feedback. The pneumatic system was not able to accurately obtain such low values.

The feedbacks from the simulator for the input profiles are plotted for one gait cycle for anterior posterior load (Figure 5-10), superior inferior displacement (Figure 5-11) and medial lateral rotation (Figure 5-12). There was no flexion extension feedback. The ML rotation was four fold higher than the ML rotation in the physiological condition.

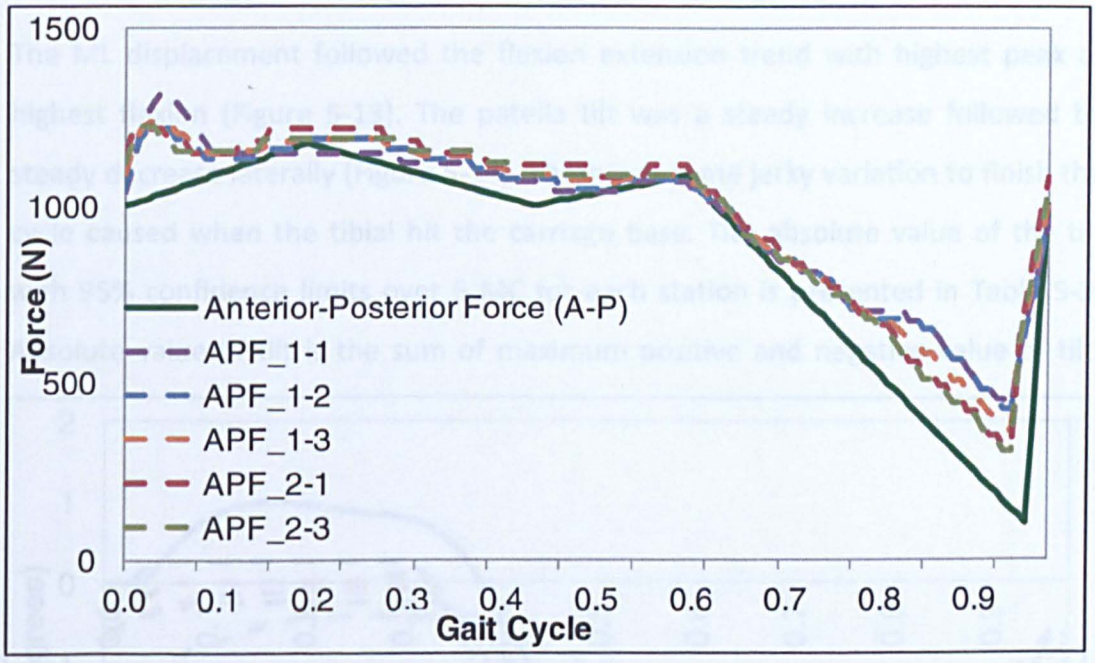

Figure 5-10 Anterior posterior load input (solid line) and simulator feedback (dotted line) plotted versus percentage of gait cycle. APF: Anterior Posterior Force

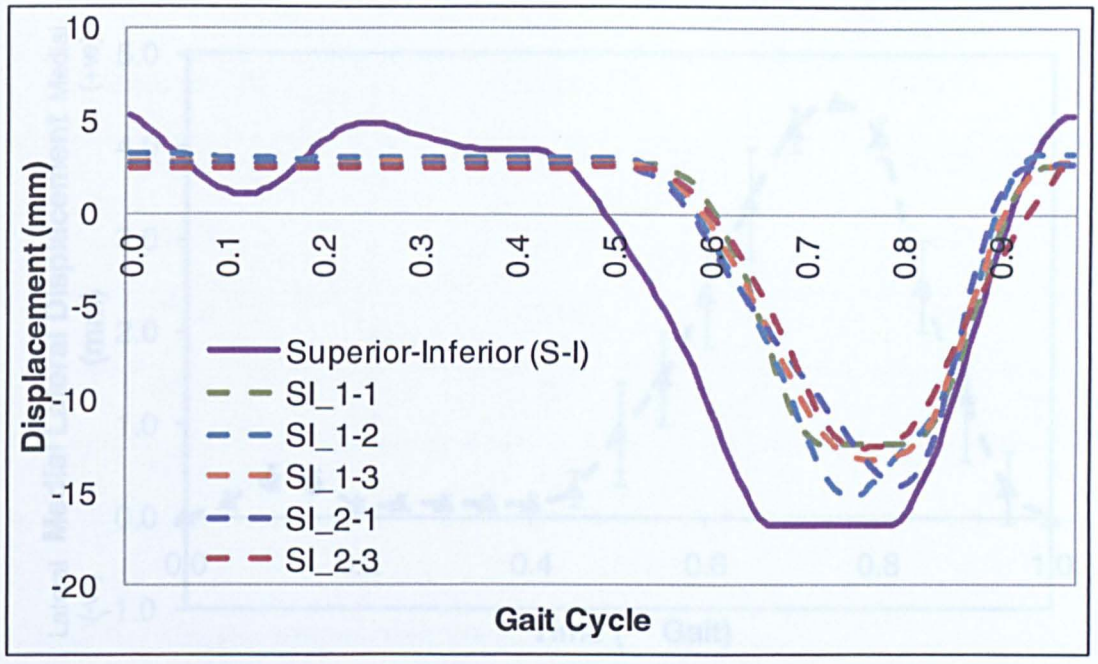

Figure 5-11 Superior inferior displacement input (solid line) and simulator feedback (dotted line) plotted versus percentage of gait cycle.

The ML displacement followed the flexion extension trend with highest peak at highest flexion (Figure 5-13). The patella tilt was a steady increase followed by steady decrease laterally (Figure 5-14). There was some jerky variation to finish the cycle caused when the tibial hit the carriage base. The absolute value of the tilt with 95% confidence limits over 6 MC for each station is presented in Table 5-3. Absolute value of tilt is the sum of maximum positive and negative value of tilt.

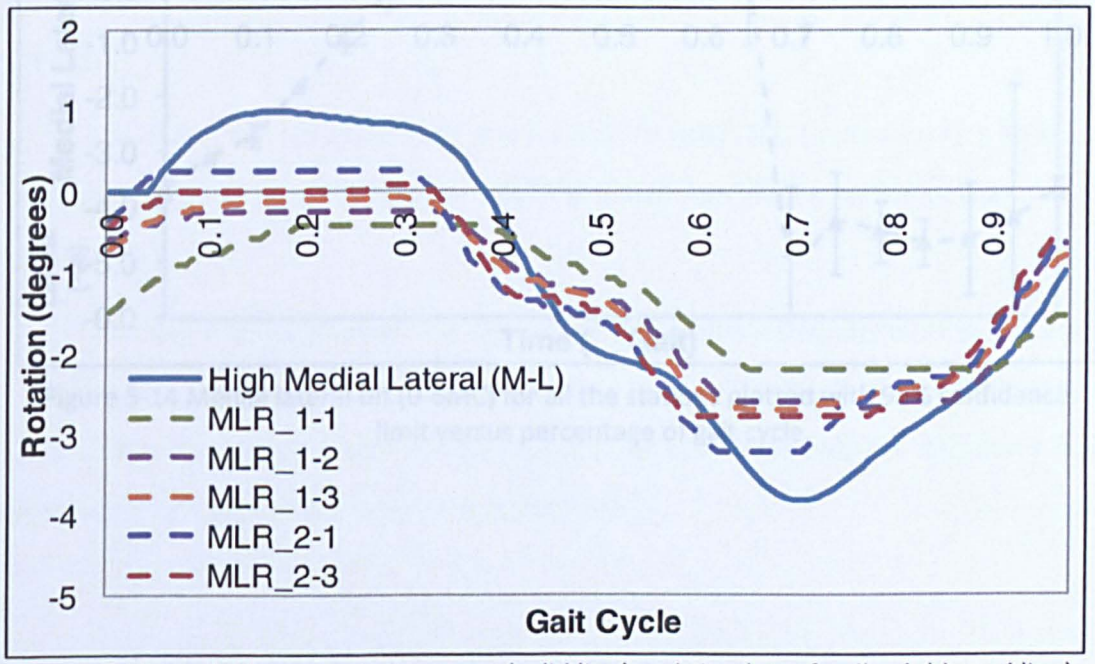

Figure 5-12 Medial lateral rotation input (solid line) and simulator feedback (dotted line) plotted versus percentage of gait cycle.

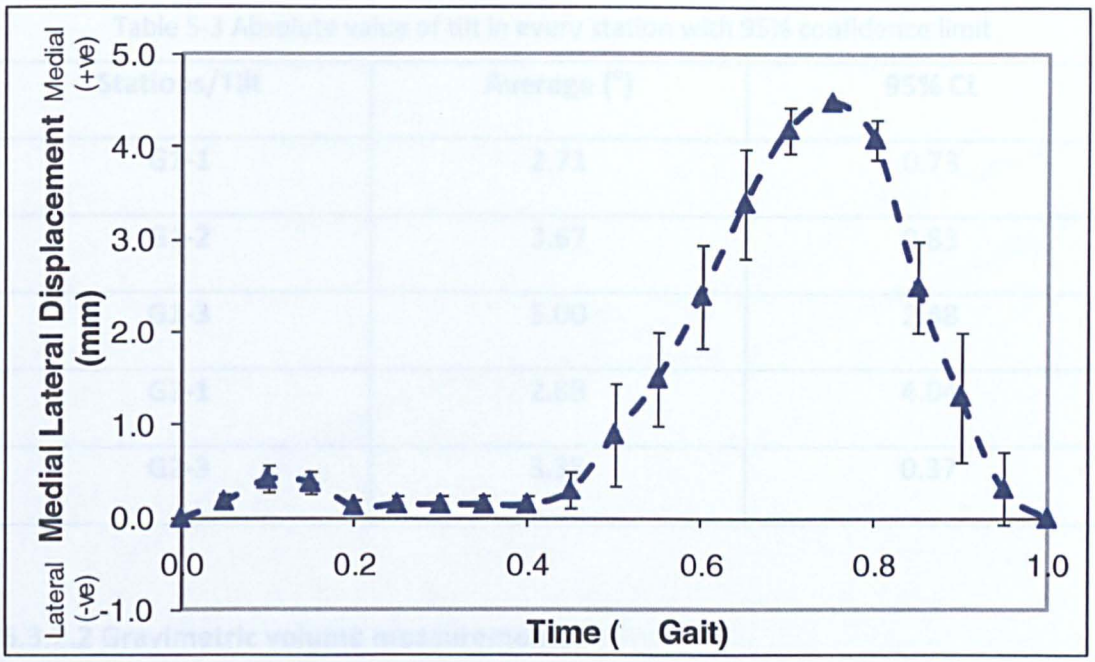

Figure 5-13 Medial lateral displacement plotted with 95% confidence limit versus percentage of gait cycle.

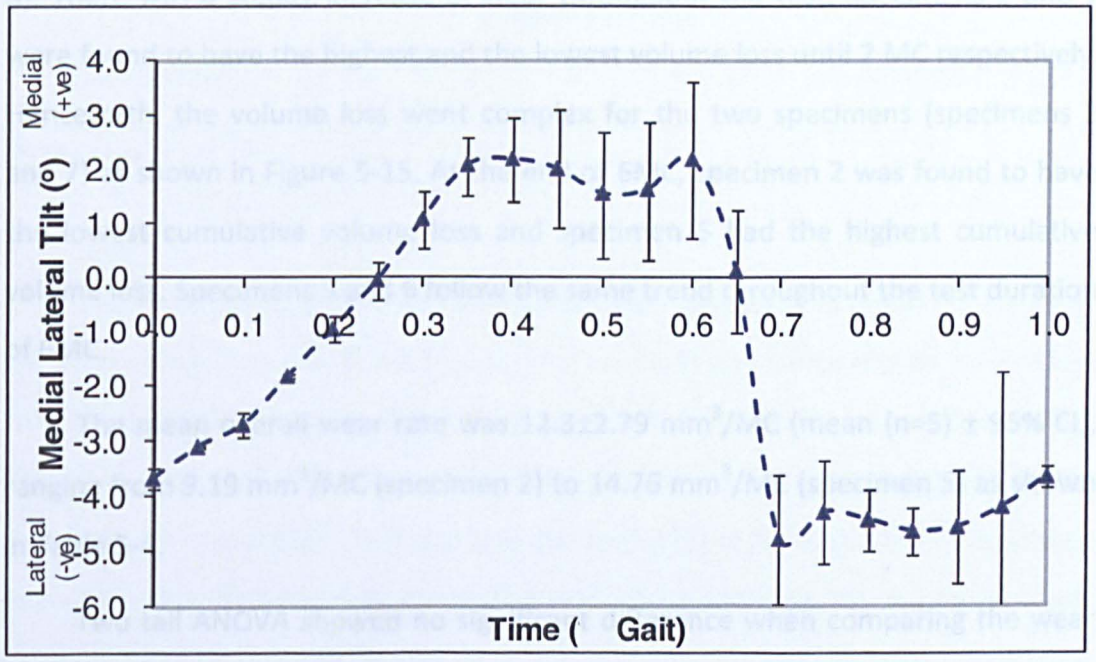

Figure 5-14 Medial lateral tilt (0-6MC) for all the stations plotted with 95% confidence limit versus percentage of gait cycle.

Table 5-3 Absolute value of tilt in every station with 95% confidence limit

Stations/Tilt	Average (°)	95% CL
G1-1	2.71	0.73
G1-2	3.67	0.83
G1-3	5.00	2.48
G2-1	2.88	4.04
G2-3	3.35	0.37

5.3.2.2 Gravimetric volume measurements

The mean cumulative volumetric wear over 6MC is shown in Figure 5-15 was 75.62±14.86 mm^3, ranging from 62.01 mm^3 (specimen 2) to 91.19 mm^3 (specimen 5). There was a steady increase in wear throughout the test. Specimens 2 and 7 were found to have the highest and the lowest volume loss until 2 MC respectively. Henceforth, the volume loss went complex for the two specimens (specimens 2 and 7) as shown in Figure 5-15. At the end of 6MC, specimen 2 was found to have the lowest cumulative volume loss and specimen 5 had the highest cumulative volume loss. Specimens 3 and 6 follow the same trend throughout the test duration of 6MC.

The mean overall wear rate was 12.3±2.79 mm^3/MC (mean (n=5) ± 95% CI), ranging from 9.19 mm^3/MC (specimen 2) to 14.76 mm^3/MC (specimen 5) as shown in Table 5-4.

Two tail ANOVA showed no significant difference when comparing the wear rate between specimens (p=0.43) or course of tests i.e. between each MC (p=0.43). This shows that there were low variability inter specimen and the simulator was producing non significant wear rate in each MC.

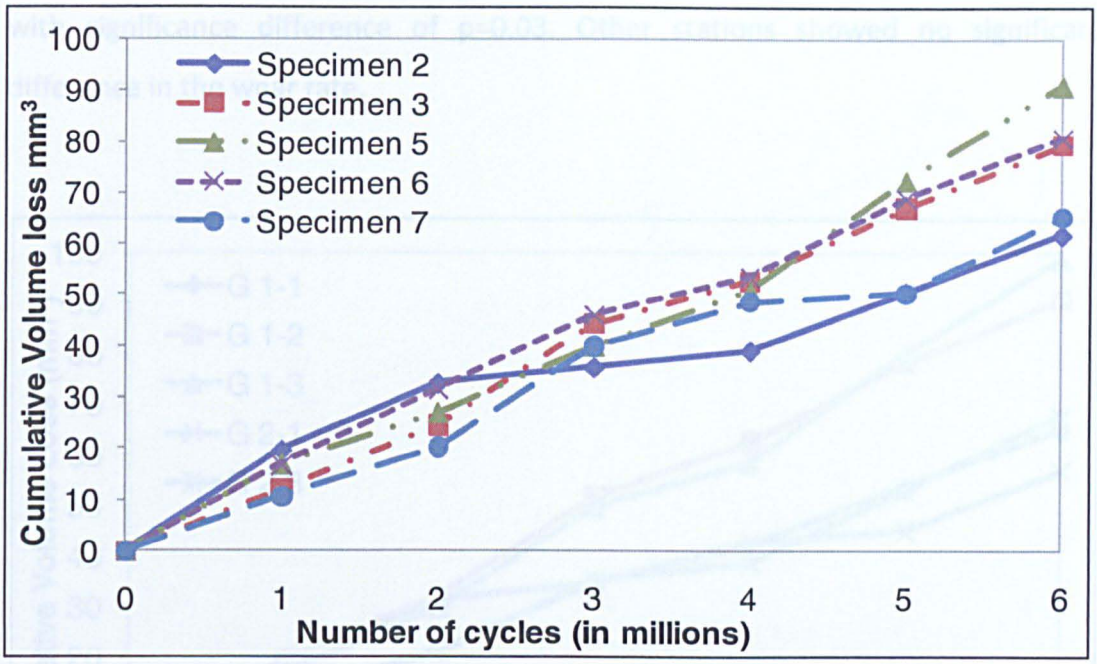

Figure 5-15 Cumulative volume loss, showing volume loss for every specimen at every MC for high ML rotation and uncontrolled ML displacement

Table 5-4 Wear rate for High ML rotation with uncontrolled ML displacement by specimen number over 6MC

Specimen No	2	3	5	6	7	Average	95%CL
Wear rate (mm^3/MC)	9.19	13.45	14.76	13.27	10.82	12.30	2.79

The cumulative volume loss per station was calculated as shown in Figure 5-16. Stations G1-2 and G1-3 had higher tilt (Table 5-3) and hence higher volume loss compared to other stations. Station G2-1 had a higher volume loss similar to G1-2 and G1-3 until 2MC. Following, the volume loss of station G2-1 decreased to the lowest at the end of 6MC. This was also due to the highest variation of tilt observed in station G2-1 (Table 5-3). Stations G1-1 and G2-2 had lowest tilt and hence lower volume throughout the wear test.

The overall wear rate for the station was 12.30±3.41mm^3/MC (mean (n=5) ± 95%CL). The mean wear rate ranged for stations from highest to lowest in station G1-3 (15.50mm^3/MC) to G2-1 (9.28mm^3/MC) as shown in Table 5-5

Variability in wear rate among station to station was performed using two tails ANOVA. Higher wear rate among station (G1-3) as compared to station (G1-1)

with significance difference of p=0.03. Other stations showed no significant difference in the wear rate.

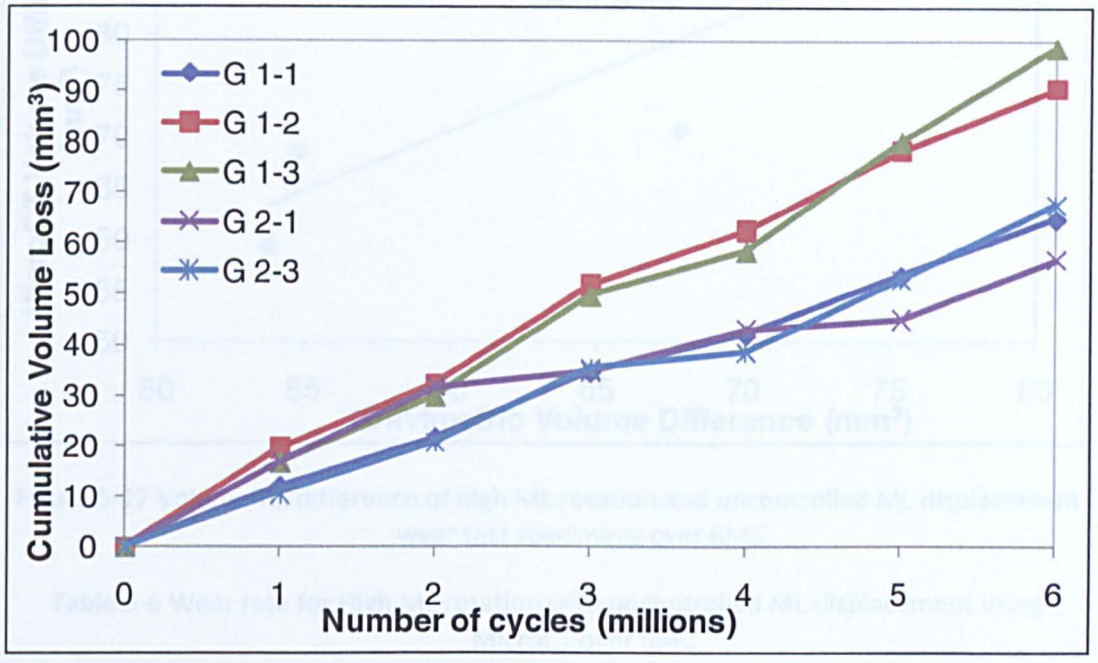

Figure 5-16 Cumulative volume loss, showing volume loss for different stations at every MC for high ML rotation and uncontrolled ML displacement

Table 5-5 Wear rate for High ML rotation with uncontrolled ML displacement by station number over 6MC

Station	G1-1	G1-2	G1-3	G2-1	G2-3	Average	95%CL
Wear rate (mm^3/MC)	10.77	14.92	15.50	9.28	11.02	12.30	3.41

5.3.2.3 MicroCT volume measurements

The volume difference obtained from MicroCT was compared with gravimetric volumetric difference. The volumes were correlated with strong linear regression (R^2) value of 0.83 as shown in Figure 5-17. The mean volume difference from MicroCT was 76±18mm^3 as compared to gravimetric of 75.62±14.86mm^3. No significant difference was found between the gravimetric and MicroCT volume determination (p=0.2). The wear rate from the MicroCT is presented in Table 5-6. The mean wear rate from the MicroCT was 12.67±3.03 mm^3/MC.

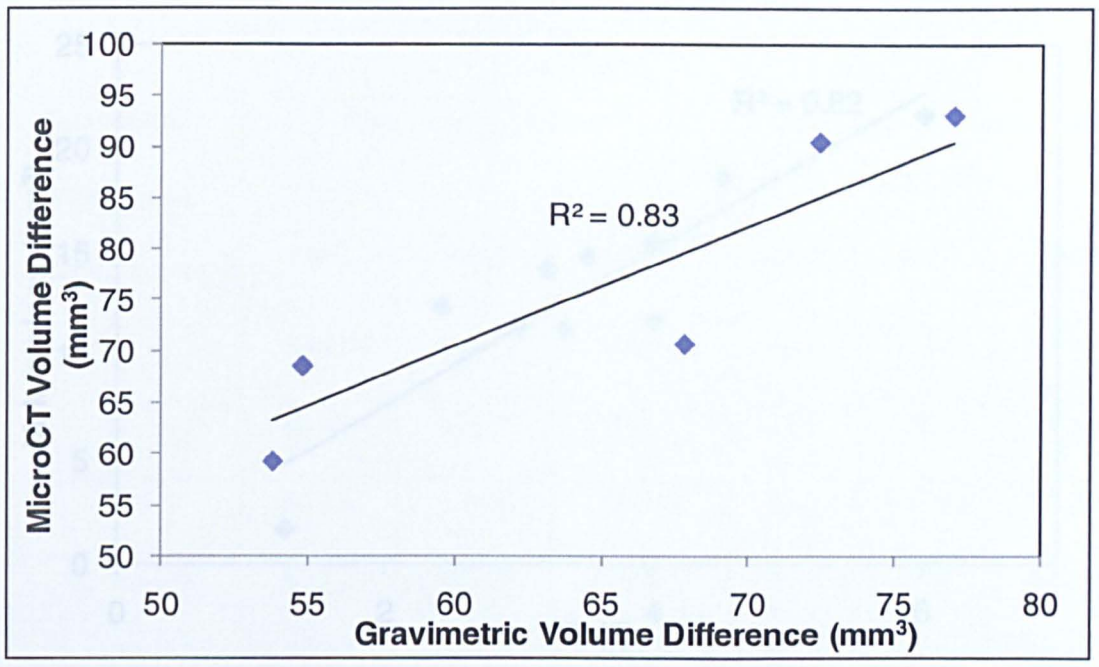

Figure 5-17 Volumetric difference of high ML rotation and uncontrolled ML displacement wear test specimens over 6MC.

Table 5-6 Wear rate for High ML rotation with uncontrolled ML displacement using MicroCT over 6MC

Specimen	2	3	5	6	7	Average	95%CL
Wear rate in mm^3/MC	9.82	11.73	15.44	15.01	11.36	12.67	3.03

5.3.2.4 Geometric volume measurements

CMM was employed to measure the volume of the specimens after 12MC. The results will be discussed in later section.

5.3.2.5 Volume loss with ML tilt

There was a linear increase in volume loss with tilt as shown in Figure 5-18. The linear correlation was strong with R^2 value of 0.82.

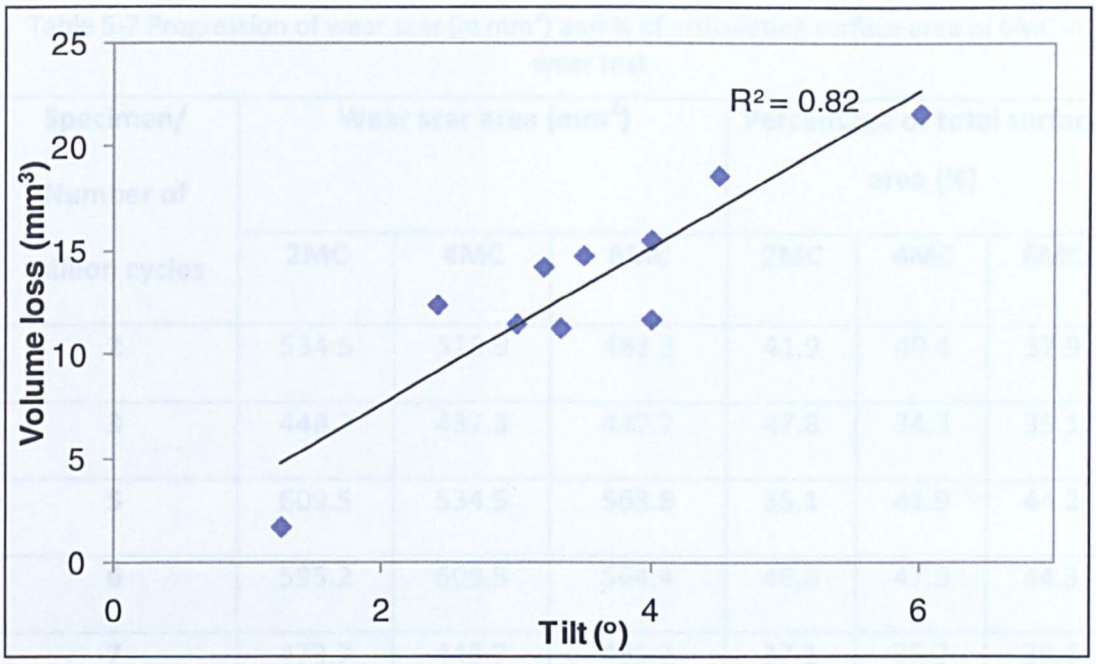

Figure 5-18 Relation of volume loss with tilt represented with linear correlation of R^2 value.

5.3.2.6 Quantification of wear scar area, surface analysis, and wear depth

Wear scar area

The wear scar areas were measured at 2, 4 and 6MC and percentage of the total surface area are represented in Table 5-7. Two tail ANNOVA were conducted for wear scar area between 2, 4 and 6MC. No significant difference was found between the wear scars (p=0.73). The wear area increased in the first two million cycles and remained the same throughout the test.

The distributions of wear scar area in the four quadrants (superior, inferior, lateral and medial) are presented in Table 5-8 in mm^2±95%CL. The wear scar area occurred in the inferior of the specimens.

The wear scar area for all the specimens after 6MC wear test are shown in Figure 5-19. Specimens 5 and 6 had the highest wear scar areas.

Table 5-7 Progression of wear scar (in mm^2) and % of articulating surface area of 6MC in wear test.

Specimen/ Number of million cycles	Wear scar area (mm^2)			Percentage of total surface area (%)		
	2MC	4MC	6MC	2MC	4MC	6MC
2	534.5	515.9	483.3	41.9	40.4	37.9
3	448.7	437.3	447.7	47.8	34.3	35.1
5	609.5	534.5	563.8	35.1	41.9	44.2
6	595.2	609.5	564.4	46.6	47.8	44.3
7	473.7	448.7	485.2	37.1	35.2	38.1
Mean±95%CL	*532.3±89*	*509.2±87*	*508.9±96*	*41.7±7*	*39.9±7*	*39.9±8*

Table 5-8 Progression of wear scar (in mm^2) in superior, inferior, lateral and medial quadrant during 6MC in wear test

Number of million cycles	Quadrant			
	Superior	Inferior	Lateral	Medial
2	23.8±18.6	138.9±20.9	190.6±15.1	171.6±30.0
4	25.2±21.3	134.8±20.8	195.5±13.3	181.6±14.9
6	27.34±41.2	153.7±23.6	180.9±38.8	145.7±25.1

The area in inferior quadrant (Table 5-8) increases whereas, area in medial quadrant decreases from 181.6mm^2 to 145.7 mm^2. This is not possible as the area increases with cycle count. It can be accounted as an measurement error.

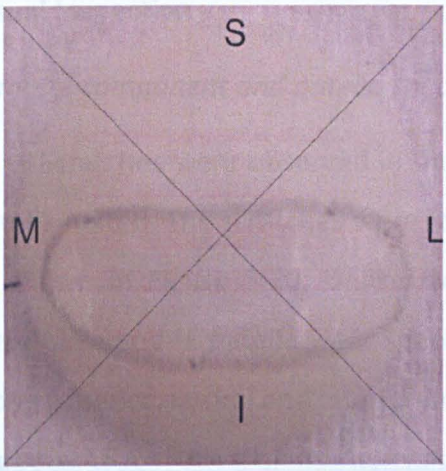

Specimen2@ 6MC

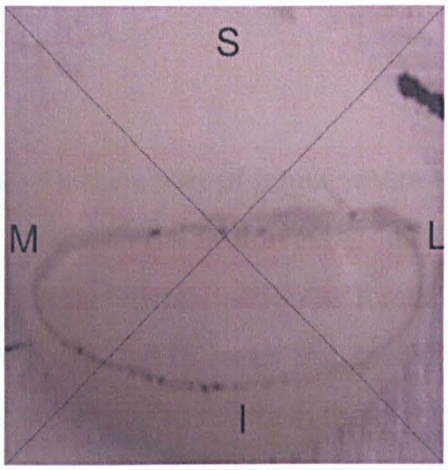

Specimen 3@6MC

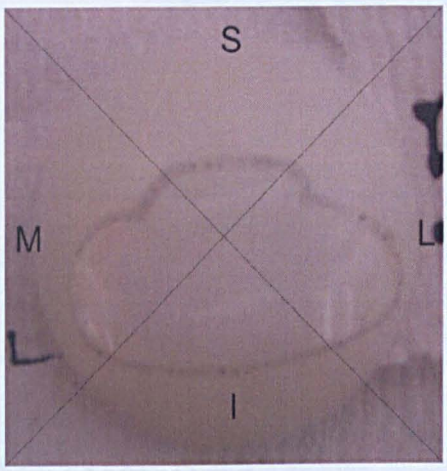

Specimen 5@ 6MC

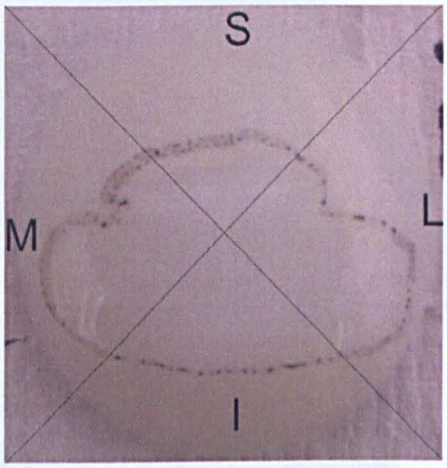

Specimen 6@ 6MC

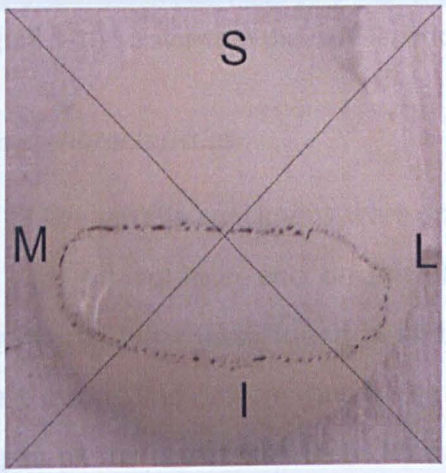

Specimen 7@6MC

Figure 5-19 Wear scar area for 5 specimens with solid line indicating worn area over 6MC.

Visual inspection

Femoral component and patella specimen

Scratches were observed in the superior articulating part of femur where the patella mated. The scratches were found to be parallel to the flexion extension axis as shown in Figure 5-20. Unlike the femoral compartment, moderate scratches were observed in patella wear specimens more compared to creep test specimen along superior, lateral and inferior quadrant and increasing to severe in the medial.

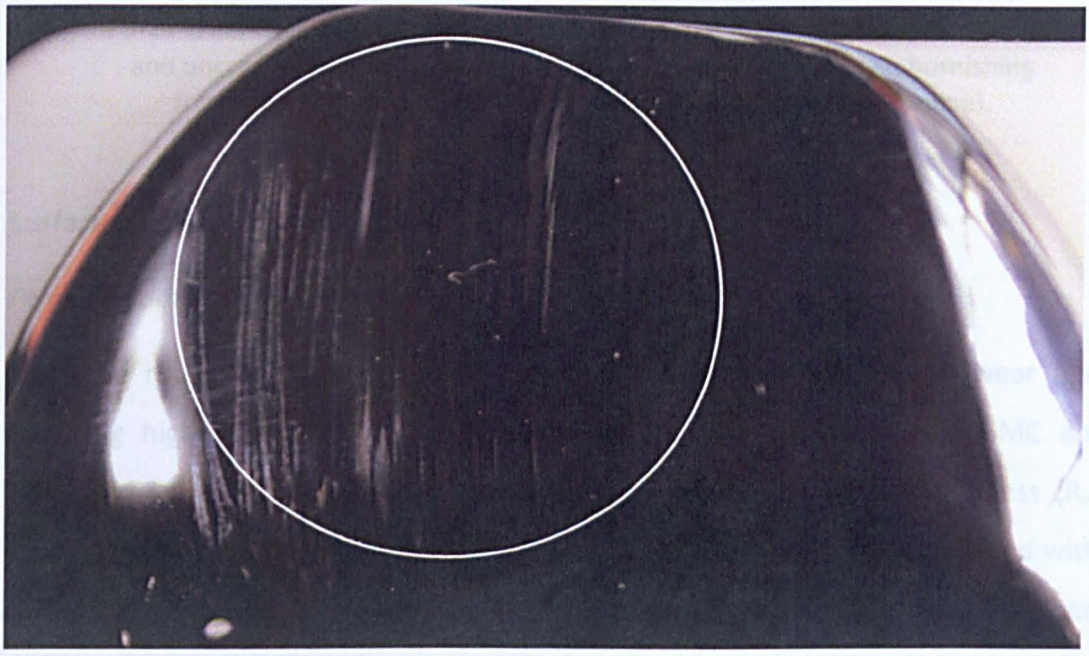

Figure 5-20 Scratches in the patella articulating femoral groove. While solid line highlights the scratches.

Wear characteristics

The patella specimens were sorted according to the wear regions after 6MC of high ML rotation and uncontrolled ML displacement wear test. Three main regimes of wear were found in all the specimens as shown in Figure 5-21. These were pitting and deformation in the middle of the specimen and burnishing on the edges of the wear scar area. Moderate scratches were observed in the patella specimens in the superior, lateral and inferior quadrants and increasing to severe scratches in the medial quadrant.

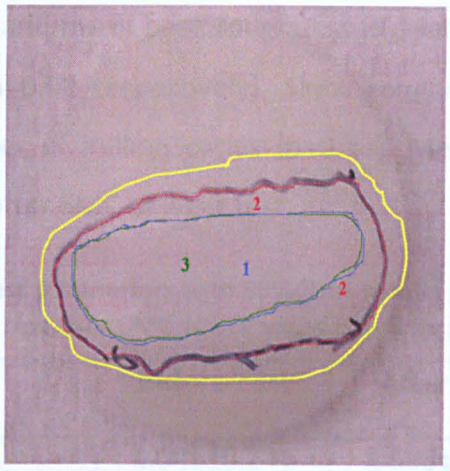

Figure 5-21 Wear characteristics of wear test specimen undergoing high ML rotation and uncontrolled ML displacement. 1: pitting wear (blue line), 2: burnishing (red line), 3: deformation (green line) and 4: scratching (yellow line).

Surface analysis

Femoral Component

The roughness parameters for femoral components during the wear test involving high ML rotation and uncontrolled ML displacements over 6MC are tabulated in Table 5-9. Average roughness (R_a) and mean valley roughness (R_v) increased significantly after the test (p=0.01). Skew roughness (R_{sk}) decreased with number of million cycles significantly (p=0.01). Mean peak roughness (R_p) remained the same after 6MC of wear test.

Table 5-9 Mean roughness parameters with 95%CL of femoral component before and after the test over 6MC with P value (*p<0.05 significant)

Parameters	Before Test	After Test	P value
R_a (μm)	0.030±0.002	0.043±0.011	0.01*
R_{sk}	0.743±0.452	-1.001±0.808	0.01*
R_p(μm)	0.105±0.004	0.099±0.018	0.79
R_v(μm)	0.071±0.003	0.095±0.023	0.01*

Patella Specimen

Similar to femoral component, changes in roughness parameters were observed in patella specimen over 6MC of wear test as shown in Table 5-10.

Average roughness (R_a) and mean peak roughness (R_p) increased significantly after the test (p=0.05 and p=0.01 respectively). Skew roughness (R_{sk}) increased non significantly with number of million cycles (p=0.13). Mean valley roughness (R_v) decreased significantly after 6MC of wear test.

Table 5-10 Mean roughness parameters with 95%CL of patella specimen before and after the test over 6MC with P value (*p<0.05 significant)

Parameters	Before Test	After Test	P value
R_a (μm)	1.049±0.241	1.593±0.612	0.05*
R_{sk}	-0.281±0.422	0.975±2.029	0.13
R_p(μm)	2.835±0.329	3.078±0.509	0.01*
R_v(μm)	3.121±0.356	2.8076±0.535	0.01*

Wear depth

Wear depth of the specimens increased with number of million cycles as shown in Table 5-11. Specimen 5 had the highest deformation over 6MC and specimens 2, 3 and 7 had the lowest deformation after the wear test.

Table 5-11 Wear depth for patella specimens over 6MC

Specimen Number	Wear depth(μm)
2	800
3	800
5	1000
6	850
7	800
Mean±95%CL	*850±108*

5.3.3 Low ML Rotation with Uncontrolled ML Displacement

This condition is the most physiological condition with ML rotation less than 1° and the ML displacement uncontrolled. This condition was run for the next 3MC.

5.3.3.1 Kinematics

The station feedbacks from simulator following the input profiles were plotted versus the gait cycle for anterior posterior load (Figure 5-22), superior inferior displacement (Figure 5-23) and medial lateral rotation (Figure 5-24). Station G2-1 was the only station that was close to the input ML rotation. However, the feedback was found to be not very smooth.

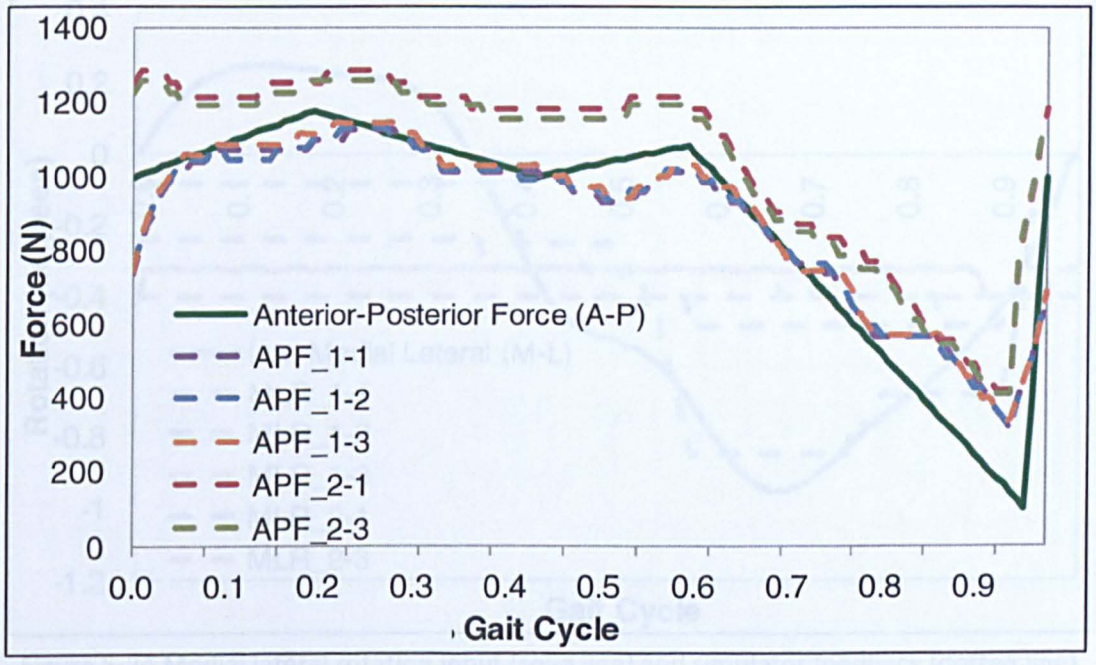

Figure 5-22 Anterior posterior load input (solid line) and simulator feedback (dotted line) plotted versus percentage of gait cycle.

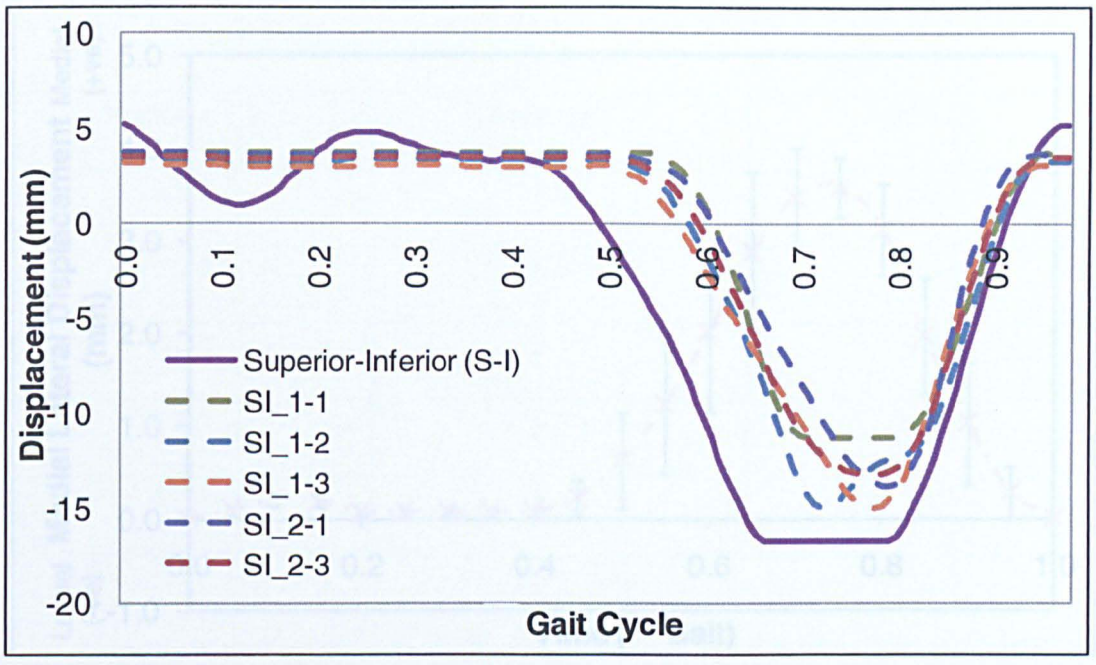

Figure 5-23 Superior inferior displacement input (solid line) and simulator feedback (dotted line) plotted versus percentage of gait cycle.

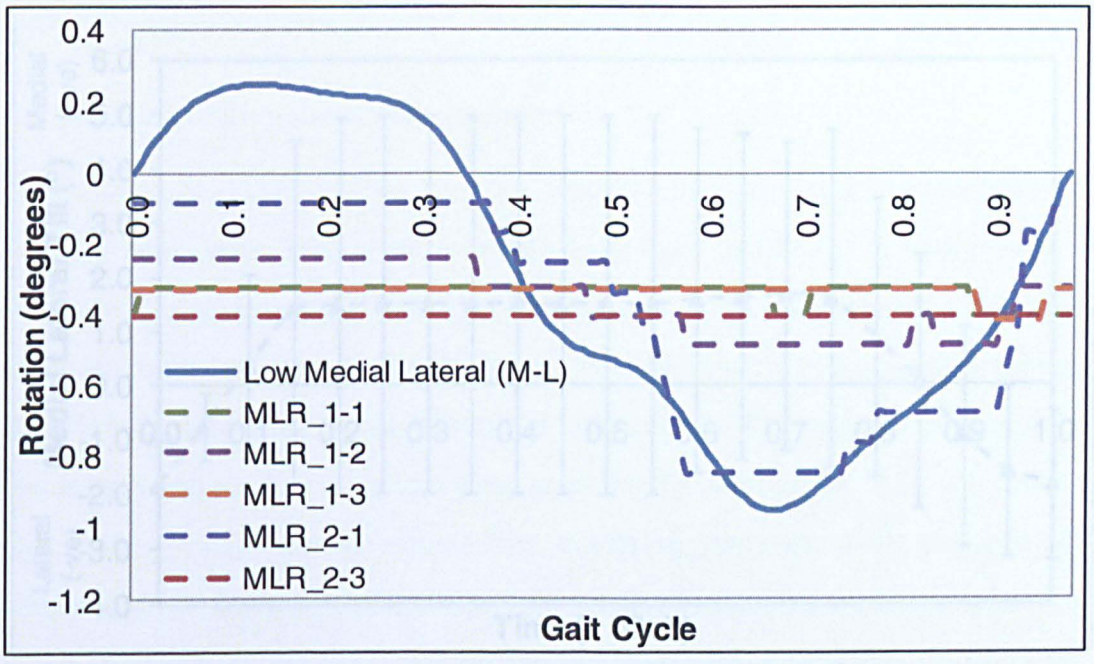

Figure 5-24 Medial lateral rotation input (solid line) and simulator feedback (dotted line) plotted versus percentage of gait cycle.

The ML displacement and tilt are shown in Figures 5-25 and 5-26. Similar to Figure 5-13, the highest ML displacement is at highest flexion. The tilt follows the same trend as in Figure 5-14. However, the magnitude is lower in this condition. The absolute values of tilt for all the stations are tabulated in Table 5-12.

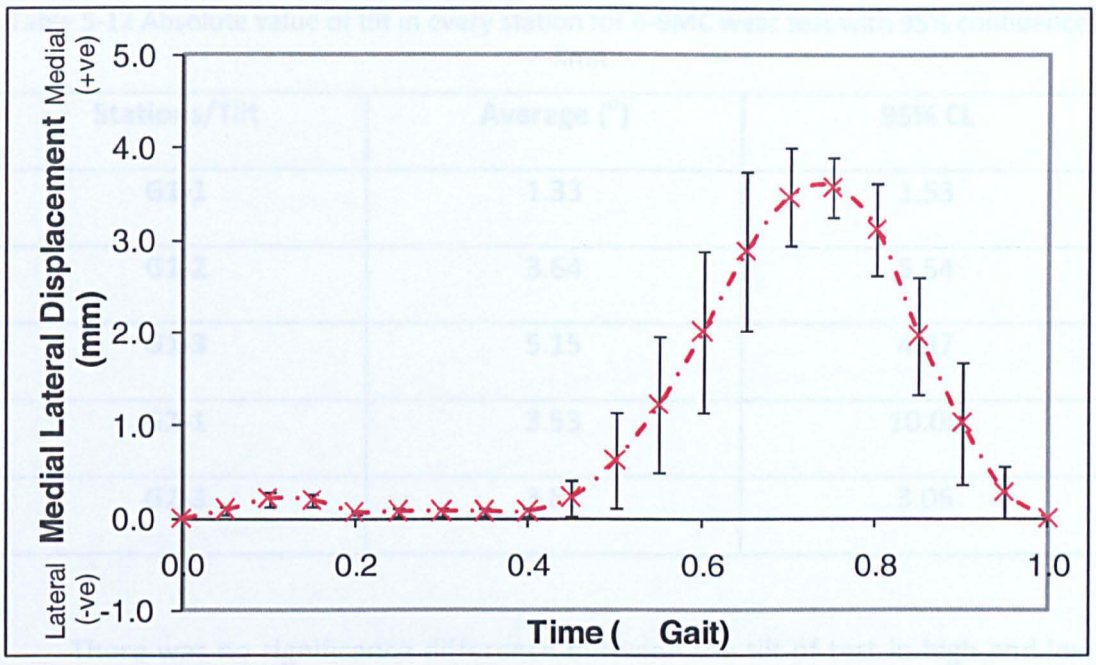

Figure 5-25 Medial lateral displacement plotted with 95% confidence limit versus percentage of gait cycle.

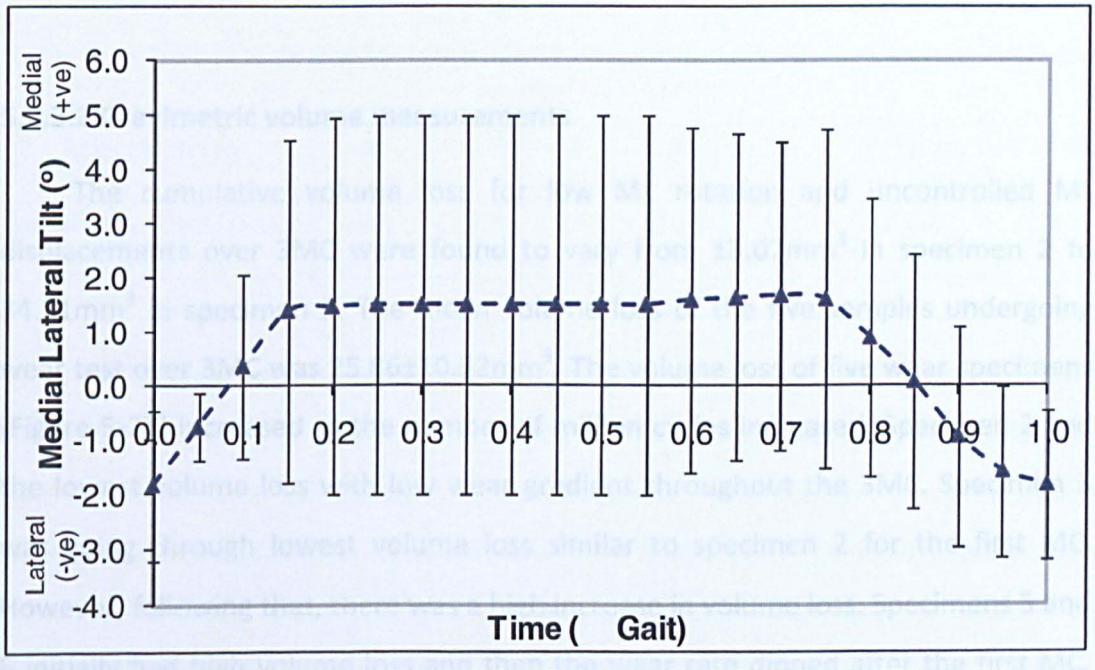

Figure 5-26 Medial lateral tilt (6-9MC) for all the stations plotted with 95% confidence limit versus percentage of gait cycle.

Table 5-12 Absolute value of tilt in every station for 6-9MC wear test with 95% confidence limit.

Stations/Tilt	Average (°)	95% CL
G1-1	1.33	1.53
G1-2	3.64	5.54
G1-3	5.15	4.87
G2-1	3.53	10.06
G2-3	3.81	3.06

There was no significance difference between the tilt of test in high and low ML rotation with uncontrolled ML displacements (p=0.97).

5.3.3.2 Gravimetric volume measurements

The cumulative volume loss for low ML rotation and uncontrolled ML displacements over 3MC were found to vary from 13.07mm^3 in specimen 2 to 34.21mm^3 in specimen 3. The mean volume loss of the five samples undergoing wear test over 3MC was 25.86±10.32mm^3. The volume loss of five wear specimens (Figure 5-27) increased as the number of million cycles increased. Specimen 2 had the lowest volume loss with low wear gradient throughout the 3MC. Specimen 3 was going through lowest volume loss similar to specimen 2 for the first MC. However, following that, there was a high increase in volume loss. Specimens 5 and 6 initially had high volume loss and then the wear rate dipped after the first MC. Specimen 7 had a complex volume loss trend with high wear rate during first and third MC and lower wear rate during 2MC.

The mean overall wear rate 8.63±3.44 mm^3/MC (mean (n=5) ± 95% CI) was calculated through gravimetric analysis, ranging from 4.68 mm^3/MC (specimen 2) to 11.63 mm^3/MC (specimen 3) as shown in Table 5-13.

Two tail ANOVA produced no significant difference while comparing the wear rate between specimens (p=0.45) during the course of test.

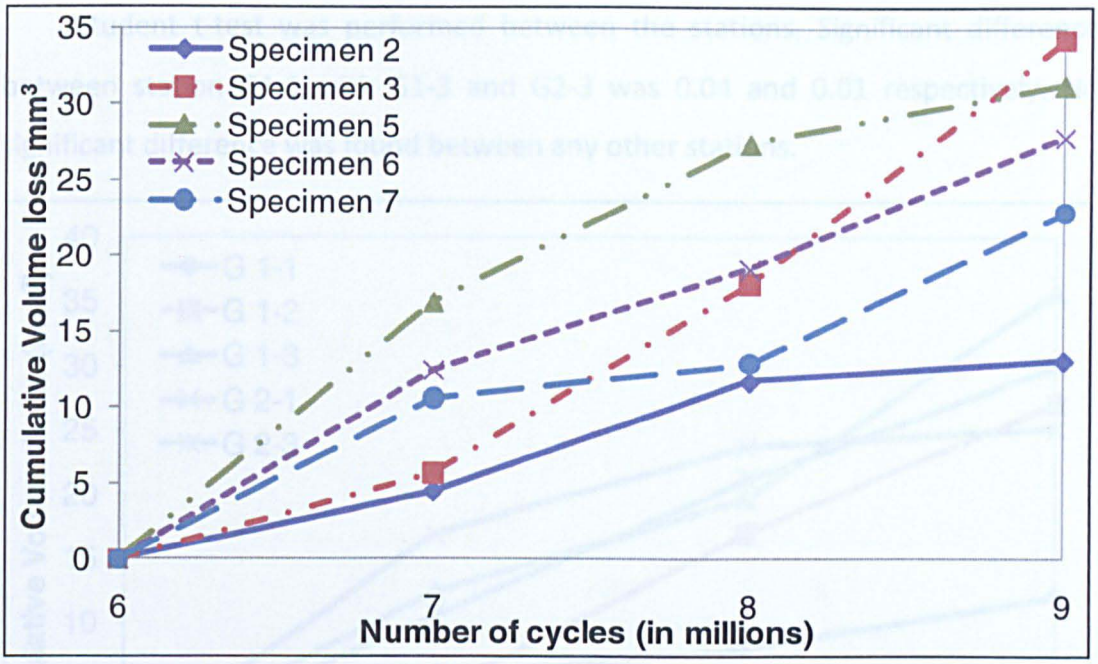

Figure 5-27 Cumulative volume loss, showing volume loss for every specimen at every MC for low ML rotation and uncontrolled ML displacement

Table 5-13 Wear rate for low ML rotation with uncontrolled ML displacement by specimen number over 3MC

Specimen No	2	3	5	6	7	Average	95%CL
Wear rate (mm^3/MC)	4.68	11.63	10.55	9.13	7.18	8.63	3.44

The volume loss for every station was calculated cumulatively for the 3MC wear test as shown in Figure 5-28. Station G2-3 had increase in volume loss with constant linear wear rate. Station G2-1 increased with the number of million cycles during the first two million cycles. In the last million cycles the wear gradient and tilt were however lower (Table 5-12). This was shown with high variation in CL (Table 5-12) and dip in the wear rate (Figure 5-28). G1-1 was the lowest wearing station over the 3MC with average absolute tilt of 1.33°. Volume loss in station G1-2 was lowest in the first MC. Following the first MC, the wear gradient was high due to an increase in volume loss. Station G1-3 had approximately linear wear gradient. The total volume loss was the highest in station G1-3 after 3MC.

The wear rate varied from 3.83mm^3/MC in station G1-1 to 11.56mm^3/MC in station G1-3. The mean wear rate from the five stations was 8.63±3.65mm^3/MC as shown in Table 5-14.

Student t-test was performed between the stations. Significant difference between station G1-1 with G1-3 and G2-3 was 0.04 and 0.01 respectively. No significant difference was found between any other stations.

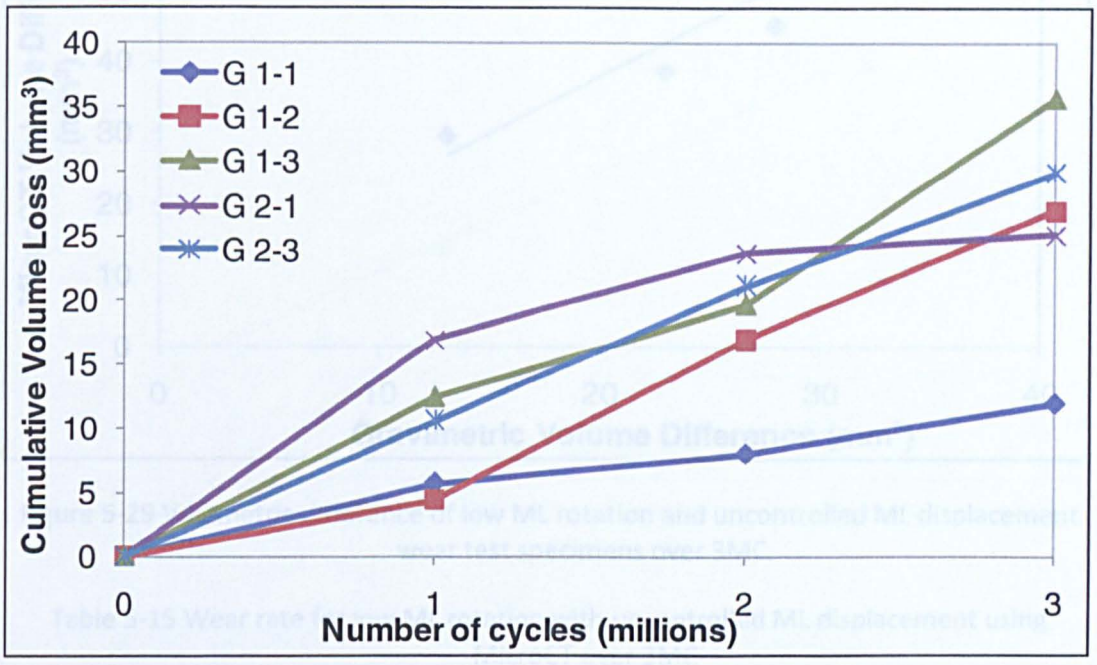

Figure 5-28 Cumulative volume loss for different stations at every MC for low ML rotation and uncontrolled ML displacement

Table 5-14 Wear rate for low ML rotation with uncontrolled ML displacement by station number over 3MC

Station	G1-1	G1-2	G1-3	G2-1	G2-2	Average	95%CL
Wear rate (mm^3/MC)	3.83	9.41	11.56	8.25	10.10	8.63	3.65

5.3.3.3 MicroCT volume measurements

The volume difference obtained from MicroCT was compared with gravimetric volumetric difference. The volumes were correlated with linear regression (R^2) value of 0.85 as shown in Figure 5-29. MicroCT mean cumulative volume difference was higher (35.32±30.9mm^3) as compared to gravimetric (25.86±10.3mm^3). The wear rate from the MicroCT analysis is presented in Table 5-15. The mean wear rate from the MicroCT from the wear test over 3MC was 7.98±4.08 mm^3/MC.

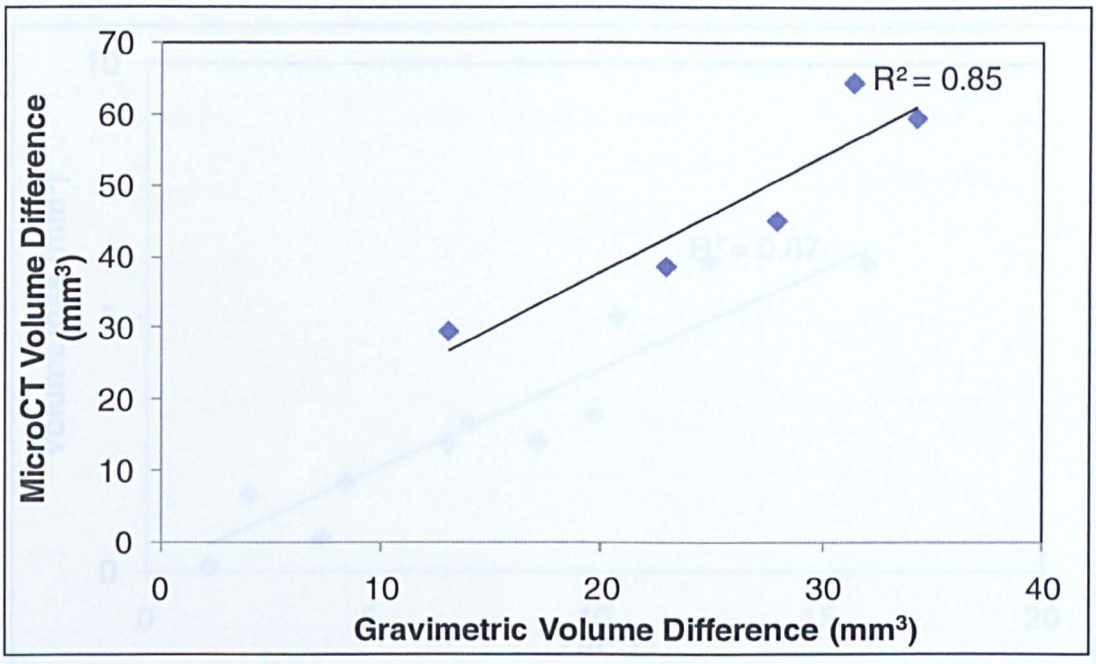

Figure 5-29 Volumetric difference of low ML rotation and uncontrolled ML displacement wear test specimens over 3MC.

Table 5-15 Wear rate for low ML rotation with uncontrolled ML displacement using MicroCT over 3MC

Specimen	2	3	5	6	7	Average	95%CL
Wear rate in mm^3/MC	5.92	9.49	12.98	6.71	4.80	7.98	4.08

5.3.3.4 Volume loss with ML tilt

There was a linear increase in volume loss with tilt similar to earlier case of high ML displacement and uncontrolled ML displacement as shown in Figure 5-30. The linear correlation was strong with R^2 value of 0.87.

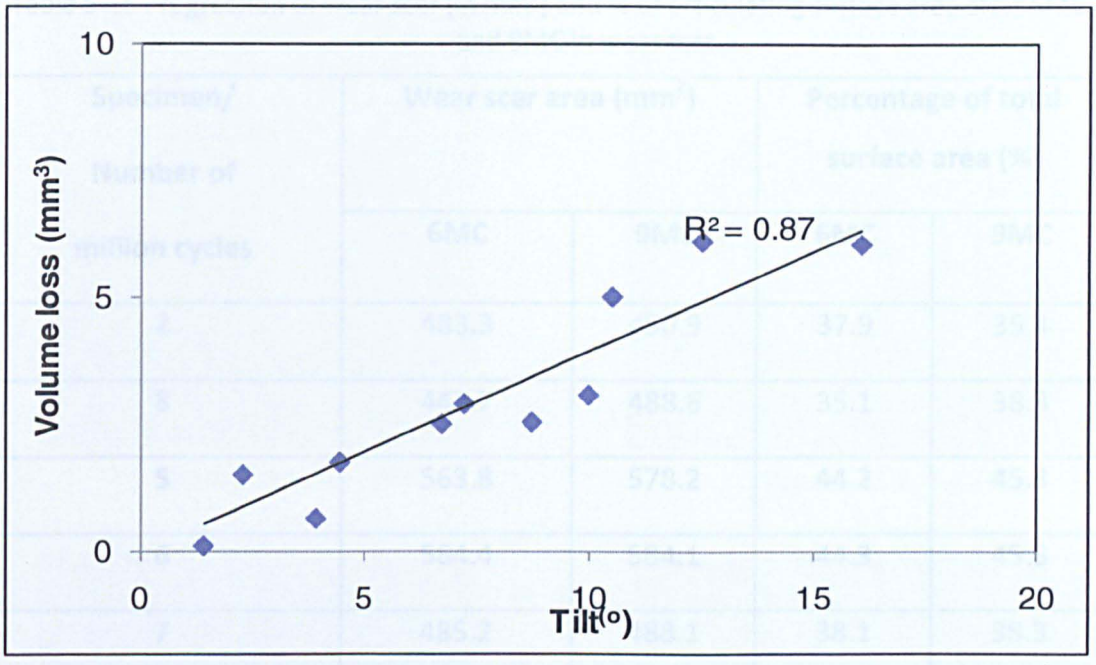

Figure 5-30 Relation of volume loss with tilt represented with linear correlation of R^2 value.

5.3.3.5 Quantification of wear scar area, surface analysis, and wear depth

Wear scar area

The wear scars were measured at 6 and 9MC. The scar area in mm^2 and percentage of the total surface area were represented in Table 5-16. Two tail ANOVAs (student t-test) were conducted for wear scar area between 6 and 9MC. The wear scars were similar and there was no significant difference (p=0.8).

The distributions of wear scar area in the four quadrants (superior, inferior, lateral and medial) are presented in Table 5-17 in mm^2±95%CL. The wear scar area occurred in the bottom half of the specimens similar to earlier scenario.

The wear scar area for all the specimens at 9MC of the wear test are shown in Figure 5-31. Specimens 5 and 6 underwent the highest wear scar area.

Table 5-16 Progression of wear scar (in mm^2) and % of articulating surface area after 6MC and 9MC in wear test

Specimen/ Number of million cycles	Wear scar area (mm^2)		Percentage of total surface area (%)	
	6MC	9MC	6MC	9MC
2	483.3	450.9	37.9	35.4
3	447.7	488.6	35.1	38.3
5	563.8	578.2	44.2	45.3
6	564.4	584.1	44.3	45.8
7	485.2	488.1	38.1	38.3
Mean±95%CL	*508.9.1±65*	*517.9±74*	*39.9±8*	*40.6±6*

Table 5-17 Progression of wear scar (in mm^2) in superior, inferior, lateral and medial quadrant during 3MC in wear test

Number of million cycles	Quadrant			
	Superior	Inferior	Lateral	Medial
6	27.34±41.2	153.7±23.6	180.9±38.8	145.68±25.1
9	33.7±40.3	153.0±11.8	179.4±12.6	172.3±28.2

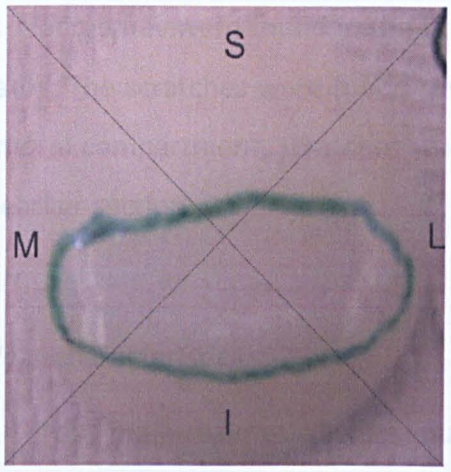

Specimen 2@ 9MC

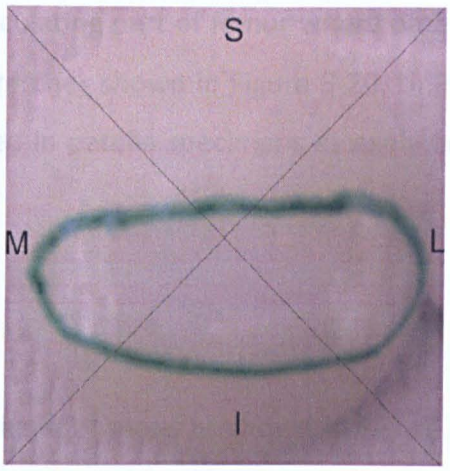

Specimen 3@9MC

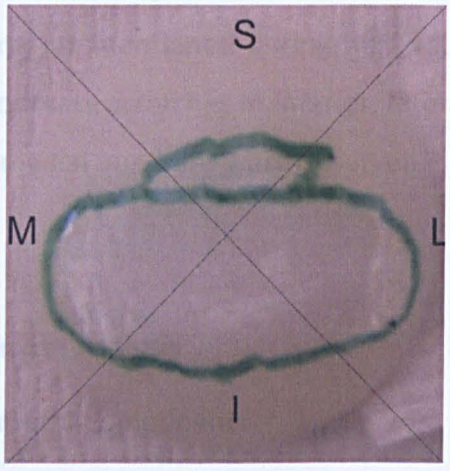

Specimen 5@9MC

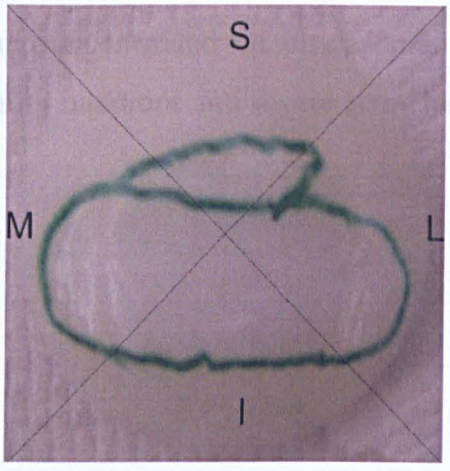

Specimen 6@9MC

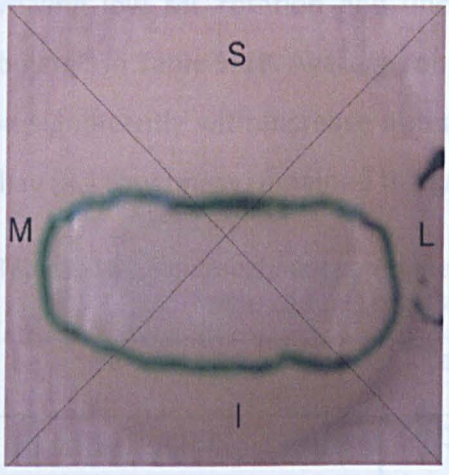

Specimen 7@9MC

Figure 5-31 Wear scar area for 5 specimens with solid line indicating worn area over 3MC.

Visual inspection

Femoral component and patella specimen

Scratches were found in the superior articulating part of femur where patella mates. The scratches were found similar to scratches shown in Figure 5-20. Unlike femoral compartment, scratches were observed in patella specimens as explained in earlier section.

Wear characteristics

Four main regimes of wear found in all the specimens as shown in Figure 5-21. These were pitting and deformation in the middle of the specimen. Burnishing and scratching were found on the edges of the wear scar area. The regimes were same as mentioned during high ML rotation and uncontrolled ML displacement. Moderate scratches in inferior, lateral and superior quadrant and severe scratches in medial quadrant were observed.

Surface analysis

Femoral Component

The roughness parameters for femoral components during the wear test involving low ML rotation and uncontrolled ML displacements from 6-9MC are tabulated in Table 5-18. Average roughness (R_a) and skew roughness (R_{sk}) increased non significantly with increase in number of million cycles ($p>0.05$). Peak (R_p) and valley (R_v) roughness remained the same over 3MC.

Table 5-18 Mean roughness parameters with 95%CL of femoral component before and after the test over 3MC with P value (*$p<0.05$ significant)

Parameters	Before Test	After Test	P value
R_a (μm)	0.040±0.011	0.052±0.011	0.08
R_{sk}	-1.000±0.808	-0.273±1.169	0.14
R_p(μm)	0.098±0.018	0.103±0.017	0.82
R_v(μm)	0.095±0.023	0.097±0.022	0.87

Patella Specimen

Some changes in roughness parameters were observed in the patella specimens over the 3MC of the wear test as shown in Table 5-19. Average (R_a), skew (R_{sk}), mean peak (R_p) and mean valley (R_v) roughness increased with the test. However, the increase was not significant ($p>0.05$).

Table 5-19 Mean roughness parameters with 95%CL of patella specimen before and after the test over 3MC with P value (*$p<0.05$ significant)

Parameters	Before Test	After Test	P value
R_a (μm)	1.594±0.612	1.703±1.306	0.83
R_{sk}	0.975±2.031	1.654±2.200	0.55
R_p(μm)	3.079±0.509	4.361±0.728	0.57
R_v(μm)	2.808±0.536	4.383±0.690	0.63

Wear depth

Wear depth of the specimens increased with number of million cycles as shown in Table 5-20. Specimens 5 and 6 had the highest deformation over 3MC and specimen 2 the lowest deformation (100 μm) after the 3MC of the wear test. The mean average wear depth over the 3MC was 110±52 μm and 960 μm over 9MC of both testing regimes.

Table 5-20 Wear depth for patella specimens over 3MC

Specimen Number	Before test (μm)	After test(μm)
2	800	850
3	800	900
5	1000	1150
6	850	1000
7	800	900
Mean±95%CL	*850±108*	*960±148*

5.3.4 Low ML Rotation with Constrained ML Displacement

This condition was run with ML rotation <1° and the ML displacement kept constrained (<1.6mm) for the next 3MC. The conditions of the test were similar to the conditions of Ellison and co authors (2008).

5.3.4.1 Kinematics

The station feedbacks from simulator following the input profiles are plotted versus the gait cycle for anterior posterior load (Figure 5-32), superior inferior displacement (Figure 5-33) and medial lateral rotation was similar as shown in Figure 5-24.

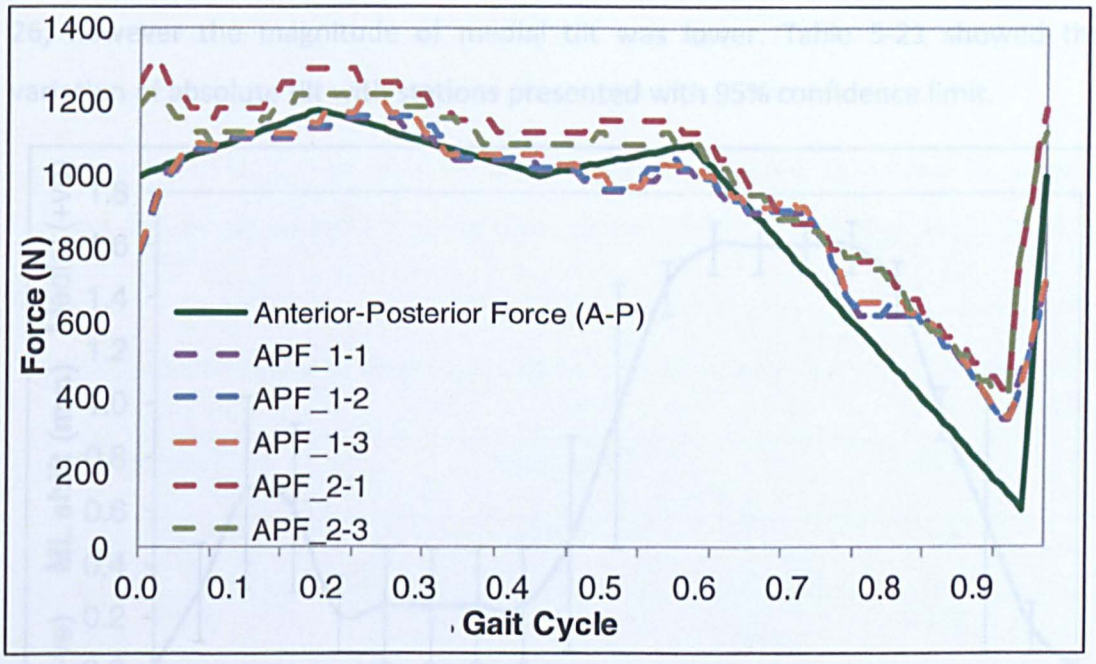

Figure 5-32 Anterior posterior load input (solid line) and simulator feedback (dotted line) plotted versus percentage of gait cycle.

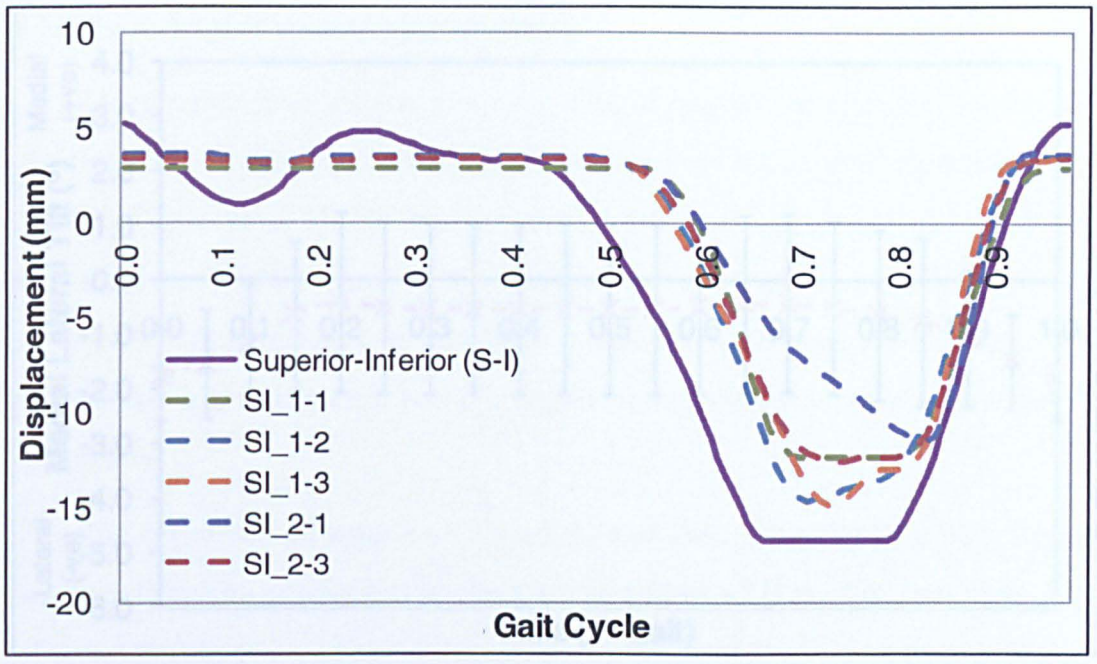

Figure 5-33 Superior inferior displacement input (solid line) and simulator feedback (dotted line) plotted versus percentage of gait cycle.

The ML displacement (Figure 5-34) increased to highest displacement of 1.6mm at highest flexion. The tilt (Figure 5-35) showed the same trend as Figure 5-26; however the magnitude of medial tilt was lower. Table 5-21 showed the variation of absolute tilt with stations presented with 95% confidence limit.

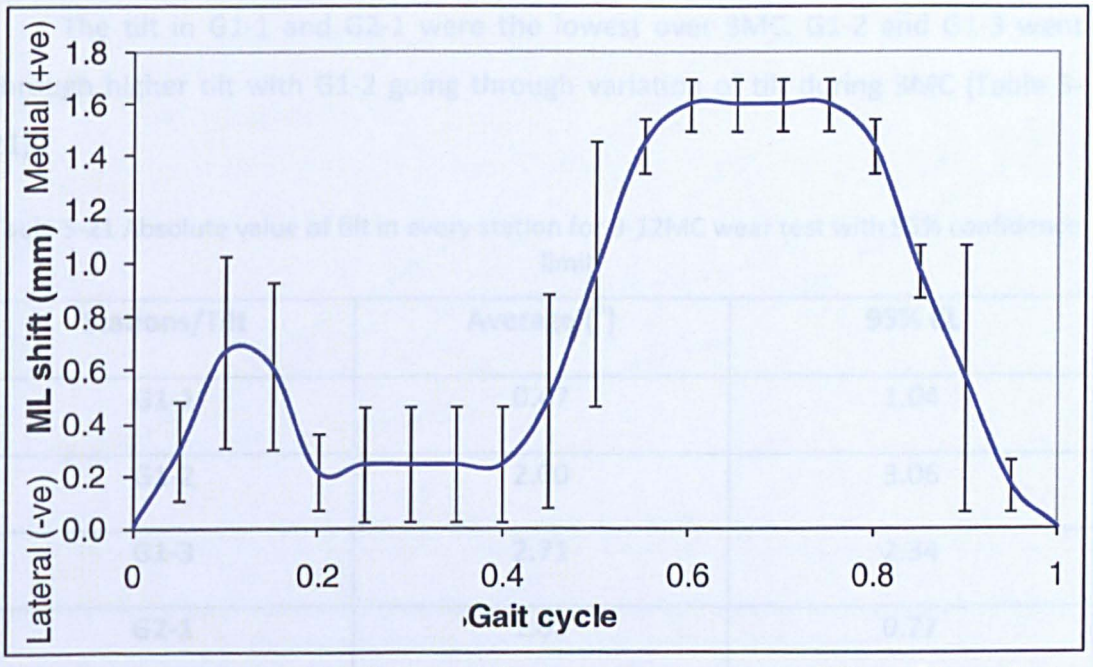

Figure 5-34 Constrained Medial lateral displacement plotted with 95% confidence limit versus percentage of gait cycle.

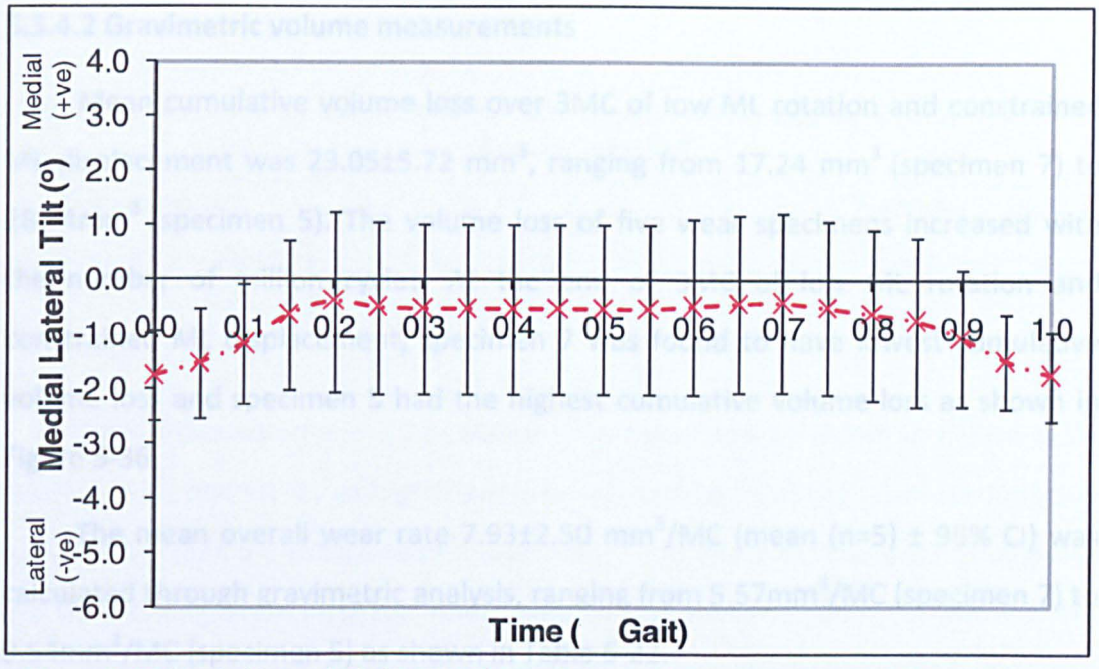

Figure 5-35 Medial lateral tilt (9-12MC) for all the stations plotted with 95% confidence limit versus percentage of gait cycle.

The tilt shown in Figure 5-35 was lower in medial tilt due to the combination of deformation and conformity. As shown in Chapter 3 Figure 3-9, the tilt was higher with low ML displacement. However, with increase in contact between the contacting surfaces the tilt decreased. This is also shown in Figure 3-13.

The tilt in G1-1 and G2-1 were the lowest over 3MC. G1-2 and G1-3 went through higher tilt with G1-2 going through variation of tilt during 3MC (Table 5-21).

Table 5-21 Absolute value of tilt in every station for 9-12MC wear test with 95% confidence limit.

Stations/Tilt	Average (°)	95% CL
G1-1	0.47	1.04
G1-2	2.00	3.06
G1-3	2.71	2.34
G2-1	1.01	0.77
G2-3	1.73	2.43

5.3.4.2 Gravimetric volume measurements

Mean cumulative volume loss over 3MC of low ML rotation and constrained ML displacement was 23.05±5.72 mm^3, ranging from 17.24 mm^3 (specimen 7) to 28.74mm^3 (specimen 5). The volume loss of five wear specimens increased with the number of million cycles. At the end of 3MC of low ML rotation and constrained ML displacement, specimen 7 was found to have lowest cumulative volume loss and specimen 5 had the highest cumulative volume loss as shown in Figure 5-36.

The mean overall wear rate 7.93±2.50 mm^3/MC (mean (n=5) ± 95% CI) was calculated through gravimetric analysis, ranging from 5.57mm^3/MC (specimen 7) to 9.54mm^3/MC (specimen 5) as shown in Table 5-22.

Two tail ANOVA produced no significant difference while comparing the wear rate between specimens (p=0.72) over every MC.

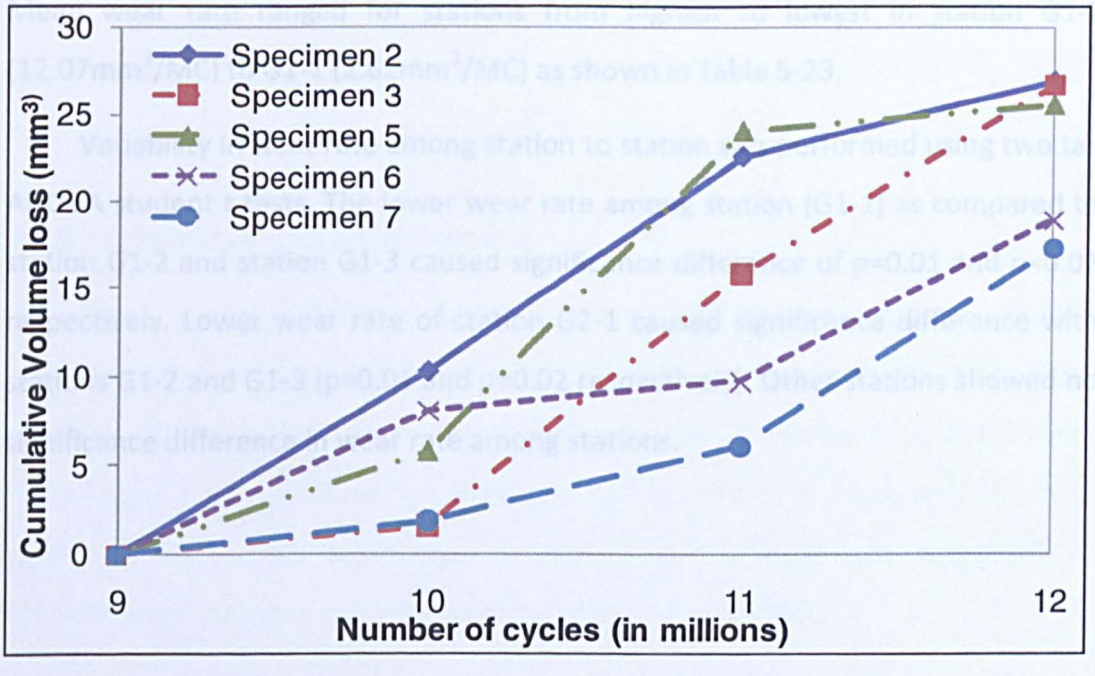

Figure 5-36 Cumulative volume loss, showing volume loss for every specimen at every MC for low ML rotation and constrained ML displacement

Table 5-22 Wear rate for low ML rotation with constrained ML displacement by specimen number over 3MC

Specimen No	2	3	5	6	7	Average	95%CL
Wear rate (mm^3/MC)	9.27	9.38	9.54	5.90	5.57	7.93	2.50

Cumulative volume loss per station was calculated as shown in Figure 5-37. Stations G1-2 and G1-3 had higher volume loss compared to the other stations due to high tilt (Table 5-21). Stations G1-1 and G2-1 had the lowest volume throughout the wear test. Station G2-2 had lower volume loss similar to G1-1 for the first MC and then the wear rate increased and the volume loss at the end of 3MC equalled the volume loss of station G1-3. This was reflected with the variation of tilt over 3MC with 95% confidence limit of ±2.43°.

The overall wear rate for all the stations was 7.93±5.45 (mean (n=5) ± 95%CL). Mean wear rate ranged for stations from highest to lowest in station G1-2 (12.07mm^3/MC) to G1-1 (2.62mm^3/MC) as shown in Table 5-23.

Variability in wear rate among station to station was performed using two tail ANOVA student t-tests. The lower wear rate among station (G1-1) as compared to station G1-2 and station G1-3 caused significance difference of p=0.01 and p=0.01 respectively. Lower wear rate of station G2-1 caused significance difference with stations G1-2 and G1-3 (p=0.01 and p=0.02 respectively). Other stations showed no significance difference in wear rate among stations.

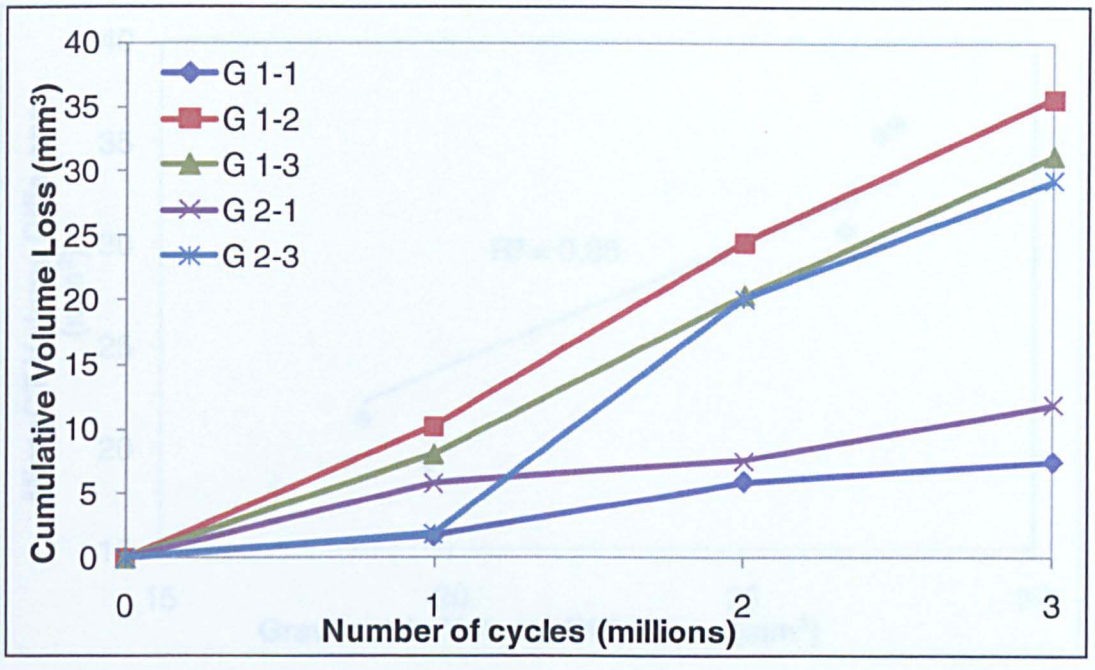

Figure 5-37 Cumulative volume loss for different stations at every MC for low ML rotation and constrained ML displacement

Table 5-23 Wear rate for low ML rotation with constrained ML displacement by station number over 3MC

Station	G1-1	G1-2	G1-3	G2-1	G2-3	Average	95%CL
Wear rate (mm^3/MC)	2.62	12.07	10.54	3.75	10.68	7.93	5.45

5.3.4.3 MicroCT volume measurements

The volume difference obtained from MicroCT was compared with gravimetric volumetric difference. The volumes were correlated with linear regression (R^2) value of 0.86 as shown in Figure 5-38. The mean volume difference from MicroCT was 29±9mm^3 as compared to gravimetric of 24±6mm^3. The wear rate from the MicroCT is presented in Table 5-24. The mean wear rate from the MicroCT from the wear test over 3MC was 9.51±3.22 mm^3/MC.

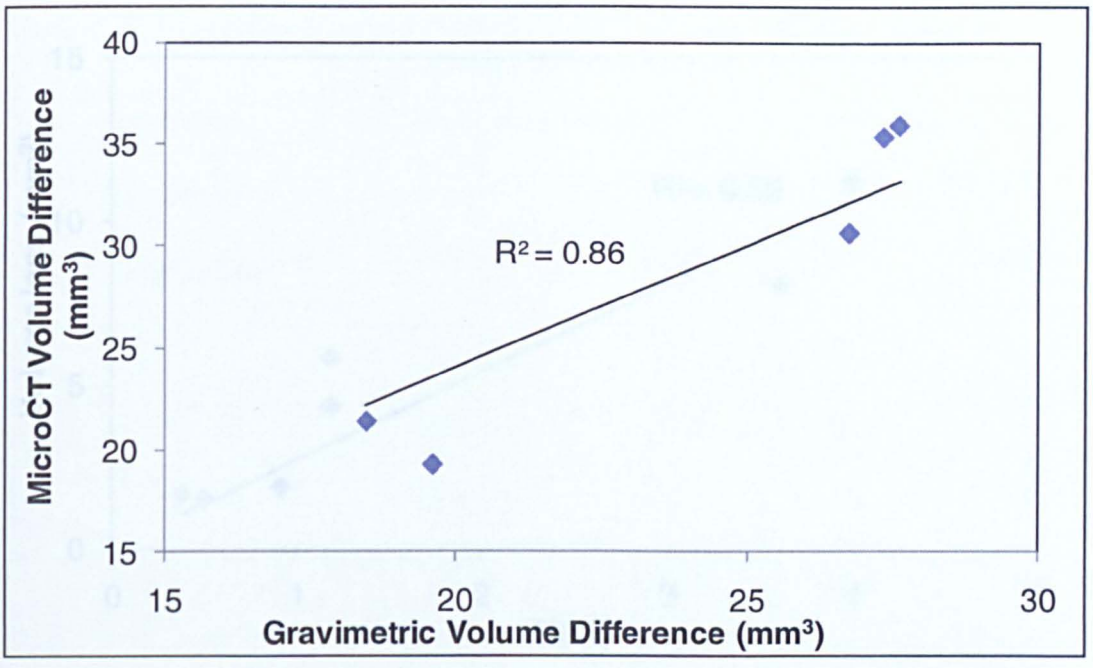

Figure 5-38 Volumetric difference of low ML rotation and constrained ML displacement wear test specimens over 3MC.

Table 5-24 Wear rate for low ML rotation with constrained ML displacement using MicroCT over 3MC

Specimen	2	3	5	6	7	Average	95%CL
Wear rate in mm^3/MC	11.98	11.80	10.22	6.42	7.14	9.51	3.22

5.3.4.4 Volume loss with ML tilt

There was a linear increase in volume loss with tilt as shown in Figure 5-39. The linear correlation was good with R^2 value of 0.85.

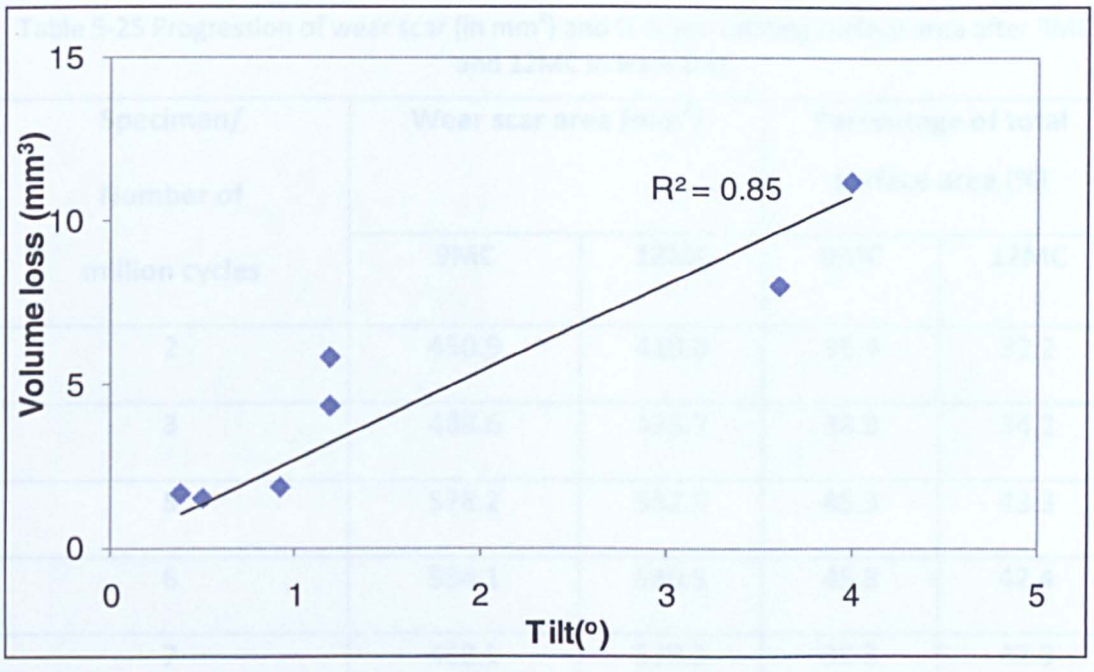

Figure 5-39 Relation of volume loss with tilt represented with linear correlation of R^2 value.

5.3.4.5 Quantification of wear scar area, surface analysis, and wear depth

Wear scar area

The wear scars were measured at 9 and 12MC. The scar area was presented in mm^2 and percentage of the total surface area as shown in Table 5-25. Two tail ANOVA were conducted for wear scar area between 9 and 12MC. No significant difference was found between the wear scars (p=0.3). The wear area remained the same throughout the 3MC test.

The distributions of wear scar area in the four quadrants (superior, inferior, lateral and medial) are presented in Table 5-26 in mm^2±95%CL. The wear scar area occurred in the inferior of the specimens.

The wear scar area for all the specimens over 3MC wear test are shown in Figure 5-40. Specimens 5 and 6 had the highest wear scar area.

Table 5-25 Progression of wear scar (in mm^2) and % of articulating surface area after 9MC and 12MC in wear test

Specimen/ Number of million cycles	Wear scar area (mm^2)		Percentage of total surface area (%)	
	9MC	12MC	9MC	12MC
2	450.9	410.0	35.4	32.2
3	488.6	435.7	38.3	34.2
5	578.2	552.5	45.3	43.3
6	584.1	540.3	45.8	42.4
7	488.1	539.3	38.3	42.3
Mean±95%CL	*517.9±74*	*495.6±81*	*40.6±6*	*38.9±6*

Table 5-26 Progression of wear scar (in mm^2) in superior, inferior, lateral and medial quadrant during 3MC in wear test

Number of million cycles	Quadrant			
	Superior	Inferior	Lateral	Medial
9	33.7±40.3	153.0±11.8	179.4±12.6	172.3±28.2
12	27.1±41.6	149.2±37.8	180.9±63.8	177.5±39.4

The area in inferior quadrant (Table 5-26) decreases whereas, area in medial quadrant increases from 172.3mm^2 to 177.5 mm^2. This is not possible as the area increases with cycle count so must have been due to measurement error.

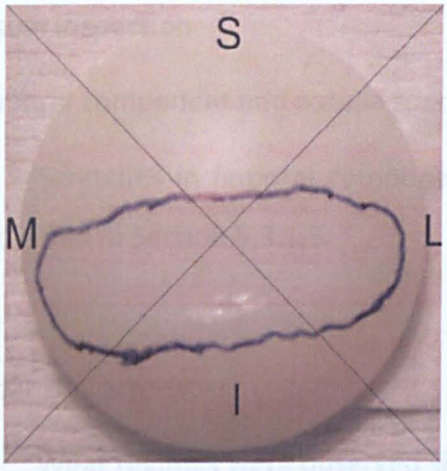

Specimen 2@12MC

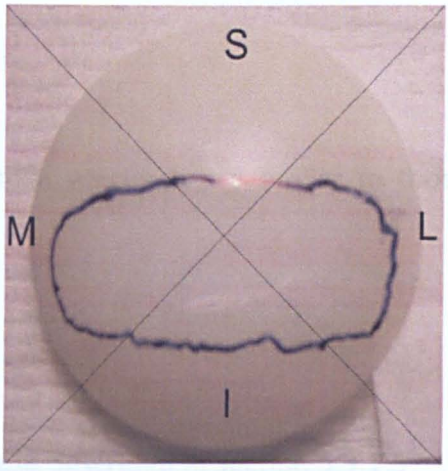

Specimen 3@12MC

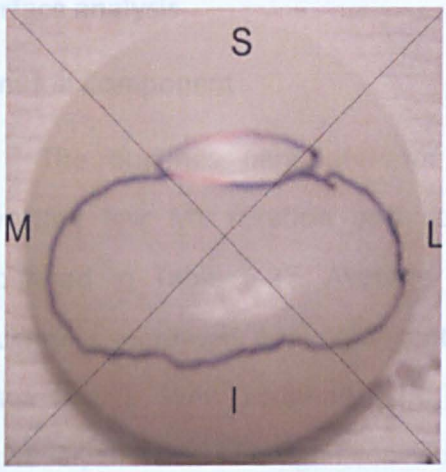

Specimen 5@12MC

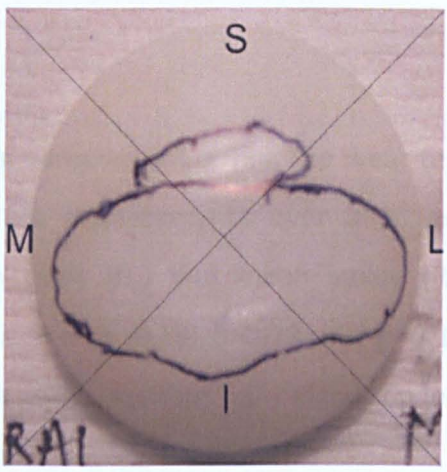

Specimen 6@12MC

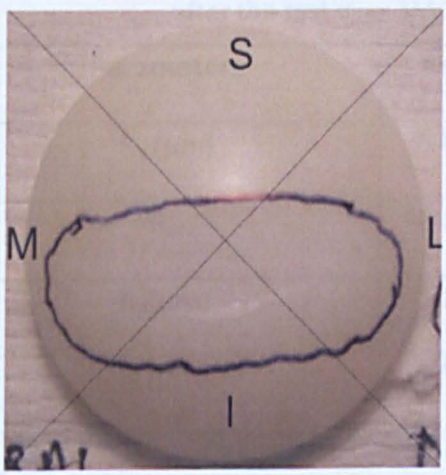

Specimen 7@12MC

Figure 5-40 Wear scar area for five specimens with solid line indicating worn area over 3MC.

Visual inspection

Femoral component and patella specimen

Scratches in femoral component and patella specimen are similar to those explained in Section 5.3.1.5.

Wear characteristics

Wear regimes were observed similar to those described in Section 5.3.1.5

Surface analysis

Femoral Component

The roughness parameters for the femoral components during the wear test involving low ML rotation and constrained ML displacements over 3MC are tabulated in Table 5-27. Average (R_a), mean peak (R_p) and mean valley (R_v) roughness increased non significantly after the test (p=0.28, p=0.13 and p=0.12 respectively). Skew roughness (R_{sk}) decreased with number of million cycles. However, there was no significance difference in the increase (p=0.14).

Table5-27 Mean roughness parameters with 95%CL of femoral component before and after the test over 3MC with P value (*p<0.05 significant)

Parameters	Before Test	After Test	P value
R_a (μm)	0.052±0.011	0.067±0.043	0.28
R_{sk}	-0.273±1.170	-1.198±1.109	0.14
R_p(μm)	0.103±0.017	0.128±0.062	0.13
R_v(μm)	0.098±0.022	0.135±0.069	0.12

Patella Specimen

Similar to femoral component, some changes in roughness parameters were observed in patella specimen over 3MC of wear test as shown in Table 5-28. Average (R_a), mean peak (R_p), mean valley (R_v) and skew (R_{sk}) increased non significantly after the test (p>0.05).

Table 5-28 Mean roughness parameters with 95%CL of patella specimen before and after the test over 3MC with P value (*p<0.05 significant)

Parameters	Before Test	After Test	P value
R_a (μm)	1.703±1.306	2.902±1.725	0.16
R_{sk}	1.655±2.200	1.885±1.109	0.80
R_p(μm)	4.361±0.728	7.061±1.381	0.23
R_v(μm)	4.384±0.690	6.201±1.108	0.18

Wear depth

Wear depth of the patella specimens increased with number of million cycles as shown Table 5-29. Specimen 6 has highest deformation over 3MC and specimen 5 had lowest deformation after the wear test. The mean wear depth over 3MC was 120±71 μm and 1080 μm over the total duration of test.

Table 5-29 Wear depth for patella specimens over 3MC.

Specimen Number	Before test (μm)	After test(μm)	Difference (over 3MC)
2	850	950	100
3	900	1050	150
5	1150	1200	50
6	1000	1200	200
7	900	1000	100
Mean±95%CL	*960±148*	*1080±143*	*120±71*

5.3.5 Round Dome Wear Test – All Results

5.3.5.1 Gravimetric analysis

Wear of the PFJ joint has been successfully quantified at various kinematic conditions until 12MC. The wear rate decreased as the ML rotation and ML

displacement were decreased as shown in Figure 5-41. Wear rate decreased from 12.3±2.79mm^3/MC at high ML rotation (<4°) and uncontrolled ML displacement to 8.6±3.44mm^3/MC mm^3/MC at low ML rotation (<1°) and uncontrolled ML displacement (p=0.05). With decrease in ML displacement, from uncontrolled to constrained displacement (<1.6mm), the wear rate changed non significantly from 8.6±3.44 mm^3/MC to 7.93±2.50 mm^3/MC. The student t-test is required to predict the significance.

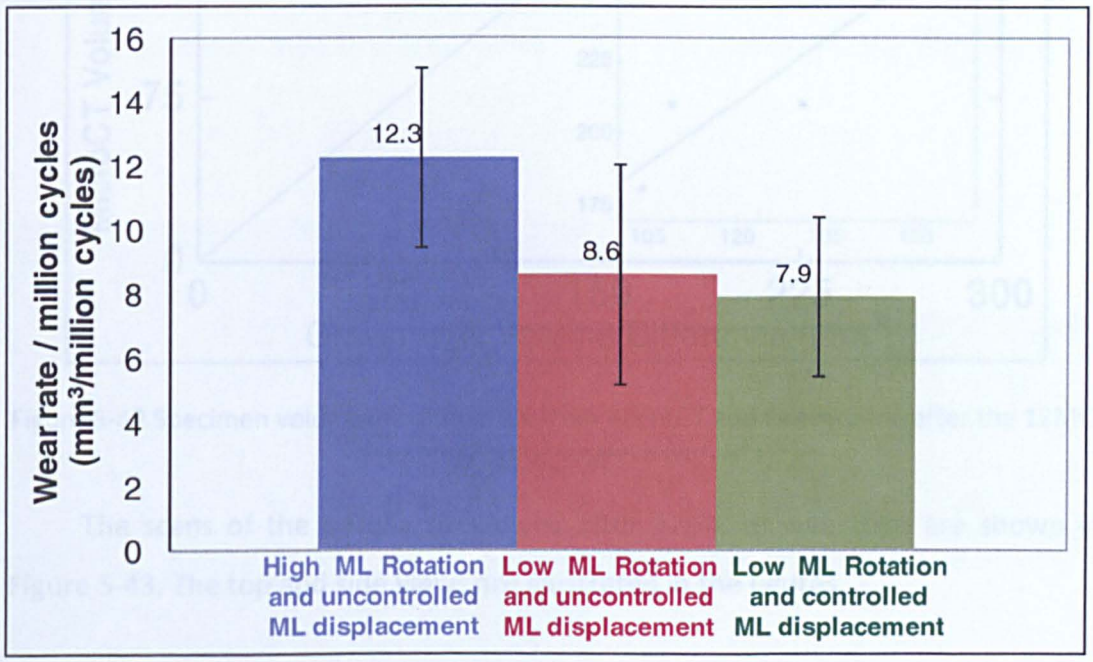

Figure 5-41 The variation of wear rate with change in kinematics.

5.3.5.2 MicroCT volumetric measurements

Pre-test MicroCT volumetric determination showed the mean volume to be 6148±62mm^3. When compared with gravimetric volumetric measurement (density =935kg/mm^3), the volume was 5780±54mm^3. It was observed that MicroCT overestimated the volume of the specimen. The R^2 value for the volume determined by MicroCT and Gravimetric methodology was 0.8.

However, as our interest was determination of volume loss of different specimen after wear test. This is shown in Figure 5-42. The R^2 (0.8) value shows a good correlation for determination of volume loss from MicroCT and Gravimetric.

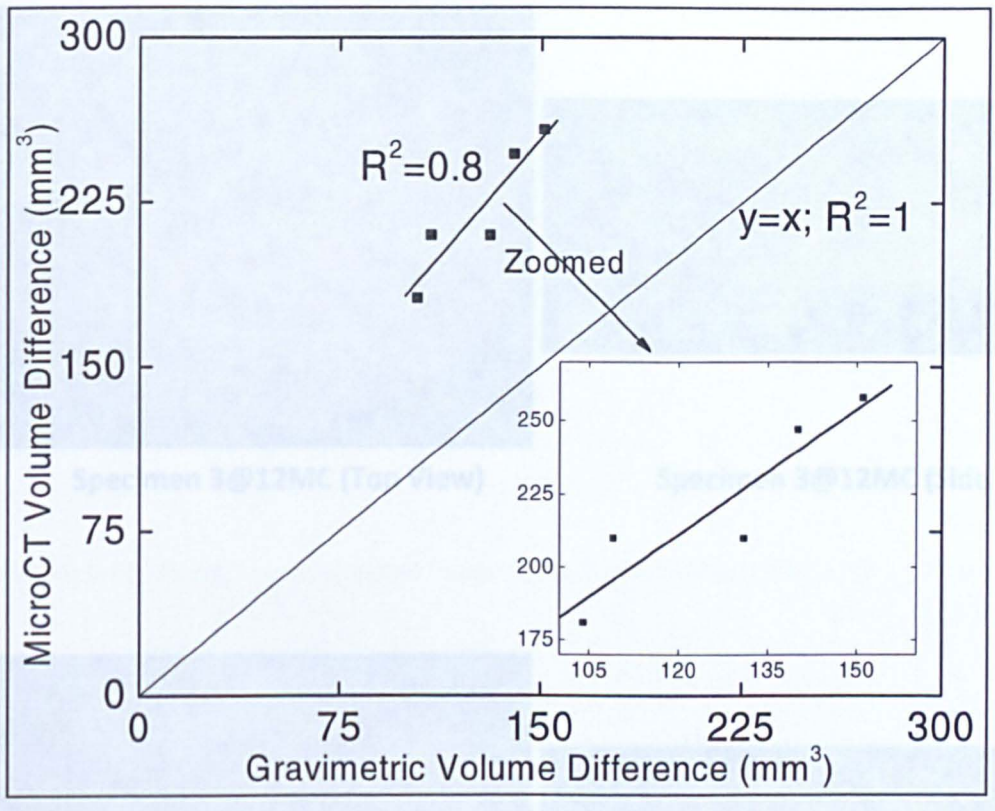

Figure 5-42 Specimen volumetric difference from MicroCT and Gravimetric after the 12MC, linear regression analysis with R^2.

The scans of the patella specimens after 12MC of wear test are shown in Figure 5-43. The top and side views are illustrated in the figures.

Specimen 2@12MC (Top View)

Specimen 2@12MC (Side View)

Specimen 3@12MC (Top View)

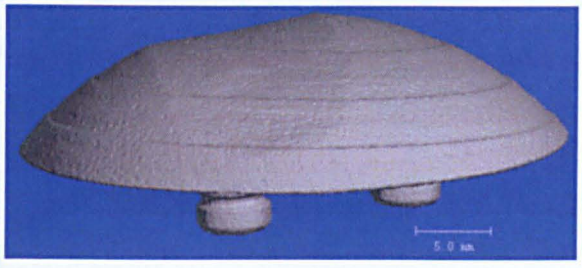

Specimen 3@12MC (Side View)

Specimen 6@12MC (Top View)

Specimen 6@12MC (Side View)

Specimen 7@12MC (Top View)

Specimen 7@12MC (Side View)

Specimen 5@12MC (Top View)

Specimen 5@12MC (Side View)

Figure 5-43 MicroCT reconstructed images of the patella specimens after 12MC wear test

5.3.5.3 Geometric volumetric measurements

The wear depth from the CMM analysis is tabulated in Table 5-30. Specimen 6 had the highest wear depth and specimen 2 had the lowest wear depth. Two tail ANOVA student t-tests between CMM wear depth and Talysurf analysis was conducted. The mean wear depth by both the methods was same with no significance difference (p=0.75). The 3D images of the patella specimens after 12MC wear test are shown in Figure 5-44.

Table 5-30 Wear depth for patella specimens over 12MC using CMM and Talysurf analysis

Specimen Number	Wear depth(μm)	Talysurf
2	1005	950
3	1019	1050
5	1282	1200
6	1128	1200
7	1008	1000
Mean±95%CL	*1088±148*	*1080±143*
4 (Creep Test)	113	115

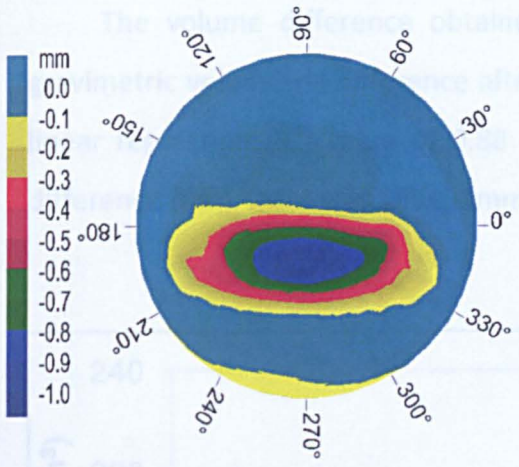

Specimen 2@12MC

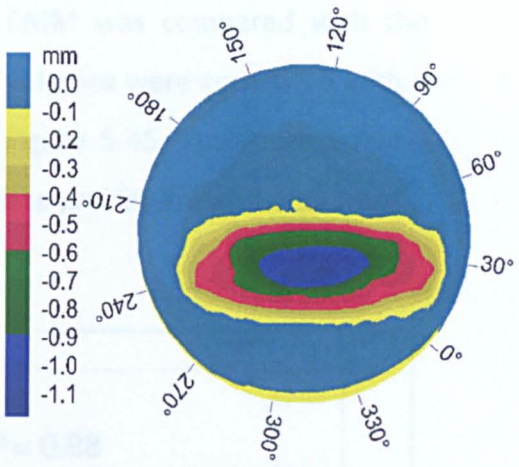

Specimen 3@12MC

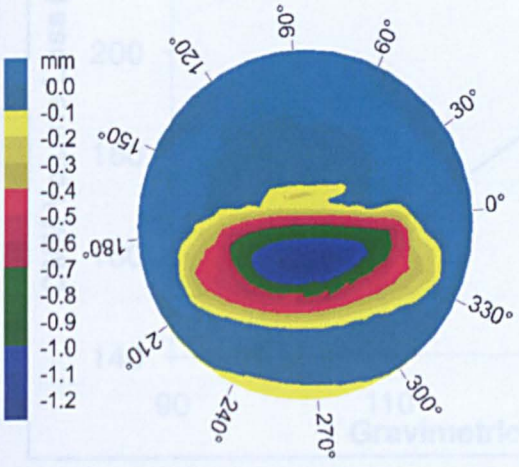

Specimen5@12MC

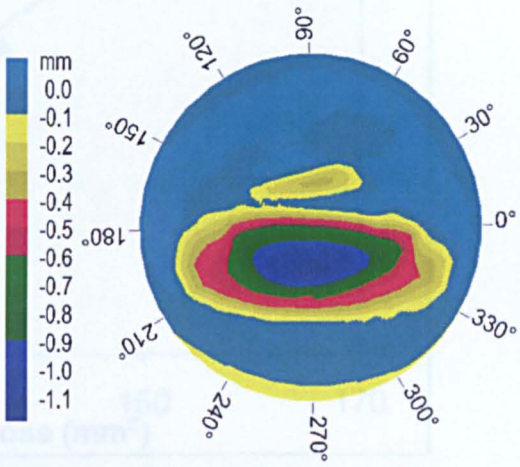

Specimen6@12MC

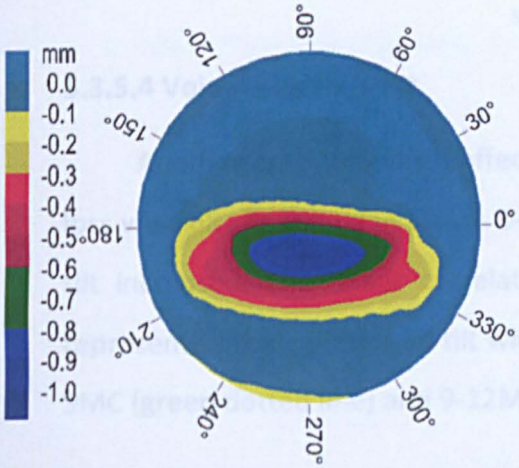

Specimen7@12MC

Figure 5-44 3D images of patella specimens after 12MC of wear test

The volume difference obtained from the CMM was compared with the gravimetric volumetric difference after 12MC. The volumes were correlated with a linear regression (R^2) value of 0.88 as shown in Figure 5-45. The mean volume difference from CMM was 185±31mm^3 as compared to gravimetric of 124±25mm^3.

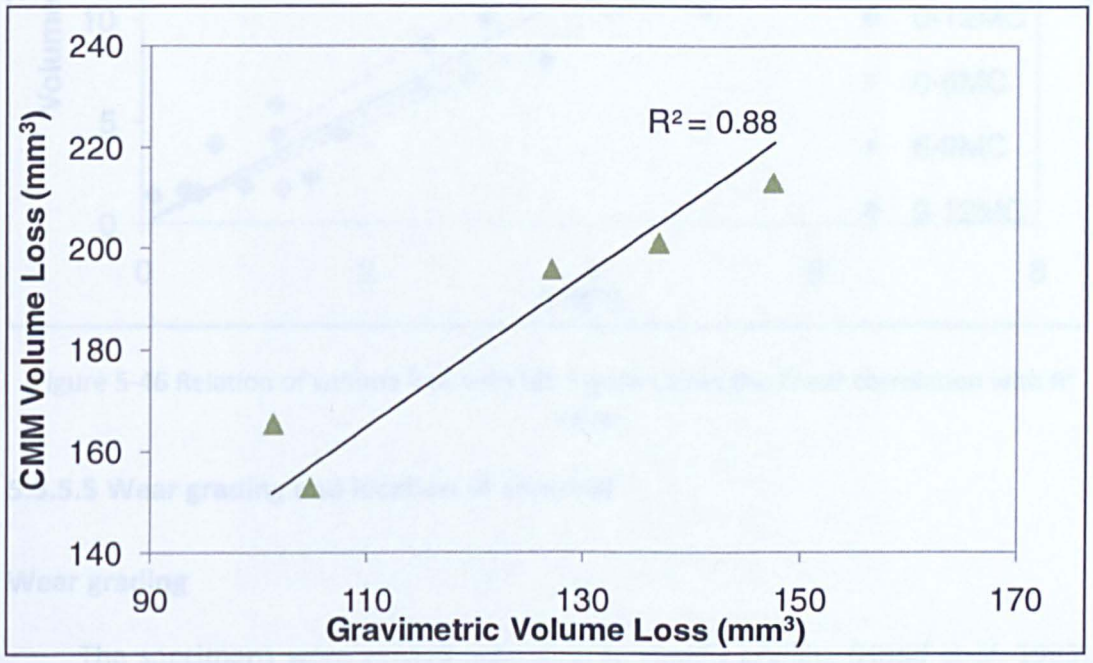

Figure 5-45 Volumetric difference of CMM with respect to gravimetric volumetric wear test specimens over 12MC.

5.3.5.4 Volume loss v/s tilt

Another criterion which affected the volume loss was the relation of volume loss with tilt. As shown in Figure 5-46 (solid blue line), volume loss increases as the tilt increased. The linear correlation R^2 was 0.80 over 12MC. The dotted line represented the variation of tilt with wear volume over 0-6MC (red dotted line), 6-9MC (green dotted line) and 9-12MC (violet dotted line).

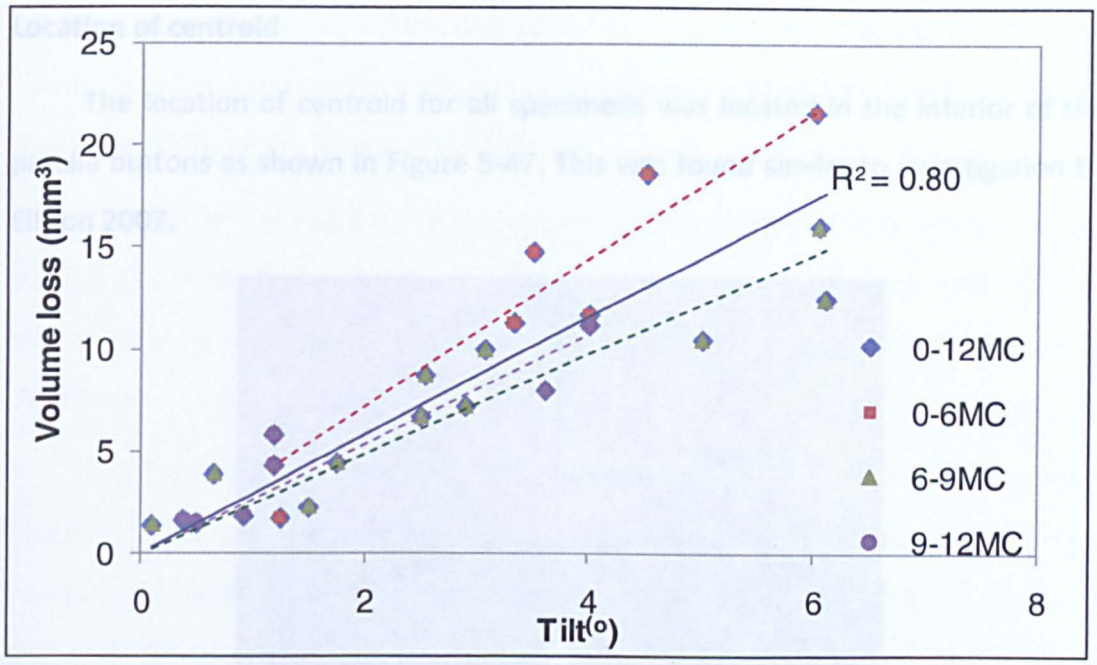

Figure 5-46 Relation of volume loss with tilt. Figure shows the linear correlation with R^2 value.

5.3.5.5 Wear grading and location of centroid

Wear grading

The specimens were graded according to Hood's grading (Hood et al. 1983). The grading for the 5 specimens is tabulated in Table 5-31. The score was moderate as compared to highest grading score of 84.

Table 5-31Wear grading of round dome test specimens using Hood *et al.*1983

Specimen Number	Score
Specimen 2	30
Specimen 3	32
Specimen 5	40
Specimen 6	40
Specimen 7	32
Average±95%CL	34.8±6

Location of centroid

The location of centroid for all specimens was located in the inferior of the patella buttons as shown in Figure 5-47. This was found similar to investigation by Ellison 2007.

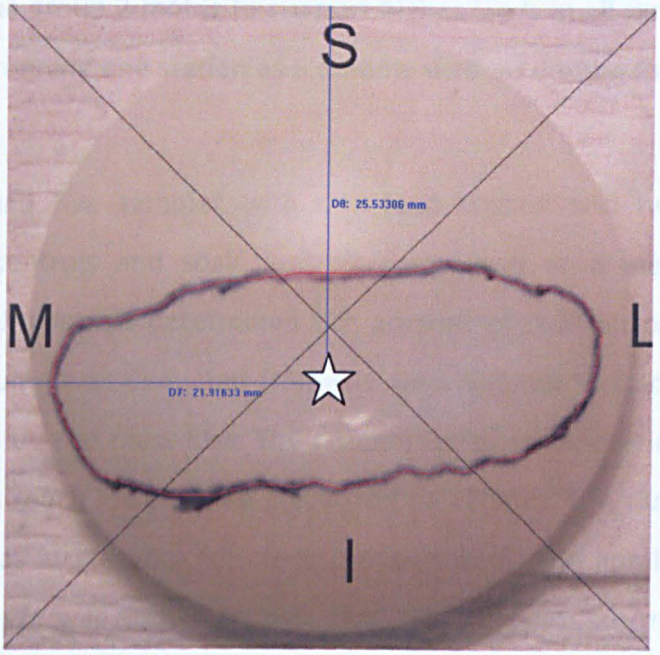

Figure 5-47 Location of centroid (in star) of the wear scar in round dome patella.

5.4 Discussion

Wear of the PFJ was dependent on the ML tilt in the joint. The repeatability of kinematics was seen to be moderate for axial load (5%) and SI displacement (11%). However, the ML rotation deviated from the input control profile due to the low demand profile operating in a pneumatic environment. The pneumatic pistons worked by expanding compressed air. There were two valves to distribute the air pressure to three pneumatic pistons. The error in air compression in such a low demand pneumatic system led to errors in force and displacement in the simulator feedback. However, the pneumatic system had good accuracy with higher demand profiles.

In the computational model (Chapter 3 Figure 3-16), it was found that tilt was dependent on AP load and ML displacement. The change in ML displacement and

AP force from station to station and presence of a separate bearing (required to constrain relative motion) in each station cradle led to variation in tilt from station to station (88%) of the lowest tilt (1.0°).

The motor in group 2 tripped at the beginning of the test. This was due to the incapability of the group 2 motor to support higher loads in all three stations. This was avoided by running one station as a dummy with no motion to avoid damaging the motor.

The test had five samples with one load control and two soak control samples. Load controls and soak controls were used as a method for active comparison. Soak controls determined the amount of fluid absorbed during the test and the volume was deducted from the wear volume to calculate the actual volume that was due to mass loss. The percentage of volume gained due to soak was 0.4mm^3 was much lower when compared to 120mm^3 lost due to wear. Load soak were used as a reference for creep measurement. The number of cycles for creep measurement was limited to only 1MC. The creep depth may change over cycle count and this was investigated in the next study on oval dome patella (Chapter 6). The creep deformation obtained in current study (115µm) was double to that obtained in the past (50µm) (Vanbiervlier *et al.* 2011). This was likely caused due to the presence of a lower load (400N) in the study by Vanbiervlier and co authors (2011) that led to a decrease in creep deformation. The creep in the current study however, was similar to Ellison et al (2008) where similar axial load was used.

The wear rate at the first million cycles was higher compared to the steady state wear, similar to investigation by Lee and Pienkowski (1998). Lee and Pienkowski (1998) investigated the initial wear of UHMWPE using pin-on-disc equipment. The 'bedding in' of the femoral components followed by cold flow and formation of wear debris as shown in Figure 5-48 led to higher wear rate at the first MC (Rostoker *et al.* 1978).

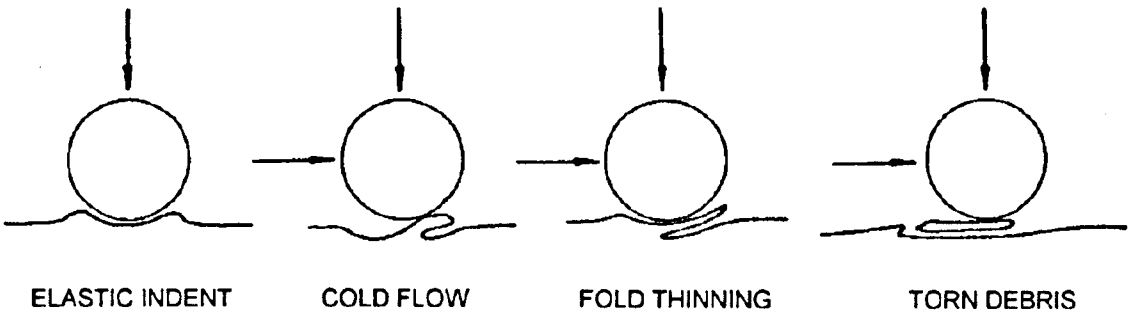

Figure 5-48 Description of creep and wear debris formation (Rostoker et al. 1978).

The wear rate decreased from 12.3±2.8mm^3/MC to 8.63±3.4mm^3/MC with decreasing in ML rotation from 4° to 1°. Wear in one directional is highly resisted due to the alignment of the polymer in that direction. As the motion gets two dimensional with addition of rotation or displacement in the perpendicular direction, strain softening in the direction perpendicular to polymer orientation caused increase in wear rate. This phenomenon is termed as cross shear. Therefore, the decrease in ML rotation by four fold caused decrease in cross shear which led to the lower wear rate. At higher ML rotation, higher strain softening occurs in the direction perpendicular to the direction of principal molecular orientation. This led to a higher wear rate as observed by Fisher *et al.* (2001) and McEwen *et al.* (2005) at a polyethylene counter face.

In contrast, a decrease in the ML displacement from 3.5mm to 1.6 mm caused no significant change in wear rate. A reduction in wear rate from 8.6±3.4 mm^3/MC to 7.9±2.5mm^3/MC was observed under this condition. The displacement in the perpendicular direction of the principal molecular orientation reduced and caused a lower cross shear ratio, leading to a lower wear rate. Wear is also directly proportional to the sliding distance according to Archard's law (1953). Hence, wear decreased as the ML displacement decreased from 3.5 to 1.6mm. However, the decrease was not linear with the change in displacement.

Volume loss was proportional to the tilt in every condition. This can be explained as the uneven loading causing uneven contact stress and additional cross shear which increased the volume loss. This was reported earlier with tibial inserts (Jennings *et al,* 2007). The lift off in the femoral condyles resulted in an increase in

wear. This change in tilt led to significance difference in the wear rate in some stations as shown in Figures 5-14, 5-26 and 5-35 and Tables 5-3, 5-12 and 5-21.

There was a significant difference ($p<0.05$) in the wear rate at low ML rotation and limited ML displacement (<1.6mm) (7.9 mm^3/MC) and wear rate in earlier investigation by Ellison and co authors (2008) (3.13 mm^3/MC) with similar conditions. One of the reasons behind the difference was the use of different machine for the PFJ joint wear simulation. The radius of rotation (Figure 5-49) in the current study was R_1 (DePuy manufacturing drawing) which was the most physiological radius obtained. In the earlier investigation the radius of rotation was R_2. The change in radius caused different contact stresses which may lead to lower wear rate in earlier investigation as compared to current. The other factors for the difference were the ML displacement was limited to 1.5 mm in current study which was limited to 1mm in previous investigation. And the application of a ligament force to the patella which replicated the ligament force in an *in vivo* scenario. These factors led to higher tilt and subsequently higher wear in the current study. The other reasons for difference may be positioning of the component, properties of component and lubricant materials.

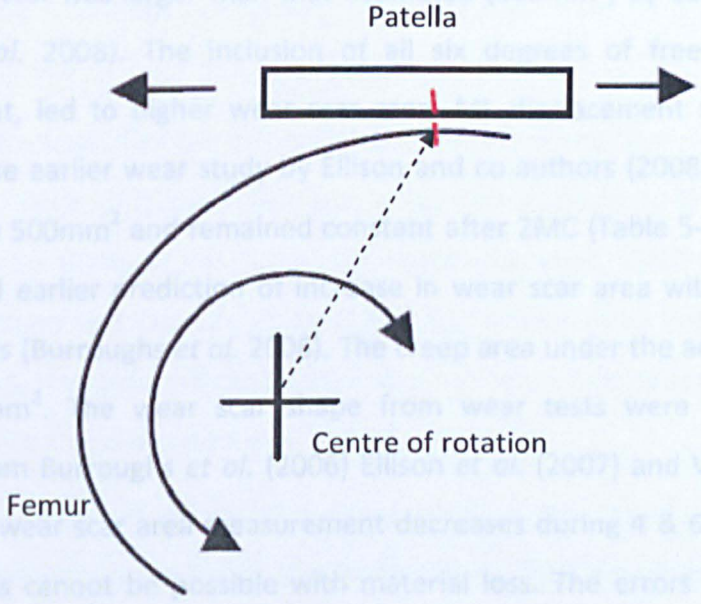

Figure 5-49 Schematics diagram of centre of rotation

Another author to predict patella wear under six degrees of freedom was Vanbiervliet *et al.* (2011). 18 Smith & Nephew femoral components were tested

against 32 mm polyethylene patella specimen at ProSim knee simulator with the tilt mechanically blocked. The wear rate was 0.91±0.21mm^3/MC, 35 times lower than wear rate at present study. The load was 3 times lower and the action of lift off was not considered. As mentioned earlier, lift off of the patella on the femoral counterpart caused higher contact stress and cross shear. The patella ML tilt was kept fixed in the investigation by Vanbiervliet and co-authors (2011) which was found to be one of the major factors for higher wear in the current study. The lubricant used in Vanbiervliet *et al.* (2011) study was a mixture of 40% new born calf bovine serum diluted with ionised water, ethylenediaminetetraacetic (EDTA) acid and sodium azide solution. The SI and ML displacements varied from -10mm to 10mm, FE rotation ranged from -10° to 100° and ML rotation was kept either at 5° medial or -5° lateral angle. Hsu and Walker (1989), Burroughs *et al.* (2006) and Korduba *et al.* (2008) also have investigated on wear of patella femoral joint. However, the number of degrees of freedom considered was limited to two (load and flexion extension rotation). This led to a lower wear rate of 3.3mm^3/MC in a walking cycle.

Wear scar area measured over 6MC was 500±22.7mm^2. The area measured in the current test was larger than that estimated (385mm^2) by earlier investigation (Ellison *et al.* 2008). The inclusion of all six degrees of freedom, mainly ML displacement, led to higher wear scar area. ML displacement was restricted to 1.0mm in the earlier wear study by Ellison and co authors (2008). Wear scar area increased to 500mm^2 and remained constant after 2MC (Table 5-7). This however, contradicted earlier prediction of increase in wear scar area with the number of million cycles (Burroughs *et al.* 2006). The creep area under the action of axial load was 171.9mm^2. The wear scar shape from wear tests were similar to those obtained from Burroughs *et al.* (2006) Ellison *et al.* (2007) and Vanbiervliet *et al.* (2011). The wear scar area measurement decreases during 4 & 6MC as compared to 2MC. This cannot be possible with material loss. The errors might be due to marking of the wear scar through visual observations.

There was a change (Tables 5-8 and 5-26) in wear scar area; in medial and inferior quadrant; measured at the end of the test conditions as compared to earlier measurement. This is not logically possible, as the area cannot decrease

with cycle count. The slight bias in wear area was due to error in the positioning of the centre of the quadrants. This led to higher or lower determination of wear scar area in the quadrants.

MicroCT and CMM were used as another way to calculate the volume of wear specimen and samples. The volume calculated using these methods were overestimated compared to the gravimetric measurement. The creep or deformation caused by 'bedding in' or initial seating of the metallic component of the polyethylene under the action of static load is the reason for higher volume estimation. This initial seating never affected the gravimetric measurement. This was avoided by calculating the volume under the action of axial load and the volume obtained was subtracted from the volume of the wear specimens for MicroCT. A good correlation between gravimetric and CMM/MicroCT was observed ($R^2 > 0.88$) using this methodology.

The wear depth increased as the number of cycles increased. The deformation increased 850±108μm after the first 6MC at high ML rotation (<4°) and free ML displacement. It further increased to 960±148μm when ML rotation was reduced by four folds (<1°). Following that with reduction of ML displacement (<1.6mm), the wear depth increased further by 120μm to 1080±143μm at the end of 12MC wear test.

Surface analyses of the creep test specimen showed lower values of average surface (R_a), skew (R_{sk}), peak (R_p) and valley (R_v) roughness. This was similar to observation by Wang et al. (1996) for acetabular cups, Elfick *et al.* (1998) for acetabular liners and Dowson *et al.* (1999) for polyethylene implants. Under the action of load, the surface became smoother as the uneven peaks and valleys were crushed. Hence there was decrease in R_a, R_{sk}, R_p and R_v.

The R_a increased as the test progressed on the femoral component and patella specimens undergoing the wear test. The scratches in the patella component were similar to those found in the tibia femoral joint (Barnett *et al.* 2002; McEwen *et al.* 2002; Burton *et al.* 2006) and patella femoral joint (Ellison *et al,* 2008) polyethylene surfaces. The average surface roughness dropped at the beginning of the cycle due to burnishing wear and the surface getting polished. The

polishing action reduced during the course of the test. No surface measurement was performed at the end of the first MC. However, the R_a increased during the course of the test.

Unidirectional scratches observed in the femur component had negative skew roughness showing that the lubrication regime must be existing. However the skew roughness value in the patella increased to a positive value. The number of peaks was higher in quantity compared to the number of valleys. Hence R_{sk} was positive in the patella surface. The peak (R_p) and valley (R_v) roughness increased as the number of cycles increased.

Four types of regimes were found in all the patella specimens (Figure 5-21). They were burnishing, scratches, pitting and deformation. Burnishing was caused due to action of metallic component with the polyethylene counterpart. Deformation was caused under the action of creep. The other wear characteristics such as adhesive fusion were absent. As the manufacturing process involved sterilisation in vacuum with higher intensity of radiation, adhesive wear was not present in the patella specimens.

There was a large variation in wear rate between the current and previous study. The introduction of a replacement patella will lead to clinical significance in the wear rate of total knee replacement. This increase in wear rate can lead to increase in wear debris which is linked to osteolysis and aseptic loosening of joint replacement (Ingham and Fisher 2000). Hence the study of patella femoral joint wear simulation is required. However, size distribution of the particles apart from volumetric wear is important (Fisher *et al.* 2001; 2004)

Summary

There was an increase in wear rate due to increase in medial lateral rotation. No significant change was observed in the wear rate when the medial lateral displacement was decreased. Wear scar area was 500mm^2 at the end of 12MC. The damage of the wear scars using Hood's method of grading was 34.8.

Chapter 6: *In vitro* wear simulation of PFC Sigma and Oval Dome Patella

6.1 Introduction

Two types of dome patella are found in the market. These are round dome and oval dome patellae. As the name suggests, the oval dome is elliptical in shape with smaller width (33mm) as compared to length (38mm). Whereas, the round dome patella has a constant diameter of 38mm. The oval dome patella has a higher bone coverage area (91%) compared to the round dome patella (78%) (Baldwin and Ken House 2005). Higher coverage of the bone provides lower contact between the bone and the metallic femoral component. This is the reason the global split of oval dome patella as compared to the round dome patella was higher; 98.8% : 1.2% (Personal communication from DePuy International Leeds, UK 2010). Galvin and co authors (2009) have investigated on the effect of wear with lower contact area. So the hypothesis tested was that the oval dome patella would have a lower wear rate than the round dome due to the lower surface contact area. The round dome patella was investigated in the last chapter.

6.2 Materials and Methods

6.2.1 Materials

The lot numbers for the femoral components and patella specimens are listed in Table 6-1. The femoral components were made of CoCr alloy and the patella specimens were all polyethylene type oval dome patella. Five wear specimens, one creep and two soak specimens were used in the test.

Table 6-1 Lot number for femoral and patella specimens

Specimen Number	Femoral lot number	Patella lot number
Group 1-1	3156739	3157694
Group 1-2	3156739	3157694
Group 1-3	3156739	3157694
Group 2-1	3157510	3157694
Group 2-2	3157510	3157694
Group 2-2	3157510	3157694
Soak Samples		3157694

6.2.2 Methods

This chapter investigates the wear rate of the patella specimen at the most appropriate physiological condition and compares the wear results with the round dome patella. The physiological conditions defined as low ML rotation (<1°) and uncontrolled ML displacement were investigated for a period of 3MC. The other degrees of freedom were flexion extension (FE) rotation from 0-22°, superior inferior (SI) displacement varying from -5 to 17mm and anterior posterior (AP) load 200 to 1200N. Five wear, one load soak and two soak samples were used during the investigation. The wear samples were placed as shown in Figure 6-1 (Scott *et al.* 1997). The two adjacent pegs in the oval dome patella were aligned to the superior of the femoral counterpart. The control routine for the test was the same as used in the investigation of round dome patella. The load soak control was acted on with an anterior posterior load varying from 200 to 1200N. All the other degrees of freedom were removed from the creep test. The soak controls were kept in 25% new born calf serum and 0.03% sodium azide solution (the same lubricant as the wear test). This is the first wear study of the oval dome patella.

Determination of the wear volume using gravimetric and CMM methods was performed. Gravimetric and CMM were used after every MC for volume measurement. In CMM, determination of the volume loss was done using the

methodology of creating an original specimen based on unworn surface. MicroCT has been ineffective in measuring lower volumes as seen in Chapter 4. Hence, measurement of volume using MicroCT was avoided for oval dome patella. Wear scar, deformation, surface analyses have also been reported every 3MC using a profilometer Talysurf. All the above mentioned techniques are discussed in Chapter 2, Section 6.2, 6.4 and 6.6.

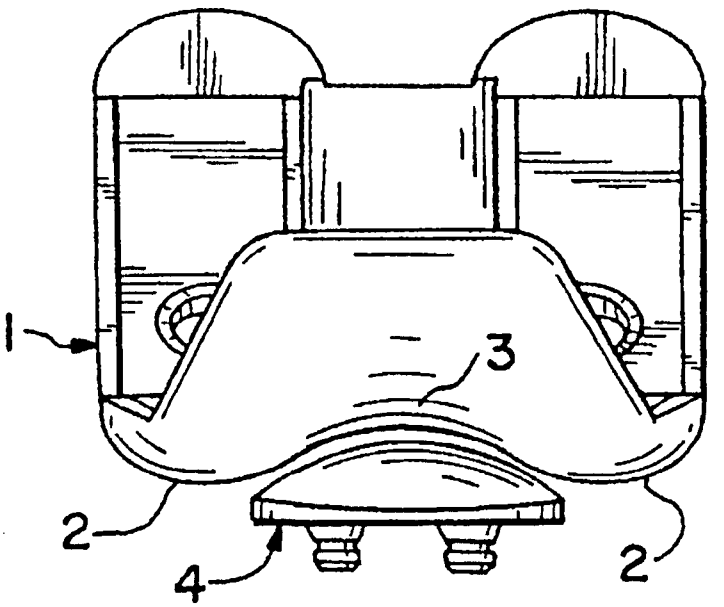

Figure 6-1 Schematic diagram showing position of oval dome with respect to femoral counterpart during a wear test (Scott *et al.* 1997)

6.3 Results

Specimen 3 was damaged due to slipping from the mating surface and was replaced by specimen 8 at the beginning of the third MC.

6.3.1 Kinematics

The input profiles of the test along with feedback for various degrees of freedom are shown in Figures 6-2 to 6-4. The feedbacks follow the input profiles in anterior posterior load and superior inferior displacement as shown in Figures 6-2 and 6-3 respectively. In the case of medial lateral rotation, the presence of pneumatic pistons led to a significant difference between the input and output feedbacks as shown in Figure 6-4 due to the low demand profile.

Excess ML tilt more than 5° was prevented. 5° was the maximum value of tilt obtained through the computational model as described in Chapter 3. Exceeding 5° led to slipping of the patella from the femoral groove contact.

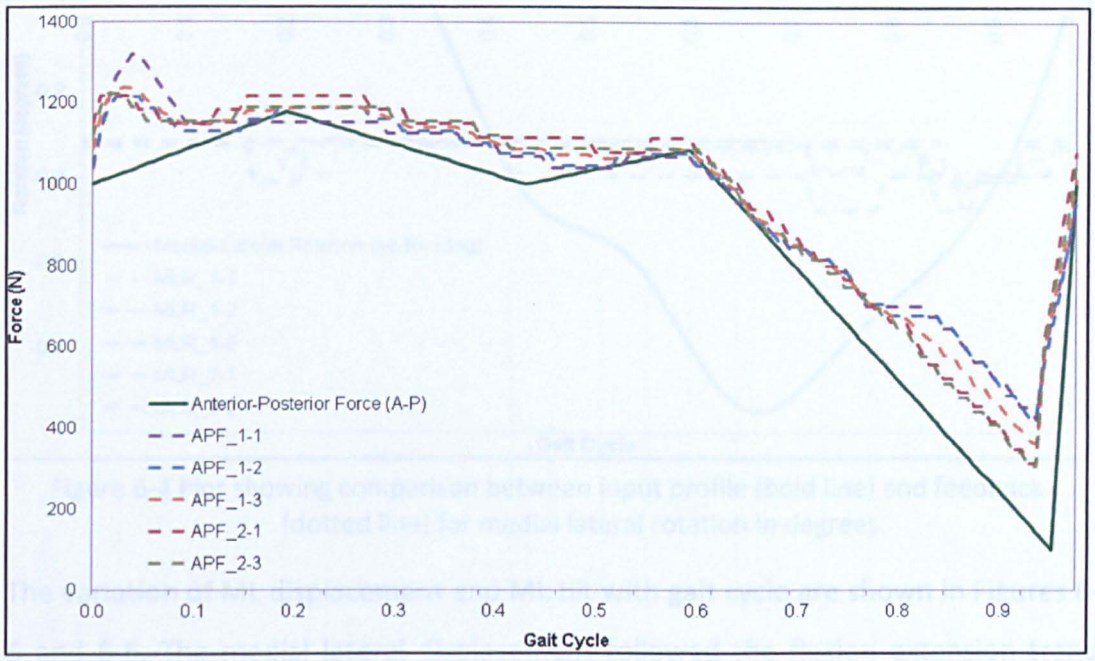

Figure 6-2 Plot showing comparison between input profile (bold line) and feedback (dotted line) for anterior posterior force in N.

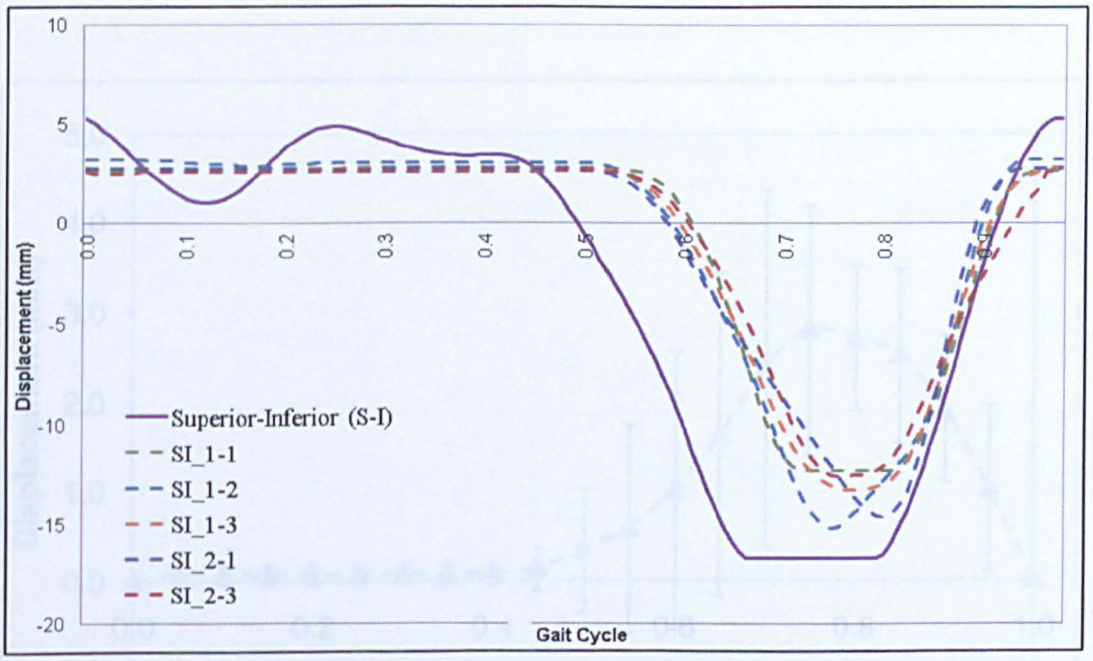

Figure 6-3 Plot showing comparison between input profile (bold line) and feedback (dotted line) for superior inferior displacement in mm.

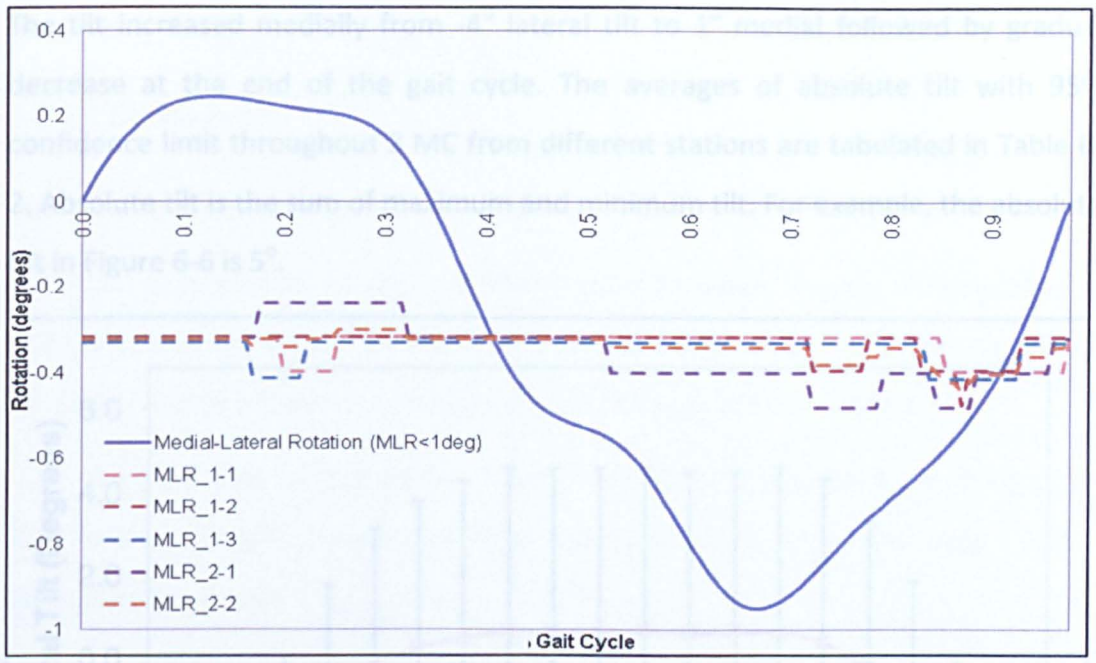

Figure 6-4 Plot showing comparison between input profile (bold line) and feedback (dotted line) for medial lateral rotation in degrees.

The variation of ML displacement and ML tilt with gait cycle are shown in Figures 6-5 and 6-6. The medial lateral displacement followed the flexion extension trend with highest displacement at highest flexion.

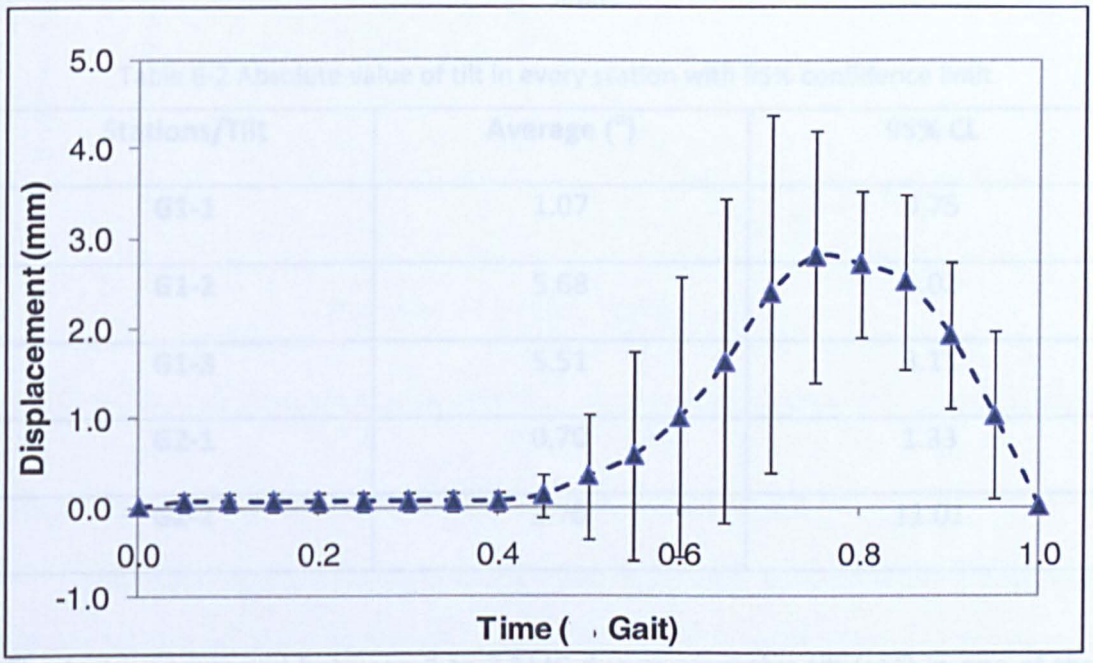

Figure 6-5 Plot showing medial lateral displacement in mm with errors bar of 95% confidence limit.

The tilt increased medially from -4° lateral tilt to 1° medial followed by gradual decrease at the end of the gait cycle. The averages of absolute tilt with 95% confidence limit throughout 3 MC from different stations are tabulated in Table 6-2. Absolute tilt is the sum of maximum and minimum tilt. For example, the absolute tilt in Figure 6-6 is 5°.

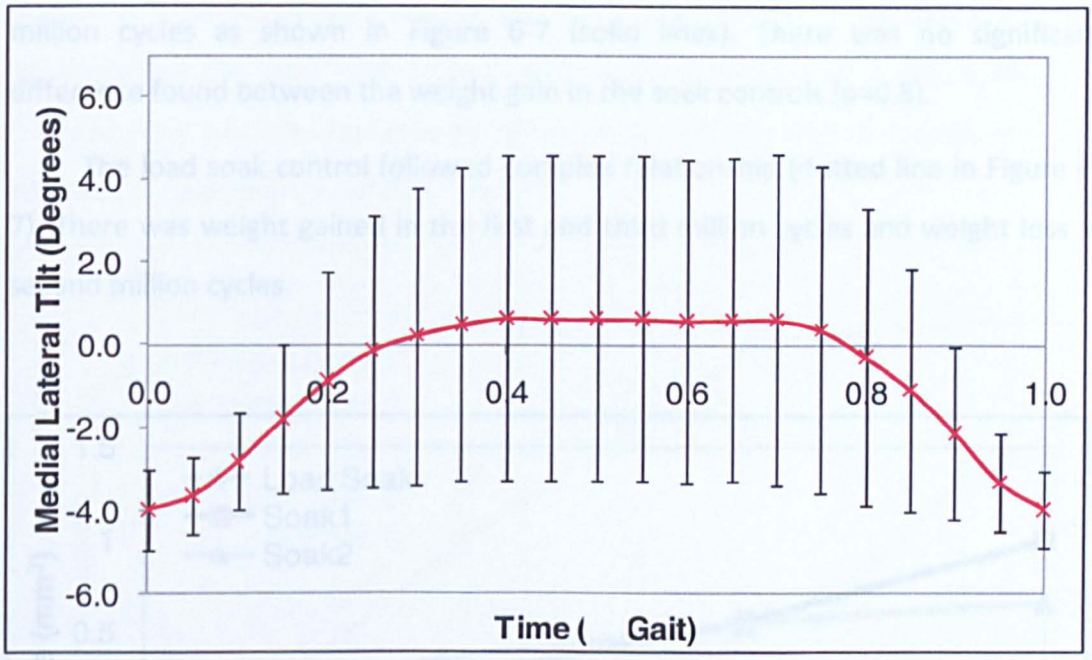

Figure 6-6 Plot showing medial lateral tilt in degrees with errors bar of 95% confidence limit.

Table 6-2 Absolute value of tilt in every station with 95% confidence limit

Stations/Tilt	Average (°)	95% CL
G1-1	1.07	0.75
G1-2	5.68	5.02
G1-3	5.51	8.11
G2-1	0.70	1.33
G2-2	3.70	11.01

The test was stopped between 2 to 2.5MC due to excessive tilt (>5°) in one of the stations; which caused the patella (specimen 3) to slip away from the femoral groove contact causing damage to the specimen. The specimen was replaced by specimen 8, which was previously used as a soak control.

6.3.2 Wear Results

6.3.2.1 Gravimetric

Soak and load soak controls

The soak control (soak1 and soak2) gained weight linearly with number of million cycles as shown in Figure 6-7 (solid lines). There was no significant difference found between the weight gain in the soak controls (p=0.8).

The load soak control followed complex relationship (dotted line in Figure 6-7). There was weight gained in the first and third million cycles and weight loss in second million cycles.

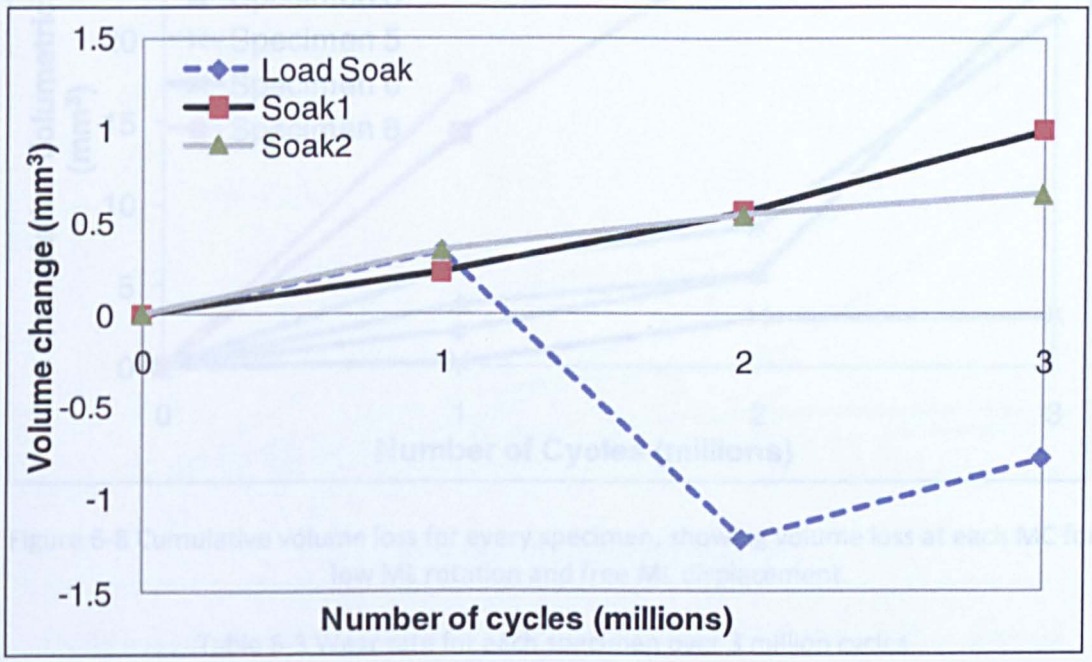

Figure 6-7 Change in weight of soak (bold line) and load soak (dotted line) specimen over 3 million cycles.

Wear results at Low ML rotation with free ML displacement

The mean cumulative volume loss over 3MC with 95% confidence limit was 20.00±18.11 mm^3, ranging from 3.11 mm^3 (specimen 5) to 28.36 mm^3 (specimen 2). Figure 6-8 shows cumulative volume loss of patella specimen over 3MC for all specimens. Specimen 2 went through higher wear during first and second million cycles. The gradient of wear was lower in the last million cycle compared to first

two million cycles. Three specimen (1, 3 and 6) followed similar trends with lower wear gradient in first two million cycles and higher gradient in the last million cycles. Specimen 5 went through lower volume loss in every million cycles. The mean wear rate of all five wear samples was 6.28±3.89 mm^3/MC (mean (n=5) ± 95% CI), ranging from 1.21 mm^3/MC (specimen 5) to 9.75 mm^3/MC (specimen 2) as shown in Table 6-3. As specimen 3 failed after 2MC, the wear rate was calculated by averaging the wear rate of four specimens between and 2 and 3 MC. The average wear rate was replaced as the wear rate of specimen 3. Specimen 3 was replaced by specimen 8 and run for a MC.

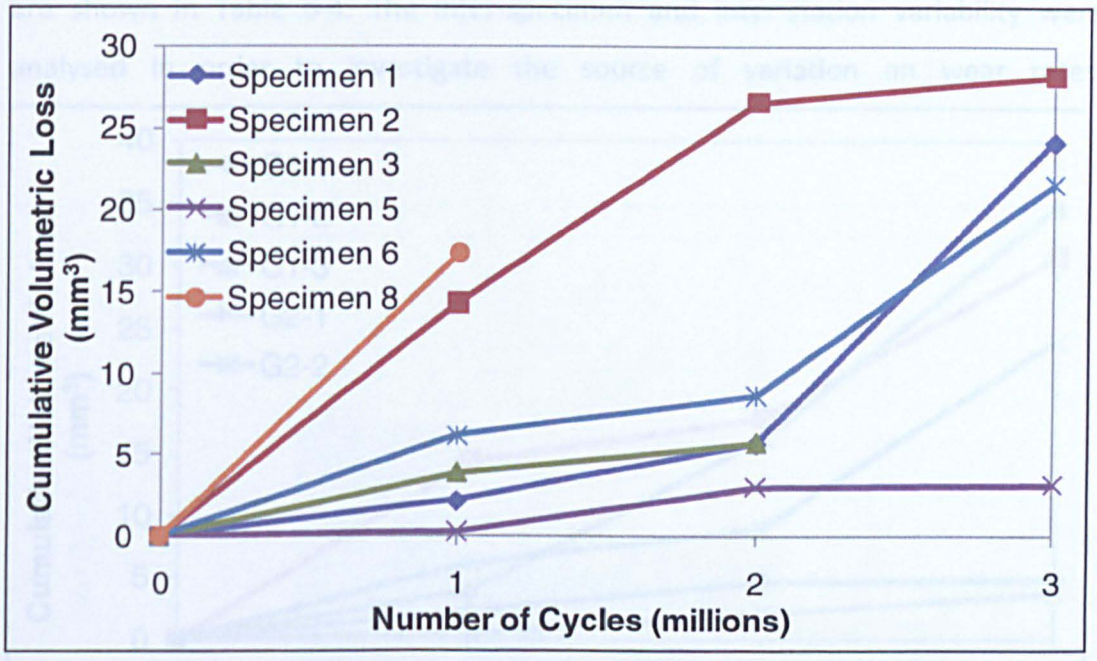

Figure 6-8 Cumulative volume loss for every specimen, showing volume loss at each MC for low ML rotation and free ML displacement.

Table 6-3 Wear rate for each specimen over 3 million cycles

Specimen No	1	2	3	5	6	Average	95% CL
0-3MC (mm^3/MC)	7.50	9.75	6.28	1.21	6.65	6.28	3.89

Figure 6-9 shows the cumulative volume loss of each specimen with respect to varied stations in the simulator. Stations G1-1 and G2-1 showed lower tilt (1.07° ±0.75°, 0.70°±1.33°) over 3 million cycles (Figure 6-6 and Table 6-2). Hence, the wear rates were lowest with 1.22mm^3/MC and 1.58mm^3/MC for stations G2-1 and G1-1 respectively. Stations G1-2 and G2-2 had a similar trend of lower wear

gradient during first and second million cycles and higher wear gradient in the last million cycles. However, the magnitude was different with station G1-2 (10.23mm^3/MC) having higher wear rate compared to G2-2 (8.00mm^3/MC). G2-2 had high variation of tilt through 3MC shown with high value of 95% CL as shown in Table 6-2 (3.70°±11.01°) compared to tilt in station G1-2 (5.68°±5.02°). Station G1-3 showed highest wear (11.55mm^3/MC) among all stations with lower wear gradient in the first million cycles and shooting to higher wear in the next two million cycles. The trend supports to highest tilt as shown in Table 6-2 with high variation in 95% confidence limit (5.5°±8.11°). The wear rate over 3 million cycles for all the stations are shown in Table 6-4. The inter-specimen and inter-station variability were analysed in order to investigate the source of variation on wear rates.

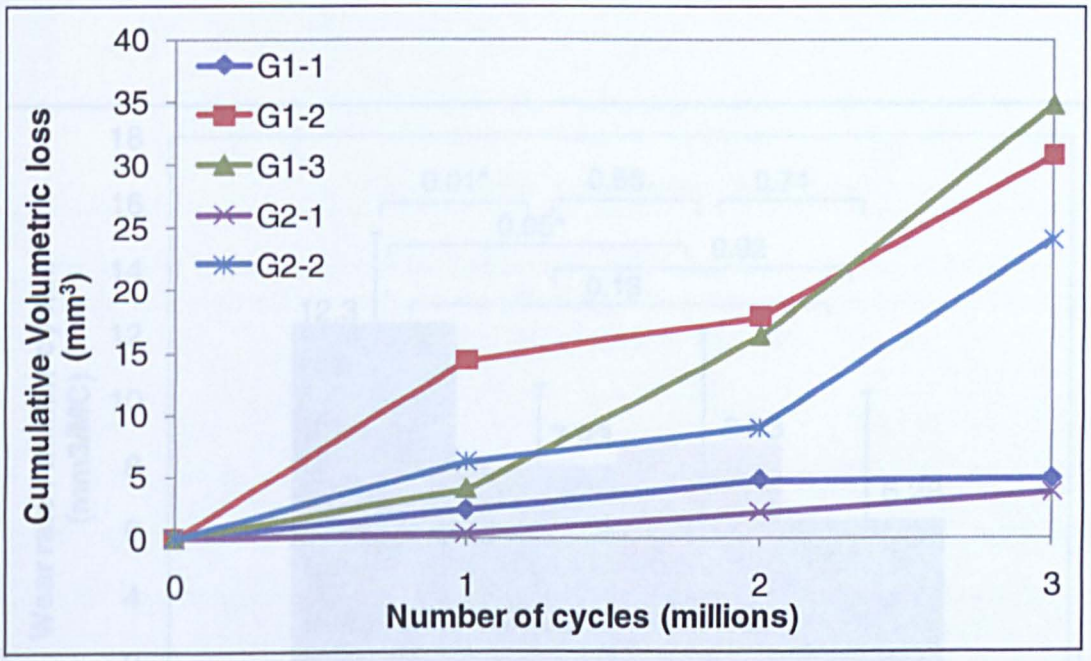

Figure 6-9 Variation of cumulative volume loss with respect to varied station, showing volume loss at each MC for low ML rotation and free ML displacement

Table 6-4 Wear rate for each stations over 3 million cycles

Station Name	G1-1	G1-2	G1-3	G2-1	G2-2	Average	95% CL
0-3MC (mm^3/MC)	1.58	10.23	11.55	1.22	8.00	6.52	6.01

Two tail ANOVA gave no significant difference while comparing the wear rate between specimens (p=0.57) or course of tests i.e. between each MC (p=0.48). This

shows that there were no inter specimen variability and the simulator was producing non significant wear rate in each MC. Variability in wear rate among station to station was performed using two tail ANOVA t-test. No significant difference (p=0.33) was found between stations.

Wear results of oval dome as compared to round dome patella

The wear rate of round and oval dome patellae under all conditions tested are shown in Figure 6-10. The change of shape from round dome to oval dome and at same condition; i.e. ML rotation and displacement uncontrolled; the wear rate decreased non significantly by 2.5mm^3/MC from round to oval dome (p=0.74).

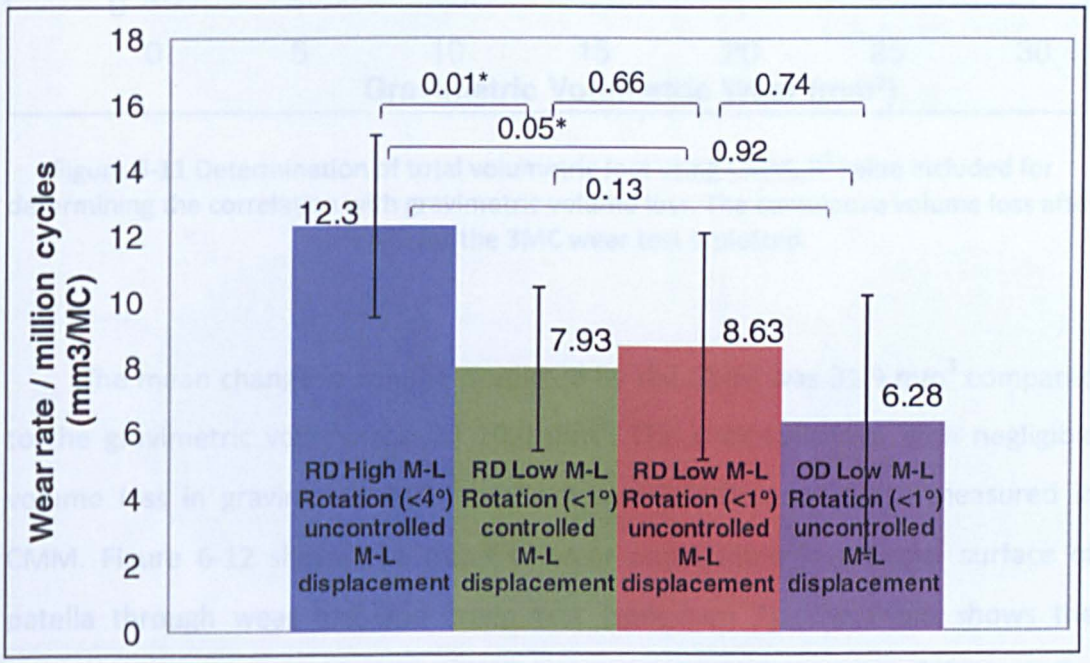

Figure 6-10 Chart showing the mean variation of wear rate (Mean with 95% confidence limit) with change in kinematics and shape of patella: RD stand for round dome and OD for oval dome patella. ANOVAs t-test are performed for each condition with significance at p<0.05

6.3.2.2 Geometrical volumetric measurements

This method was used for determination of volumetric wear after every million cycles of wear test on the oval dome patella wear specimens using CMM. The results were compared to the cumulative volume loss obtained from gravimetric measurements. Volumetric wear determined by CMM was sum of

creep and material removed. Still, good correlation with the gravimetric (R^2>0.8) was obtained at every million cycles as shown in Figure 6-11.

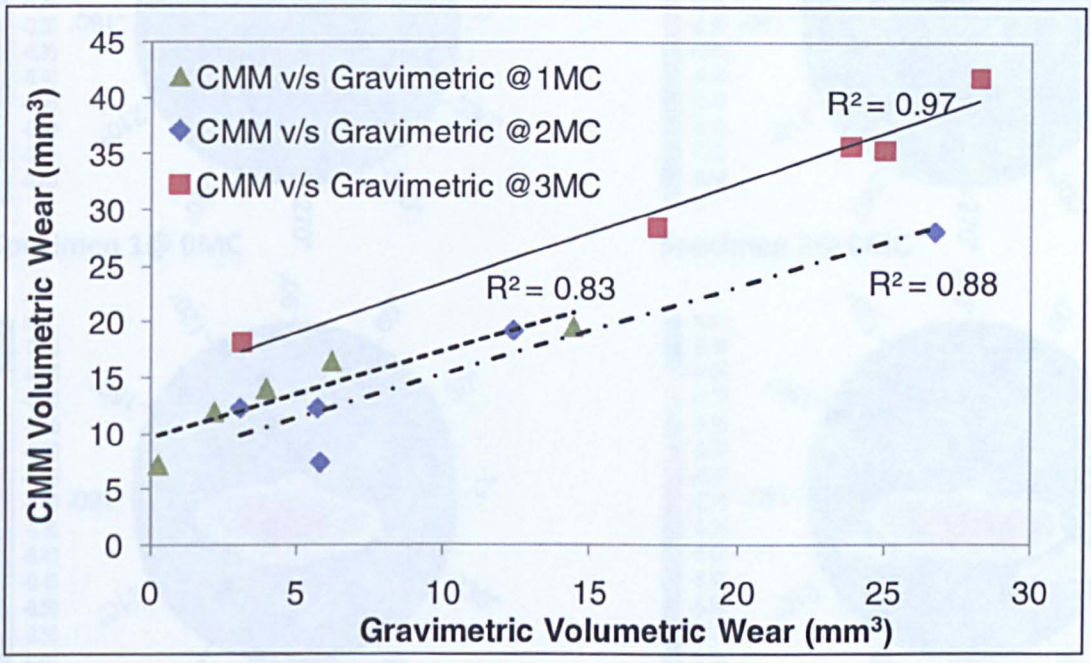

Figure 6-11 Determination of total volumetric loss using CMM; R^2 value included for determining the correlation with gravimetric volume loss. The cumulative volume loss after every MC for the 3MC wear test is plotted.

The mean change in volume predicted by the CMM was 31.9 mm^3 compared to the gravimetric volume loss of 20.0 mm^3. The soak specimen with negligible volume loss in gravimetric had 3mm^3 volumetric difference when measured in CMM. Figure 6-12 shows the trend of wear penetration in articular surface of patella through wear test and creep test (specimen 7). The trend shows the penetration continued to increase with every MC. At the beginning of the test, the machining marks could be seen in every specimen. The scale of the penetration was higher (-0.60mm) on the edges of certain CMM scans. The error was due to error in measurement. This however did not affect the volumetric wear determination as the scars were located near the centre not in the edges.

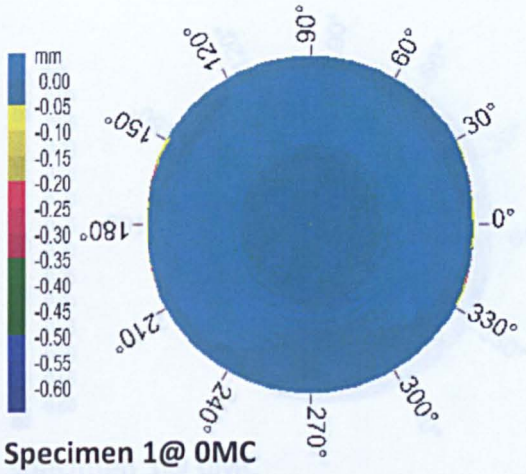

Specimen 1@ 0MC

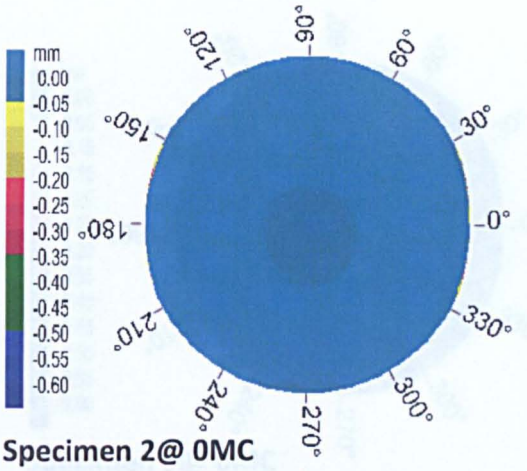

Specimen 2@ 0MC

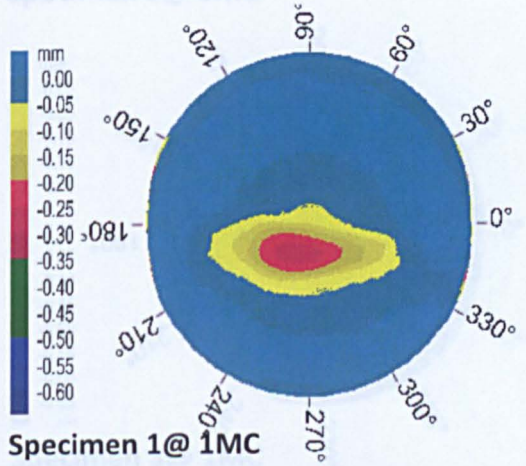

Specimen 1@ 1MC

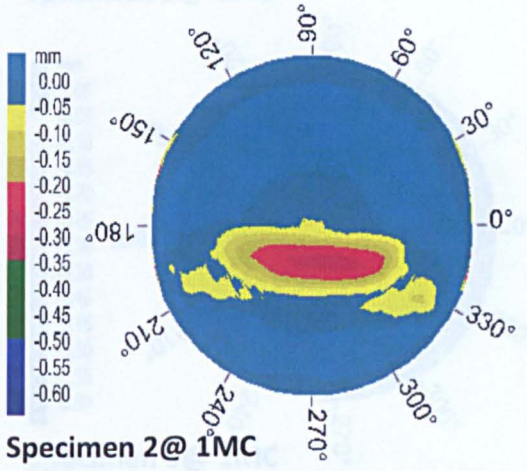

Specimen 2@ 1MC

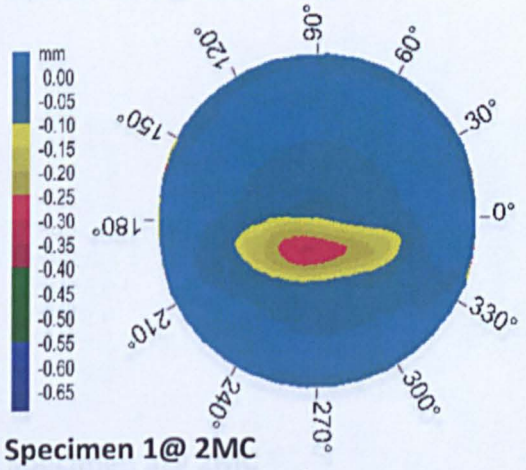

Specimen 1@ 2MC

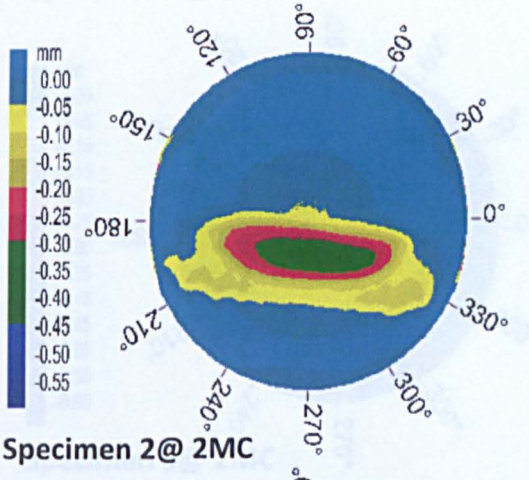

Specimen 2@ 2MC

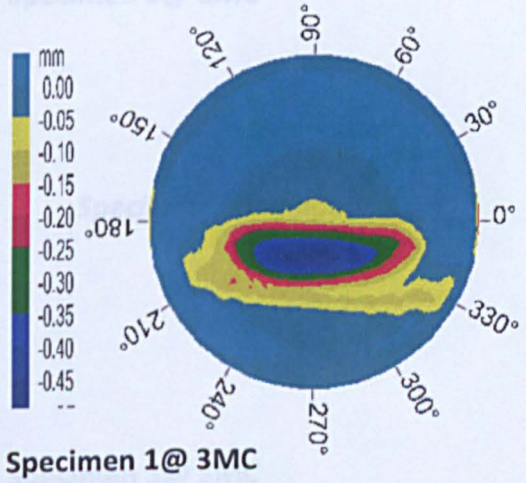

Specimen 1@ 3MC

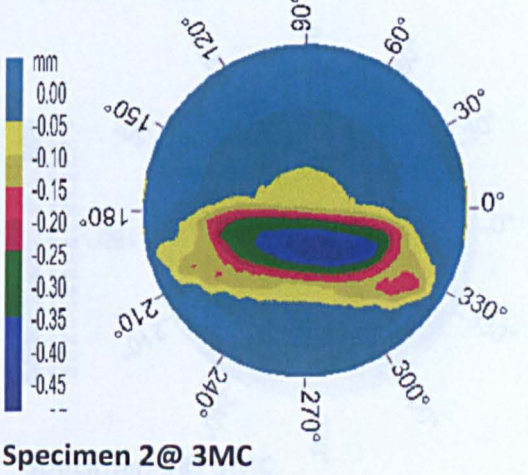

Specimen 2@ 3MC

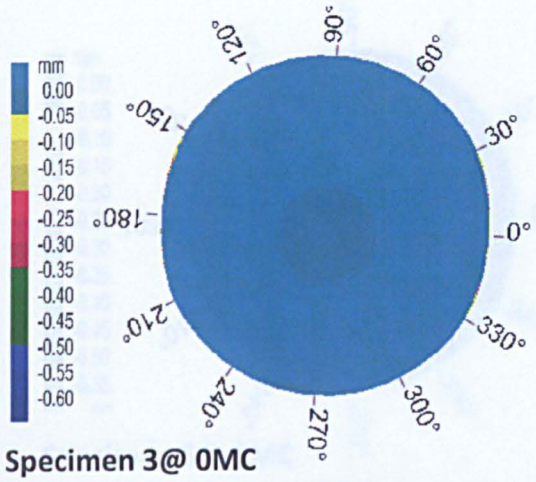

Specimen 3@ 0MC

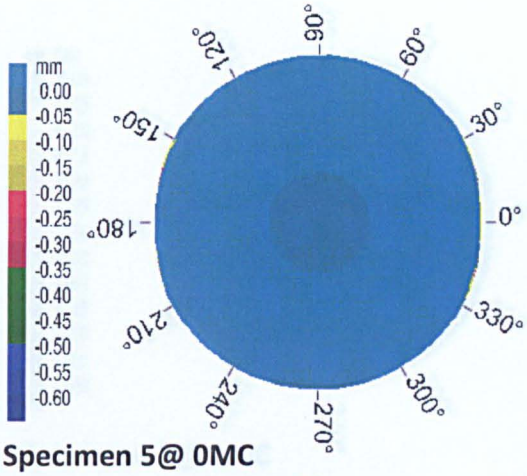

Specimen 5@ 0MC

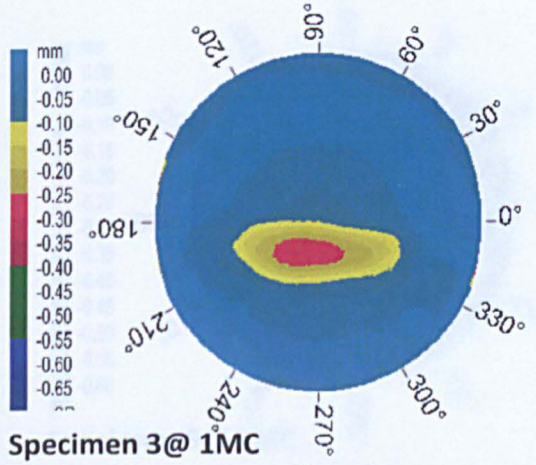

Specimen 3@ 1MC

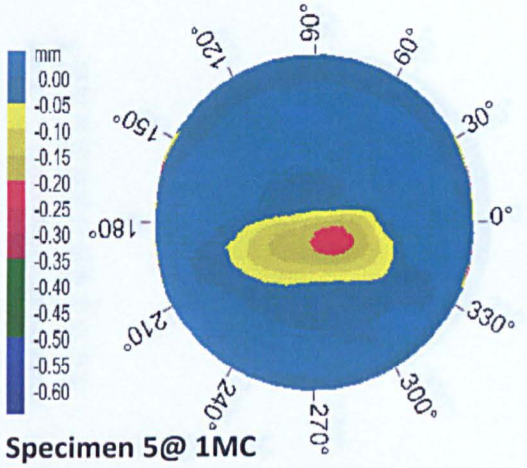

Specimen 5@ 1MC

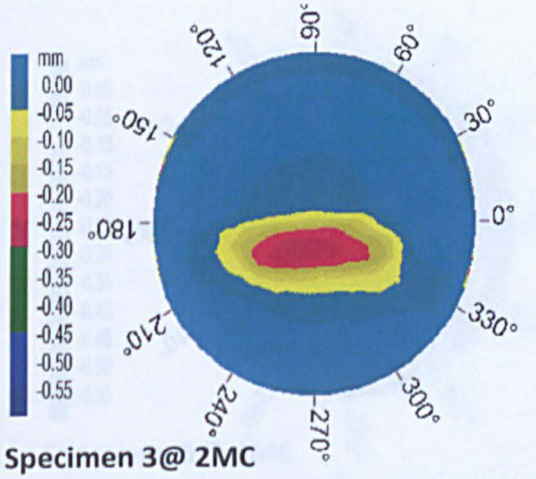

Specimen 3@ 2MC

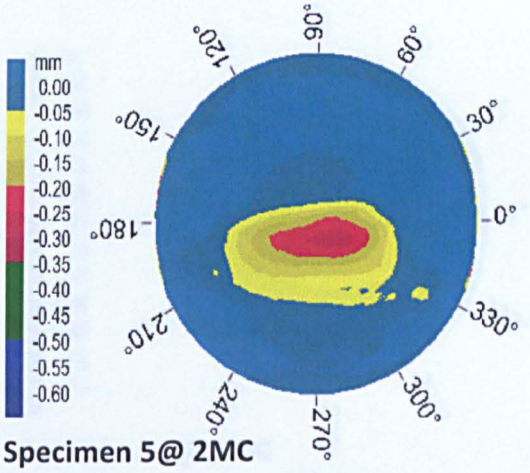

Specimen 5@ 2MC

Specimen 3 damaged

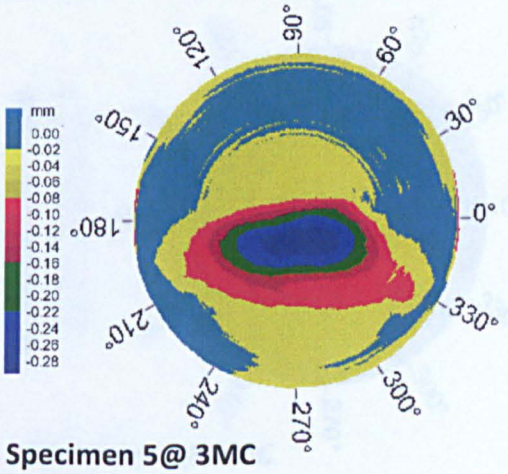

Specimen 3@ 3MC

Specimen 5@ 3MC

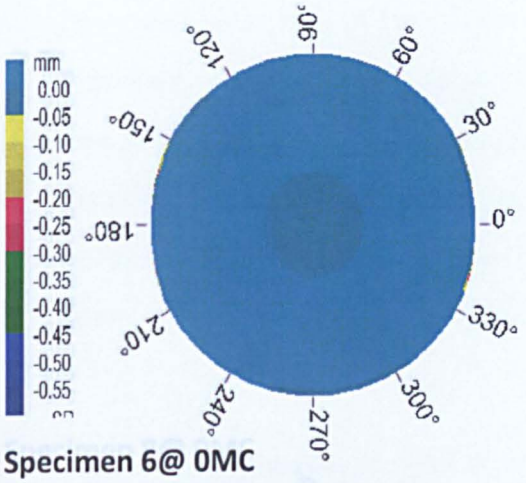

Specimen 6@ 0MC

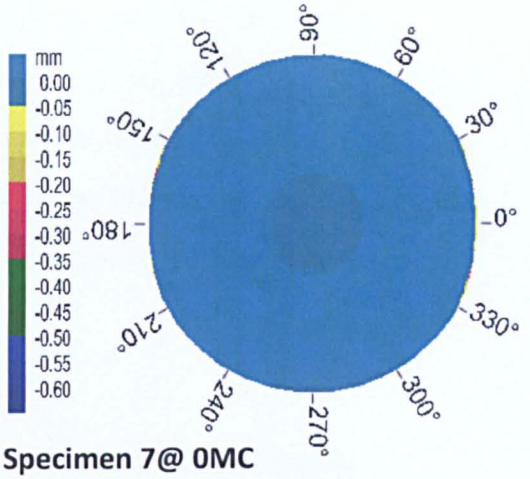

Specimen 7@ 0MC

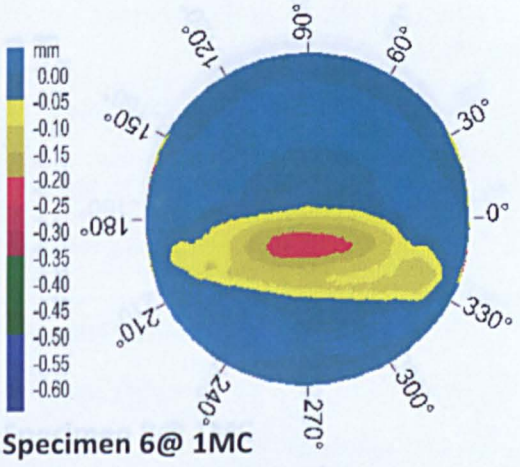

Specimen 6@ 1MC

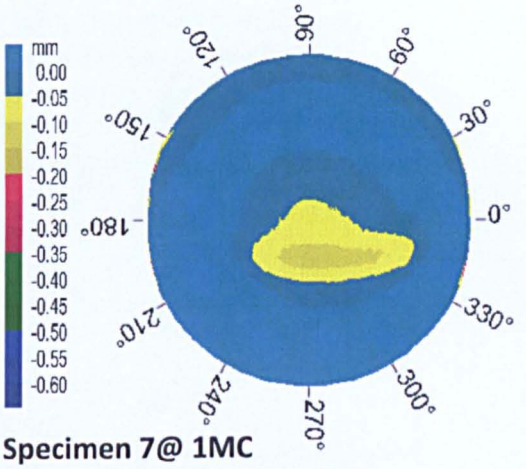

Specimen 7@ 1MC

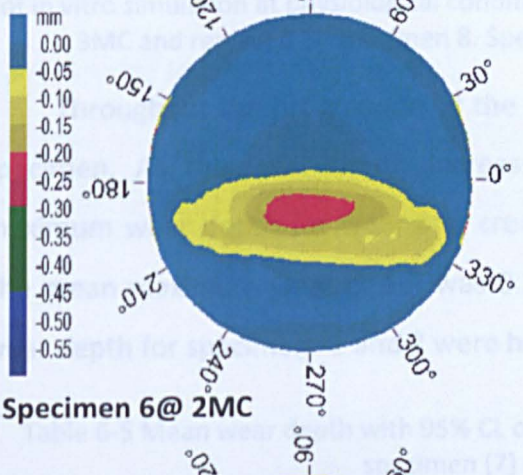

Specimen 6@ 2MC

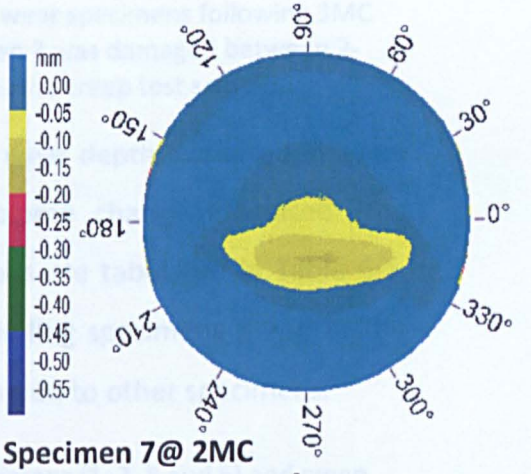

Specimen 7@ 2MC

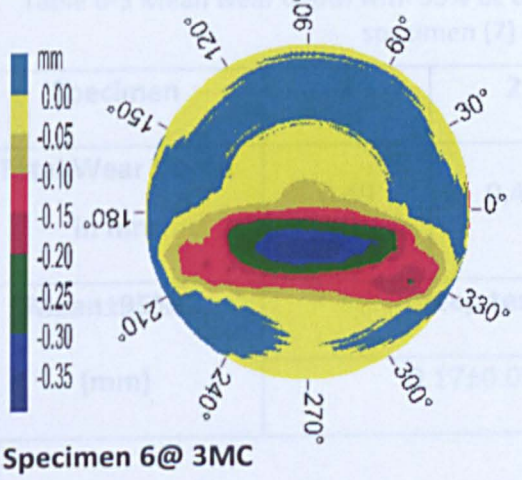

Specimen 6@ 3MC

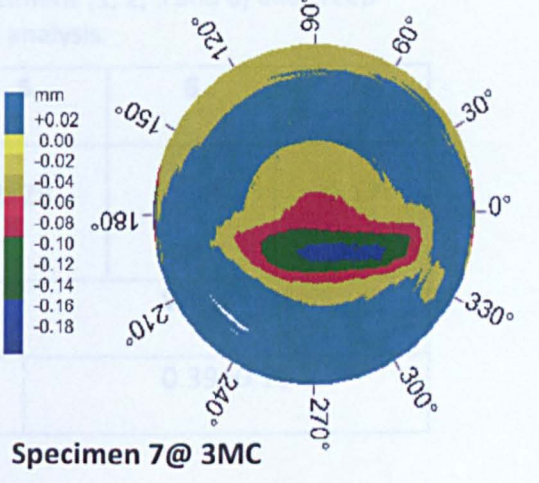

Specimen 7@ 3MC

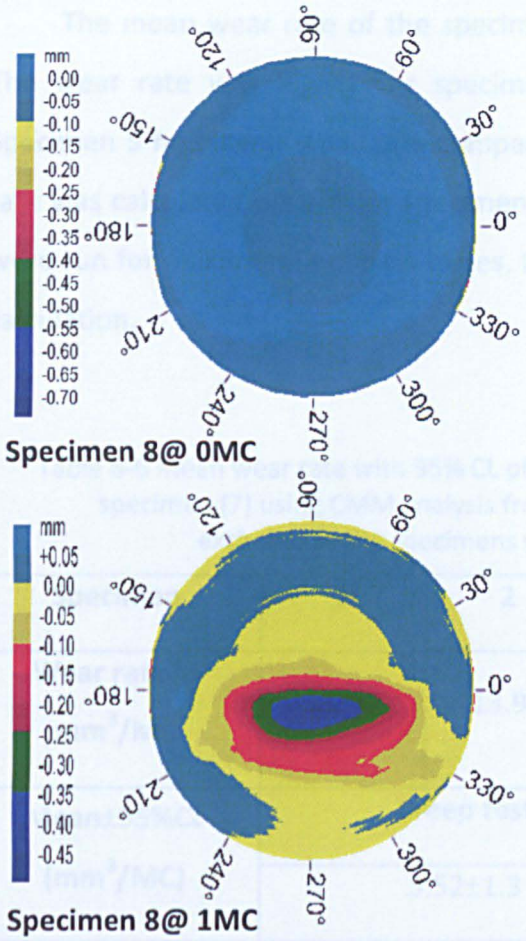

Figure 6-12 CMM analysis of wear penetration of all five wear specimens following 3MC of in vitro simulation at physiological condition. Specimen 3 was damaged between 2-3MC and replaced by specimen 8. Specimen 7 was the creep test sample.

Throughout the progression of the study, the wear depth increased in every specimen. As the wear depth increased, the volume change increased. The maximum wear depth for wear and creep specimens are tabulated in Table 6-5. The mean maximum wear depth was 0.39mm excluding specimens 3 and 8. The wear depth for specimens 1 and 2 were higher compared to other specimens.

Table 6-5 Mean wear depth with 95% CL of worn specimens (1, 2, 5 and 6) and creep specimen (7) using CMM analysis.

Specimen	**1**	**2**	**5**	**6**	**7**
Total Wear Depth in mm	0.49	0.41	0.28	0.38	0.17
Mean±95%CL (mm)	**Creep test**		**Wear test**		
	0.17±0.05		0.39±0.13		

The mean wear rate of the specimen using CMM is presented in Table 6-6. The wear rate was higher for specimen 8 as compared to other specimens. Specimen 5 had lower wear rate compared to other wear specimens. Mean wear rate was calculated on n=4 for specimen (1, 2, 5 and 6). As the specimens 3 and 8 were run for maximum 2 million cycles, they were not included in mean wear rate calculation.

Table 6-6 Mean wear rate with 95% CL of worn specimens (1, 2, 5 and 6) and creep specimen (7) using CMM analysis from 3 million cycles. Specimen 3 and 8 were excluded as the specimens were run less than 2 million cycles.

Specimen	**1**	**2**	**5**	**6**	**7**
Wear rate in mm^3/MC	11.90	13.95	6.05	11.80	3.52
Mean±95%CL (mm^3/MC)	**Creep test**		**Wear test**		
	3.52±1.3		10.92±5.43		

6.3.3 Volume Loss with ML Tilt

The volume loss increased with increased in tilt. Strong correlation of 0.98 was found between the two entities as shown in Figure 6-13

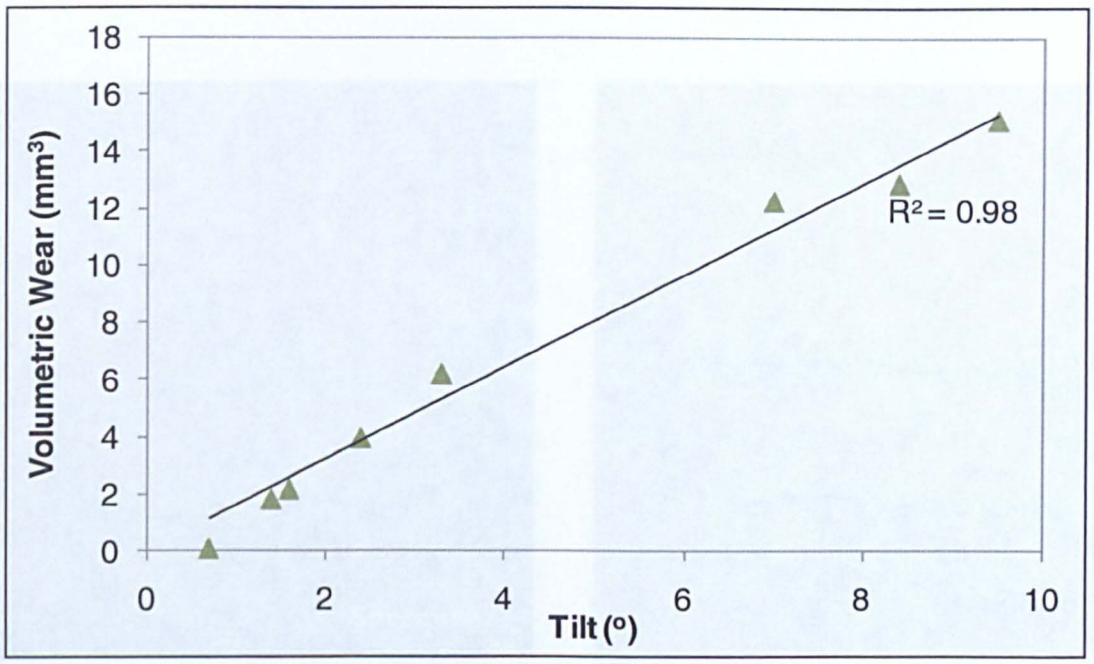

Figure 6-13 Relation of wear volume with tilt. Figure shows the linear correlation with R^2 value.

6.3.4 Quantification of Wear Area, Centroid of the Scar Area, Surface Analysis and Wear Depth

6.3.4.1 Scar area

The wear scar appeared towards the superior quadrant in all the oval dome patella specimens, spreading from the medial to the lateral periphery (Figure 6-14). No wear or surface change was seen on the edges or the backside of the patella specimen. This showed that the patella specimen was rigidly fixed in the holder during the wear test. The width of articulation scar area of specimen 7 undergoing creep was lower compared to the other specimens. The wear specimens had the higher increase in the wear scar area during the first million cycles and the wear scar area stabilised after the first million cycles as shown in Figure 6-15 and Table 6-7.

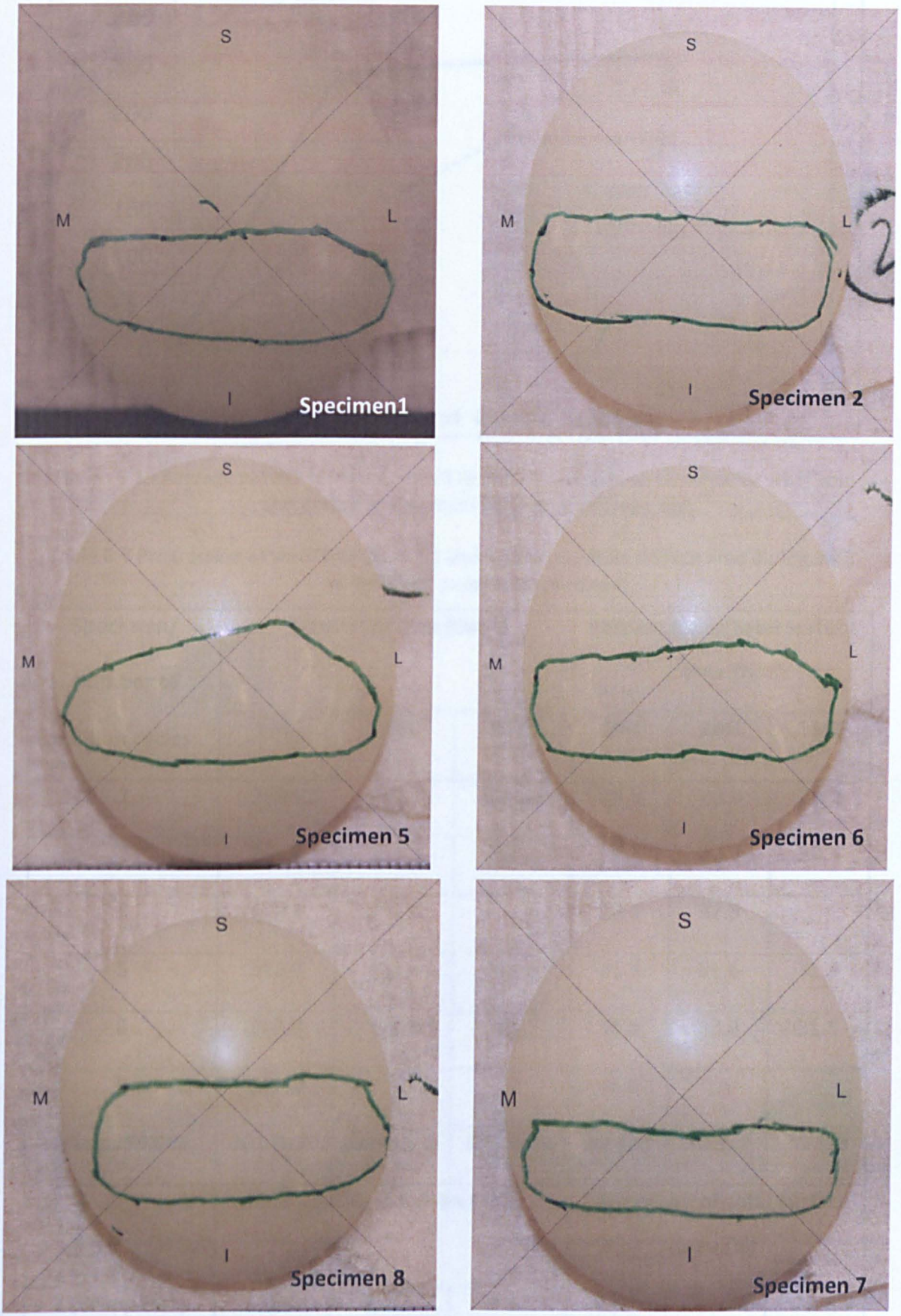

Figure 6-14 Wear Scar for all 5 specimens with solid line indicating total worn area. Specimen 7 underwent creep test.

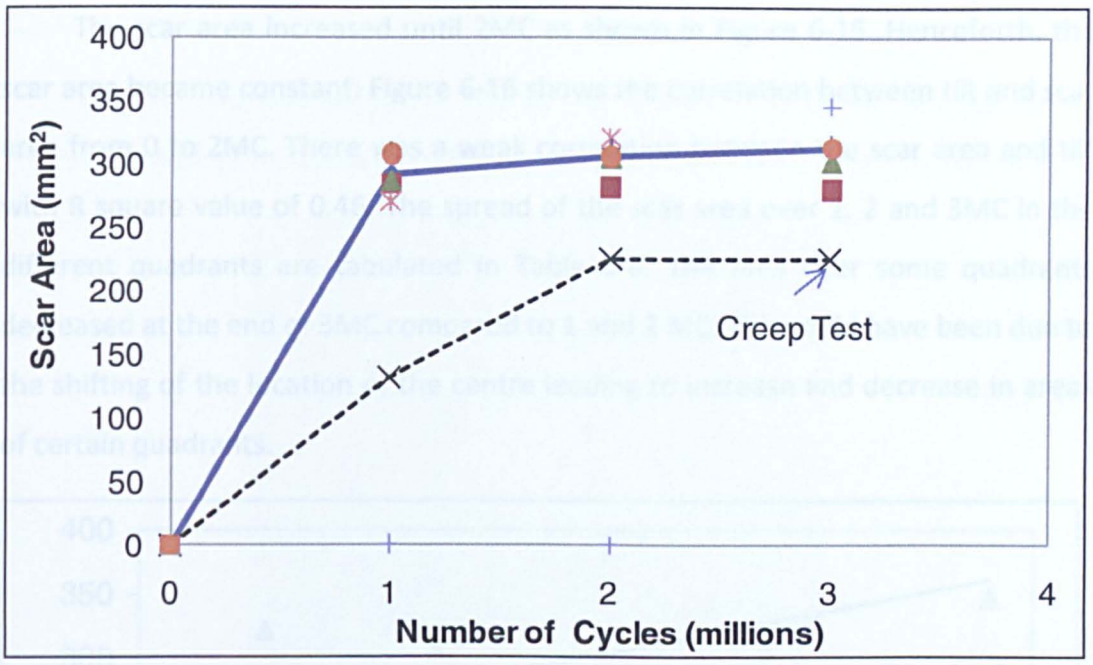

Figure 6-15 Average patella scar area from 0 to 3MC. The solid line denotes for wear test and dotted line denotes increment of creep test.

Table 6-7 Progression of wear scar (in mm^2) and % of articulating surface area during 3MC in wear and creep test specimens

Specimen/ Number of million cycles	Wear scar area (mm^2)			Percentage of total surface area (%)		
	1MC	2MC	3MC	1MC	2MC	3MC
1	283.8	281.7	280.0	28.6	28.4	28.2
2	286.8	305.3	302.4	28.9	30.7	30.4
3	270.1	320.8		27.2	32.3	
5	310.8	313.8	316.8	31.3	31.6	31.9
6	307.7	306.5	313.2	31.0	30.8	31.5
8	347.0			34.9		
Mean±95%CL	*301.0±29*	*305.6±18*	*303.1±26*	*30.3±3*	*30.8±2*	*30.5±3*
	Articulating scar area (mm^2)			Percentage of total surface area (%)		
7 (Creep test)	132.4	226.6	226.5	13.3	22.8	22.8

The scar area increased until 2MC as shown in Figure 6-15. Henceforth, the scar area became constant. Figure 6-16 shows the correlation between tilt and scar area from 0 to 2MC. There was a weak correlation between the scar area and tilt with R square value of 0.46. The spread of the scar area over 1, 2 and 3MC in the different quadrants are tabulated in Table 6-8. The area over some quadrants decreased at the end of 3MC compared to 1 and 2 MC. This could have been due to the shifting of the location of the centre leading to increase and decrease in areas of certain quadrants.

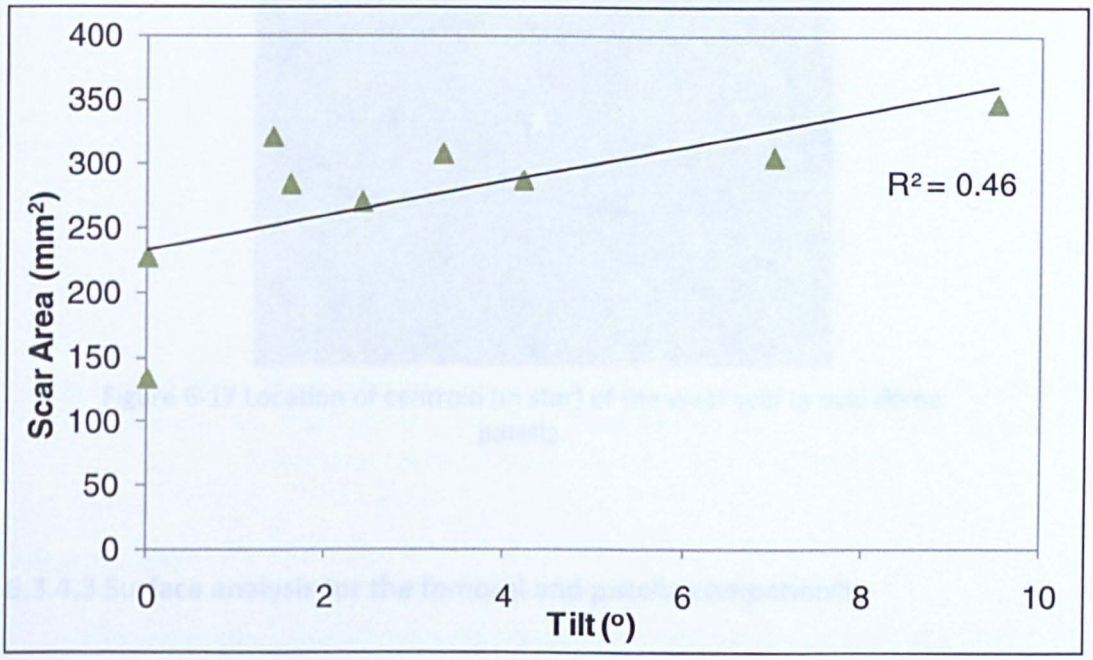

Figure 6-16 Relation of wear volume with tilt. Figure shows the linear correlation with R^2 value.

Table 6-8 Progression of wear scar (in mm^2) in superior, inferior, lateral and medial quadrant during 3MC in wear test

Number of million cycles	Quadrant			
	Superior	Inferior	Lateral	Medial
1	7.5±5.7	87.2±24.8	127.3±13.4	114.1±17.7
2	10.4±12.4	88.1±12.7	129.4±13.0	123.5±16.9
3	1.88±4.67	109.7±18.9	106.7±15.0	94.0±31.1

6.3.4.2 Location of centroid

The centroid was located in the inferior quadrant as shown in Figure 6-17. This was similar to the location of the centroid in round dome patella (Chapter 5).

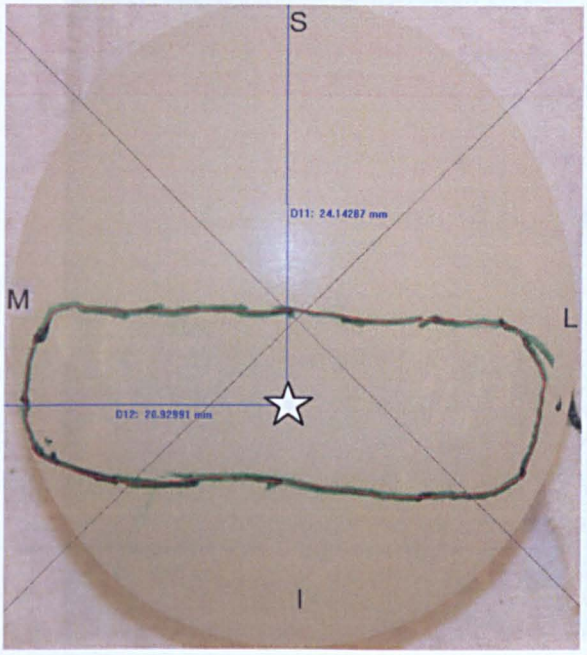

Figure 6-17 Location of centroid (in star) of the wear scar in oval dome patella.

6.3.4.3 Surface analysis for the femoral and patella components

Visual observations

Femoral component and patella specimens

Scratches similar to the round dome wear test were observed in the femur (Figure 5-20) using visual inspection. The scratches were parallel to the flexion extension axis. There were a few scratches found in the patella specimens. The number of scratches varied significantly between the components tested in creep and wear tests with the former having minimal scratches.

Wear characteristics

A few regimes of wear were observed as shown in Figure 6-18. The blue and green regime represents the pitting and deformation respectively. These regimes

were embedded inside the regime shown in red line which was the burnishing wear regime. Scratches were found outside the burnishing regime as shown by the yellow line. Similar scratches to round dome were observed in oval dome patellae.

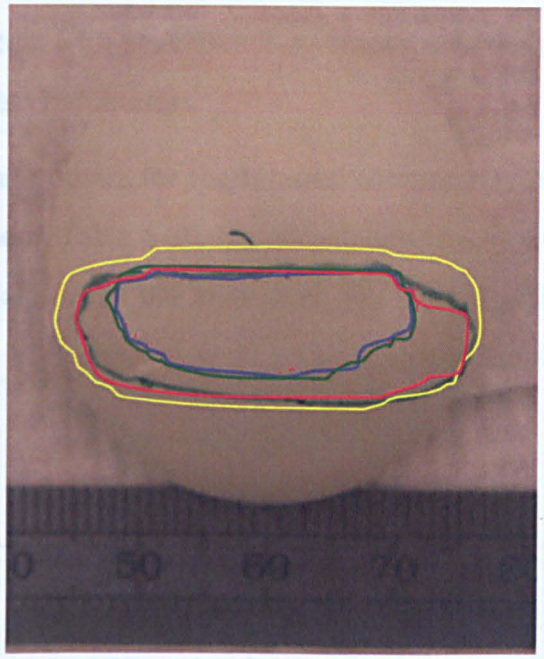

Figure 6-18 Wear characteristics of wear test specimens undergoing low ML rotation and uncontrolled ML displacement. 1: pitting wear (blue line), 2: burnishing (red line), 3: deformation (green line) and 4: scratching (yellow line).

Wear grading

The oval dome specimens were graded according to Hood et al. (1983). The grading of the four specimens is presented in Table 6-9. Embedded PMMA particles and abrasion was absent in the grading. The grading was lower than the round dome patella (34.8±5.9).

Table 6-9 Grading of wear damage in oval dome test specimen

Specimen	**Score**
Specimen 1	29
Specimen 2	30
Specimen 5	32
Specimen 6	29
Average±95%CL	30±2.25

Surface analysis

Femoral component

A typical calculation of the roughness parameters for a femoral component undergoing the wear test with specimen 2 as an example is shown in Figure 6-19 along with the roughness parameters.

The roughness parameters for the femoral components before and after the wear test are tabulated in Table 6-10. Significant differences were found between R_a, R_{sk} and R_v before and after the wear test. However, R_p was not significantly different. R_a, Rp and R_v increased with progression of the test. However, R_{sk} decreased after 3MC.

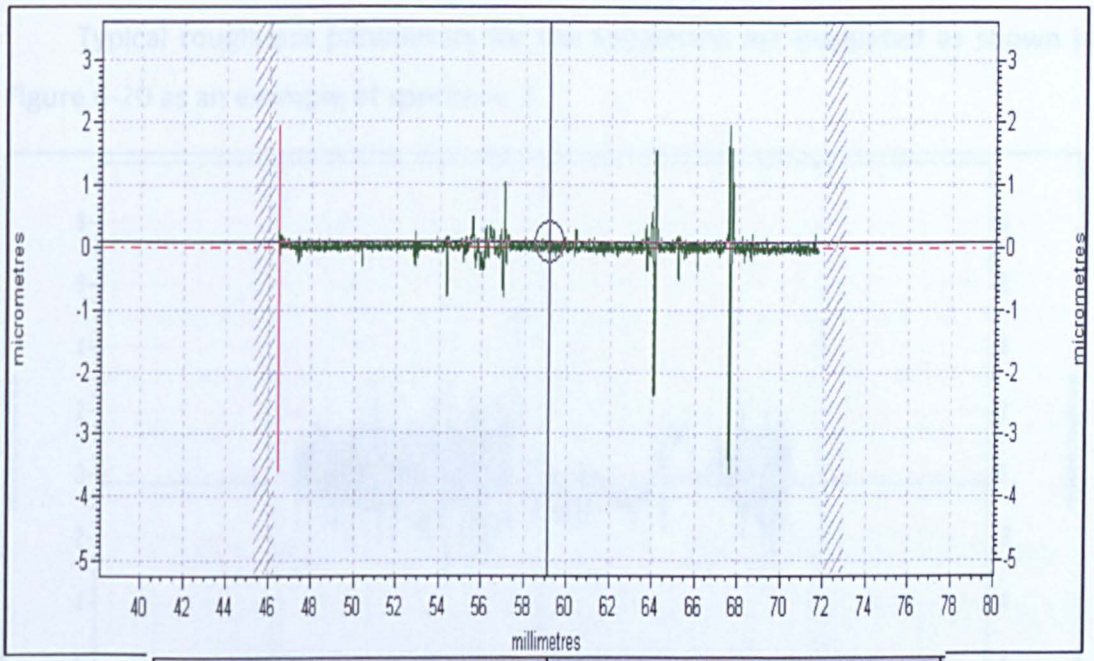

Ra	0.0729	µm	Rq	0.2164	µm
Rsk	-6.1374		Rku	115.5931	
Rp	0.1708	µm	Rv	0.1931	µm
RLo	25.2510	mm	Rt	5.5736	µm
Rlq	107.91	µm			
			Rz	0.3639	µm
RS	27.71	µm	RSm	3025.57	µm
Rln	25.2500	mm	Rc	2.1475	µm

Figure 6-19 Roughness of femoral component mating with wear specimen 2. The table shows average (R_a), skew (R_{sk}), peak (R_p) and valley (R_v) roughness of the femoral component

Table 6-10 Roughness parameters for the femoral components before and after the wear simulation test. Significant difference between the test interval with *p<0.05

Parameters	Pre-Test	Post-Test	P value
R_a(μm)	0.027±0.01	0.037±0.01	0.021*
R_{sk}	0.58±0.51	-2.53±1.26	0.0001*
R_p(μm)	0.092±0.01	0.097±0.02	0.44
R_v(μm)	0.067±0.01	0.092±0.02	0.005*

Patella specimen

Similar to femoral component, the oval dome patella were measured under Talysurf profilometer for measurement of average surface and skew roughness parameters.

Typical roughness parameters for the specimens are evaluated as shown in Figure 6-20 as an example of specimen 2.

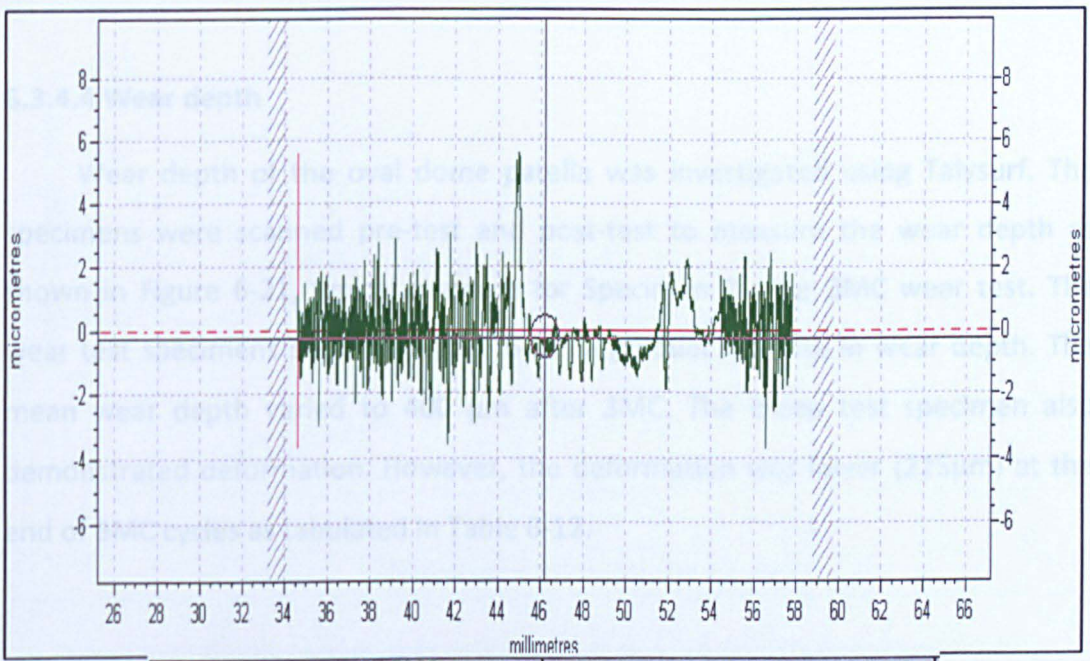

Radius	27.7693	mm			
Ra	0.7644	μm	Rq	1.0321	μm
Rsk	0.9676		Rku	6.7639	
Rp	1.8130	μm	Rv	1.8212	μm
RLo	23.2413	mm	Rt	9.2638	μm
Rlq	106.56	μm			
			Rz	3.6342	μm
RS	58.38	μm	RSm	234.14	μm
Rln	23.2000	mm	Rc	2.6188	μm

Figure 6-20 Roughness of wear patella specimen 2 after running for 3MC.

The roughness parameters R_p, R_v, R_a and R_{sk} before and after the wear test along with p value are presented in Table 6-11. The mean average surface roughness (R_a) remained constant (0.83μm) throughout the 3MC. Skew roughness R_{sk} significantly increased from -0.28 μm to 0.42 μm at 3MC. R_p and R_v decreased with the wear test. However, the change was significant and non significant for R_p and R_v respectively

Table 6-11 Roughness parameters for the patella specimen before and after the wear test. Significant difference between the test interval with *p<0.05

Parameters	Pre-Test	Post-Test	P value
R_a(μm)	0.83±0.09	0.83±0.15	0.97
R_{sk}	-0.28±0.22	0.42±0.81	0.03*
R_p(μm)	2.45±0.21	1.99±0.49	0.05*
R_v(μm)	2.58±0.20	2.10±0.66	0.10

6.3.4.4 Wear depth

Wear depth of the oval dome patella was investigated using Talysurf. The specimens were scanned pre-test and post-test to measure the wear depth as shown in Figure 6-21, typical example for Specimen 2 after 3MC wear test. The wear test specimens showed (Figure 6-22) a gradual increase in wear depth. The mean wear depth varied to 400 μm after 3MC. The creep test specimen also demonstrated deformation. However, the deformation was lower (225μm) at the end of 3MC cycles as tabulated in Table 6-12.

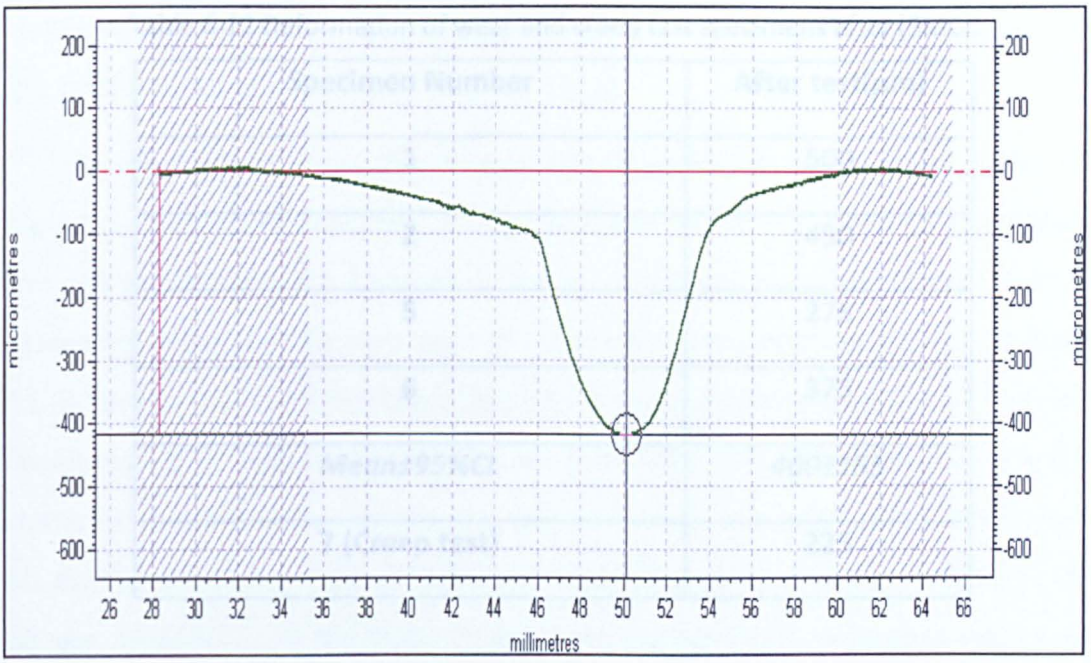

Figure 6-21 Wear depth of wear patella specimen 2 after running for 3MC.

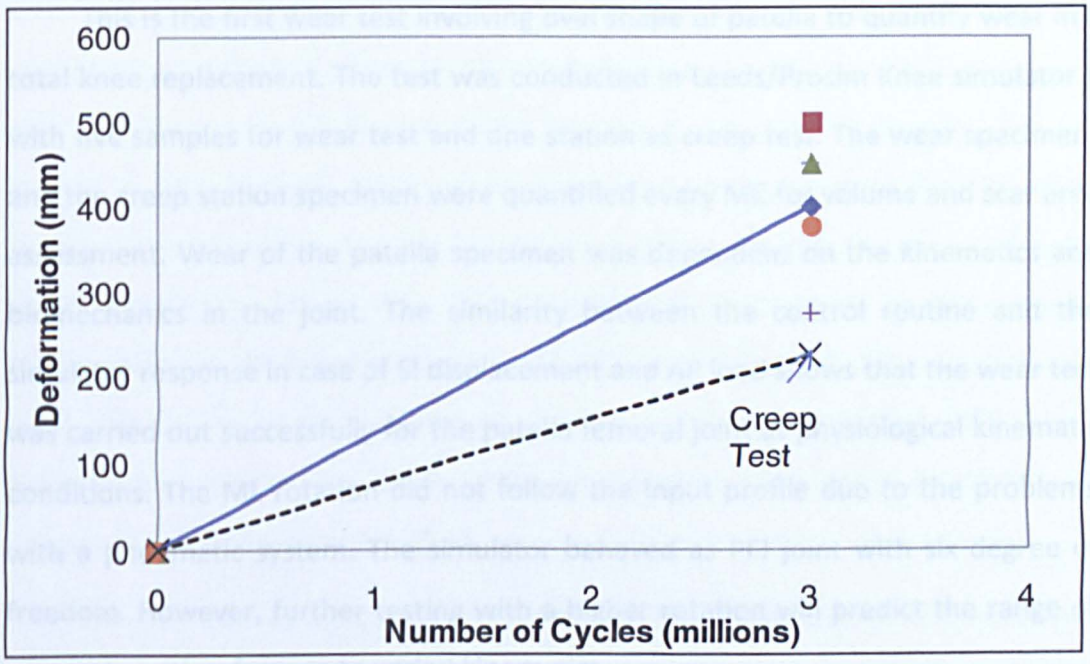

Figure 6-22 Scatter plot of wear depth/deformation of the patella specimen during physiological conditions; ML rotation (<1°) and free ML displacement.

Table 6-12 Deformation of wear and creep test specimens after (3MC).

Specimen Number	After test(μm)
1	500
2	450
5	275
6	375
Mean±95%CL	*400±155*
7 (Creep test)	225

6.4 Discussion

This is the first wear test involving oval shape of patella to quantify wear in a total knee replacement. The test was conducted in Leeds/Prosim Knee simulator 1 with five samples for wear test and one station as creep test. The wear specimens and the creep station specimen were quantified every MC for volume and scar area assessment. Wear of the patella specimen was dependent on the kinematics and biomechanics in the joint. The similarity between the control routine and the simulator response in case of SI displacement and AP load shows that the wear test was carried out successfully for the patella femoral joint at physiological kinematic conditions. The ML rotation did not follow the input profile due to the problems with a pneumatic system. The simulator behaved as PFJ joint with six degree of freedom. However, further testing with a higher rotation will predict the range of wear rate with reference to varied kinematics.

Similar to the round dome patella, the oval dome patella wear test had five samples with one load control and two soak control specimens. Load controls and soak controls were used as a method for active comparison. Soak controls determined the amount of fluid uptake during the test and the volume was deducted from the wear volume to determine the actual material loss. Load soak were used as a reference for creep measurement. The creep test specimen

stabilised after 2MC. This was in support of earlier investigation of creep wear in the knee stabilising after 2-3MC (Stanley 2011).

In the current study, the volume loss of specimen 2 was found to be the highest compared to specimen 5. This was due to the transition of specimen 5 through station G2-1, G2-2 and G1-1. The three stations were having low tilt which caused the wear volume from each of them lower compared to stations G1-2 and G1-3. Specimen 2 was transferred from G1-2 to G1-3 followed by G2-1 which was having higher tilt leading to higher volume loss (Table 6-2). The tilt was lower in few stations due to following reasons: the rigidity of the bearings to resist torque, lower ML displacement and the axial load was lower as compared to other stations. The tilt was different in all the stations. However, no significant difference was found between each stations ($p=0.29$).

As shown in Figure 6-13, wear volume increased as the tilt increased with linear regression R square 0.98. This can be explained as the uneven loading causing uneven contact stress which increases the wear. This was reported earlier with tibial inserts (Jennings *et al.* 2007). Jennings and co authors reported that the lift off in the femoral condyles resulted in increase in wear for the tibial components. The other factor which affected the wear was the effect of cross shear. Due to the ML rotation, higher strain softening occurs in the direction perpendicular to the direction of principal molecular orientation. This led to higher wear rate as predicted by Fisher *et al.* (2001) and McEwen *et al.* (2005) in a polyethylene counter face. Weak correlation between wear scar area and tilt was observed with R square vale of 0.46.

The wear rate of the oval dome patella was lower than the round dome. With the identical physiological condition; low ML rotation and free ML displacement, the wear rate of oval dome was $6.28mm^3$/MC as compared to $8.63mm^3$/MC in case of round dome patella as shown in Figure 6-10. The smaller wear scar area of the oval dome patella among the two shapes of specimen (oval (31.2%) and round dome (39.9%) patella) caused the difference in the wear rate. As the area was lower in oval dome, the contact stress increased (Archard's law 1953). The wear

rate was lower similar to earlier investigation by Wang et al. (2001) and Galvin et al. (2009).

CMM was used as another way to calculate the volume of wear specimen. The volume change was different compared to gravimetric. The creep or wear depth caused by 'bedding in' of the metallic component in the polyethylene under the action of axial load was the reason for higher volume estimation. A good correlation between gravimetric and CMM at every MC was observed ($R^2 > 0.88$). The deformation in one of the soak specimen (specimen 8) subsequently used for wear testing was higher than any other specimen. Similar results were observed by Stanley (2011) when a soak specimen was used as load soak specimen after soaking in lubricating medium. However, a conclusion cannot be derived based on single specimen.

The creep area under the action of axial load was 132mm^2 at 1MC to constant value of 226mm^2 at 2 and 3 MC. The wear scar was lower as the specimen was acted on by axial or anterior posterior load. As shown in Figure 6-15, the wear scar area remained constant after 2MC contradicting Burroughs and co authors (2006) theory of varying wear scar area on testing of Sombero style patella button. As the degree of freedom considered in Burroughs and co-authors (Burroughs et al. 2006) were FE rotation and axial load, the effect of sliding distance due to SI and ML displacement were not noticed. This led to incorrect prediction of wear rate and wear scar area. As mentioned earlier wear is a function of material removal, creep and contact area translation. Burroughs and co author's wear model lacked the contact area translation. However, the shape of the scar was similar to the literature and biased towards inferior side of the patella.

Wear characteristics of the oval dome patella specimen showed scratching, burnishing, pitting and surface deformation. Fusion defects were removed by using gamma radiation procedure. The grading of the oval dome was moderate (30±1.5). However it was lower than the round dome patella (34.8±5.9) as the round dome went through higher number of cycles.

The wear depth increased with the number of million cycles. The wear depth increased from 0μm to 410 μm at the end of 3MC at low ML rotation and free ML

displacement. The metallic component seating action on the patella and the movement due to the tilt led to higher wear scar area. The lift off of the femoral component as described by (Jennings *et al.* 2007) caused more wear depth on the medial lateral plane. The higher the tilt led to increase in wear scar area. Similarly for creep test specimen, the wear depth after 3MC under the action of load alone was 225μm.

Surface roughness (Ra) increased for femoral component with increase in number of million cycles. Unidirectional scratches observed in the femur surface had negative skew roughness showed that the lubrication regime must be existing. Average roughness remained constant for patella specimens. However the skew roughness value in patella increased to positive value. The increase in skew roughness parameter implied that patella lacked lubrication between the articulating surface and was action of wear (Affatato *et al.* 2006). The peak (R_p) and valley (R_v) roughness increased as the number of cycles increased signifying peaks and troughs in the patella surface due to pitting or scratching.

Summary

There was a decrease in wear rate due to change in shape from round to oval dome patella buttons. However, this was not significant. The wear scar area of the oval dome specimen was 303mm^2 at the end of 3MC. The damage of the wear scars using Hood's method of grading was 30.0.

Chapter 7: Tribological Analysis of Patella Femoral Joint Retrievals

7.1 Introduction

The comparison of specimens from *in vitro* wear simulations with *in vivo* retrievals is essential for clinical relevance and validation of the *in vitro* simulation. Several attempts have been made to classify the surface characteristics of patella retrievals in the literature (Hood *et al.* 1983; Schwartz *et al.* 2002). However, only limited attempts have been made to compare *in vitro* specimens with clinical data (Ellison *et al.* 2010).

Once retrievals are received, determination of wear and hence, comparison with *in vitro* specimens can be challenging. The challenge in comparison may be due to the absence of data on the orientation of the retrievals and pre-wear measurements stage. Secondly, the motions in the simulators are mainly sliding contact. *In vivo*, the ligaments and impact loading conditions may lead to non proportional tribological characteristics. The ligaments can stabilise the bone thereby reducing damage. The impact loading can increase the contact stress and lead to high wear. Pre-wear data is important to determine the volume of the wear specimens (retrievals and *in vitro*). Measurement of the wear volume gravimetrically is only possible when volume before the wear process is known. However, with absence of pre-wear data, it becomes difficult to accurately determine the cumulative volume. The coordinate measuring machine (CMM) remains the only available method for the current author to evaluate the volume without pre-wear data. Comparison of other tribological characteristics like wear scar area and wear area spread in quadrants (Figure 7-1) are also difficult to analyse without adequate information on the orientation. Figure 7-1(a) shows a typical representation of wear area spread in four quadrant labelled 'S' for superior, 'I' for inferior, 'M' for medial and 'L' for lateral. However, if the orientation of wear scar was changed Figure 7-1 (a-d), a different spread of wear scar around quadrants was observed. This can lead to completely different wear characteristics.

In this chapter, retrievals obtained have been qualitatively evaluated for wear scar area, location of wear scar over varied quadrants, location of centroid for the wear scar, roughness, modes of UHMWPE damage and volumetric wear. Further, to this an active comparison with the simulation/*in vitro* specimens is made to validate the experimental simulations.

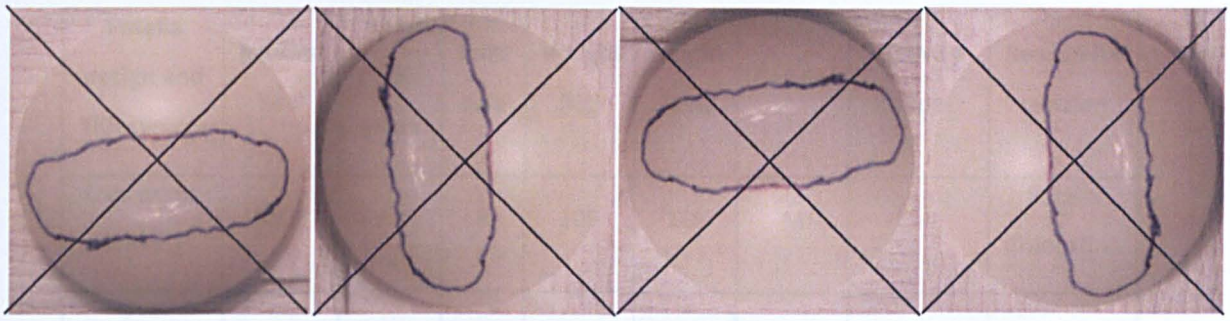

Figure 7-1 Wear scar area spread around quadrants ('M' for medial, 'L' for lateral, 'S' for superior and 'I' for inferior). Orientation of wear scar at (a) 0°, (b) 90° clockwise, (c) 180° clockwise and (d) 270° clockwise.

7.2 Materials and Method

The specimens (n=10) were retrievals collected from different hospitals over a period of 5 years (2003-2008) and are detailed in Table 7-1. The reasons for the failure were patella dislocation (20%), joint pain (30%), aseptic loosening (10%) and osteolysis (10%). The reasons for failure in 2 specimens (D, G) were unknown. The division of specimens in terms of gender was 60% female and 20% male, for the remaining 20% data was not available. The number of years *in situ* ranged from 2.1-13.1 years with 60% right knees and 30% left knees. Details of the remaining 10% knees were not known. The average weight and height was 81±14 kg and 164±10cm (average (n=10) ±95% CFL) respectively. The details of manufacturer for some of the selected retrievals were not known (Table 7-1). Oval and round dome retrievals were graded by 2 users to classify the retrievals based on intensity, area and type of wear scars according to the method by Hood *et al.* (1983).

The wear scar measurements, centroid location and wear scar over quadrants were captured using high zoom Camera (Cannon SLR) and analysed in Image ProPlus (Media Cybenetics, MD USA). Determination of the volumetric wear of the retrievals was performed in CMM and later analysed in SR3D software version 4.2

(Tribosol Ltd). Roughness parameters (R_a, R_{sk}, R_v and R_p) were determined using Talysurf profilometer. Finally, wear characteristics were evaluated using visual inspection. The details of methodologies are presented in the chapter 2: Materials and Methods.

Table 7-1 Clinical data of patella retrievals (Retrieval database, University of Leeds)

Patella design and TKR system	Implant Year	No of in situ years	Joint side	Weight (kg)	Height (cm)	Gender	Activity type	Reason for revision
Oval dome & PFC ∑	2002	3.9	R	105	186	M	-	Patella dislocation
Oval Sombero & PFC	1998	2.1	R	63	160	F	No support	Joint Pain
Oval Dome & PFC∑	2002	3.4	R	76	157	F	Sedentary	Aseptic loosening
Oval dome & PFC ∑	-	-	L	-	-	-	Sticks	-
Oval Sombero & PFC	1999	7.2	R	87	177	M	Stick	Joint Pain
Oval Sombero & PFC	2001	5.5	L	77	152	F	Sedentary	Joint pain.
Oval Dome	-	-	-	-	-	-	-	-
Sombero & Kinemax	2003	2.9	R	106	155	F	Manual	Tibia failure
Round Sombero & Leicester PFK	1997	9.2	L	69	155	F	Sticks	Osteolysis
Round Flat & Accord knee	1993	13.1	R	65	170	F	Stick	Dislocation

7.3 Results

7.3.1 Position of Wear Scar Area

The wear scars resulting from experimental simulation showed the spread of wear scar towards the inferior of the patella specimen (Figure 7-1a). The rationale for selection of the position of wear scar in the retrievals was based on the fact that majority of the wear scars appeared in inferior side as shown in Figure 7-2 and Figure 7-3. Figure 7-2 (a, b, c) shows the contact of patella with the femur during the rotation of femoral component at flexion and movements of patella in superior inferior direction in the sagittal plane. At 0° of flexion or full extension, the contact was at the top edge of the patella. At 10° of flexion, the point of contact moves from top edge to the inferior of the patella. At higher degrees of flexion, the contact is spread in inferior of the patella surface.

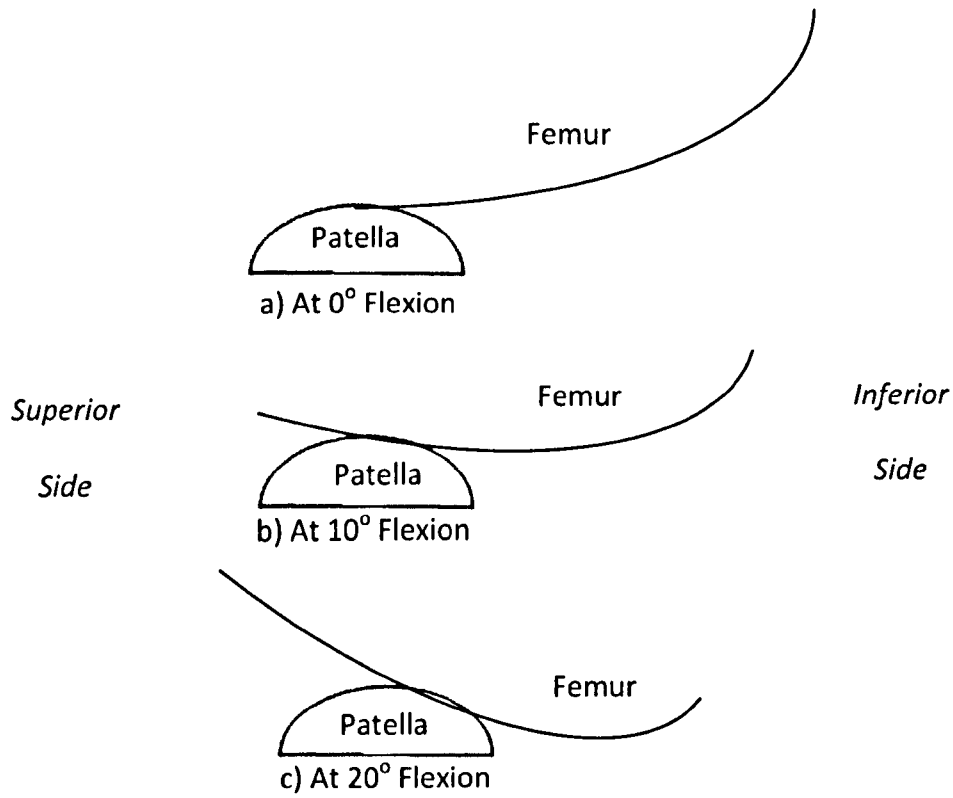

Figure 7-2 Position of patella with respect to femur during a) 0° b) 10° and c) 20° of femoral flexion in sagittal plane.

In the frontal plane, the tilt combined with ML displacement led to formation of the wear scar on the medial and lateral sides of patella in the patella femoral joint as shown in Figure 7-3 (a, b and c). The scenario was as obtained in the

experimental simulation. At the beginning of flexion, the patella tilt was towards lateral side (medial tilt) due to the presence of ligament load. Following movement of the patella towards the medial side, there was lateral patella tilt at 20° flexion. During this changeover from medial to lateral tilt, the patella crossed through 0° tilt at 10° flexion.

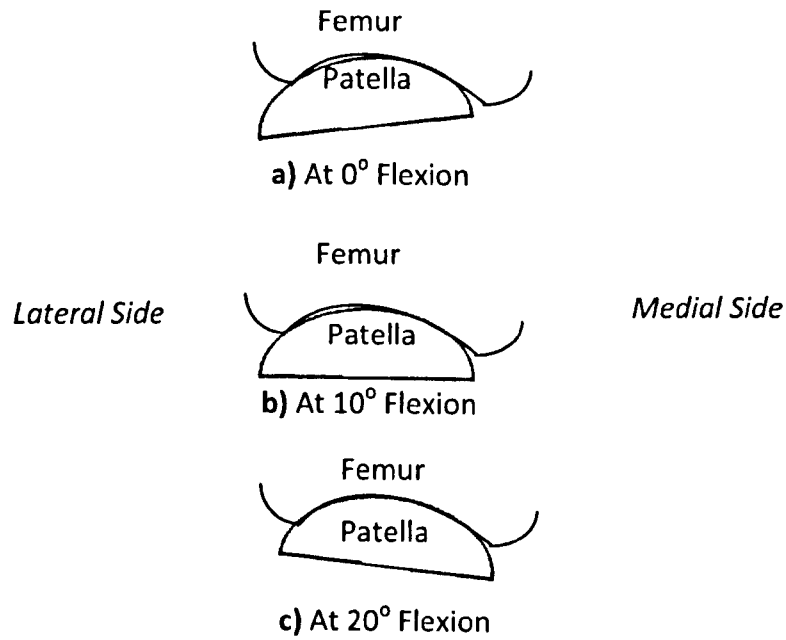

Figure 7-3 Position of patella with respect to the femur during a) 0°, b) 10° and c) 20° of femoral flexion in the frontal plane.

Following this rationale from the experimental simulations results, all the ten retrievals were rotated to locate the wear scar in the inferior of the patella.

7.3.2 Oval Patella Retrievals

7.3.2.1 Geometric volumetric measurements

Volumetric analysis was performed using CMM measurement as shown in Figure 7-4. The volumetric loss (using three repeated measurements) varied from 1.19 (retrieval D) to 65.46mm^3 (retrieval A) for the oval patella retrievals (A to H) as tabulated in Table 7-2. The scale in the CMM measurement showed positive reading. The positive readings were on the edges which do not affect the wear volume calculation as the area of interest was the inferior periphery.

The wear rate varied from 1.08mm^3/year (retrieval C) to 26.76 mm^3/year (retrieval B). The average wear rate was 9.09±9.39mm^3/year as shown in Table 7-3

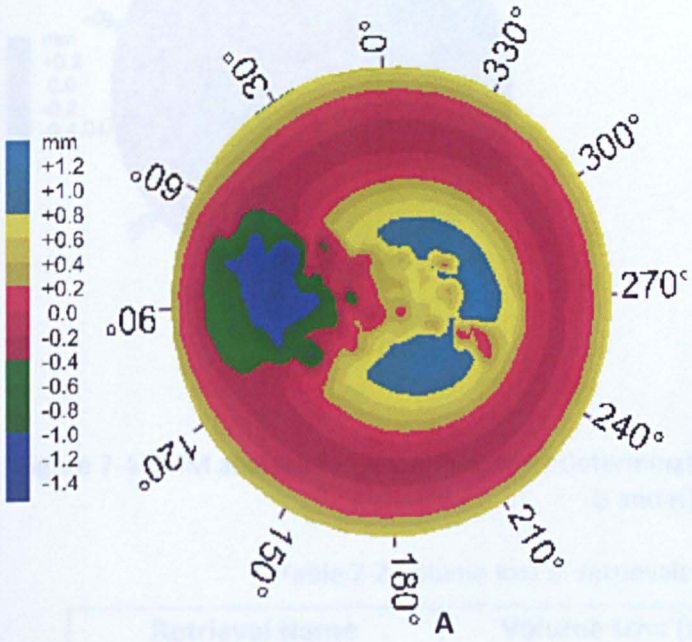

A

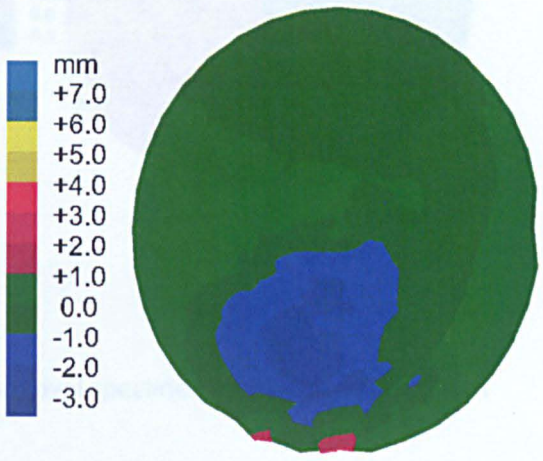

B

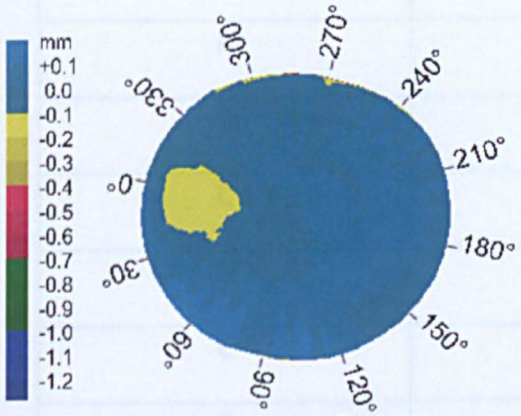

C

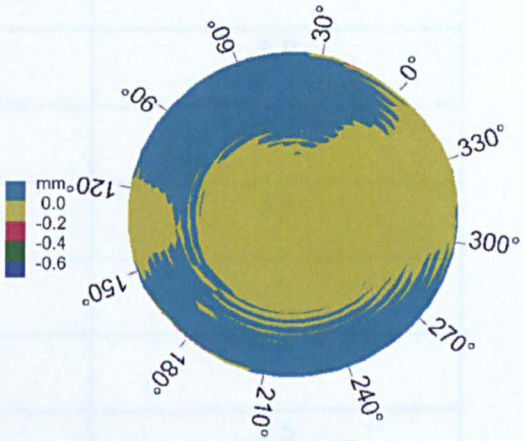

D

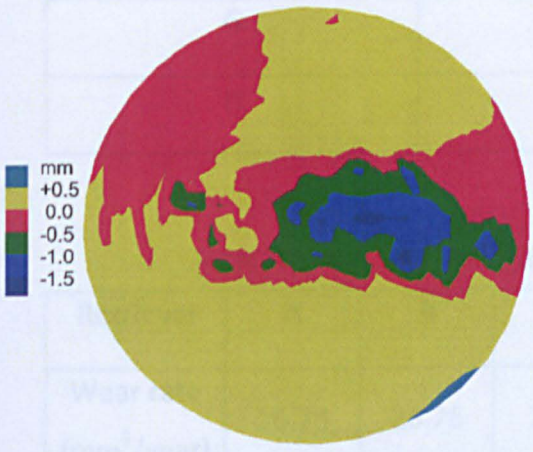

E

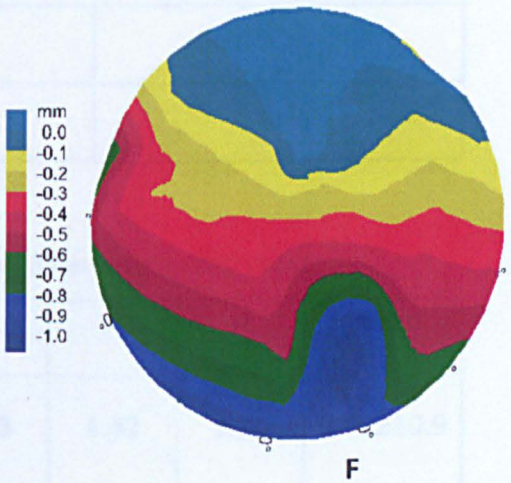

F

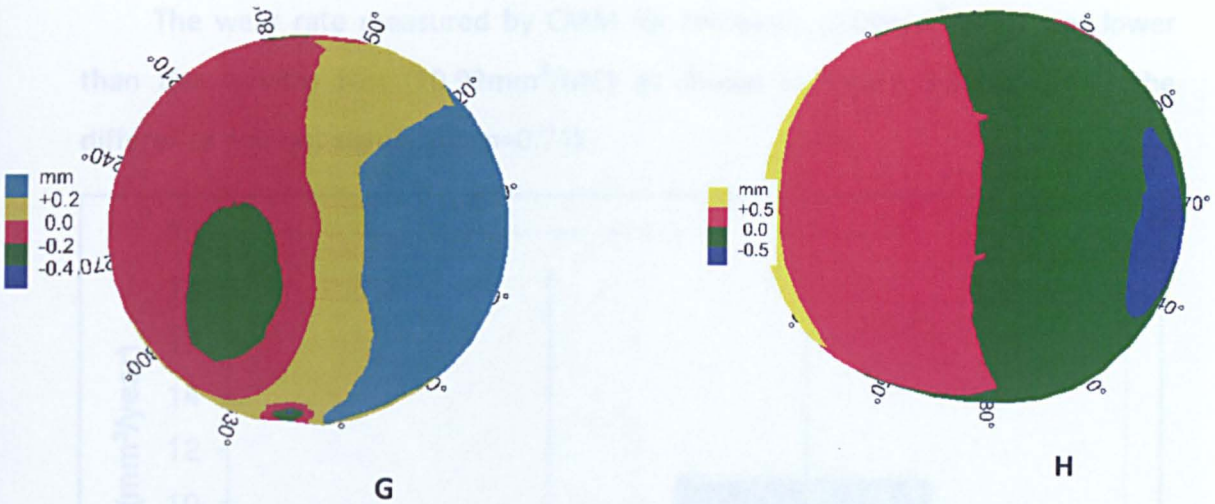

Figure 7-4 CMM analysis for volumetric wear determination (oval specimen A to F; round specimen G and H).

Table 7-2 Volume loss of retrievals determined using CMM

Retrieval Name	Volume Loss (mm^3)	Number of *in situ* years
A	65.46±5.06	3.9
B	56.19±7.01	2.1
C	3.66±2.41	3.4
D	1.19±0.26	-
E	28.33±3.23	7.2
F	26.59±2.20	5.5
G	3.25±0.01	-
H	3.31±2.25	2.9

Table 7-3 Wear rate (mm^3/year) of retrievals determined using CMM.

Retrieval	A	B	C	E	F	H	Mean
Wear rate (mm^3/year)	16.78	26.76	1.08	3.93	4.82	1.14	9.09±10.9

The wear rate measured by CMM for retrievals (9.09mm^3/year) was lower than the *in vitro* test (10.92mm^3/MC) as shown in Figure 7-5. However, the difference was not significant (p=0.74).

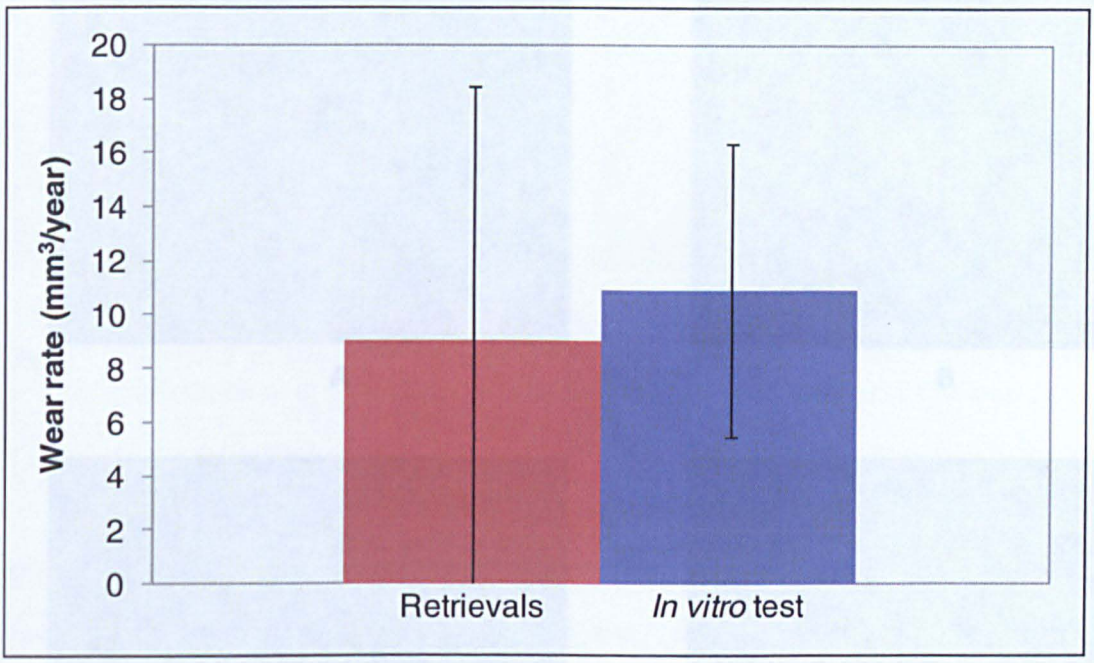

Figure 7-5 CMM analysis for volumetric wear determination (retrievals and *in vitro* test).

7.3.2.2 Quantification of surface analysis

Visual inspection

Scratches

Few scratches were found in retrievals G and H. Scratches in retrieval G was due to handling and scratches in retrieval H was due to third body wear particles as shown yellow solid lines in Figure 7-6 (G and H).

Wear characteristics

The various types of wear regimes found in the selected oval patella retrievals were scratching, burnishing, pitting, delamination and surface deformation as shown in Figure 7-6. The retrievals F and G were the least damaged specimens with respect to the varied regimes found. In terms of worn damage, specimens B and E were found to be the worst damaged wear specimens.

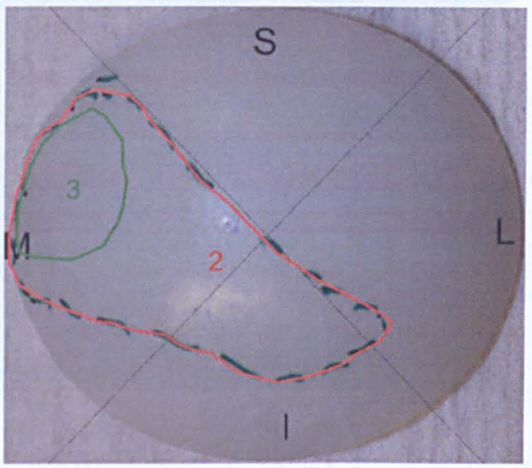

A

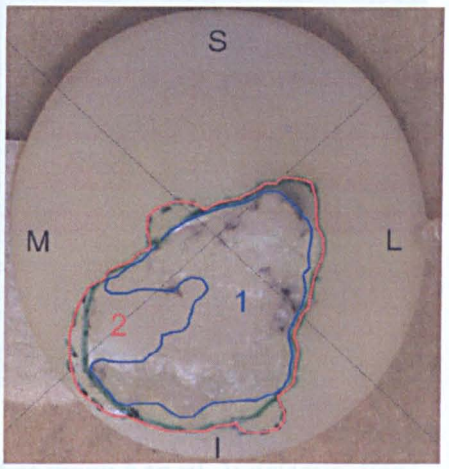

B

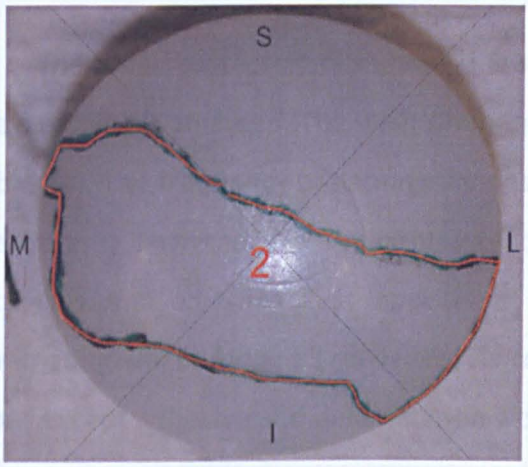

C

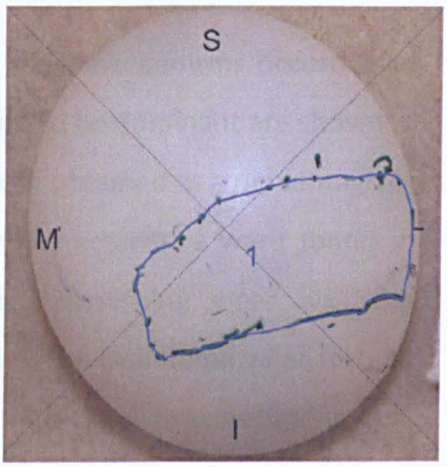

D

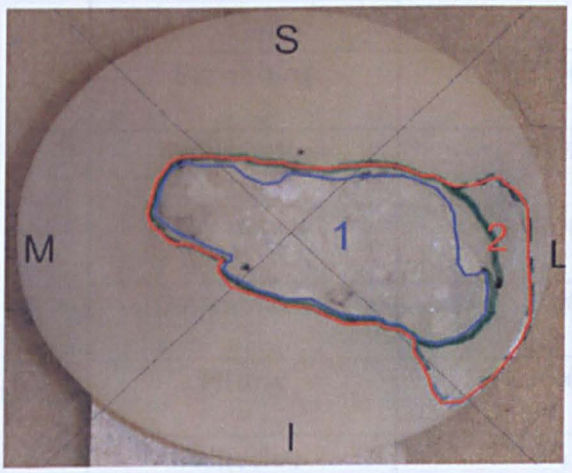

E

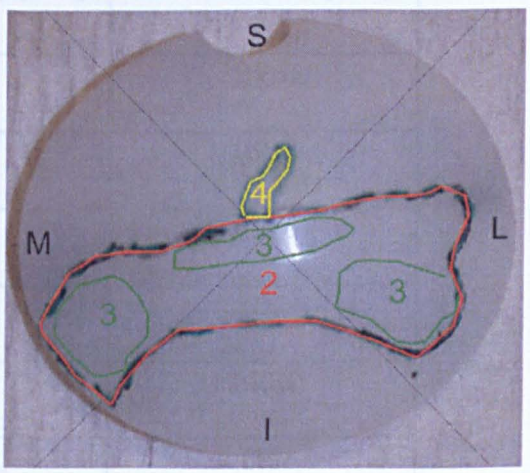

F

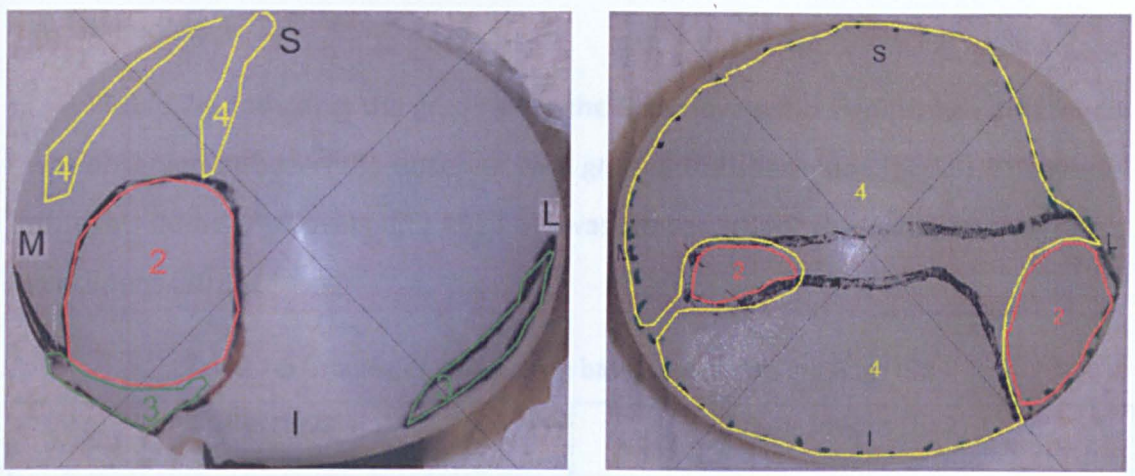

G H

Figure 7-6 Wear characteristics for oval patella retrievals (Specimen A to H). 1: delamination/ pitting wear, 2: burnishing, 3: deformation, 4: scratching, 5: adhesive wear.

The wear characteristics showed a series of wear mechanisms occurring in the 8 retrievals analysed. The wear phenomena found to be dominant are shown in Table 7-4. The frequency of damage modes (n=8) were obtained as a percentage of the dataset analysed. No similarities of the wear characteristics were found in retrievals and *in vitro* test specimens. However, burnishing wear was the dominating wear among all retrievals. As compared to the oval dome wear test, all types except adhesive and delamination wear were found in all five specimens.

Table 7-4 Frequency of patella damage with respect to the 8 retrievals dataset analysed

Type of wear	Present Study (n=8)	*In vitro* Study (n=5)
Burnishing	80%	100%
Deformation	50%	100%
Scratches	30%	100%
Delamination	30%	0%
Pitting	10%	100%
Adhesive	0%	0%

Wear grading

Table 7-5 tabulates the grading for the 8 retrievals. No significance difference was observed between the observer who graded the specimens (p=0.5). The grade of oval dome retrievals (12.25±3.6) was lower than the experimental test specimens (30±1.5).

Table 7-5 Grading of oval patella based on Hood's grading (1983)

Retrievals	Grade {mean (n=2) }
A	9.5
B	14.5
C	18
D	5.5
E	17
F	9
G	14
H	10.5
Average	12.25±3.6

Wear scar area and location of centroid

The wear area of the patella was spread from medial to lateral with bias towards the inferior side as shown in Figure 7-7. Mean wear scar areas of 279.78±49.97mm^2 (average n=8 ± 95% CFL) were found for the oval patella retrievals. In total among 8 retrievals, the wear area was 27.5±7.1% of the total surface area for the retrievals wear as in Table 7-6. The spread of the worn area was mostly towards inferior side with 11.4±9.7mm^2 in superior, 77.5±58.0mm^2 in inferior, 110.1±48.9mm^2 in lateral and 88.6±66.4mm^2 in medial part of the patella retrievals. The correlation between the wear scar area and the number of years *in situ* was R^2=0.65 as shown in Figure 7-8.

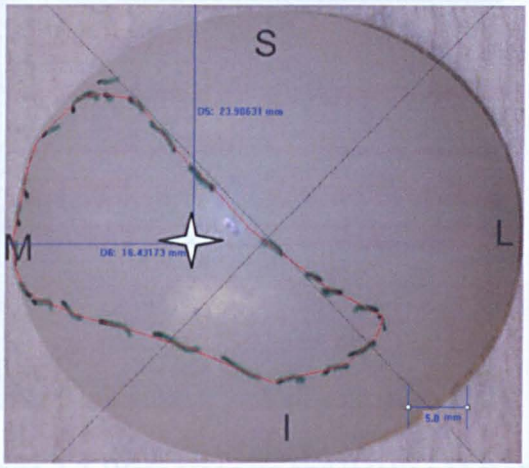

A

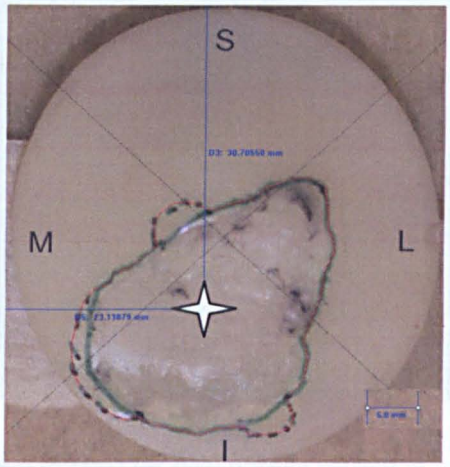

B

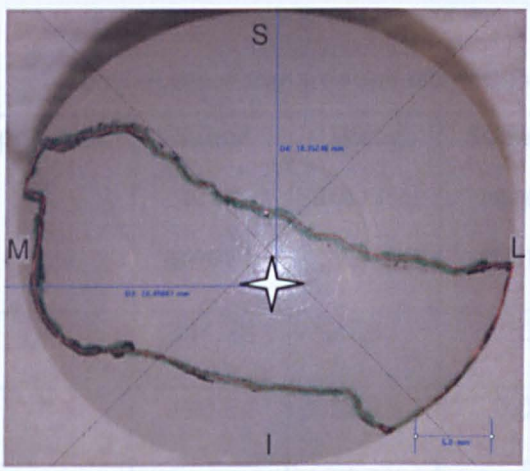

C

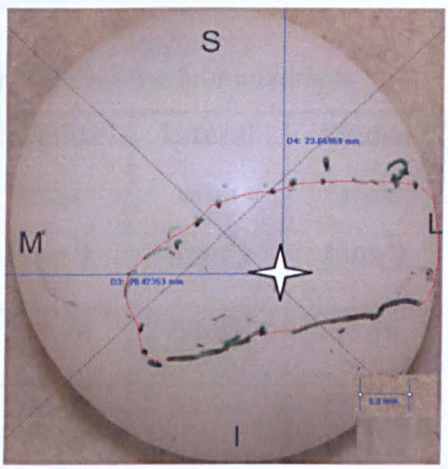

D

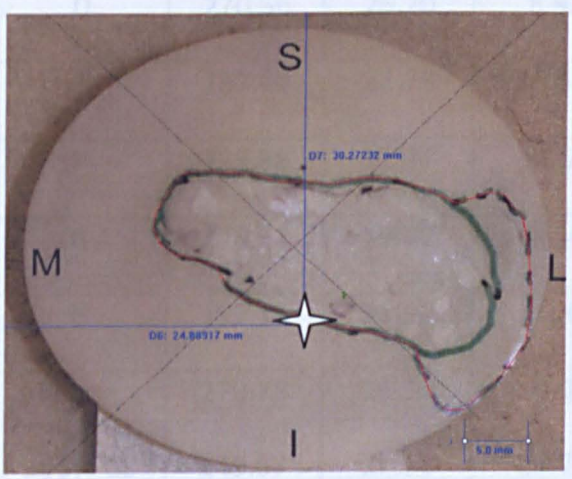

I

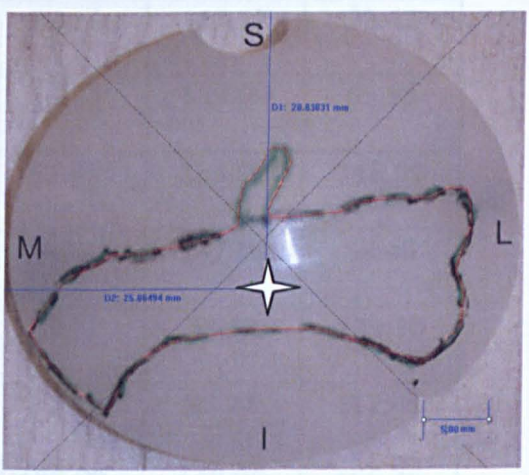

I

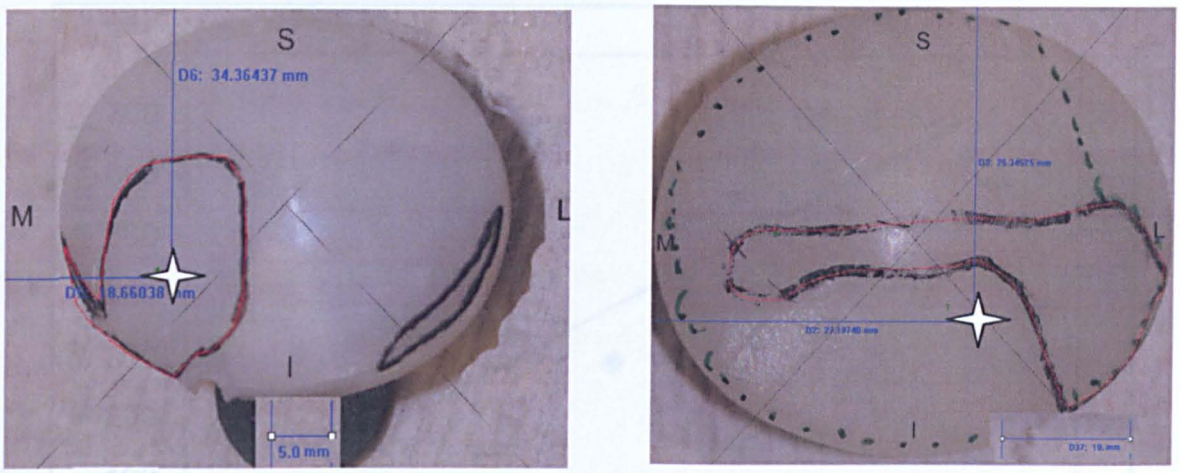

Figure 7-7 Wear scar area and location of centroid (shown in star) for oval patella retrievals (Specimen A to H).

Table 7-6 Wear scar area and distribution of wear scar over the four quadrants

Specimen	Wear area (mm^2)	Wear area (%)	Superior area (mm^2)	Inferior area (mm^2)	Lateral area (mm^2)	Medial area (mm^2)
A	344.28	27.81	12.33	231.76	68.83	66.46
B	230.64	17.23	0.00	108.55	11.14	279.09
C	350.85	44.10	5.47	84.08	90.06	154.57
D	270.56	25.20	8.92	92.18	147.17	28.41
E	287.40	22.78	35.5.2	36.73	159.04	65.98
F	333.88	31.37	14.56	52.97	135.00	116.99
G	228.51	19.42	3.24	6.83	147.03	58.48
H	192.10	21.98	0.00	38.27	23.62	129.30
Mean	279.78	26.24	10.00	81.42	97.74	112.41
±95% CL	±49.97	±7.11	±9.71	±58.00	±48.86	±66.36

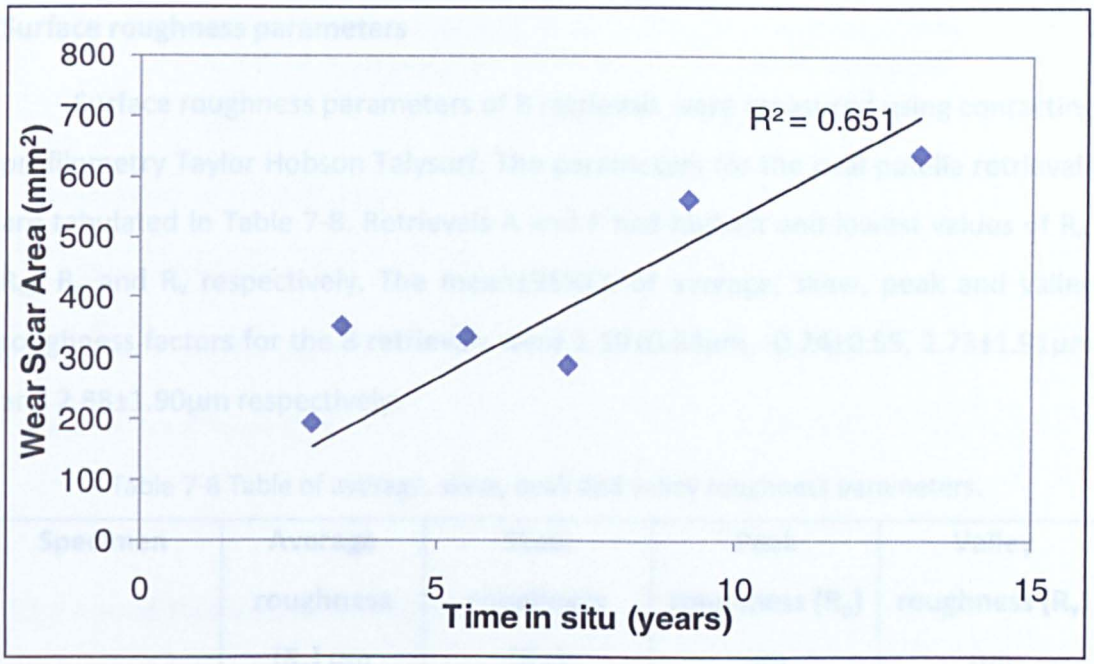

Figure 7-8 Wear scar area (square mm) with respect to time in situ (in years) with linear trend line and linear correlation (R^2).

As compared to the *in vitro* experimental simulation over 3MC, the wear scar area was 303.1 ± 45 mm^2 and 31.0±3% of the total area was covered in wear scar. There was no significant difference between the wear area (0.47) and percentage of area covered (0.35). The comparison of the wear areas of retrievals in superior, inferior, lateral and medial quadrant compared to in vitro specimens are shown in Table 7-7.

Table7- 7 Table of wear area in superior, inferior, lateral and medial quadrants of retrievals and *in vitro* specimens with p test between the two.

Wear Area (mm^2)	Retrievals	*In vitro Test*	P test
Superior	11.4±9.7	1.9±4.7	0.18
Inferior	77.5±58.0	107.1±18.9	0.94
Lateral	110.1±48.9	100.2±15.0	0.77
Medial	88.6±66.4	95.4±31.1	0.52

The locations of the centroid in the retrievals are shown in Figure 7-7. For *in vitro* oval dome patella (Figure 6-17), the centroid location was in inferior region.

Surface roughness parameters

Surface roughness parameters of 8 retrievals were measured using contacting profilometry Taylor Hobson Talysurf. The parameters for the oval patella retrievals are tabulated in Table 7-8. Retrievals A and F had highest and lowest values of R_a, R_{sk}, R_p and R_v respectively. The mean±95%CL of average, skew, peak and valley roughness factors for the 8 retrievals were 1.19±0.83μm, -0.24±0.55, 2.73±1.91μm and 2.88±1.90μm respectively.

Table 7-8 Table of average, skew, peak and valley roughness parameters.

Specimen	Average roughness (R_a) μm	Skew roughness (R_{sk})	Peak roughness (R_p) μm	Valley roughness (R_v) μm
A	3.06	0.77	6.63	7.11
B	0.56	-0.92	1.34	1.63
C	0.62	-0.90	1.50	1.75
D	0.79	0.59	1.85	1.76
E	2.37	0.15	5.97	5.59
F	0.41	-0.45	0.92	0.97
G	0.44	-0.75	0.96	1.10
H	1.26	-0.38	2.67	3.14
Mean±95% CL	1.19±0.83	-0.24±0.55	2.73±1.91	2.88±1.90

The roughness of *in vitro* oval dome patella cannot be compared with the surface parameters tabulated in Table 7-8 as the retrievals were retrieved through range in years (2.1 to 7.2 years). The oval dome patella was run in the simulator for 3MC. The roughness parameters of retrieval specimens (A, B, C and H) were compared to oval dome *in vitro* test specimens with student t-test for significance as shown in Table 7-9. There were no significance difference found between the R_a, R_{sk}, R_p and R_v values of retrievals as compared to *in vitro* specimens.

Table7-9: Table of average, skew, peak and valley roughness parameters of specimen (A, B, C and H) in mean±95% confidence limit and significance p test.

Type	Retrievals	*In vitro specimen*	P test
Average roughness (R_a) µm	1.38±1.83	0.83±0.15	0.27
Skew roughness (R_{sk})	-0.36±1.26	0.58±0.81	0.10
Peak roughness (R_p) µm	3.03±3.93	1.99±0.49	0.33
Valley roughness (R_v) µm	3.41±4.07	2.10±0.66	0.25

7.3.3 Round Dome Patella Retrievals

7.3.3.1 Geometric volumetric measurements

The volumetric analysis was performed using CMM analysis as shown in Figure 7-9. Due to the shape of the patella retrievals used in the CMM analysis currently applicable to spherical shape, one out of two retrievals was analysed. The second retrieval (J) could not be analysed using CMM as it was a flat round retrieval. The software was based on spherical shape geometry. Anything other than spherical shape could not be analysed. The volume difference using three repeated measurements was positive difference i.e. volume gain 176.00±83.44mm^3. As there was no volume loss, the wear rate could not be determined. The *in vitro* test specimens did not go through adhesive wear. Hence, a comparison with the retrieval volumetric wear could not be generated.

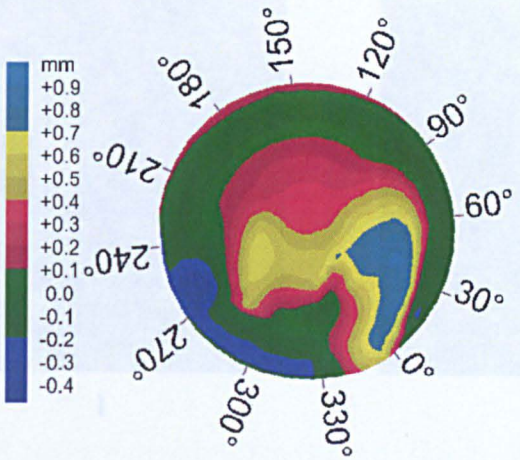

Figure 7-9 CMM analysis for volumetric wear determination (round retrieval I).

7.3.3.2 Quantification of surface analysis

Visual inspection

Scratches

Few scratches were found in retrieval J as shown by the yellow solid lines in Figure 7-10 (J).

Wear characteristics

The various types of wear regimes found in the selected round patella retrievals were scratching, burnishing, pitting, delamination and surface deformation as shown in Figure 7-10 (J). Adhesive wear was found in retrieval I.

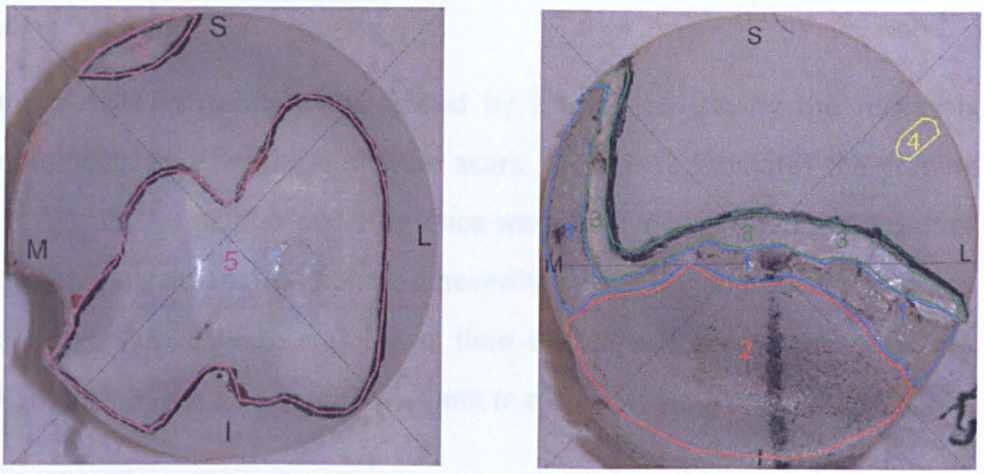

I J

Figure 7-10 Wear characteristics for retrievals (Specimen I to J). 1: delamination/ pitting wear, 2: burnishing, 3: deformation, 4: scratching, 5: adhesive wear.

The wear characteristics showed a number of wear mechanism occurring in the 2 retrievals analysed. The following wear phenomena were found to dominate as shown in Table 7-10. The frequency of damage modes were obtained as a percentage of two retrievals dataset analysed. Pitting wear was dominant in the two round patella retrievals.

Table 7-10 Frequency of patella damage with respect to the 2 retrievals dataset and *in vitro* test specimens analysed

	Present Study (n=2)	***In vitro* test (n=5)**
Burnishing	50%	100%
Deformation	50%	100%
Scratches	50%	100%
Delamination	50%	0%
Pitting	100%	100%
Adhesive	50%	0%

Wear grading

Round patella retrievals were graded by 2 users to classify the retrievals based on intensity, area and type of wear scars. Table 7-11 tabulates the grading for the 2 retrievals. No significance difference was observed between the observer who graded the specimens (p=0.6). The severity of the damage in round dome patella retrievals (19.75±43.6) was lower than the experimental test specimens (34.8±5.9). However, the 95% confidence limit in retrievals was very high.

Table 7-11 Grading of round patella based on Hood's grading (1983)

Retrievals	Grade {mean (n=2) }
I	23.5
J	16
Average	19.75±47.7

Wear scar area and location of centroid

The wear area on the patella was spread from medial to lateral with bias towards the inferior side as shown in Figure 7-11 similar to the oval dome patella retrievals. A mean wear scar areas of 598.11±51.43mm^2 (mean n=2 ± 95% CFL) was found for the round patella retrievals. In total among 2 retrievals, the wear scar area covered 54.60±4.11% of the total surface area of the retrievals. Similar spread of the worn area was mostly towards inferior region with 28.27±26.71mm^2 in superior, 224.86±564.00mm^2 in inferior, 154.57±148.86mm^2 in lateral and 159.47±642.36mm^2 in medial part of the patella retrievals as shown in Table 7-12.

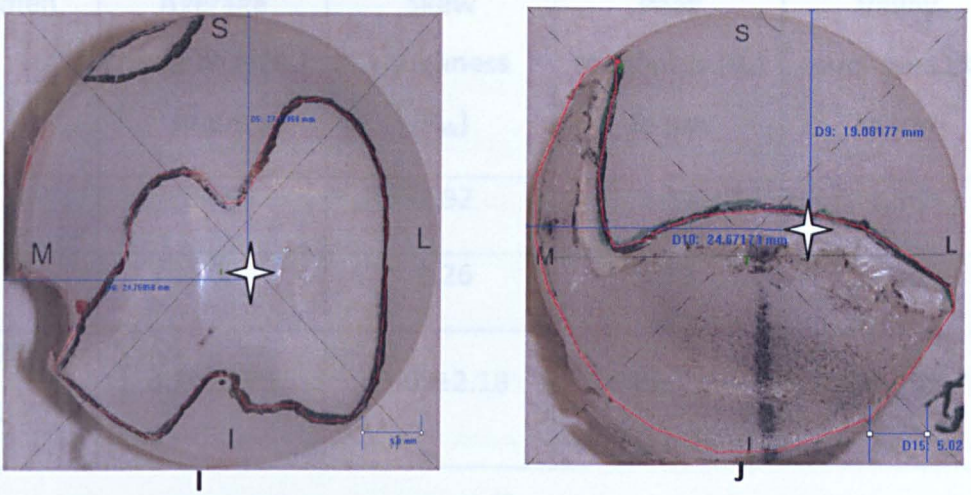

Figure 7-11 Wear scar area and location of centroid (shown in star) for oval patella retrievals (Specimen I and J).

Table 7-12 Wear scar area and distribution of wear scar over the four quadrants

Specimen	Wear area (mm^2)	Wear area (%)	Superior area (mm^2)	Inferior area (mm^2)	Lateral area (mm^2)	Medial area (mm^2)
I	561.18	52.40	48.86	180.41	166.46	101.05
J	635.03	56.80	7.69	269.30	142.69	217.89
Mean	598.91	54.60	28.27	224.86	154.57	159.47
±95% CL	±469.23	±27.90	±261.57	±564.73mm^2	±150.99	±742.30

Surface roughness parameters

The surface roughness parameters of 2 retrievals were measured using contacting profilometry (Talysurf, Taylor Hobson). The parameters for the oval patella retrievals are tabulated in Table 7-13. As the roughness parameters varied with cycle count, the parameters of the *in vitro* test specimens cannot be compared with the retrievals.

Table 7-13 Table of average, skew, peak and valley roughness parameters.

Specimen	Average roughness (R_a) in µm	Skew roughness (R_{sk})	Peak roughness (R_p) in µm	Valley roughness (R_v) in µm
I	0.49	-2.92	1.13	1.36
J	1.08	-3.26	1.73	3.40
Mean±95% CL	0.79±3.75	-3.09±2.18	1.43±3.77	2.38±12.97

7.4 Discussion

The selection for the location of the wear scar was based on experimental simulations and nature of wear scar observed in literature (Hood et al. 1983; Schwartz *et al.* 2002; Ellison *et al.* 2010). Hood *et al.* (1983) found wear patterns distributed along medial lateral quadrants. Schwartz et al. (2002) and Lindsay et al. (2010) suggested the 'bow tie' shape wear patterns in their studies. These types of wear pattern were observed in experimental simulations (round and oval dome patellae) and retrievals C, F and J in the current study.

Oval dome retrieval volume varied from 1.19 to 65.46mm^3 and time *in situ* varied from 2.1 to 13.1 years. No linear correlation between the two data set was observed (R^2=-0.311). Out of 8, only 6 of the retrievals could be analysed for wear rate per year due to absence of data. The average wear rate per year was 9.09±9.39 mm^3/year (average n=7±95%CFL). The wear rate obtained from CMM analysis of *in vitro* oval dome specimens was 10.92±5.43mm^3/MC. No significant difference was observed between the two set of data. The volumetric wear for retrievals ranged from 1.08 to 26.76mm^3/year. The maximum value shows the clinical significance for concern over production of wear debris leading to osteolysis. In round dome retrievals, the data was not sufficient enough to calculate the wear rate. One of the retrievals selected underwent adhesive wear

and the other retrieval could not be analysed in CMM. This was the first attempt to compare two types of wear specimen with retrievals.

Various regimes of wear were observed in oval dome retrievals. The total damage consisted of delamination, burnishing, deformation, scratching and pitting. Burnishing wear was the highest damage mode (80%) among all the 8 oval dome retrieval patellar buttons. The in vitro wear characteristics involved similar regimes of wear. However, the frequency of the damage mode was 100% (Table 7-4). Previous literature (Hood et *al.* 1983; Schwartz *et al.* 2002; Ellison *et al.* 2010) also reported the most common damage mode was burnishing. Data regarding adhesive wear formation was not included in the other two studies (Hood *et al.* 1983; Schwartz *et al.* 2002). In round dome retrievals, apart from earlier mentioned wear damages, adhesive wear was observed in one specimen. The *in vitro* specimen did not show any adhesive damage. This was due to the improvement in manufacturing process and packaging. The *in vitro* specimen showed 100% of pitting wear similar to the damage mode in patellar buttons. As the number of components was too small, a comparison between the similarity in damage modes of the retrievals and in vitro specimens could not be made. The other damage modes present in the retrievals were observed to be less than 50%.

The wear grading of oval dome patella buttons compared to the oval dome retrievals specimen showed no significance difference. The wear grading for retrieval was 12.25 compared to test specimen of 30. For round dome, the grade from experimental simulation was 34.6 and retrievals were 19.75. The in vitro specimen was found to have higher grade compared to retrievals. However, the damage was moderate. As there was no dependency of grading with cycle count, the Hood's grading system has limitations.

The centroid was located in the inferior of the *in vitro* round and oval dome patella (Figure 7-12). The position was similar to the location of centroid in retrievals (oval dome B, C, E, F, H and round dome I). As compared to Schwartz et al (2002), the location of the centroid was in the centre of the quadrants.

Wear scar area spread over quadrants was found to be in the inferior region of the patella in medial lateral quadrant with bias towards the inferior side similar

to experimental. However, student t-test show significance difference between superior and inferior quadrant and no difference between medial and lateral quadrant at 5% level in retrievals. The highest area was covered in lateral side similar to investigation by Lindsey and co-authors (2010). The wear scar was spread in medial lateral quadrant as suggested by Hood and co authors (1981, 1983 and 2002) and the shape was found to be similar to the bow tie as suggested by Schwartz, *et al.* (2002). A comparison between the wear area of retrievals, experimental simulations, and investigation by Schwartz and co authors (2002) are presented in Figure 7-12.

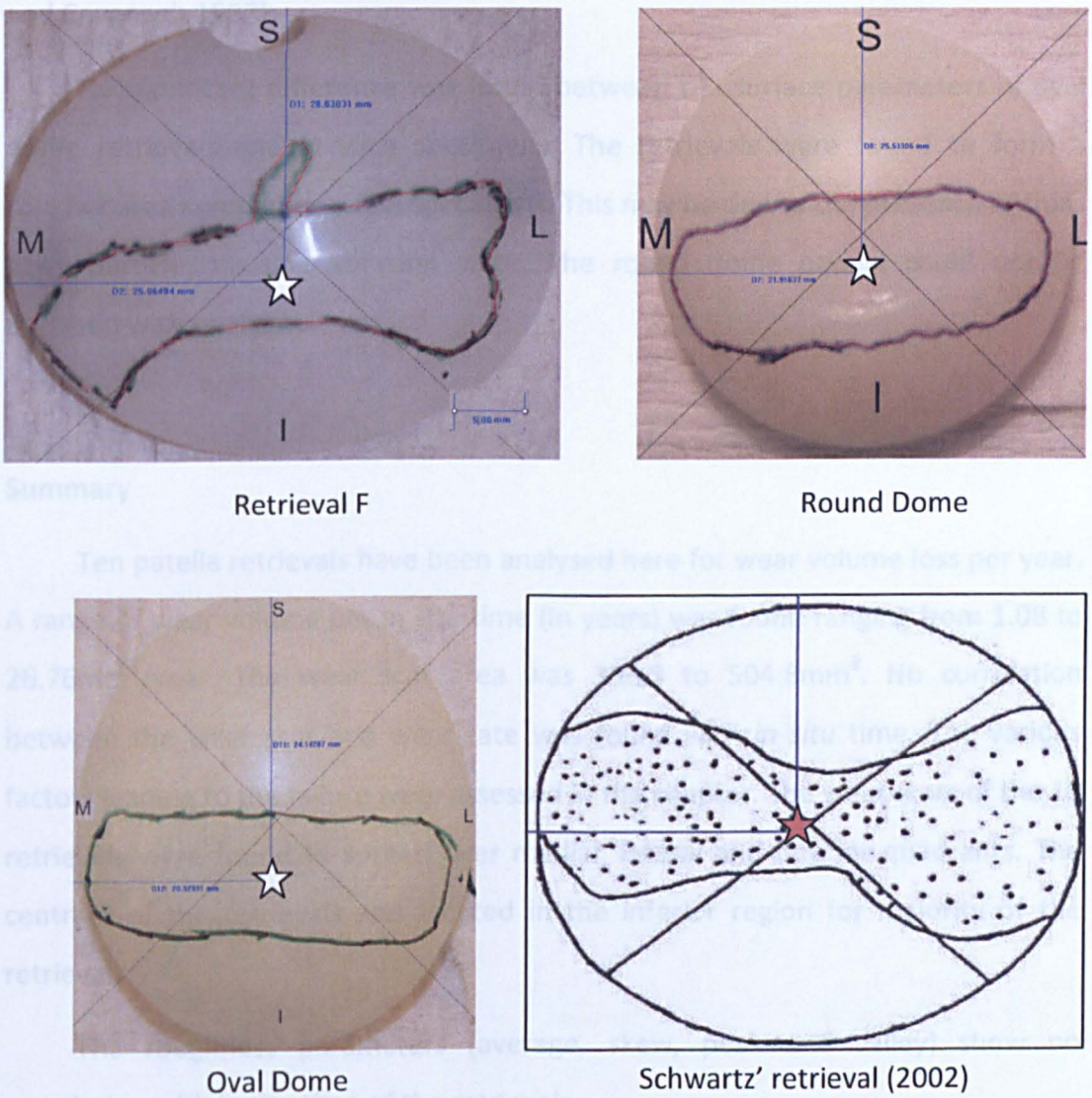

Retrieval F

Round Dome

Oval Dome

Schwartz' retrieval (2002)

Figure 7-12 Comparison of wear scar area and location of centroid (in star) between retrieval F, round dome and oval dome patella from experimental simulations and Schwartz's retrieval analysis (2002).

The wear scar area of oval dome retrievals and test specimens were 279.78±50 mm^2 and 303.1±45 mm^2 respectively. In percentage 27.5% and 31.0% of area was covered with wear scar for oval dome retrievals and experimental specimens respectively. The wear scar area of round dome retrievals was 598.91±52mm^2 and 54.6% of the total surface area. Similar, wear scar area of retrievals (400.07±87mm^2) investigated by Schwartz and co authors (2002) were observed. However, no significant difference was found between the two sets of wear scar areas in retrievals. The variation of wear scar reflects among different studies suggest the movement of patella as predicted in natural knees (Lafortune and Cavanagh 1987).

No significant difference was found between the surface parameters of oval dome retrievals and *in vitro* specimens. The retrievals were found to form a rougher area compared to test specimens. This may be due to the presence of third body particles causing abrasion wear. The round dome patella could not be assessed with retrievals.

Summary

Ten patella retrievals have been analysed here for wear volume loss per year. A range of wear volume per in situ time (in years) was found ranging from 1.08 to 26.76mm^3/year. The wear scar area was 306.8 to 504.8mm^2. No correlation between the wear scar and wear rate was found with *in situ* time. The various factors leading to the failure were assessed in the chapter. The wear scars of the 10 retrievals were found to spread over medial, lateral and inferior quadrants. The centroid of the retrievals was located in the inferior region for majority of the retrievals.

The roughness parameters (average, skew, peak and valley) show no correlation with in situ time of the retrievals.

90% of the retrievals show variation of wear mechanism like burnishing (80%), deformation (50%), scratching (30%), delamination (30%) and pitting wear (10%). Adhesive wear was found in one retrieval out of the ten retrievals assessed.

Similar to experimental simulations, the medial lateral displacement, tilt, weight, implant type were categorised as the reason for failure in most of the retrieval. However, the flexion extension rotation, ligament and muscle forces can lead to similar failures but with no data present are difficult to assess.

Chapter 8: Overall Discussion and Conclusion

8.1 Overall Discussion

A total knee replacement (TKR) remains the final treatment for patients suffering with knee arthritis providing relief from the pain and improvement in function. Despite the fact that the common reason for revisions of TKR is due to problems regarding patella femoral joint (Berger *et al.* 1998; Fehring *et al.* 2000; Sharkey *et al.* 2002; Amis *et al.* 2005; Stiehl *et al.* 2005; Berti *et al.* 2006; Ma *et al.* 2007; Kessler *et al.* 2008; Anglin *et al.* 2009), the use of the patella during TKA varies from country to country with popularity in USA (90%), Denmark (76%), Australia (43%), England and Wales (33%), Sweden (14%) and Norway (11%) (Robertsson *et al.* 2010, Clements *et al.* 2010 and National Joint Registry for England and Wales 2009, 2010). Limited research has been performed in the past for determination of volumetric wear in the patella femoral joint (Hsu and Walker 1989; Korduba *et al.* 2008; Ellison *et al.* 2008; Vanbiervliet *et al.* 2011). However, the degrees of freedom controlled were limited to five.

The aim of this study was to develop and evaluate a six axis patella femoral joint knee simulator and study the influence of kinematics (displacement and rotation) and change in patella button shapes on the wear rate of the patella femoral joint. The other axes were superior inferior displacement, axial load, flexion extension and medial lateral rotations

The six axis patella femoral joint simulator was developed by modifying the existing Leeds/ProSim knee simulator. The initial stages included development of the new fixtures in computational Model (MSc.Software Adams/VIEW). This helped in saving initial cost and man hours required to develop and manufacture the simulator fixtures. The computational simulator was used to investigate the contact and kinematics in patella femoral joint. Good correlation between the experimental and computational model was observed. The validation of kinematics from computational modelling with experimental results was the first step in creating a

wear model. The kinematics of the patella femoral joint was investigated at two varied radius of rotation. At constrained medial lateral (ML) displacement, the tilt was similar in trend for both radius of rotation. However, constant lateral tilt was recorded when the radius of rotation was higher (R_2) with uncontrolled ML displacement. ML and anterior posterior (AP) displacements had highest displacement at highest flexion.

ML displacement and rotation induced cross shear as stated in earlier investigations (Johnson 1987; Saikko and Calonius, 2003; Fisher *et al.* 2005; Kang *et al.* 2008), which increased wear rate. In an earlier investigation, the medial lateral displacement was limited to 1mm (Ellison *et al. 2008*). Other investigators have reported ML displacement to be higher than 1mm (Lafortune and Cavanagh 1987; Chew *et al.* 1997; Barink *et al.* 2007 and Belvedere *et al.* 2007). Galvin *et al.* 2009 have stated that the wear rate decreased with decrease in wear area. As the oval dome patella had lower bone coverage (Baldwin and Ken House 2005) hence, lower articulating area and thus the surface wear was hypothesised. Hence, the current study investigated

- The effect of higher ML rotation (<4°) and uncontrolled ML displacement which investigates the effect of higher kinematics.
- The ML rotation was reduced to <1° and ML displacement uncontrolled also known as the physiological condition,
- The effect of ML displacement by controlling the displacement to 1.6mm and low ML rotation (<1°) which investigates lower kinematics.
- The change in design of patellar buttons at low ML rotation (<1°) and uncontrolled ML displacement on wear rate at the physiological condition.

The wear rate was 12.3±2.8mm^3/million cycles at highest ML rotation (<4°) and uncontrolled ML displacement. The wear rate significantly (p=0.05) decreased to 8.6±3.4mm^3/million cycles when the ML rotation was decreased by four fold. The reduction of ML rotation caused reduction in cross shear leading to reduction in wear rate. At higher ML rotation, higher strain softening occurred in the

direction perpendicular to the direction of molecular orientation. This led to higher wear at the articulating surface (Fisher *et al.* 2001; McEwen *et al.* 2005). A reduction of ML displacement from uncontrolled to constrained (<1.6mm) led to no significant change from 8.6±3.4mm^3/MC to 7.9±2.5mm^3/MC in the wear rate. When the patellar button design was changed from round to oval at low ML rotation (<1^o) and uncontrolled ML displacement, the wear rate decreased non significantly by 2.5mm^3/MC from 8.6±3.4mm^3/MC to 6.3±3.9mm^3/MC. The decrease was as hypothesised by Galvin *et al.* (2009); the wear scar area was lower in oval dome (31.2%) design compared to the round dome patellae design (39.9%). The wear rates of the PFJ were generally lower compared to the tibia femoral joint (5-40mm^3/MC) (Barnett *et al.* 2002; McEwen *et a*l. 2005; Affatato *et al.* 2008; Wang *et al.* 2008).

A good correlation between tilt and wear volume was observed throughout the test with the R squared value more than 0.8. The increase in tilt resulted in an increase in volume loss. This was similar to the observation by Jennings and co-authors (Jennings *et al.* 2007). The lift off of the patella specimen with the femoral component caused increased cross shear. The increase in cross shear led to increase volume loss (Fisher *et al.* 2001; McEwen *et al.* 2005).

The wear rate of *in vitro* test specimens was compared to retrievals for clinical relevance. Gravimetric analysis is the standard and validated method of measuring wear (Affatato et al. 2002; D'Lima et al. 2003). However problems regarding fluid intake, backside wear, mass of fixturing attached to specimens and absence of pre-wear data in retrievals (Bills et al. 2005; Bills et al. 2007) led to development of new methods of measuring volumetric wear. Coordinate measuring machine (CMM), Pycnomatic ATC (Pycnometer) and Micro computed tomography (MicroCT) have been recently used for measuring volumetric wear (Keng 1970; Raimondi *et al.* 2000; Bills *et al.* 2007; Vicars *et al.* 2009). However, none have been used for measuring patella volumetric wear. These methods were tested for accuracy and repeatability and compared with gravimetric for measuring three stages of artificially removed material (5, 10 and 15mm^3) from a polyethylene specimen. The Pycnometer failed to measure the volume accurately as the specimen covered only 10% of the chamber volume. It was recommended that 66-

75% of the chamber should be filled with the specimen for increased accuracy in determining the volume of specimen (Pycnomatic and Pycnomatic ATC Instruction Manual2007; Viana *et al.* 2002). CMM surface fit (±0.13mm^3) and MicroCT reference methods (±15.94mm^3) showed repeatability in measurement of volume. However, the accuracy of MicroCT reference method was higher when the volume loss was higher. The CMM surface fit method was identified as the preferred method to measure the volumetric wear of retrievals.

The wear rate of the oval dome patella retrievals (n=8) from CMM surface fit analysis was 9.09±10.9mm^3/year was not significantly different (p=0.74) from the wear rate of *in vitro* test (n=5) specimens (10.92±5.43mm^3/MC). The wear scar in the test specimens were similar to shape ('bow tie') of the retrievals and to the past studies (Schwartz et al. 2002). The retrievals and test specimens were compared based on the severity of damage using Hood's grading (Hood *et al.* 1983). The severity of the damage in test specimens (oval dome and round dome were 30 and 39 respectively) was found to be higher than retrievals (oval dome and round dome were 12.3 and 19.7 respectively).

There was a large variation in wear rate between current (6.28mm^3/MC to 12.30mm^3/MC) and previously compared studies (3.13mm^3/MC). The higher wear rate in the current test was due to an increase in ML displacement which was restricted to 1mm in the earlier test (Ellison *et al.* 2008). The other possible reasons may be the use of different simulators and radius of rotation of patella over femoral articulating surface. The results suggest that the introduction of a patella will lead to significant increased in clinical wear rates of total knee replacement (18-64% of total knee replacement wear). This increase in wear rate can lead to increases in wear debris which has been linked to osteolysis and aseptic loosening of joint replacements (Ingham and Fisher 2000). Hence, the inclusion of the patella femoral joint in wear simulation is important. However, size distribution of the particles as well as from volumetric wear is important (Fisher *et al.* 2001; 2004)

8.2 Conclusion

A 6-axis PFJ simulator was developed to investigate the influence of kinematics and patellar button design on wear rate. The use of computational model was found to be a valuable tool in predicting patella kinematics. The model was the first step in modifying the existing knee simulator as patella femoral joint simulator. Good agreement in kinematics from the model and experimental results were observed. The kinematics of the patella femoral joint was investigated at varied radii of rotation. At constrained medial lateral (ML) displacement; the tilt was similar in trend for both radius of rotation. However, constant lateral tilt was recorded when the radius of rotation was higher (R_2) with uncontrolled ML displacement. ML and anterior posterior (AP) displacements had highest displacement at highest flexion. At highest flexion, there was higher tilt, AP and ML displacements in unworn compared to worn patella specimen through both the computational and experimental model. This was due to presence of conformity between worn patella and femur which led to lower kinematics values.

Gravimetric assessment remains the most accurate and quickest way to determine wear volume. CMM can be used for retrievals when no pre-wear data exists and offers additional information on the geometry, penetration depth and deformation.

The influence of ML rotation was observed in the wear rate. The wear rate increased by 42% (12.3mm^3/MC) when ML rotation was increased by four folds and ML displacement was uncontrolled (8.63mm^3/MC). However, controlling the ML displacement (<1.6mm) from uncontrolled state did not show any significant change in wear rate (7.93mm^3/MC). Sliding distance was less effective in generating wear as compared to change in ML rotation. The change in design of the patellar button from round to oval dome at low ML rotation (<1°) and uncontrolled ML displacement led to non significant decrease in wear rate from 8.63 to 6.28mm^3/MC. As the area was low, the wear rate was low. This is the reason for higher sale of oval dome in the market.

The round dome and oval dome wear scars increased to 506mm^2 and 306mm^2 respectively at the end of 2MC and remained constant throughout the test.

CMM analysis of the oval dome test specimen and retrievals showed no significant difference in wear rate (10.92mm^3/MC and 9.09mm^3/year). The wear scar was situated in the inferior of the patella similar to retrievals and earlier investigation by Hood *et al.* (1983) and Schwartz *et al.* (2002). This shows that the positions of wear scar are similar to retrievals showing good correlation of retrievals and *in vitro* wear specimens. The damage based on Hood's method of grading (Hood et al. 1983) in the test specimens (round dome 39 and oval dome 30) were higher compared to respective retrievals (round 19.7 and oval 12.3).

Adhesive wear were absent in the test specimen due to presence of an improved manufacturing method in UHMWPE polyethylene. Other wear mechanisms present in both the retrievals and test specimens were abrasion, pitting, deformation, scratching and burnishing. However, the frequency of the wear damage was different for both cases.

8.3 Future work

The study considered investigation of the wear rate with change in kinematics and shape of patellar buttons. Further investigations and efforts in understanding should focus on the following

- Investigation of different types of TKR.
- Investigation of wear at higher rotation and displacements.
- A constant ligament load was considered to act as the ligament force opposing the medial lateral displacements. Springs should be incorporated with a coefficient equivalent to ligament tension and the variation of wear rate should be investigated.
- A computational wear model based on the kinematics model validated in the current study should be developed.
- Wear debris analysis should be performed to compare the size distribution of the wear debris and compare with earlier investigations.

References

Abbas, G., C. Diss (2011). "Patellar tracking during the gait cycle." Journal of orthopaedic surgery (Hong Kong) **19**(3): 288-291.

Affatato, S., L. Cristofolini, W. Leardini, P. Erani, M. Zavalloni, D. Tigani, M. Viceconti (2008). "A New Method of In Vitro Wear Assessment of the UHMWPE Tibial Insert in Total Knee Replacement." Artificial Organs **32**(12): 942-948.

Ahmed, A. M., D. L. Burke, A. Yu (1983). "Invitro measurement of static pressure distribution in synovial joints .2. Retropatellar surface." Journal of Biomechanical Engineering-Transactions of the Asme **105**(3): 226-234.

Ahmed, A. M., N. A. Duncan and M. Tanzer (1999). "In vitro measurement of the tracking pattern of the human patella." J Biomech Eng **121**(2): 222-8.

Amis, A. and F. Farahmand (1996). "Biomechanics of the knee extensor mechanism." The Knee **3**(1-2): 73-81.

Amis, A. A., W. Senavongse, P. Darcy (2005). "Biomechanics of patellofemoral joint prostheses." Clinical Orthopaedics and Related Research (436): 20-29.

Anglin, C., J. M. Brimacombe, D. R. Wilson, B.A. Masri, N.V. Greidanus, J. tonetti, A. J. Hodgson (2009). "Biomechanical consequences of patellar component medialization in total knee arthroplasty." Journal of Arthroplasty **25**(5): 793-802.

Archard, J. F. (1953). "Contact and Rubbing of Flat Surfaces." Journal of Applied Physics **24**(8): 981-988.

Arthritis Research Campaign OA. "Osteoarthritis of the Knee " Retrieved 16th June, 2008, from http://www.arc.org.uk/arthinfo/patpubs/6027/6027.asp.

Arthritis-NHS choices. "Arthritis" Retrieved 16th January, 2011, from http://www.nhs.uk/Conditions/Arthritis/Pages/Introduction.aspx

ASTM-F75-01 (2001). "Standard Specification for Cobalt-28 Chromium-6 Molybdenum Alloy Castings and Casting Alloy for Surgical Implants (UNS R30075)."

Baldwin, J. L. and C. K. House (2005). "Anatomic dimensions of the patella measured during total knee arthroplasty." Journal of Arthroplasty **20**(2): 250-257.

Baldwin, M. A., C. Clary, L. P. Maletsky, P. J. Rullkoetter (2009). "Verification of predicted specimen-specific natural and implanted patellofemoral kinematics during simulated deep knee bend." Journal of Biomechanics **42**(14): 2341-2348.

Barbour, P. S. M., M. H. Stone, J. Fisher (2000). "A hip joint simulator study using new and physiologically scratched femoral heads with ultra high molecular weight polyethylene acetabular cups." Proceedings Instituition Mechanical Engineers. Part H: Journal of Engineering in Medicine **214**: 569-576.

Barink, M., H. Meijerink, N. Verdonschot, A. vanKampen, M. D. Malefit (2007). "Asymmetrical total knee arthroplasty does not improve patella tracking: a study without patella resurfacing." Knee Surgery Sports Traumatology Arthroscopy **15**(2): 184-191.

Barnett, P. I., J. Fisher, D. D. Auger, M. H. Stone, E. Ingham (2001). "Comparison of wear in a total knee replacement under different kinematic conditions." J Mater Sci Mater Med **12**(10-12): 1039-42.

Barnett, P. I. (2002). Wear and Wear Debris in Fixed Bearing Knee Prostheses. School of Mechanical Engineering. Leeds, The University of Leeds.

Bayer, R. G. (2002). "Wear Analysis for Engineers" HNB Publisher. ISBN Number: 0-9664286-5-X.

Bell, C. J., P. S. Walker (1998). "Effect of oxidation on delamination of ultrahigh-molecular-weight polyethylene tibial components." J Arthroplasty **13**(3): 280-90.

Belvedere, C., F. Catani, A. Ensini, J. L. M. de la Barrera and A. Leardini (2007). "Patellar tracking during total knee arthroplasty: an in vitro feasibility study." Knee Surgery Sports Traumatology Arthroscopy **15**(8): 985-993.

Berger, R. A., L. S. Crossett, J. J. Jacobs, H. E. Rubash (1998). "Malrotation causing patellofemoral complications after total knee arthroplasty." Clinical Orthopaedic Related Research **356**: 144-153.

Berti, L., M. G. Benedetti, A. Ensini, F. Catani, S. Giannini (2006). "Clinical and biomechanical assessment of patella resurfacing in total knee arthroplasty." Clinical Biomechanics **21**(6): 610-616.

Besong, A. A., J. L. Hailey, E. Ingham, M. Stone, B. M. Wroblewski, J. Fisher (1997). "A study of the combined effects of shelf ageing following irradiation in air and counterface roughness on the wear of UHMWPE." Biomed Mater Eng **7**(1): 59-65.

Bills, P., L. Blunt, X. Jiang (2007). "Development of a technique for accurately determining clinical wear in explanted total hip replacements." Wear **263**: 1133-1137.

Bowden, A. E., S. M. Kurtz, A. A. Edidin (2005). "Validation of a micro-CT technique for measuring volumetric wear in retrieved acetabular liners." Journal of Biomedical Materials Research Part B-Applied Biomaterials **75B**(1): 205-209.

Brockett, C. L., L. M. Jennings, J. Fisher "The wear of fixed and mobile bearing unicompartmental knee replacements." Proceedings of the Institution of Mechanical Engineers Part H-Journal of Engineering in Medicine **225**(H5): 511-519.

Bruckner, P., and K. Khan (2002). "Anterior knee Pain" Clinical Sports Medicine 2nd Edition. New York, N.Y. : McGraw-Hill, 464-493.

Buechel, F. F.,Pappas, M. J and D'Alessio, (2001). "Twenty-year evaluation of meniscal bearing and rotating platform knee replacements." Clinical Orthopaedics and Related Research 388:41-50.

Burroughs, B. R., H. E. Rubash, D. Estok, M. jasty, J. Krevolin, O. K. Muratoglu (2006). "Comparison of conventional and highly crosslinked UHMWPE patellae evaluated by a new in vitro patellofemoral joint simulator." Journal of Biomedical Materials Research Part B-Applied Biomaterials **79B**(2): 268-274.

Cannon, A., M. Stolley, B. Wolf and A. Amendola (2008). "Patellofemoral resurfacing arthroplasty: Literature review and description of a novel technique." The Iowa Orthopaedic journal **28**.

Charnley, J., (1979). "Low friction Arthroplasty" Berlin: Springer-Verlag. ISBN Number: 3540088938.

Chew, J. T. H., N. J. Stewart, A. D. Hanssen, Z. P. Luo, J. A. Rand and K. N. An (1997). "Differences in patellar tracking and knee kinematics among three different total knee designs." Clinical Orthopaedics and Related Research: 87-98.

Childers, J. C. and S. C. Ellwood (1979). "Partial chondrectomy and subchondral bone drilling for chondromalacia." Clinical Orthopaedics and Related Research(144): 114-120.

Clements, W. J., L. Miller, S. L. Whitehouse, S.E. Graves, P. Ryan, R. W. Crawford (2010). "Early outcomes of patella resurfacing in total knee arthroplasty." Acta Orthopaedics **81**(1): 108-113.

Collier, J. P., J. L. McNamara, V. A. Surprenat, R. E. Jensen, H. P. Surprenant (1991). "All-polyethylene patellar components are not the answer." Clin Orthop(273): 198-203.

Crowninshield, R. D., A. G. Rosenberg, S. M. Sporer (2006). "Changing demographics of patients with total joint replacement." Clinical Orthopaedics and Related Research(443): 266-272.

DELRIN product and properties, 2000.

DePuy Manufacturing drawing (2009). DePuy International Ltd.

Ding, M., A. Odgaard, I. Hvid (1999). "Accuracy of cancellous bone volume fraction measured by micro-CT scanning." Journal of Biomechanics **32**(3): 323-326.

Dixit, S., J. P. Difiori, M. Burton, B. Mines (2007). "Management of Patellofemoral Pain Syndrome." American Family Physician **75**(2): 194-202.

Dowson, D. and B. Jobbins (1988). "Design and development of a versatile hip joint simulator and a preliminary assessment of wear and creep in Charnley total replacement hip joints." Engineering in medicine **17**(3): 111-7.

Duncan, R., G. Peat, E. Thomas, L. Wood, E. Hay, P. Croft (2009). "Does isolated patellofemoral osteoarthritis matter?" Osteoarthritis and cartilage **17**(9): 1151-1155.

D'Lima, D. D., P. C. Chen, M. A. Kester, C. W. Jr. Colwell (2003). "Impact of patellofemoral design on patellofemoral forces and polyethylene stresses." J Bone Joint Surg Am **85-A Suppl 4**: 85-93.

Eckhardt, R. (2002) EORS abstract. 12th annual meeting. Switzerland 11-13th February 2002

Engh, G. A., K. A. Dwyer, C. K. Hanes (1992). "Polyethylene wear of metal-backed tibial components in total and unicompartmental knee prostheses." Journal of Bone and Joint Surgery-British Volume **74**(1): 9-17.

Elfick, A. P., R. M. Hall, A. Unsworth, I. M. Pinder (1998). "Surface topography of retrieved PCA acetabular liners: proposal of a novel wear mechanism." Journal of Materials Science Letters **17**(13): 1085-1088.

Ellison, P. (2007). Investigation of Wear within the Patellofemoral Joint of Total Knee replacement. Leeds, University of Leeds: 221.

Ellison, P.,Barton, D. C.,Esler, C.,Shaw, D. L.,Stone, M. H. and Fisher, J. (2008). "In vitro simulation and quantification of wear within the patellofemoral joint replacement." Journal of Biomechanics. **41**(7):1407-1416.

Ellison, P., J. Fisher (2010). "Assessment of the damage in retrieved Patellar components" Journal of long-term effects of Medical Implants **20**(1): 57-72.

Endo, M. M., P. S. Barbour, D.C. Barton, J. Fisher, M. H. Stone (2001). "Comparative wear and wear debris under three different counterface conditions of crosslinked and non-crosslinked ultra high molecular weight polyethylene." Biomed Mater Eng **11**(1): 23-35.

Fajardo, R. J., T. M. Ryan, J. kappelman (2002). "Assessing the accuracy of high-resolution X-ray computed tomography of primate trabecular bone by comparisons with histological sections." American Journal of Physical Anthropology **118**(1): 1-10.

Fehring, T. K. (2000). "Rotational Malalignhmentof the femoral component in total knee arthroplasty." Clinical Orthopaedics and Related Research (380):72-79.

Fisher, J.,Dowson, D.,Hamdzah, H. and Lee, H. L. (1994). "The effect of sliding velocity on the friction and wear of UHMWPE for use in total artificial joints." Wear **175**(1-2):219-225.

Fisher, J., P. Firkins, E. A. Reeves, J. L. Hailey, G. H. Isaac (1995). "The influence of scratches to metallic counterfaces on the wear of ultra-high molecular weight polyethylene." Proc Inst Mech Eng [H] **209**(4): 263-4.

Fisher, J., E. A. Reeves, G. H. Isaac, K. A. Saum and W. M. Sanford (1997). "Comparison of the wear of aged and non aged UHMWPE sterilized by gamma

irradiation and by gas plasma." Journal of Materials Science: Materials in medicine **8**: 375-378.

Fisher, J., McEwen, H M J., Barnett, P.I., Bell, C J., Stewart, T D., Stone, M H. and Ingham, E. (2001). "Wear of polyethylene in artificial knee joints" Current Orthopaedics **15**(6):399-405.

Fisher, J., H. M. McEwen, J. L. Tipper, A. L. Galvin, J. Ingram, A. kamali, M. H. Stone, E. Ingham (2004). "Wear, debris, and biologic activity of cross-linked polyethylene in the knee: benefits and potential concerns." Clin Orthop Relat Res(428): 114-9.

Fisher, J., A. Galvin, J. Tipper, T. Stewart, M. Stone, E. Ingham (2005). "Comparison of the functional Biological activity and osteolytic potential of ceramic on ceramic and cross linked polyethylene bearings in the hip." 10th International BIOLOX Symposium.Br

Flitney, R. K., M. W. Brown (2007). "Seals and Sealing handbook" 5th Edition, Butterworth-Heinemann Publishing unit, Oxford MA, USA. ISBN Number: 9781856174619.

Fulkerson, J. P. (1997). "Arthroscopic Surgery, Part II: the Knee" Clinics in sports medicine **16**(1): 175 pages, W. B. Saunders publishing.

Fulkerson, J. P. (2005). "Alternatives to patellofemoral arthroplasty." Clinical Orthopaedics and Related Research(436): 76-80.

Galvin, A. L., L. Kang, I. Udopia, L. M. Jennings, H. M. J. McEwen, Z. M. Jin, J. Fisher (2009). "Effect of conformity and contact stress on wear in fixed-bearing total knee prostheses." Journal of Biomechanics **42**(12): 1898-1902.

Garth, J. W. P. (2001). "Clinical biomechanics of the patellofemoral joint." Operative Techniques in Sports Medicine **9**(3): 122-128.

Gill, H. S. and J. J. O'Connor (1995). "Calculation of human patellar loads during activity." Gait & Posture **3**(3): 177.

Godest, A. C.,Beaugonin, M.,Haug, E.,Taylor, M. and Gregson, P. J. (2002). "Simulation of a knee joint replacement during a gait cycle using explicit finite element analysis." Journal of Biomechanics **35**(2):267-275.

Goldblatt, J. P. and J. C. Richmond (2003). "Anatomy and biomechanics of the knee." Operative Techniques in Sports Medicine **11**(3): 172-186.

Gray, H. (1858). Anatomy - Descriptive and Surgical, John W Parker and Sons.

Hall, S. J., (1995) *Basic biomechanics / Susan J. Hall.*, St. Louis ; London :, Mosby.

Halloran, J.P., Easley, S.K., Petrella, A.J., Rullkoetter, P.J., (2005a). "Comparison of deformable and elastic foundation finite element simulations for predicting knee replacement mechanics." J. Biomech. Eng. **127**, 813–818.

Halloran, J. P., A. J. Petrella and P. J. Rullkoetter (2005b). "Explicit finite element modeling of total knee replacement mechanics." Journal of Biomechanics **38**(2): 323-31.

Halloran, J., Maletsky, L.P., Taylor, M., Clary, C., Petrella, A., Rullkoetter, P., (2006). "Validation of Predicted TKR Kinematic Variation with Implant Design." 52nd Annual Meeting of the Orthopaedic Research Society 31, 0588.

Halloran, J. P., C. W. Clary, L. P. Maletsky, M. taylor, A. J. Petrella, P. J. Rullkoetter (2010). "Verification of Predicted Knee Replacement Kinematics During Simulated Gait in the Kansas Knee Simulator." Journal of Biomechanical Engineering-Transactions of the Asme **132**(8).

Hara, T., E. Tanck, J. Homminga, R. Huiskes (2002). "The influence of microcomputed tomography threshold variations on the assessment of structural and mechanical trabecular bone properties." Bone **31**(1): 107-109.

Harsha, A. P. and T. J. Joyce "Challenges associated with using bovine serum in wear testing orthopaedic biopolymers." Proceedings of the Institution of Mechanical Engineers Part H-Journal of Engineering in Medicine **225**(H10): 948-958.

Haut, R. C. (1989). "Contact pressures in the patellofemoral joint during impact loading on the human flexed knee." Journal of Orthopaedic Research **7**(2): 272-280.

Heatley, F. W., P. R. Allen and J. H. Patrick (1986). "Tibial tubercle advancement for anterior knee pain - a temporary or permanent solution." Clinical Orthopaedics and Related Research (208): 215-224.

Heegaard, J., P. F. Leyvraz, et al. (1995). "The biomechanics of the human patella during passive knee flexion." Journal of Biomechanics **28**(11): 1265-1279.

Hendrickson, T. (2002). Massage for Orthopaedic conditions, Lippincott Williams and Wilkins.

Hollinghurst, D., J. Stoney, T. Ward, H. Pandit, D. Beard, D. W. Murray (2007). "In vivo sagittal plane kinematics of the Avon patellofemoral arthroplasty." Journal of Arthroplasty **22**(1): 117-123.

Hood, R. W., T. M. Wright, A. H. Burstein (1983). "Retrieval Analysis of Total Knee Prostheses - A Method and its Application to 48 Total Condylar Prostheses." Journal of Biomedical Materials Research **17**(5): 829-842.

Hooper, G. (2002). Patella Complications, LCS Mobile Bearing Knee Arthroplasty - 25 Years of Worldwide Experience, Springer Berlin: 260-263.

Hsu, H. P. and P. S. Walker (1989). "Wear and deformation of patellar components in total knee arthroplasty." Clin Orthop(246): 260-5.

Huang, C. H., J. J. Liau, F. Y. Ho, C. Y. Lin, T. H. Young, C. K. Cheng (2005). "Polyethylene failure of the patellar component in New Jersey low-contact stress total knee arthroplasties." J Arthroplasty **20**(2): 202-8.

Huberti, H. H. and W. C. Hayes (1984). "Patellofemoral contact pressures - The influence of Q-angle and tendofemoral contact." Journal of Bone and Joint Surgery-American Volume **66A**(5): 715-724.

Huberti, H. H. and W. C. Hayes (1988). "Contact pressures in chondromalacia patellae and the effects of capsular reconstructive procedures." Journal of Orthopaedic Research **6**(4): 499-508.

Hunter, D. J., T. D. Spector (2003). "The role of bone metabolism in osteoarthritis" Current rheumatology reports **5**(1): 15-19.

Ingham, E. and J. Fisher (2000). "Biological reactions to wear debris in total joint replacement." Proc Inst Mech Eng [H] **214(H1)**: 21-37.

ISO:14242-3 (2009). "Implants for surgery - Wear of total hip-joint prostheses - Part 3."

ISO:14243-2 (2009). "Implants for surgery - Wear of total knee joint prostheses - Part 2: Methods of measurement."

ISO:4287 (1997). " Geometrical Product Specifications (GPS) -- Surface texture: Profile method -- Terms, definitions and surface texture parameters."

ISO:7207-2 (2011). "Implants for surgery: Components for partial and total knee joint prostheses. Part 2: Articulating surfaces made of metal, ceramic and plastics materials."

John, K. S. "The Effect of Serum Protein Concentration on Wear Rates in a Hip Simulator." Journal of Biomaterials Applications **25**(2): 145-159.

Johnson, K. L. (1985). Contact Mechanics, Cambridge University Press.

Jennings, L. M., C. J. Bell, E. Ingham, R. D. Komistek, M. H. Stone, J. Fisher(2007). "The influence of femoral condylar lift-off on the wear of artificial knee joints." Proceedings of the Institution of Mechanical Engineers Part H-Journal of Engineering in Medicine **221**(H3): 305-314.

Kang, L., A. L. Galvin, Z. M. Jin, J. Fisher (2006). "A simple fully integrated contact-coupled wear prediction for ultra-high molecular weight polyethylene hip implants." Proceedings of the Institution of Mechanical Engineers Part H-Journal of Engineering in Medicine **220**(H1): 33-46.

Kang, L., A. L. Galvin, T. D. Brown, Z. M. Jin, J. Fisher (2008). "Quantification of the effect of cross-shear on the wear of conventional and highly cross-linked UHMWPE." Journal of Biomechanics **41**(2): 340-346.

Karlsson, J., L. Sward and O. Lansinger (1992). "Bad results after anterior advancement of the tibial tubercle for patellofemoral pain syndrome." Archives of Orthopaedic and Trauma Surgery **111**(4): 195-197.

Kaufer, H. (1979). "Patellar biomechanics." Clin Orthop(144): 51-4.

Kerckhofs, G., J. Schrooten, T. Van Cleynenbreugel, S. V. Lomov, M. Wevers (2008). "Validation of x-ray microfocus computed tomography as an imaging tool for porous structures." Review of Scientific Instruments **79**(1).

Keng, E. Y. H. (1970). "Air and Helium Pycnometer." Powder Technology **3**(3): 179-185.

Kessler, O., S. Patil, C.W. Colwell, D.D. D'Lima (2008). "The effect of femoral component and malrotation on patellar biomechanics." Journal of Biomechanics **41**(16): 3332-3339.

Knight, L. A., S. Pal, et al. (2007). "Comparison of long-term numerical and experimental total knee replacement wear during simulated gait loading." Journal of Biomechanics **40**(7): 1550-1558.

Koh, T. J., M. D. Grabiner, R. J. Deswart (1992). "Invivo tracking of the human patella." Journal of Biomechanics **25**(6): 637-&.

Komistek, R. D., J. B. Stiehl, D. A. Dennis, R. D. Paxson, R. W. Soutas-Little (1997). "Mathematical model of the lower extremity joint reaction forces using Kane's method of dynamics." Journal of Biomechanics **31**(2): 185-189.

Komistek, R. D., D. A. Dennis, J. A. Mabe and S. A. Walker (2000). "An in vivo determination of patellofemoral contact positions." Clinical Biomechanics **15**(1): 29-36.

Kooijman, H. J., A. Driessen, J. R. van Horn (2003). "Long-term results of patellofemoral arthroplasty - A report of 56 arthroplasties with 17 years of follow-up." Journal of Bone and Joint Surgery-British Volume **85B**(6): 836-840.

Korduba, L. A., J. Longaray, P. Lancin, A. Essner, A. Wamg, R. M. Meneghini (2008). Development of an aggressive wear test for patella implants. 54th Orhopaedic Research society. San Francisco, California.

Kornaat, P. R., J. L. Bloem, R. Y. T. Ceulemans, N. Riyazi, F. R. Rosendaal, R. G. Nelissen, W. O. carter, M. P. H. Le Graverand, M. Kloppenburg (2006). "Osteoarthritis of the knee: Association between clinical features and MR imaging findings" Radiology **239**(3): 811-817.

Kuhn, J. L., S. A. Goldstein, L. A. Feldkamp, R. W. Goulet, G. Jesion (1990). "Evaluation of a MicroCT system study trabecular bone structure." Journal of Orthopaedic Research **8**(6): 833-842.

Kurtz, S. M., O. K. Muratoglu, M. Evans, A. A. Edidin (1999). "Advances in the processing, sterilisation and crosslinking of UHMWPE for total joint arthroplasty" Biomaterials **20**: 1659-1688.

Kurtz, S. M., A. van Ooij, R. Ross, J. de Waal Malefijt, J. Peloza, L. Ciccarelli, M. L. Villarraga (2007). "Polyethylene wear and rim fracture in total disc arthroplasty." Spine J **7**(1): 12-21.

Lafortune, M. A. and P. R. Cavanagh (1987). "Three-Dimensional Kinematics of the Patella During Walking." Biomechanics X-A / editor: Bengt Jonsson. **6A**: 337-341.

Lafortune, M. A., P. R. Cavanagh, H. J. Sommer, A. Kalenak (1992). "3-Dimensional kinematics of the human knee during walking." Journal of Biomechanics **25**(4): 347-357.

Lee, K. Y. and D. Pienkowski (1998). "Compressive creep characteristics of extruded ultrahigh-molecular-weight polyethylene." Journal of Biomedical Materials Research **39**(2): 261-265.

Leeds Standard operating procedure. "Operating procedure for simulator studies"

Li, S., A. H. Burstein (1994). "Ultra high molecular weight polyethylene." The Journal of Bone and joint surgery **76-A**(7): 1080-1090.

Lievers, W. B., V. Lee, S. M. Arsenault, S. D. Waldman, A. K. Pilkey (2007). "Specimen size effect in the volumetric shrinkage of cancellous bone measured at two levels of dehydration." Journal of Biomechanics **40**(9): 1903-1909.

Lindsey, J. A., D. Conner, P. Godleski, B. Perkinson, W. M. Mihalko, J. L. Williams (2010). "Patellar Button wear patterns in well functioning Total Knee Arthroplasty Retrievals" Journal of long-term effects of Medical Implants **20**(1): 73-79.

Liao, Y. S., H. McKellop, Z. Lu, P. Campbell, P. Benya (2003). "The effect of frictional heating and forced cooling on the serum lubricant and wear of UHMW polyethylene cups against cobalt-chromium and zirconia balls." Biomaterials **24**(18): 3047-59.

Livingston, B. J., M. J. Chmell, M. Spector, R. Poss (1997). "Complications of total hip arthroplasty associated with the use of an acetabular component with a Hylamer lining." The journal of Bone and Joint Surgery **79-A**(10): 1529-38.

Lombardi, A. V., G. A. Engh, R. G. Volz, J. L. Albrigo, B. J. Brainard (1988). "Fracture dissociation of the polyethylene in metal-backed patellar components in total knee arthroplasty." Journal of Bone and Joint Surgery-American Volume **70A**(5): 675-679.

Ma, H. M., Y. C. Lu, T. G. Kwok, F. Y. Ho, C. Y. Huang, C. H. Huang (2007). "The effect of the design of the femoral component on the conformity of the patellofemoral joint in the total knee replacement." Journal of Bone and Joint Surgery. **89**(3): 408-412.

Martelli, S. and V. Pinskerova (2002). "The shapes of the tibial and femoral articular surfaces in relation to tibiofemoral movement." Journal of Bone and Joint Surgery-British Volume **84B**(4): 607-613.

McAlindon, T. E., S. Snow, C. Cooper, P. A. Dieppe (1992). "Radiographic Patterns of Osteoarthritis of the knee joint in the community – The importance of patellofemoral joint" Annals of the Rheumatic diseases **51**(7) : 844-849.

McEwen, H. M., P. I. Barnett, C. J. Bell, R. Farrar, D. D. Auger, M. H. Stone, J. Fisher (2005). "The influence of design, materials and kinematics on the in vitro wear of total knee replacements." J Biomech **38**(2): 357-65.

Miller, R. K., J. W. Goodfellow, D. W. Murray, J. J. O'Connor (1998). "In vitro measurement of patellofemoral force after three types of knee replacement." Journal of Bone and Joint Surgery-British Volume **80B**(5): 900-906.

Mountney, J., D. R. Wilson, M. Paice, B. A. Masri, N. V. Greidanus (2008). "The Effect of an augmentation Patella Prosthesis Versus Patelloplasty on Revision Patellar Kinematics and Quadriceps Tendon Force: An Ex Vivo Study." The Journal of Arthroplasty **23**(8): 1219-1231.

Mow, V. C. and R. Huiskes (2005). Basic orthopaedic biomechanics and mechano-biology, Lippincott Williams and Wilkins.

MSC.Software (2008). ADAMS/View R3 help manual.

National Joint Registry for England and Wales (2010). "7th Annual Report: Surgical data to December 2009".

Nicol, S. G., J. M. Loveridge, A. E. Weale, C. E. Ackroyd, J. H. Newman (2006). "Arthritis progression after patellofemoral joint replacement" Knee **13**(4): 290-295.

NationalJointRegistry (2010). National Joint Registry for England and Wales - 8th Annual Report.

NJR.uk (2003). National Joint Registry Dataset.

Ostermeier, S., O. Buhrmester, C. Hurschler and C. Stukenborg-Colsman (2005). "Dynamic in vitro measurement of patellar movement after total knee arthroplasty: an in vitro study." BMC Musculoskelet Disord **6**: 30.

Personal communication from DePuy International Leeds, UK (2010).

Peters, Jr. P. C., G. A. Engh, K. A. Dwyer, T. N. Vinh (1992). "Osteolysis after total knee arthroplasty without cement" The Journal of Bone and Joint Surgery **74-A** (6): 864-876.

Petersilge, W. J., C. S. Oishi, K. R. Kaufman, S. E. Irby, C. W. Jr. Colwell (1994). "The effect of trochlear design on patellofemoral shear and compressive forces in total knee arthroplasty." Clin Orthop Relat Res(309): 124-30.

Piraino, D., B. Richmond, H. Freed, G. Belhobek, J. Schils, B. Stulberg (1990). "Total knee replacement – radiologic findings of failure of porous-coated metal backed patellar component." American Journal of Roentgenology **155**(3): 555-558.

Pycnomatic and Pycnomatic ATC Instruction Manual (2007). Pycnomatic And Pycnomatic ATC (Automatic Temperature Control) Instruction Manual. Milan: 120.

Rao, S. S. (1995). Mechanical Vibrations, Addison-Wesley.

Raimondi, M. T., R. Sassi, R. Pietrabissa (2000). "A method for the evaluation of the change in volume of retrieved acetabular cups." Proceedings of the Institution of Mechanical Engineers Part H-Journal of Engineering in Medicine **214**(H6): 577-587.

Rawlinson, J. J., B. D. Furman, S. Li, T.M. Wright, D. L. Bartel (2006). "Retrieval, experimental, and computational assessment of the performance of total knee replacements." Journal of Orthopaedic Research **24**(7): 1384-1394.

Reeves, E. A., D. C Barton, D. P. FitzPatrick, J. Fisher (1998). "Comparison of gas plasma and gamma irradiation in air sterilization on the delamination wear of

UHMWPE knee replacement components." Transaction of 44th Annual Meeting, Orthopaedic Research Society, New Orleans: 16-19 March 1998, 778

Reilly, D. T. and M. Martens (1972). "Experimental Analysis Of Quadriceps Muscle Force And Patello-Femoral Joint Reaction Force For Various Activities." Acta Orthopaedica Scandinavica **43**(2): 126-130.

Robertsson, O., S. Bizjajeva, A. M. Fenstad, O. Furnes, L. Lidgren, F. Mehnert (2010). "Knee arthroplasty in Denmark, Norway and Swedon." Acta Orthopaedics **81**(1): 82-89.

Rostoker, W., E. Y. S. Chao, J. O. Galante (1978). "The appearances of wear on polyethylene--a comparison of in vivo and in vitro wear surfaces." J Biomed Mater Res **12**(3): 317-35.

Saikko, V. and O. Calonius (2003). "An improved method of computing the wear factor for total hip prostheses involving the variation of relative motion and contact pressure with location on the bearing surface." J Biomech **36**(12): 1819-27.

Saikko, V., O. Calonius, J. Keranen (2004). "Effect of slide track shape on the wear of ultra-high molecular weight polyethylene in a pin-on-disk wear simulation of total hip prosthesis." Journal of Biomedical Materials Research Part B-Applied Biomaterials **69B**(2): 141-148.

Saleh, K. J., E. A. Arendt, J. Eldridge, J. P. Fulkerson, T. Minas and K. J. Mulhall (2005). "Symposium - Operative treatment of patellofemoral arthritis." Journal of Bone and Joint Surgery-American Volume **87A**(3): 659-671.

Schai, P. A., T. S. Thornhill, R. D. Scott (1998). "Total knee arthroplasty with the PFC system: RESULTS AT A MINIMUM OF TEN YEARS AND SURVIVORSHIP ANALYSIS." J Bone Joint Surg Br %R 10.1302/0301-620X.80B5.8368 **80-B**(5): 850-858.

Schmalzried, T. P., F. J. Dorey, H. Mckellop (1998). "Commentary: The Multi factorial Nature of Polyethylene Wear in Vivo." The Journal of Bone and Joint Surgery **80A**: 1234-42.

Schonholtz, G. J. (1989). "Arthroscopic debridement of the knee-joint." Orthopedic Clinics of North America **20**(2): 257-263.

Scott, R. D., T. S. Thornhill, J. Slamin (1997). Oval domed shaped patella prosthesis. USA, JOHNSON and JOHNSON PROFESSIONAL, INC.: 1076.

Schwartz, O., J. Aunallah, M. Levitin, D. G. Mendes (2002). "Wear pattern of retrieved patellar implants." Acta Orthop Belg **68**(4): 362-9.

Semlitsch, M., (1991). "The historical development of UHMWPE as a slide bearing in joint endoprostheses." In Willert, H., G. Buchhorn, amd P. Eyerer, Ultra high molecular weight polyethylene as a biomaterial in orthopaedic surgery. Toronto: Hogrefe and Huber Publishers: 1-5.

Seymour, R (2002). "Prosthetics and Orthotics: lower limb and spinal". Lippincott Williams and Wilkins, Second Edition: 0-485.

Sharkey, P. F., W. J. Hozack, R. H. Rothman, S. Shastri, S. M. Jacoby (2002). "Why are total knee arthroplasties failing today?" Clinical Orthopaedics and Related Research (404): 7-13.

Sheenan, F T. and Drace, J E (1999). "Quantitative MR measures of three-dimensional patellar kinematics as a research and diagnostic tool." Medicine and Science in Sports and Exercise **31**(10):1339-1405.

Singerman, R., J. Berilla, G. Kotzar, J. Daly, D. T. Davy (1994). "A six-degree-of-freedom transducer for in vitro measurement of patellofemoral contact forces." J Biomech **27**(2): 233-8.

Singerman, R., D. T. Davy, V. M. Goldberg (1994). "Effects of patella alta and patella infera on patellofemoral contact forces." Journal of Biomechanics **27**(8): 1059-1065.

Singerman, R., S. M. Gabriel, C. B. Maheshwer and J. W. Kennedy (1999). "Patellar contact forces with and without patellar resurfacing in total knee arthroplasty." Journal of Arthroplasty **14**(5): 603-609.

Sips, R. J. A., L. Mulder, J. H. Koolstra, T. M. G. J. van Eijden (2008). "Development of the micro architecture and mineralization of the basilar part of the pig occipital bone." Connective Tissue Research **49**(1): 22-29.

SJR.se (2007). Swedish knee arthroplasty register.

Stachowiak, G. W. and A. W. Batchelor (2005). "Engineering Tribology" 3rd Edition Elsevier Inc. Oxford UK.

Stanley unpublished data (2011). University of Durham. UK

Steihl, J. B. (2005). "A clinuical overview patellofemoral joint and application of total knee arthroplasty." Journal of Biomechanics **38**(2): 209-214.

Szebenyi, B., A. P. Hollander, P. Dieppe, B. Quilty, J. Duddy, S. Clarke, J. R. Kirwan (2006). "Associations between pain, function and radiographic features in osteoarthritis of the knee" Arthritis and Rheumatism **54**(1): 230-235.

Tipper, J. L., E. Ingham, J. L. Hailey, A. A. Besong, J. Fisher, B. M. Wroblewski, M. H. Stone (2000). "Quantitative analysis of polyethylene wear debris, wear rate and head damage in retrieved Charnley hip prostheses." J Mater Sci Mater Med **11**(2): 117-24.

Tennant, S., A. Williams, V. Vedi, C. Kinmont, W. Gedroyc, D. M. Hunt (2001). "Patello-femoral tracking in the weight-bearing knee: a study of asymptomatic volunteers utilising dynamic magnetic resonance imaging: a preliminary report." Knee Surgery Sports Traumatology Arthroscopy **9**(3): 155-162.

Uvehammer, J., L. Regner, J. Karrholm (2001). "Flat vs. concave tibial joint surface in total knee arthroplasty: randomized evaluation of 39 cases using radiostereometry." Acta Orthop Scand **72**(3): 257-65.

United States Patent – Modular knee replacement 1998, DePuy manufacturing drawing

United States Patent – oval dome patella 1997

Vanbiervliet, J., J. Bellemans, C. Verlinden, J. P. Luyckx, L. Labey, B. Innocenti, H. Vandenneucker (2011). "The influence of Malrotation and femoral Component material on patellofemoral wear during gait" The Journal of Bone and Joint Surgery **93-B**: 1348-1354.

Van Kampen, A. and R. Huiskes (1990). "The 3-dimensional tracking pattern of the human patella." Journal of Orthopaedic Research **8**(3): 372-382.

Viana, M., P. Jouannin, C. Pontier, D. Chulia (2002). "About pycnometric density measurements." Talanta **57**(3): PII S0039-9140(02)00058-9.

Vicars, R., J. Fisher, R. Hall (2009). "The accuracy and precicion of a micro computer tomography volumetric measurement technique for the analysis of in-vitro tested total disc replacements." Proceedings of the Institution of Mechanical Engineers Part H-Journal of Engineering in Medicine.

Wang, A., C. Stark, J. H. Dumbleton (1996). "Mechanisticv and morphological origins of ultra high molecular weight opolyethylene wear debris in total joint replacement prostheses." Proceedings Instituition Mechanical Engineers. Part H: Journal of Engineering in Medicine **210**: 141-155.

Wang, A. G., S. S. Yau, A. Essener, L. Herrera, M. Manley, J. Dembleton (2008). "A highly crosslinked UHMWPE for CR and PS total knee arthroplasties." Journal of Arthroplasty **23**(4): 559-566.

Whelan, A., J. Goff (1990). "Injection molding of Thermoplastics materials" Volume 2. New York: Van Nostrand Reinhold.

Whittle, M. W. (2001). Gait analysis : an introduction / Michael W. Whittle. Oxford :, Butterworth-Heinemann,.

Wilson, M. G., K. Kelley, T. S. Thornhill (1990). "Infection as a complication of total knee-replacement arthroplasty. Risk factors and treatment in sixty-seven cases." Journal of Bone and Joint Surgery-American Volume **72**: 878-883.

Wright, T. M. and D. L. Bartel (1986). "The problem of surface damage in polyethylene total knee components." Clin Orthop(205): 67-74.

Wright, T. M., C. M. Rimnac, P. M. Faris, M. Bansal (1988). "Analysis of surface damage in retrieved carbon fiber-reinforced and plain polyethylene tibial components from posterior stabilized total knee replacements." J Bone Joint Surg Am **70**(9): 1312-9.

Yercan, H. S., T. A. S. Selmi, P. Neyret (2005). "The treatment of patellofemoral osteoarthritis with partial lateral facetectomy." Clinical Orthopaedics and Related Research(436): 14-19.

Zachman, N. J., B. M. Hillberry, D. B. Kettelkamp (1978). "Design of a Load Simulator for Dynamic Evaluation of Prosthetic Knee Joints." ASME publication n 78-DET-59.

Zavatsky, A. B., P. T. Oppold, A. J. Price (2004). "Simultaneous In Vitro Measurement of Patellofemoral Kinematics and Forces." Journal of Biomechanical Engineering **126**(3): 351-356.

Appendix (List of Conference Publications)

Raman Maiti, John Fisher, Zhongmin Jin, Peter Ellison and Louise Jennings

Computational Modelling and Experimental Validation of Patella-Femoral Kinematics of Total Knee Joint Replacements during Gait Cycle

World Congress on Biomechanics, August 2010, Singapore

Raman Maiti, John Fisher, Zhongmin Jin, Liam Rowley and Louise Jennings

Effect of Kinematics on the Wear Rate of the Patella Femoral ARTIFICIAL Joint

ASME Summer Bioengineering Conference, June 2011, Pennsylvania, USA

Raman Maiti, John Fisher, Zhongmin Jin and Louise Jennings

An Experimentally Validated Computational Model of a Six Axis Artificial Patella Femoral Joint Simulator during the Gait Cycle

Pre-ORS, February 2012, San Francisco, USA

Raman Maiti, John Fisher, Zhongmin Jin and Louise Jennings

Influence of Kinematics on the Wear Rate of the Artificial Patella Femoral Joint

Orthopaedic Research Society, February 2012, San Francisco, USA

Appendix A

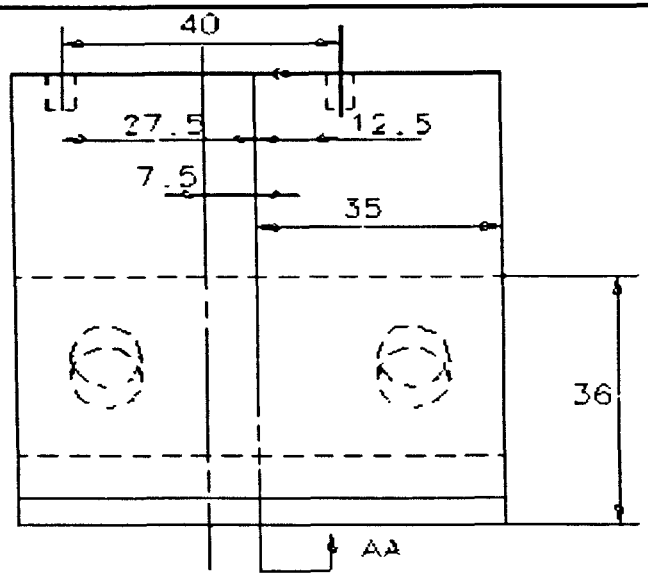

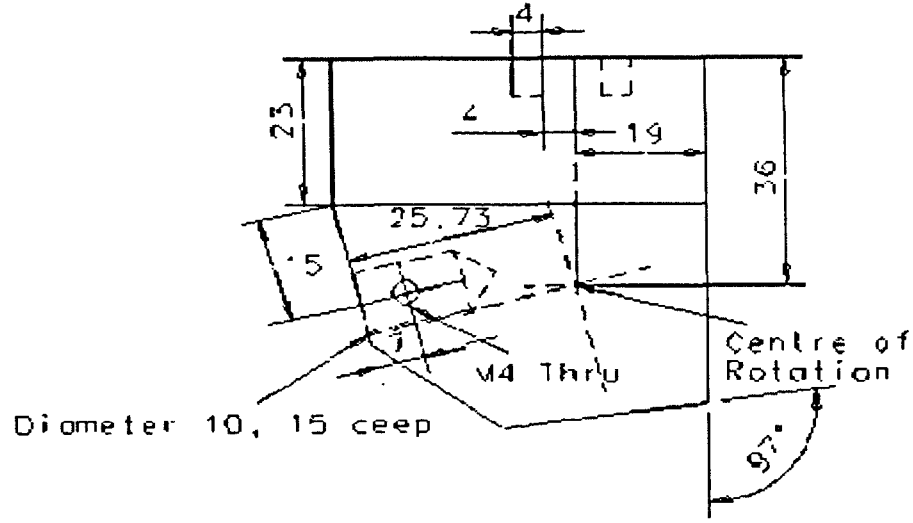

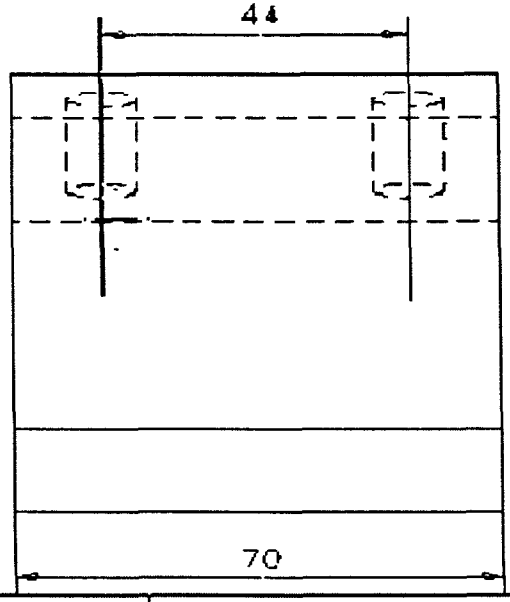

Section AA-AA

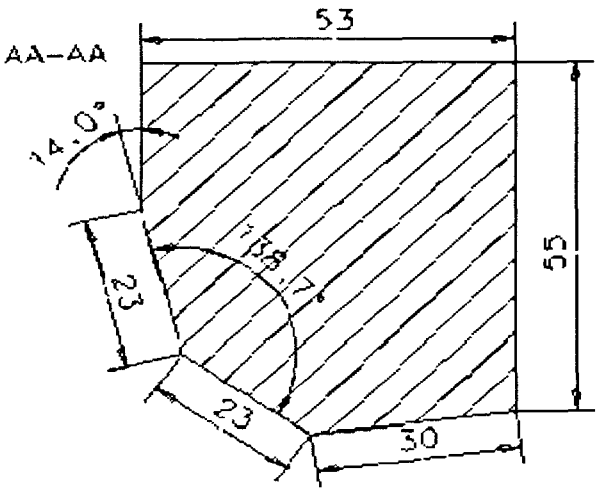

REMOVE ALL SHARP EDGES ALL CHAMFER 45 DEG x mm

6 Piece Manufacture

45 DEG x 1mm
CHAMF

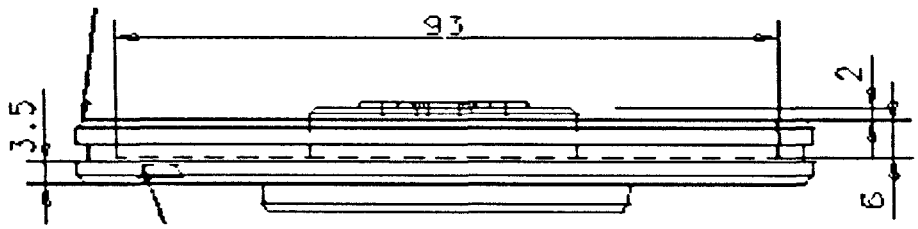

SINK WITH SLOT DRILL
6 mm DIA +/- 0.02 x 1.8 DEEP
DON NOT BREAK THRO

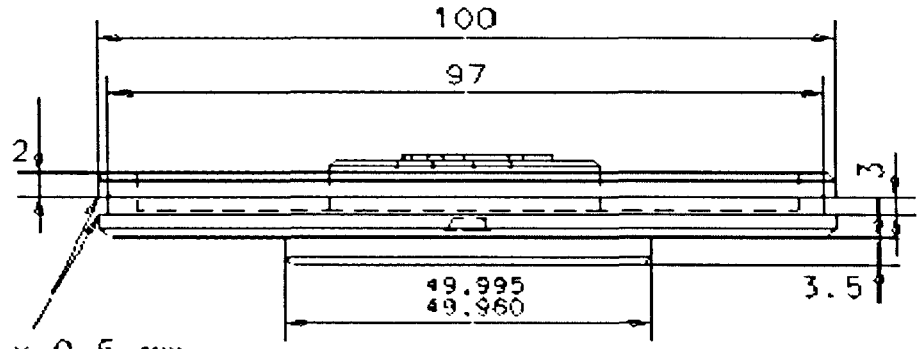

45 DEG x 0.5 mm
Chamf

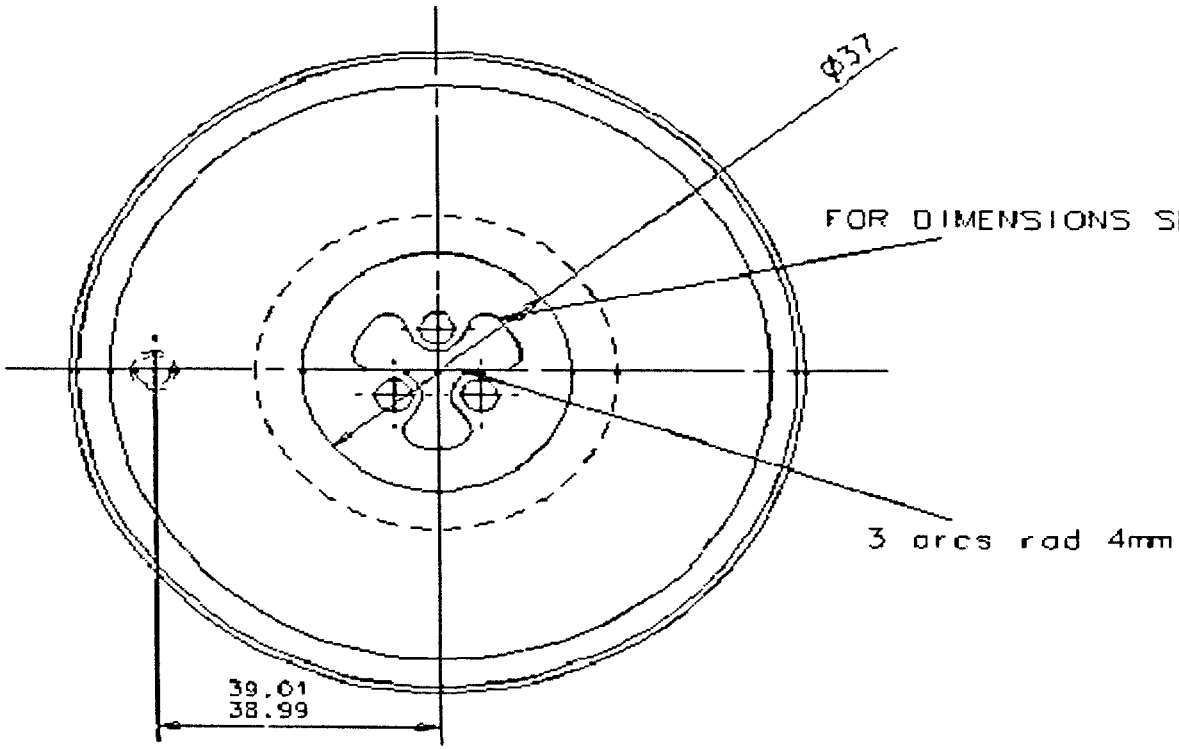

FOR DIMENSIONS SEE PATELLA BACKING

3 arcs rad 4mm

REMOVE ALL SHARP EGDES
ALL CHAMFERS 45 DEG x 1 mm

5 pieces monufacture

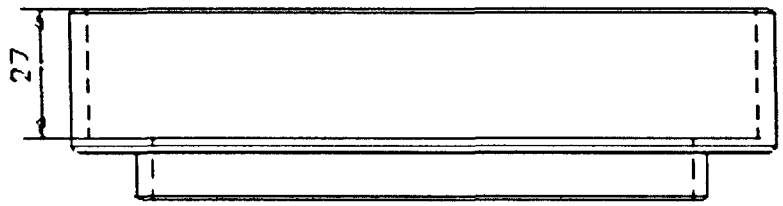

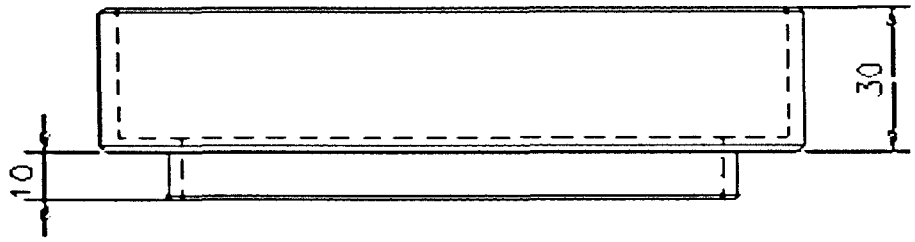

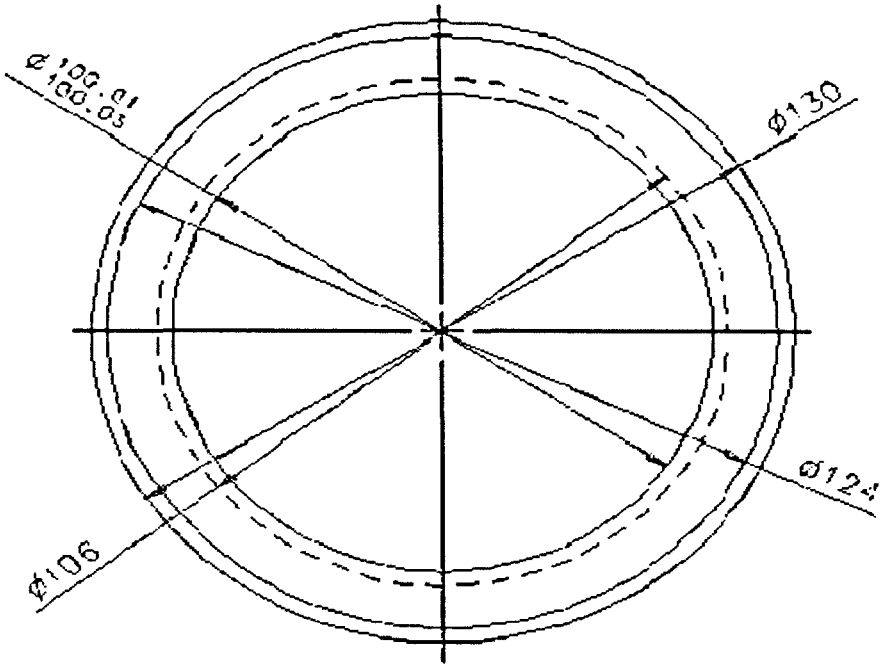

REMOVE ALL SHARP EDGES
ALL CHAMFER 45 DEG x 1 mm

5 Pieces Manufacture

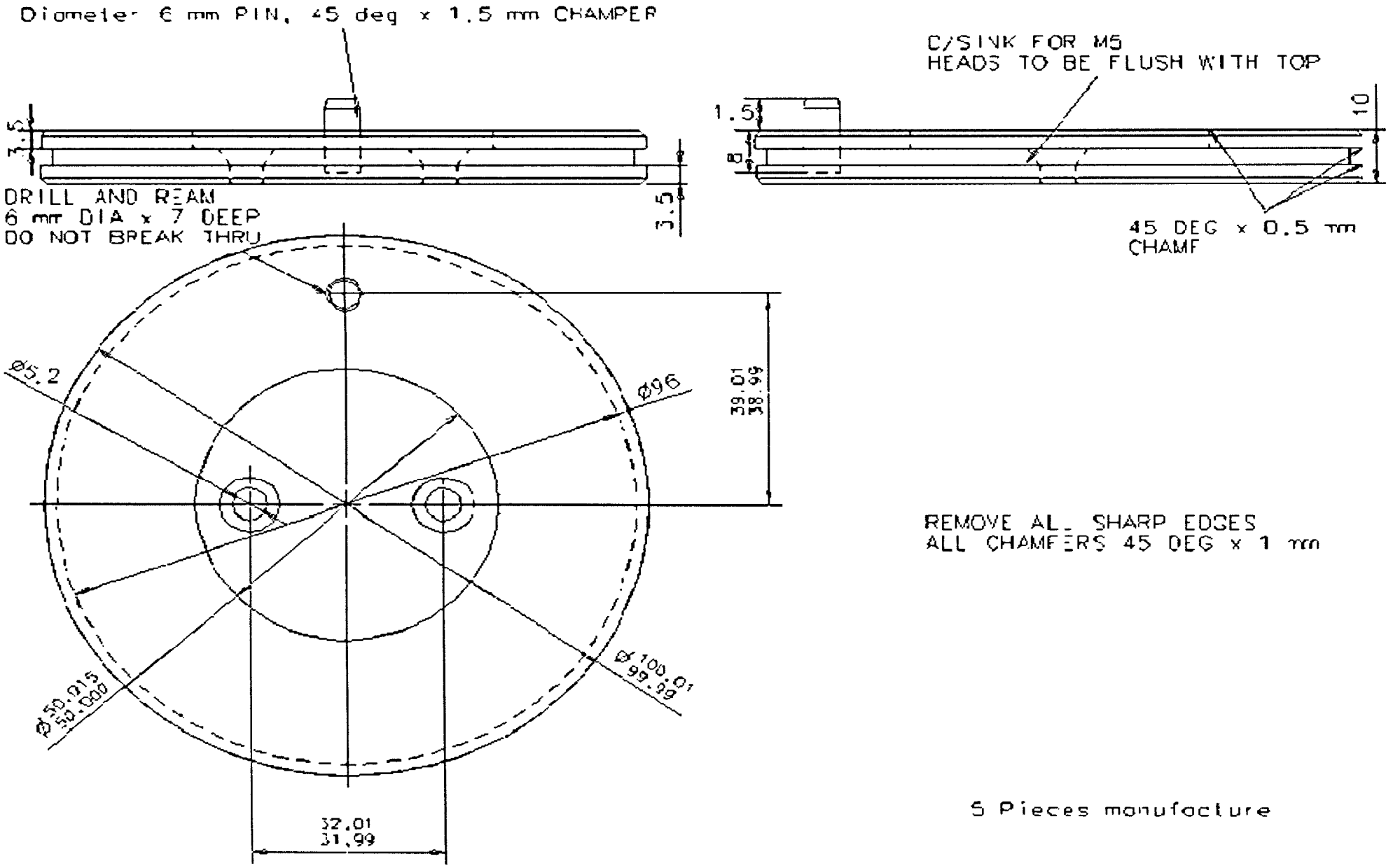
Diameter 6 mm PIN, 45 deg x 1.5 mm CHAMFER
C/SINK FOR M5
HEADS TO BE FLUSH WITH TOP
3.5
3.5
1.5
8
10
DRILL AND REAM
6 mm DIA x 7 DEEP
DO NOT BREAK THRU
45 DEG x 0.5 mm
CHAMF
Ø5.2
Ø96
39.01
38.99
Ø50.015
50.000
Ø100.01
99.99
32.01
31.99
REMOVE ALL SHARP EDGES
ALL CHAMFERS 45 DEG x 1 mm
5 Pieces manufacture

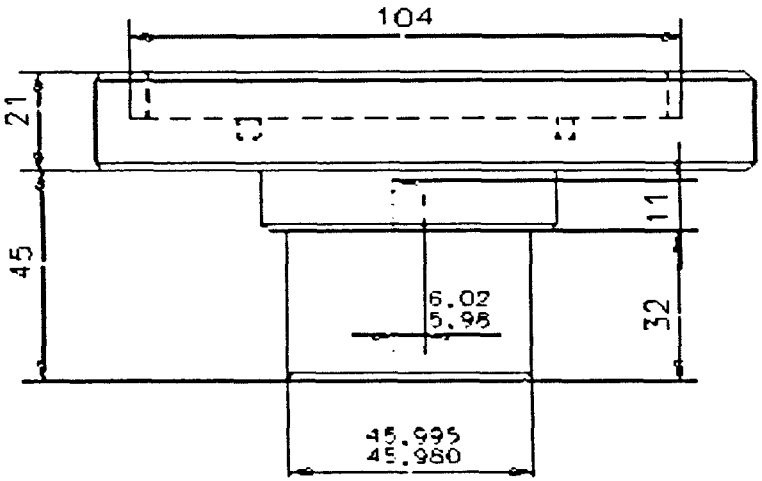

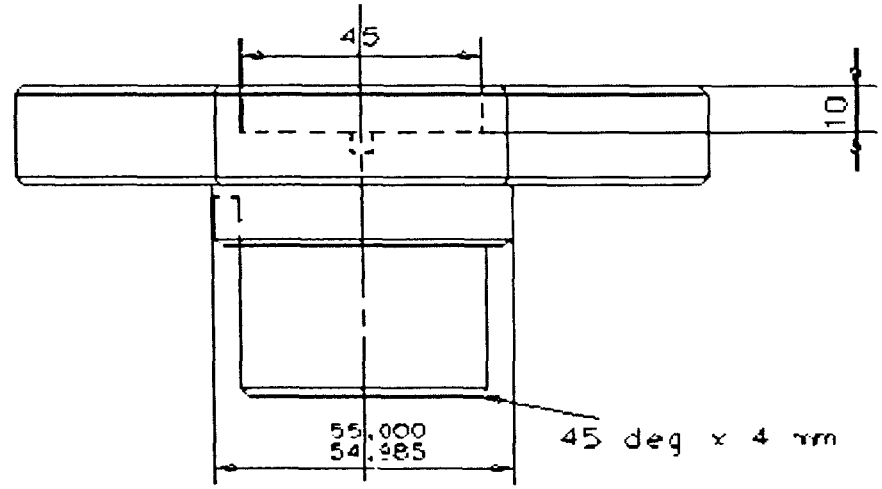

2 holes M5. DRILL + TAP 4 mm deep
DO NOT BREAK THRU

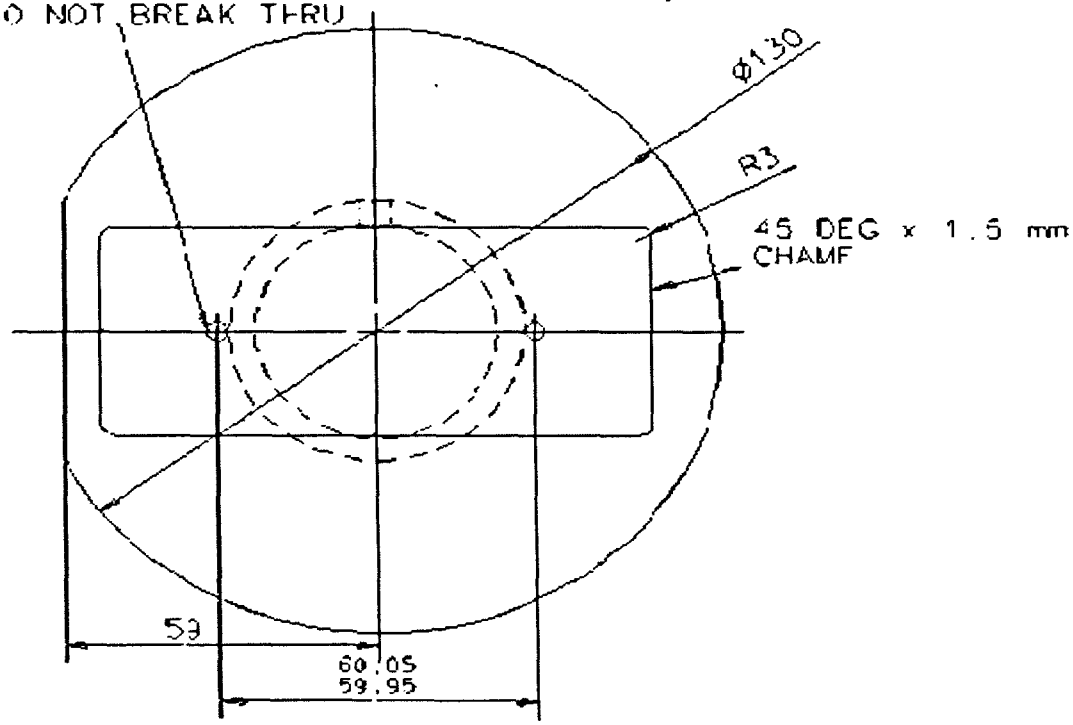

REMOVE ALL SHARP EDGES
ALL CHAMFERS 45 DEG x 1.5 MM
UNLESS STATED

5 Piece Manufacture

	Axial load	IE rotation	IE rotation zero	AP displacement	AP displacement zero	AP load
G1-1	0.03495	12.1	133	13	172	
G1-2	0.03593	12.1	134	12.9	146	0.116429
G1-3	0.03649	12.3	139	13.4	148	
Average	0.03579	12.2		13.1		
G2-1	0.02883	12.0	124	13	147	
G2-2	0.02923	12.3	138	12.9	145	0.117214
G2-3	0.03246	12.2	138	12.9	227	
Average	0.03017	12.2		12.9		